

**Civilian Radioactive Waste Management System
Management & Operating Contractor**

**Waste Package Related Impacts of Plutonium Disposition Waste Forms in a Geologic
Repository**

TDR-EBS-MD-000003 REV 01 ICN 01

January 2000

Prepared for:

U.S. Department of Energy
Office of Civilian Radioactive Waste Management
1000 Independence Avenue SW
Washington, D.C. 20585

Prepared by:

Civilian Radioactive Waste Management System
Management & Operating Contractor
1211 Town Center Drive
Las Vegas, Nevada 89144

Under Contract Number
DE-AC08-91RW00134

DISCLAIMER

This report was prepared as an account of work sponsored by an agency of the United States Government. Neither the United States Government nor any agency thereof, nor any of their employees, nor any of their contractors, subcontractors or their employees, makes any warranty, expressed or implied, or assumes any legal liability or responsibility for the accuracy, completeness, or any third party's use or the results of such use of any information, apparatus, product, or process disclosed, or represents that its use would not infringe privately owned rights. Reference herein to any specific commercial product, process, or service by trade name, trademark, manufacturer, or otherwise, does not necessarily constitute or imply its endorsement, recommendation, or favoring by the United States Government or any agency thereof or its contractors or subcontractors. The views and opinions of authors expressed herein do not necessarily state or reflect those of the United States Government or any agency thereof.

QA: QA

**Civilian Radioactive Waste Management System
Management & Operating Contractor**

**Waste Package Related Impacts of Plutonium Disposition Waste Forms in a Geologic
Repository**

TDR-EBS-MD-000003 REV 01 ICN 01

January 2000

Prepared for:

U.S. Department of Energy
Office of Civilian Radioactive Waste Management
1000 Independence Avenue SW
Washington, D.C. 20585

Prepared by:

Civilian Radioactive Waste Management System
Management & Operating Contractor
1211 Town Center Drive
Las Vegas, Nevada 89144

Under Contract Number
DE-AC08-91RW00134

*WM-11
NMS527*

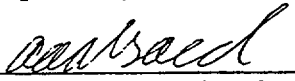
**Civilian Radioactive Waste Management System
Management & Operating Contractor**

**Waste Package Related Impacts of Plutonium Disposition Waste Forms in a Geologic
Repository**

TDR-EBS-MD-000003 REV 01 ICN 01

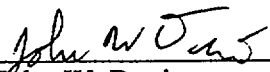
January 2000

Prepared By:


Abdelhalim A. Alsaed

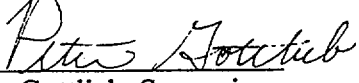
Date: 4/21/2000

Checked By:

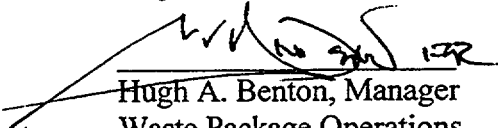

John W. Davis

Date: 4/21/00

Approved By:


Peter Gottlieb, Supervisor
Degraded and External Criticality

Date: 4/21/00


Hugh A. Benton, Manager
Waste Package Operations

Date: 4/21/00

INTENTIONALLY LEFT BLANK

HISTORY OF CHANGE

<u>Rev/Change Number</u>	<u>Date</u>	<u>Description and Reason for Change</u>
REV 00	September 1999	Initial Issue
REV 00 ICN 01	January 2000	Editorial Changes The results, conclusions, and recommendations did not change; however, editorial changes were made. Pages affected are: x, 2-3, 2-10, 2-11, 6-2, 6-12, 6-32, 6-34, 6-45, 6-64, 8-2, 8-3, and 8-4.
REV 01	January 2000	External Criticality Evaluations are added in Section 7 and summarized in the executive summary and in Section 8. Editorial changes throughout the document are identified with vertical bars.
REV 01 ICN 01	March 2000	Addition of explanation of Heavy Metal Mass calculation in Table 2-1 Page 2-1 and correction of page number from which the information was taken in CRWMS M&O 1998a in response to DR# LVMO-00-D-010.

INTENTIONALLY LEFT BLANK

EXECUTIVE SUMMARY

This report provides a comprehensive summary of the waste package (WP) related impacts of the Plutonium Disposition waste forms that are being developed and evaluated by the Office of Fissile Materials Disposition of the DOE. These waste forms are of two distinct types. One type is mixed oxide spent nuclear fuel (MOX SNF), which would be received from one or more commercial nuclear reactors using MOX fuel prepared from surplus weapons plutonium. The other type is plutonium immobilized in ceramic disks, which would be embedded in HLW glass in the standard HLW glass disposal canister. The ceramic disks would occupy approximately 12% of the HLW canister volume, while most of the remaining 88% of the volume would be occupied by HLW glass.

The studies reported here have been ongoing for five years, and much of the work has been presented in one of four previous annual reports. This is the first of the reports to be subject to requirements of the Office of Civilian Radioactive Waste Management Quality Assurance Requirements (DOE 1998a and CRWMS M&O 1999p). This compliance is necessary in order that the results presented here be applicable to the major upcoming OCRWM project statutory and licensing documents: the Site Recommendation, and the License Application. It is, therefore, necessary to confirm some of the results from the prior year's reports. A summary distinguishing the results that are new this year is given at the end of this executive summary.

The two basic WP designs used for this study are identical to those that have been used for the commercial SNF and the HLW glass; they are used here for the MOX SNF and the immobilized plutonium, respectively. These WP designs were used for the OCRWM *Viability Assessment of a Repository at Yucca Mountain (VA)* document, which was recently delivered to the United States Congress. The improved performance expected with these new WP designs will be covered in the Waste Package Related Impacts report for next year.

MOX

This study is primarily concerned with evaluating the criticality potential of the intact and degraded forms of the MOX SNF. Two variations of the WP VA design have been used: the 21 PWR WP and the 12 PWR WP. The 21 PWR WP holds 21 MOX fuel assemblies and is used for moderately burned MOX SNF. The latter holds only 12 MOX fuel assemblies and is used for the highest burned MOX SNF, in order to satisfy peak temperature limits. This study also includes an evaluation of the structural, thermal, and shielding impacts of the MOX SNF WPs.

The design and irradiation cycle of the MOX fuel will be specified by the contractor selected by the DOE. In the meantime a typical design and cycle developed by Westinghouse has been used for preliminary impact assessment. When the final fuel design and irradiation cycle are developed, they will be evaluated for compliance with repository acceptance criteria. The criticality characteristics of the five different assembly enrichment-burnup combinations for the MOX design and irradiation cycle that are evaluated in this document fall within the envelope of criticality characteristics of commercial LEU SNF assemblies, many of which have worse criticality characteristics than the MOX SNF. Therefore, the criticality evaluations for the MOX SNF follow the methods of criticality analysis that have been established for LEU SNF:

1. Evaluate the criticality of the intact configuration to demonstrate the effectiveness of the criticality control measures.
2. Use the geochemistry code EQ6 to determine the configurations of materials in WPs in which the basket structure and SNF matrix have degraded.
3. Evaluate the criticality implications of simultaneous fuel matrix degradation, assembly collapse, and fission product loss.
4. Evaluate the criticality implications of simultaneous fuel matrix degradation, assembly collapse, and loss of the iron oxide that comes from the corrosion of the carbon steel basket within the WP.

Major Findings for the MOX Waste Form

The following findings are based on currently available data on the hypothetical Westinghouse MOX fuel design and irradiation cycle.

1. Assuming that the MOX SNF will not be emplaced sooner than 10 years following discharge from the reactor, those assemblies having low burnup (≤ 46 GWd/MTHM) can be loaded into the standard commercial 21 PWR WP, and those assemblies having high burnup (> 46 GWd/MTHM) can be loaded into the standard commercial 12 PWR WP. This strategy will meet the maximum thermal output design criteria of 11.8 kW per package. With the expected distribution of burnups in the MOX SNF, this strategy will result in approximately half the MOX assemblies being placed in each of the two types of waste package. This emplacement strategy will ensure that:
 - The MOX SNF waste package meets applicable regulatory requirements
 - That there is no credible intact or degradation scenario leading to an internal criticality in the waste packages.
2. The most severe structural hazard to the waste package is a tipover accident. A finite-element analysis shows that the peak stress in the waste package will be at least 15% less than the ultimate material tensile strength of the material. This shows that the structural behavior of both the 21 PWR WP and the 12 PWR WP will be within design limits. The calculated stresses on the WPs containing MOX SNF are very similar to stresses calculated for WPs containing ordinary commercial SNF. This result is to be expected because the MOX and ordinary commercial assemblies weigh very nearly the same.
3. Assuming that the MOX SNF will be emplaced at least 10 years following discharge, the maximum initial heating rates for the MOX SNF were 798 W/assembly for the 21 PWR WP and 1070 W/assembly for the 12 PWR WP. These values are less than the 850 W/assembly and 1500 W/assembly used as the thermal design basis (maximum thermal output of 18 kW per WP) for commercial LEU PWR SNF, indicating that the MOX assemblies are well within the design envelope of the commercial SNF WP. The peak

cladding temperature calculated for the 21 MOX PWR WP was approximately 336°C, and that for the 12 MOX PWR was approximately 302°C. These temperatures are below the established design limit of 350°C.

4. Dose rates from both neutron and gamma radiation were calculated for the 21 PWR WP loaded with the highest burnup MOX SNF and the shortest cooling period after reactor discharge (10 years) to serve as a worst case that would give the highest dose rates. Maximum dose rates at the exterior surfaces of the waste package were less than 110 rad/hr. Maximum dose rates from the MOX SNF were much less than those from commercial LEU PWR SNF of similar burnup, which were calculated to be greater than 150 rad/hr. The 12 MOX PWR WP design has an equivalent amount of shielding with a smaller radiation source, which should result in smaller surface dose rates.

The design limit of 100 rad/hr on the WP surface was specified so that no significant increase would occur in the corrosion rate of the waste package barrier due to any radiolytic compounds synthesized from moist air. For both waste packages, the SNF surface dose rate exceeded the design limit only during the period immediately following emplacement when humidity in the repository environment is expected to be low. It is concluded, therefore, that no increase in corrosion rates from radiolysis will occur.

The following items deal with the criticality. Most of the conclusions are with respect to the conservative criticality threshold of $k_{\text{eff}} = 0.92$. Only very unlikely configurations would cause the MOX SNF waste package k_{eff} to exceed this value. Therefore, it is expected that the MOX SNF will satisfy the anticipated risk-based regulatory requirements. Furthermore, the MOX SNF is more robust with respect to criticality than a significant fraction of the commercial LEU SNF.

5. Criticality evaluations were performed for configurations internal to the MOX SNF WP, for conditions ranging from intact to fully degraded fuel and basket. Configurations that could lead to $k_{\text{eff}} > 0.92$ were found to be extremely unlikely. Specifically, it was found that:
 - The loss of all fission products from the SNF matrix while the fuel pins are still uncollapsed produced k_{eff} greater than 0.92, but less than 0.95.
 - The loss of 75% of the iron oxide (which came from the corrosion of the carbon steel basket) can produce a k_{eff} just above 0.95. Such high oxide loss was evaluated for comparison purposes only; there is no known physical mechanism for causing such a high iron oxide loss from the waste package in the repository environment.
 - Since the k_{eff} calculations took principal isotope burnup credit, it will be necessary for the reactor operator to provide data sufficient for reactor criticality benchmark calculations.
6. The probabilities of criticality have been estimated by considering worst case configurations. For the worst-case fission-product-loss scenario, the expected number of criticalities in 100,000 years is approximately 0.08. For the worst case iron-oxide-loss

scenario, the expected number of criticalities in 100,000 years is less than 0.07.

7. For a worst case steady state criticality lasting 10,000 years, the maximum radionuclide inventory increment at 1,000 years following the criticality shutdown is 18% of the radionuclide inventory (in Curies) that would be present at that time without the criticality. At 20,000 years following the criticality shutdown the increment will have decayed to only 2.5% (in Curies) more than would be present without the criticality. These comparisons are with respect to the least burned MOX SNF, because that is the only type that can go critical. If comparison were made to the average burnup MOX, which has approximately 25% more radionuclide inventory to begin with, the percent increments would be correspondingly smaller.
8. For a transient criticality with a fairly rapid insertion rate, the peak overpressure and temperature are inversely correlated with the available exit area of the holes in the waste package barrier. For a total opening area of 0.1 cm^2 (which is extremely unlikely to permit enough water to enter and exit the waste package) the peak overpressure is less than 60 atmospheres and the peak temperature is only 220°C . Both these parameters are less than the values experienced in a PWR reactor. Therefore, they are not likely to cause any damage to the waste package barrier or to the fuel cladding, both of which are important in limiting radionuclide release. The radionuclide inventory increment for the transient event will be negligible, since the burnup received from the transient criticality is less than 10^{-7} GWd/MTHM .
9. The concentration of fissile material in the MOX source term for external criticality is too small to produce a significant accumulation external to the waste package.

CERAMIC

As with the MOX waste form, the principal waste package impact issue is criticality. However, regulatory requirements also dictate structural and shielding evaluations. If the structural evaluation can show that canister breach from the worst-case handling accident is a beyond-design-basis event (i.e., less than $10^{-6}/\text{year}$), then there can be no plutonium release and no offsite radiation dose from such an accident. The purpose of the thermal evaluation is to ensure correct accounting of the contribution of this waste form to the overall repository thermal loading strategy.

For the ceramic waste form, the principal criticality control measure is the incorporation of gadolinium (Gd) and hafnium (Hf) neutron absorbing materials in the waste form. The potential for criticality is determined primarily by the amount of neutron absorber material remaining in the waste package if, and when, water breaches the waste package subjecting its contents to aqueous corrosion. Under such conditions the waste form can corrode; however, the fissile material in the waste form (^{239}Pu and its decay product ^{235}U) will remain in the waste package for hundreds of thousands of years, because it is very insoluble under most water chemistry conditions. The neutron absorber Hf is even less soluble than the fissile material so it will also remain in the WP. However, Gd, the more effective neutron absorber, becomes more soluble under some conditions (particularly $\text{pH} < 6$) and could eventually be flushed from the waste

package. The geochemistry part of this study identifies the degradation rates for the waste form, HLW glass, and steel that can lead to low pH, and consequently significant Gd loss.

Because of the importance of the criticality issue for the immobilized Pu waste form, the following explanation is useful. The expected degradation scenarios depend on the following processes:

- a. Local breach of the waste package by aqueous corrosion, and wetting of all interior surfaces
- b. Local breach of the stainless steel HLW canisters containing the HLW filler glass and the Pu ceramic waste form
- c. Dissolution of the HLW glass
- d. Breach of the inner cans that actually contain the Pu ceramic disks
- e. Corrosion of the stainless steel of the canisters and cans
- f. Dissolution of the ceramic waste form
- g. Removal of the fissile material from the waste package
- h. Removal of the neutron absorber material from the waste package
- i. Accumulation of the fissile material in the external environment.

Many of these processes will overlap in time. In fact, the removal of fissile material and neutron absorber take place over hundreds of thousands of years (because of the small solubility of the fissile and absorber materials) and must, therefore, overlap. Furthermore, the largest loss of Gd occurs when the HLW glass is not dissolved, but the Pu cans are breached, the canisters and cans are fully corroded, and the ceramic waste form is dissolved. The fact that the glass is expected to degrade faster than the stainless steel or ceramic makes the maximum-Gd-loss scenario extremely unlikely.

The range of possible degraded configurations internal to the waste package that have some potential for criticality can be represented by two general classes. (1) *Partly degraded configurations* in which the fissile material is still contained within the ceramic disks, but the neutron absorbing Gd and Hf has leached from the disks and become distributed uniformly throughout the waste package. Such configurations have the greatest potential for separating the fissile material and the neutron absorber material. (2) *Fully degraded configurations* in which the fissile material has become distributed uniformly throughout the sludge formed from the solid degradation products of all the waste package components and enough water for optimum moderation. Both of these configuration classes are safely sub-critical throughout the credible range of degradation conditions.

Major Findings for the Pu Ceramic Waste Form

Based on the current design for the HLW canister loading and the current ceramic formulation (27 kg of Pu per canister), this study finds that:

1. The ceramic Pu waste form can be emplaced in the repository at a loading of 5 Pu-containing HLW canisters per waste package; this permits the disposal of immobilized Pu in the same waste package as will be used for the disposal of HLW glass.
 - The ceramic Pu waste package meets applicable regulatory requirements.
 - There is no credible degradation scenario leading to criticality internal to the waste package. Furthermore, beyond 40,000 years after emplacement so much of the ^{239}Pu will have decayed to the less reactive ^{235}U that criticality will no longer be physically possible within the waste package.
 - Thermal and shielding impacts are comparable to, or less than, those of the corresponding HLW waste package.
 - The canister containing the Pu-bearing ceramic disks and the HLW glass can withstand a corner drop from a height of 9.14 meters without being breached.
2. Criticality for the intact configuration is not possible, since the maximum calculated $k_{\text{eff}} = 0.11$ when all of the void space in the waste package is filled with water.
3. Criticality is not possible for partly degraded configurations, in which there is maximum credible separation between fissile material and neutron absorber. The maximum calculated $k_{\text{eff}} = 0.54$ for this partly degraded configuration.
4. Criticality is not credible for fully degraded configurations (defined above as having a uniform distribution of fissile material and neutron absorber throughout the WP with varying degrees of neutron absorber loss from the waste package). The maximum Gd loss predicted by the geochemistry calculations is 78%. The k_{eff} for this case is less than 0.5. Furthermore, such a large loss of Gd only occurs under very unlikely conditions.
5. Accumulation of a critical mass external to the waste package requires a high concentration of fissile material in the source term that may flow out of the waste package. This high fissile concentration can only occur if the ceramic aqueous degradation rate is at least 10 times larger than the current estimate provided by the Office of Fissile Materials Disposition. Even with this unlikely occurrence, there are a number of additional unlikely conditions required before criticality can occur.

RELATION TO PREVIOUS STUDIES

As mentioned above, this report is the fifth in an annual series on the waste package related impacts of the Plutonium Disposition waste forms. These reports have dealt with two sets of

impacts: (1) the early impacts, thermal, structural, and shielding and (2) the principal long-term impact: criticality. These reports have covered both the MOX and the Pu-ceramic alternatives. They have generally found the impacts to be within the repository design envelope.

This study advances those previous studies in the following respects:

- The requirements of Quality Assurance have been applied to ensure the acceptability of the results for Site Recommendation and License Application.
- Several important issues with respect to the immobilized plutonium waste package have been resolved:
 - The canister containing the immobilized plutonium ceramic disks and the high level waste filler glass has been shown analytically to survive a drop from 9.14 meters, landing on a bottom corner (the maximum drop test performed on a HLW canister).
 - All possible combinations of degradation rates for the waste package components (ceramic disks, filler glass, and canister stainless steel) have been evaluated to identify the maximum loss of gadolinium. It was found to be possible to lose 78% of the initial gadolinium loading, which still leaves more than enough in the waste package to prevent criticality. There were several different scenarios having gadolinium loss greater than 20%, but they were all characterized by very high corrosion rates for the ceramic waste form. Such high corrosion rates are possible, but very unlikely; the ceramic waste form was chosen for its robustness with respect to aqueous corrosion.
 - For the gadolinium remaining in the waste package, the worst case separation from the fissile material (defined as having the fissile material remain in the degraded ceramic disks at the bottom of the waste package while gadolinium is distributed throughout the water filled waste package) was found to have $k_{eff} < 0.54$.
- For MOX criticality, a wider range of parameters characterizing degraded configurations has been considered. These include consideration of up to 75% loss of the iron oxide (corrosion product of the steel components of the waste package basket) which provides a significant criticality control function. As stated under MOX section, finding #5, these high oxide loss scenarios were evaluated for comparison purposes only; there is no known physical mechanism for causing such a high iron oxide loss from the waste package in the repository environment.

- Several important new studies have been added:
 - The probability of criticality internal to the waste package has been evaluated for the MOX SNF for a distribution of the degradation parameters characterizing the degraded configurations.
 - The consequences have been evaluated for both steady state and transient MOX criticality (internal to the waste package), and both were shown to have insignificant effects.

CONTENTS

	Page
EXECUTIVE SUMMARY.....	vii
MOX.....	vii
CERAMIC.....	x
RELATION TO PREVIOUS STUDIES.....	xii
ACRONYMS	xxv
1. INTRODUCTION AND BACKGROUND.....	1-1
2. WASTE FORM AND WASTE PACKAGE DESCRIPTIONS	2-1
2.1 MOX	2-1
2.1.1 MOX SNF Characteristics	2-1
2.1.2 Waste Package Description.....	2-3
2.1.2.1 Material Properties	2-6
2.1.3 Waste Stream Quantities	2-6
2.1.4 Waste Package Criticality Control Measures.....	2-7
2.1.5 Criteria for Evaluating Impacts of MOX Disposal	2-7
2.1.5.1 Structural Criteria.....	2-7
2.1.5.2 Thermal Criteria	2-8
2.1.5.3 Shielding Criterion	2-8
2.1.5.4 Criteria Related to Postclosure Criticality.....	2-8
2.2 CERAMIC.....	2-9
2.2.1 Waste Stream Quantities	2-9
2.2.2 Waste Form Description.....	2-9
2.2.2.1 Dimensions.....	2-9
2.2.2.2 Mass	2-10
2.2.2.3 Chemical/Isotopic Composition of the Ceramic Waste Form	2-10
2.2.2.4 Characteristics of HLW Filler Glass	2-12
2.2.2.5 Corrosion Rates.....	2-13
2.2.3 Plutonium Disposition Canister	2-14
2.2.3.1 Canister Dimensions	2-15
2.2.3.2 Canister Mass	2-15
2.2.4 Waste Package Description.....	2-17
2.2.5 Waste Package and Canister Quantities	2-19
2.2.6 Criteria for Evaluating Impacts of Disposal of the Ceramic Waste Form	2-19
2.2.6.1 Structural Criteria.....	2-19
2.2.6.2 Thermal Criteria	2-20
2.2.6.3 Shielding Criterion	2-20
2.2.6.4 Criteria Related to Postclosure Criticality.....	2-20
2.3 ENVIRONMENTAL CONDITIONS.....	2-20
2.3.1 Chemical Composition of J-13 Well Water	2-20
2.3.2 Drip Rate of J-13 Water into a WP	2-20
3. STRUCTURAL ANALYSIS.....	3-1

CONTENTS (Continued)

	Page
6.2.3.1	Geochemistry Evaluations of the Degradation Processes and Scenarios6-34
6.2.3.2	Degraded Configurations6-48
6.3	PROBABILITY OF INTERNAL CRITICALITY6-56
6.3.1	Method6-56
6.3.2	Probability Distributions of Secondary Degradation Processes.....6-58
6.3.3	Criticality Probability6-59
6.4	INTERNAL CRITICALITY CONSEQUENCES6-62
6.4.1	Transient Criticality.....6-63
6.4.1.1	Transient Criticality Methodology6-64
6.4.1.2	Transient Criticality Results.....6-64
6.4.2	Steady State Criticality.....6-68
6.4.2.1	Steady State Criticality Methodology6-68
6.4.2.2	Steady State Criticality Results.....6-70
7.	EXTERNAL CRITICALITY.....7-1
7.1	SOURCE TERMS.....7-1
7.1.1	Source Term from the MOX Waste Package.....7-1
7.1.2	Source Term from the Ceramic Waste Package.....7-2
7.2	ACCUMULATION OF FISSILE MATERIAL7-6
7.2.1	Accumulation from the MOX Source Term7-6
7.2.2	Accumulation from the Ceramic Source Term7-6
7.2.2.1	Accumulation in the Invert.....7-6
7.2.2.2	Accumulation in the Far-Field7-10
7.3	CRITICALITY EVALUATIONS OF EXTERNAL ACCUMULATIONS.....7-18
7.3.1	Criticality Evaluations for Accumulations in the Near-Field.....7-18
7.3.2	Criticality Evaluations for Accumulations in the Far-Field7-19
7.4	PROBABILITY OF EXTERNAL CRITICALITY7-21
7.4.1	Occurrence of Criticality.....7-21
7.4.2	Upper Bound to the Probability of Criticality7-22
8.	FINDINGS AND CONCLUSIONS.....8-1
8.1	MOX8-1
8.1.1	Structural8-1
8.1.2	Thermal8-1
8.1.3	Shielding.....8-2
8.1.4	Criticality.....8-2
8.2	CERAMIC.....8-3
8.2.1	Structural8-3
8.2.2	Thermal8-3
8.2.3	Shielding.....8-3
8.2.4	Criticality.....8-4
9.	REFERENCES.....9-1

CONTENTS (Continued)

	Page
9.1 DOCUMENTS CITED.....	9-1
9.2 SOURCE DATA.....	9-9

FIGURES

	Page
2-1. Thermal Power Generation from MOX SNF Actinide Composition.....	2-2
2-2. 21 PWR UCF Waste Package Assembly.....	2-4
2-3. 12 PWR UCF Waste Package Assembly.....	2-5
2-4. Can-in-Canister Sketch.....	2-16
2-5. 5-DHLW Waste Package to be Used for Plutonium Immobilized in Ceramic.....	2-18
3-1. Canister Shell Strain Contours Along the Target Surface for 11.58 m Vertical Drop.....	3-3
3-2. Orientation of Vertical and Corner Drops.....	3-4
3-3. Canister Shell Strain Contours Along the Target Surface for 9.14 m Corner Drop.....	3-5
4-1. Temperature Histories for 21 PWR MOX WP.....	4-2
4-2. Temperature Histories for 12 PWR MOX SNF WP.....	4-3
4-3. Waste Package Temperature Distribution.....	4-4
4-4. Temperature versus Time since Emplacement for Selected Points in the WP.....	4-5
5-1. Waste Package Surfaces for Radial Dose Rate Calculation.....	5-4
5-2. Radiation Dose Rate Over Time from the 21 MOX PWR WP Mid-Region.....	5-6
5-3. Axial Profile of Dose Rates at the Outside Surface of the 21 MOX PWR WP.....	5-7
5-4. MCNP Shielding Representation of 5-DHLW WP Containing Can-in-Canister.....	5-8
6-1. Degradation Sequence of the 21 PWR Basket Structure Following WP Breach.....	6-4
6-2. Intact 21 PWR MOX Fuel Waste Package.....	6-5
6-3. Intact 12 PWR MOX Fuel Waste Package.....	6-6
6-4. Time Effects on k_{eff} for Intact MOX SNF and Intact Baskets in a 21 PWR Absorber Plate WP.....	6-7
6-5. Time Effects on k_{eff} for Intact MOX SNF and Intact Baskets in a 12 PWR WP.....	6-8
6-6. Time Effects on k_{eff} for Intact MOX SNF and Intact Baskets in a 12 PWR WP with Al Shunts.....	6-9
6-7. Retention History of Elements of Principal Interest for Criticality Remaining in WP.....	6-13
6-8. Degraded 21 PWR MOX Fuel Waste Package with Uniform Corrosion Product Distribution	6-15
6-9. Degraded 21 PWR MOX Waste Package With Settled Corrosion Product Distribution (58% solid content).....	6-16
6-10. Degraded 12 PWR MOX Fuel Waste Package with Uniform Corrosion Product Distribution.....	6-16
6-11. Degraded 12 PWR MOX Waste Package With Settled Corrosion Product Distribution (58% solid content).....	6-17
6-12. Time Effects on k_{eff} for Intact MOX and LEU SNF in a 21 PWR WP with a Fully Degraded Basket (No Boron Remaining) and Uniformly Distributed Corrosion Products.....	6-18
6-13. Time Effects on k_{eff} for Intact MOX SNF in a 21 PWR WP with a Fully Degraded Basket (No Boron Remaining) and Settled Corrosion Products.....	6-19
6-14. Time Effects on k_{eff} for Intact MOX SNF in a 12 PWR WP with a Fully Degraded Basket and Uniformly Distributed Corrosion Products.....	6-20
6-15. Time Effects on k_{eff} for Intact MOX SNF in a 12 PWR WP with a Fully Degraded Basket and Settled Corrosion Products.....	6-21
6-16. Degraded 21 PWR Fuel Waste Package with Uniform Corrosion Product Distribution.....	6-22

FIGURES (Continued)

	Page
6-17. k_{eff} as a Function of Fission Product Loss (4.0 wt%, 35.6 GWd/MTHM) (CRWMS M&O 1999h, Fig. 6-1).....	6-26
6-18. k_{eff} as a Function of Iron Oxide Loss (4.0 wt%, 35.6 GWd/MTHM) (CRWMS M&O 1999h, Fig. 6-2).....	6-27
6-19. Degraded 21 PWR MOX WP with Fuel Rods Collapsed to Bottom of Package Surrounded by Uniformly Distributed Basket Corrosion Products.....	6-28
6-20. Fully Degraded Fuel and Basket Material Uniformly Distributed Throughout Interior Volume of 21 PWR WP.....	6-29
6-21. Time and Fuel Degradation Effects on k_{eff} for 21 PWR WP with a Fully Degraded Basket, Square Lattice Collapsed Rods (MOX and LEU), and Uniformly Distributed Corrosion Products.....	6-30
6-22. Time and Fuel Degradation Effects on k_{eff} for a 21 PWR WP with Fully Degraded Basket and Fuel, and Uniformly Distributed Corrosion Products.....	6-31
6-23. Sensitivity of Aqueous Gd Molalities (CRWMS M&O 1999c, Fig. 5-5).....	6-39
6-24. Effect of fO_2 on pH (CRWMS M&O 1999c, Fig. 6-1).....	6-44
6-25. Aqueous Concentrations of Important Elements and pH for Case 3 (CRWMS M&O 1999c, Fig. 6-2).....	6-46
6-26. Aqueous Concentrations of Important Elements and pH for Case 26 (CRWMS M&O 1999c, Fig. 6-3).....	6-47
6-27. A Cross-sectional View of a Horizontally Emplaced Waste Package for the Partial Degradation Configuration (CRWMS M&O 1999k, Fig. 5-1).....	6-49
6-28. A Cross-sectional Front View of a Horizontally Emplaced Waste Package for the Full Degradation Configuration (CRWMS M&O 1999k, Fig. 5-2).....	6-51
6-29. MCNP k_{eff} for Case 14 (49% Gd lost, CRWMS M&O 1999k, Fig. 6-1).....	6-52
6-30. MCNP k_{eff} for Case 14 with All Gd and Hf Removed (CRWMS M&O 1999k, Fig. 6-2)6-53	53
6-31. MCNP k_{eff} for Case 14 with Partial Gd and Hf Removed (CRWMS M&O 1999k, Fig. 6-3).....	6-54
6-32. Minimum Hf Required to Maintain Subcriticality versus Time since Discharge	6-55
6-33. Calculated k_{eff} for Maximum Gd Loss Cases	6-56
6-34. Expected Criticalities for Alternative Fission Product Loss Scenarios (CRWMS M&O 1999l, Fig. 6-1)	6-60
6-35. Expected Criticalities for Alternative Iron Oxide Loss Scenarios (CRWMS M&O 1999l, Fig. 6-2).....	6-61
6-36. Expected Criticalities with Alternative Coefficients of Variance for Oxide Loss and Fission Product Loss (CRWMS M&O 1999l, Fig. 6-3).....	6-62
6-37. Pressure for 0.158 \$/s Insertion Rate (CRWMS M&O 1999m, Fig. 6.1-3).....	6-66
6-38. Fuel Temperature for 0.158 \$/s Insertion Rate (CRWMS M&O 1999m, Fig. 6.1-4)	6-67
6-39. Exit Flow 0.158 \$/s Insertion Rate (CRWMS M&O 1999m, Fig. 6.1-9).....	6-67
6-40. Pressure for 0.0004 \$/s Insertion Rate (for both 10.0 cm ² and 0.1 cm ² exit areas) (CRWMS M&O 1999m, Fig. 6.2-1).....	6-68
7-1. EQ3/6 Pu Source Terms.....	7-4
7-2. EQ3/6 U Source Terms.....	7-5

FIGURES (Continued)

	Page
7-3. Schematics of Handling of Dilution: a) Local Dilution; b) Classical Dispersion (CRWMS M&O 2000c, Figure 2-1)	7-12
7-4. Spatial Distribution of Actinide Minerals after 2,500 Years of Precipitation (SA=1,000,000 cm ²) (CRWMS M&O 2000c, Figure 6-4).....	7-13
7-5. Moles of Pu and U Minerals Precipitated as a Function of Cell Number (SA=20,000 cm ² for 2,500 years) (CRWMS M&O 2000c, Figure 6-6)	7-14
7-6. Total Number of Moles of Actinide Precipitated as a Function of Dilution (SA=20,000 cm ²) (CRWMS M&O 2000c, Figure 6-11)	7-16
7-7. Sensitivity Analysis for Surface Areas (dilution factor of 10%) (CRWMS M&O 2000c, Figure 6-12).....	7-17
7-8. Total Number of Moles of Actinide Precipitated as a Function of Surface Area (dilution factor of 10%) (CRWMS M&O 2000c, Figure 6-13).....	7-17
7-9. Invert Dimension (not to scale) (CRWMS M&O 1999q, Figure 5).....	7-18
7-10. Fracture Matrix with Aperture Detail (not to scale) (CRWMS M&O 2000d, Figure 5-2)	7-20

INTENTIONALLY LEFT BLANK

TABLES

	Page
2-1. Mechanical Parameters for Westinghouse 17x17 MOX Fuel Assemblies.....	2-1
2-2. Initial Heavy Metal Isotopic Content (wt%) of MOX SNF Assemblies	2-1
2-3. MOX Assembly Selection Criteria	2-1
2-4. Material Properties of 21 PWR WP Components	2-6
2-5. Input Composition of the Baseline Ceramic Waste Form	2-10
2-6. Impurities in the Pu Process Input Stream.....	2-11
2-7. Average wt% Isotopic Composition of the Pu and U Feed in 2010	2-12
2-8. Curies per kg of Total Plutonium plus Americium in 2010	2-12
2-9. HLW Filler Glass Composition	2-13
2-10. Corrosion Rates Used for EQ6 Analyses.....	2-14
2-11. The Main Physical Characteristics of the Five High-Level Waste Canister Waste Package	2-18
2-12. Numbers of Canisters Required for Disposal of Immobilized Pu	2-19
2-13. Compositions of J-13 Well Water (from LL980711104242.054)	2-21
5-1. Major Isotopes Contributing to the Fuel Region Radiation Source.....	5-3
5-2. Major Isotopes Contributing to the End Fittings Region Radiation Source	5-3
5-3. 10-Year Dose Rates from 21 MOX PWR SNF at External Surface of Waste Package	5-5
5-4. 10-Year Dose Rates at the External Surface from Commercial LEU SNF in the 21 PWR Waste Package	5-5
5-5. Dose Rate Results for the 5-DHLW/DOE Spent Fuel Disposal Container WP Shielding Calculations.....	5-10
6-1. Corrosion Products Remaining Following Basket Degradation in the 21 PWR WP	6-12
6-2. Results for the 4.0 wt%/35.6 GWd/MTHM Fuel, 0% Collapse (CRWMS M&O 1999h, Table 6-1).....	6-24
6-3. Results for the 4.0 wt%/35.6 GWd/MTHM Fuel, 100% Collapse (CRWMS M&O 1999h, Table 6-5).....	6-25
6-4. Results of the Iron Oxide for 4.0 wt%/35.6 GWd/MTHM Fuel (CRWMS M&O 1999h, Table 6-11).....	6-25
6-5. Peak k_{eff} for Degraded PWR MOX SNF	6-32
6-6. Percent Loss of Gadolinium, for Entire WP, Thermodynamic Data Sensitivity Study (CRWMS M&O 1999c, Table 5-6)	6-39
6-7. Gd, Pu, and U% Losses for Indicated Deviations from J-13 Incoming Water Composition (CRWMS M&O 1999c, Table 5-7)	6-40
6-8. Sensitivity of Gd Loss to Glass Composition (CRWMS M&O 1999c, Table 5-9).....	6-41
6-9. Gd, Pu, and U Losses for EQ6 Cases (CRWMS M&O 1999c, Tables 5-10, 5-11, 5-12, and 6-1).....	6-42
6-10. Gd Loss Characteristics and pH of Selected Cases (CRWMS M&O 1999c, Table 6-2)	6-43
6-11. MCNP Calculated k_{eff} for Partially Degraded Cases (CRWMS M&O 1999k, Table 6-1)6- 50	6-54
6-12. Minimum Hf Required to Maintain Subcriticality.....	6-54
6-13. Expected Number of Criticalities for 83 MOX Waste Packages (CRWMS M&O 1999l, Table 6-1).....	6-59

TABLES (Continued)

	Page
6-14. Maximum Temperature and Pressure Values for PWR MOX SNF for a Reactivity Insertion Rate of 0.158 \$/s (CRWMS M&O 1999m, Table 6.1-1).....	6-66
6-15. Total Activity for 21 PWR MOX SNF Waste Package for Steady State Criticality Event (CRWMS M&O 1999m, Table 6.3-1).....	6-70
7-1. Aqueous Concentration for Low Drip Rate and High Pu Solubility	7-2
7-2. Aqueous Concentration for High Drip Rate and High Pu Solubility.....	7-2
7-3. Pu-ceramic Degradation Rates for Source Term Calculations	7-3
7-4. Summary of Invert U and Pu Accumulations (CRWMS M&O 2000b, Table 6-1)	7-10
7-5. Summary of Results (pe0a1231): Accumulation Starts 2,500 Years After Breach Time for 2,500 Years(CRWMS M&O 2000c, Table 6-1)	7-15
7-6. Summary of Results for Case pe0a1231 for Different Pu Decay (SA=20,000 cm ²) (CRWMS M&O 2000c, Table 6-3).....	7-15
7-7. Summary of Results for Case pe0a1231 for Different Pu Decay (SA=1,000,000 cm ²) (CRWMS M&O 2000c, Table 6-4).....	7-15
7-8. Summary of Results for Case pw2a1231 for Different Pu Decay (SA=20,000 cm ²) (CRWMS M&O 2000c, Table 6-5).....	7-16
7-9. Summary of Results for Case pw2a1231 for Different Pu Decay (SA=1,000,000 cm ²) (CRWMS M&O 2000c, Table 6-6).....	7-16
7-10. Tuff Composition (CRWMS 1997m, Table 4.1.3-1).....	7-18
7-11. Near-Field Criticality Evaluation of Plutonium Disposition Ceramic Waste Form (CRWMS M&O 2000d, Table 5-2 and Table 6-1).....	7-19
7-12. Far-Field Criticality Evaluation of Plutonium Disposition Ceramic Waste Form (CRWMS M&O 2000d, Table 5-3 and Table 6-2).....	7-21

ACRONYMS

2-D	Two Dimensional
3-D	Three Dimensional
5-DHLW WP	5 Defense High Level Waste Package
AML	Areal Mass Loading
B&W	Babcock and Wilcox
B-SS	Borated Stainless Steel
CDF	Cumulative Distribution Function
CL	Critical Limit
CPA	Controlled Project Assumption
CRWMS	Civilian Radioactive Waste Management System
CSCI	Computer Software Configuration Item
cv	Coefficient of Variation
DBE	Design Basis Event
DHLW	Defense High-Level Waste Package
DOE	United States Department of Energy
EDA-II	Second Enhanced Design Alternative
ff	Frequency Function
FP	fission products
FPL	Fission Product Loss
Gd	Gadolinium
GWd	Gigawatt Days
Hf	Hafnium
HEU	Highly Enriched Uranium
HLW	High-Level Waste
HM	Heavy Metal
k_{eff}	k effective
LEU	Low Enriched Uranium
LLNL	Lawrence Livermore National Laboratory
M&O	Management & Operating
MGR	Monitored Geologic Repository
MOX	Mixed Oxide Fuel
MT	metric tons
MTHM	Metric Tons Heavy Metal
MTU	metric ton uranium
OCRWM	Office of Civilian Radioactive Waste Management
OIC	other internal components
pdf	Probability Density Function
PI	Principal Isotopes
PNNL	Pacific Northwest National Laboratory
Pu	Plutonium
PWR	Pressurized Water Reactor
SCFT	Solid Centered Flow Through
SDD	System Description Document
SKB	Swedish Nuclear Fuel and Waste Management Co.

ACRONYMS (Continued)

		Page
SNF	Spent Nuclear Fuel	
SRS	Savannah River Site	
SS	stainless steel	
TBV	to be verified	
TSPA	Total System Performance Assessment	
U	Uranium	
UCF	Uncanistered Fuel	
VA	Viability Assessment	
WF	Waste Form	
WP	Waste Package	
wt%	weight percentage	
vol%	volume percentage	

1. INTRODUCTION AND BACKGROUND

This report provides a comprehensive summary of the waste package (WP) related impacts of the Plutonium Disposition waste forms that are being developed/evaluated by the Office of Fissile Materials Disposition of the United States Department of Energy (DOE). These waste forms are of two distinct types. One type is mixed oxide spent nuclear fuel (MOX SNF) that would be received from one or more commercial nuclear reactors using MOX fuel prepared from surplus weapons Pu. The other type is Pu immobilized in ceramic disks, which would occupy approximately 12% of the volume of the standard canister being used for the disposal of high-level waste (HLW) glass. Most of the remaining 88% volume of the HLW canister is filled with the HLW glass. This report is in support of the work outlined in Civilian Radioactive Waste Management System (CRWMS) Management & Operating Contractor (M&O) (1999b).

To properly represent the two waste forms, each of the major sections of the report has two main subsections, the first for MOX SNF, and the second for the ceramic waste form.

The two basic waste package designs used for this study are described in Section 2. These designs are identical with those that have been used for the commercial SNF and the HLW glass; they are used here for the MOX SNF and the immobilized Pu, respectively. These are the designs that were used for the OCRWM Viability Assessment of a Repository at Yucca Mountain (VA) document, which was recently delivered to the United States Congress. These designs have been superseded by designs that are expected to have lifetimes of over 100,000 years before water penetration. The improved performance expected with these new designs will be covered in the Waste Package Related Impacts report for next year.

The remaining contents of the report are as follows:

- Section 3 discusses the structural analyses conducted on the waste packages, and for the ceramic waste form, the individual canisters that go inside the waste package.
- Section 4 discusses the thermal analyses conducted on the waste packages.
- Section 5 discusses the radiation shielding analyses conducted on the waste packages.
- Section 6 discusses the internal criticality evaluations. The criticality evaluations for each waste form are preceded by a degradation analysis using a geochemistry code. This degradation analysis serves to define the characteristics of the solution (water plus solutes) in the waste package and the composition of the solid degradation products. Section 6.3 provides an estimate of the probability of criticality (expressed as the cumulative expected number of criticalities as a function of time) for the MOX SNF. Section 6.4 summarizes the consequences for the MOX criticality, both steady state and transient. There are no corresponding probability or consequence calculations for the ceramic waste form because none of the configurations discussed in Section 6.2 has k_{eff} sufficiently close to 1, to make such calculations relevant.

- Section 7 is intended for the external criticality counterpart of Section 6. Because of the delayed delivery of ceramic degradation data from LLNL, the external accumulation of fissile material could not be completed in time for REV 00 of this document. All external criticality entries to this section will be completed for the next revision of this document, to be delivered at a later date.
- Section 8 summarizes the major findings from this study.

2. WASTE FORM AND WASTE PACKAGE DESCRIPTIONS

2.1 MOX

2.1.1 MOX SNF Characteristics

The potential use of MOX fuel in power reactors has been investigated through the development of conceptual designs for commercial pressurized water reactor (PWR) equilibrium reload cycles fueled with MOX assemblies (Westinghouse Electric Corporation 1994 and 1998). The most recent design, documented in Westinghouse Electric Corporation (1998), requires 92 fresh MOX assemblies per reload cycle. Two values of fissile Pu, given as weight percent (wt%) fissile Pu in the heavy metal (HM), were used in this design (Westinghouse Electric Corporation 1998, p. 18). The fresh reload batch consisted of 20 assemblies with a 4.5 wt% fissile Pu in HM and 72 assemblies with a 4.0 wt% fissile Pu in HM. The core loading for this design was 81.6 metric tons of heavy metal (MTHM) (Westinghouse Electric Corporation 1998, p. 16) resulting in an average Pu content of 18.48 kg/assembly. The average burnup for assemblies was targeted at 45 to 50 GWd/MTHM and ranged from a low value of approximately 35 to a high value of approximately 56 GWd/MTHM (Westinghouse Electric Corporation 1998, p. 43). The steady state discharge distribution consists of 83 assemblies burned for two cycles and 9 assemblies for three cycles (Westinghouse Electric Corporation 1998, p. 31). All assemblies burned for three cycles were of the 4.0 wt% fissile Pu in HM type.

The conceptual core design documented in Westinghouse Electric Corporation (1998) utilized the Westinghouse 17x17 Vantage 5 commercial assembly type (DOE 1992, p. 2A-30) and is the reference design for this study. Detailed mechanical parameters for these assemblies are given in Table 2-1. Assembly dimensions are given primarily in English units and converted into metric units to maintain consistency between calculations using either set of units. Assembly weights are used in the structural analysis (Section 3).

The initial heavy metal isotopic content of the PWR MOX Westinghouse Vantage 5 assembly fuel important for repository considerations is given in Table 2-2.

Table 2-1. Mechanical Parameters for Westinghouse 17x17 MOX Fuel Assemblies

Parameter	Vantage 5 Assembly		
	Value Metric Units	Value English Units	Reference
Fuel Length	365.76 cm	144 in.	Westinghouse Electric Corporation 1998, Table 1.2-1
Heavy Metal Mass	422.8 kg ^a	932.1 lb	CRWMS M&O 1998a, page 7
Assembly Weight	618.8 kg	1364.2 lb	CRWMS M&O 1998k, page 6
Weight of Non-fuel Material/Assembly	54.4 kg	120 lb	CRWMS M&O 1998k, page 6

^a This value was determined by dividing the Core Heavy Metal Mass by the Number of Assemblies given in Table 5.1-1 on Page 7 of CRWMS M&O 1998a.

Table 2-2. Initial Heavy Metal Isotopic Content (wt%) of MOX SNF Assemblies

Isotopes	Vantage 5 Assemblies (4.0 wt% Fissile Pu in HM) ^a	Vantage 5 Assemblies (4.5 wt% Fissile Pu in HM) ^a
²³⁵ U	0.191	0.190
²³⁸ U	95.550	95.019
²³⁹ Pu	3.983	4.481
²⁴⁰ Pu	0.251	0.282

^a Derived from isotopic wt% (Westinghouse Electric Corporation 1998, p. 17). Isotopes comprising < 0.01 wt% not listed.

The characterization of the potential MOX assemblies with respect to the content of those SNF isotopes of greatest abundance or of most neutronic significance was calculated (CRWMS M&O 1998a) with the SAS2H computer code and the ORIGEN-S computer code. The SAS2H and ORIGEN-S codes are part of the SCALE Code System, Version 4.3 (Computer Software Configuration Item [CSCI]: 30011 V4.3) (CRWMS M&O 1997a). SCALE4.3 was previously obtained from SCM in accordance with appropriate procedures. SCALE 4.3 is qualified and used only within the range of validation as documented in the SQR (CRWMS M&O 1997a). A one axial node SAS2H representation of the MOX assembly was developed to perform the depletion steps. The multi-cycle burnup histories were derived from the equilibrium MOX core load map (Westinghouse Electric Corporation 1998, Fig. 1-2.8, p. 31). Results from this analysis formed the source data for criticality, thermal, and radiation shielding evaluations of waste package designs for MOX assemblies in the Monitored Geologic Repository (MGR). The particular cases selected under the above criteria are given in Table 2-3 together with the controlling criteria.

Table 2-3. MOX Assembly Selection Criteria

Case ID ^a	Fissile Pu in HM (wt%)	Discharge Burnup (GWd/MTHM)	Controlling Criteria for Selection
1	4.0	56.5	Heat Generation
2	4.5	46.5	Heat Generation
3	4.0	50.1	Heat Generation; Criticality
4	4.0	35.6	Criticality
5	4.5	39.4	Criticality

^a ID = identification number.

Results from the analysis of Westinghouse MOX SNF relevant to the purpose of this calculation include the thermal power generation and isotopic content of the MOX SNF assemblies as a function of time after discharge from the reactor (CRWMS M&O 1998a). Representative results from the analyses are given in Figure 2-1 for the thermal power generation in the MOX SNF assemblies.

The total thermal power per assembly generated for each of the heat generation cases as shown in Figure 2-1 is for a period of 10,000 years beginning 10 years after discharge from the reactor (CRWMS M&O 1997b, Section 3.2). The total thermal power in the figure is the sum of the thermal power generated by radioactive decay of activated light elements, actinides, and fission products. The heating rate contribution from the different components varies with the assembly burnup value since the SNF isotopic composition is burnup dependent. Over short time periods, heating rates show a direct correlation with burnup due to the short-lived isotopes. This correlation does not hold over longer time periods as can be seen by comparing the two lower curves of Figure 2-1 for times beyond 40 years. This effect results in a larger source for MOX SNF at times greater than 100-1,000 years than is present for Low Enriched Uranium (LEU) SNF (CRWMS M&O 1998m, Fig. 5.1). These heating rate values are used as source terms for thermal calculations for the waste packages discussed in Section 4.

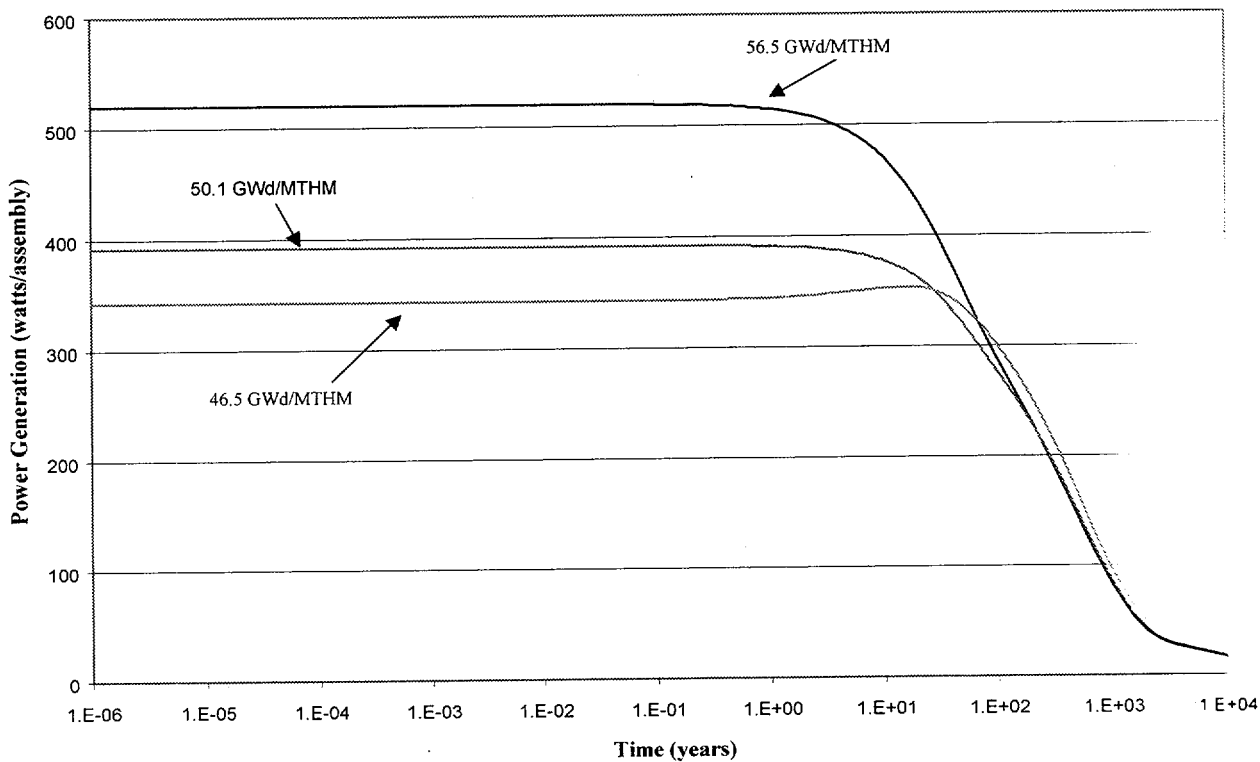


Figure 2-1. Thermal Power Generation from MOX SNF Actinide Composition.

Principal Isotope (PI) burnup credit is assumed to be an acceptable method to account for reduced reactivity of SNF in criticality evaluations (Controlled Project Assumption (CPA) 030, CRWMS M&O 1999a). A list of 29 "Principal Isotopes" for long-term criticality control in SNF has been previously established (CRWMS M&O 1997c, p. 3-26). The concentrations of these isotopes as a function of time derived from the SAS2H/ORIGEN-S analysis of the MOX SNF (CRWMS M&O 1998a) are used in the criticality analysis discussed in Section 6.

2.1.2 Waste Package Description

Waste packages considered for MOX SNF are the 21 PWR Uncanistered Fuel (UCF) WP and the 12 PWR UCF waste package which are the same as the Viability Assessment designs for commercial LEU SNF (CRWMS M&O 1997d, Section 8 and CRWMS M&O 1997e, Section 8). The 21 PWR WP holds 21 MOX fuel assemblies and is used for moderately burned MOX SNF. The latter holds only 12 MOX fuel assemblies and is used for the highest burned MOX SNF, in order to satisfy peak temperature limits. These waste packages are illustrated in Figure 2-2 and in Figure 2-3, respectively. These illustrations depict the waste packages, their internals, and the material specifications. Both designs incorporate techniques to limit the maximum anticipated temperatures in the waste package and fuel cladding materials. The 21 PWR WP design also incorporates borated stainless steel (B-SS) plates in the basket assembly for criticality control. The absorber plates are needed because the MOX assemblies proposed for disposal in this waste package design have the lowest burnup levels and consequently greater fissile Pu content. The nominal 12 PWR WP design does not contain B-SS absorber plates since it is to be used only for high burnup assemblies and the analysis is more conservative by not considering such absorber plates. Borated stainless steel absorber plates can be used in the 12 PWR WP but are not required for criticality control. Use of absorber plates in the 12 PWR WP would decrease the criticality potential of the 12 PWR WP even further and, thus, was not considered in the criticality analyses. In the UCF WP design, SNF assemblies are placed directly into the steel basket assemblies enclosed within the corrosion resistant and corrosion allowance barriers. The VA design for the corrosion barrier includes a corrosion allowance outer barrier material and a corrosion resistant inner barrier material.

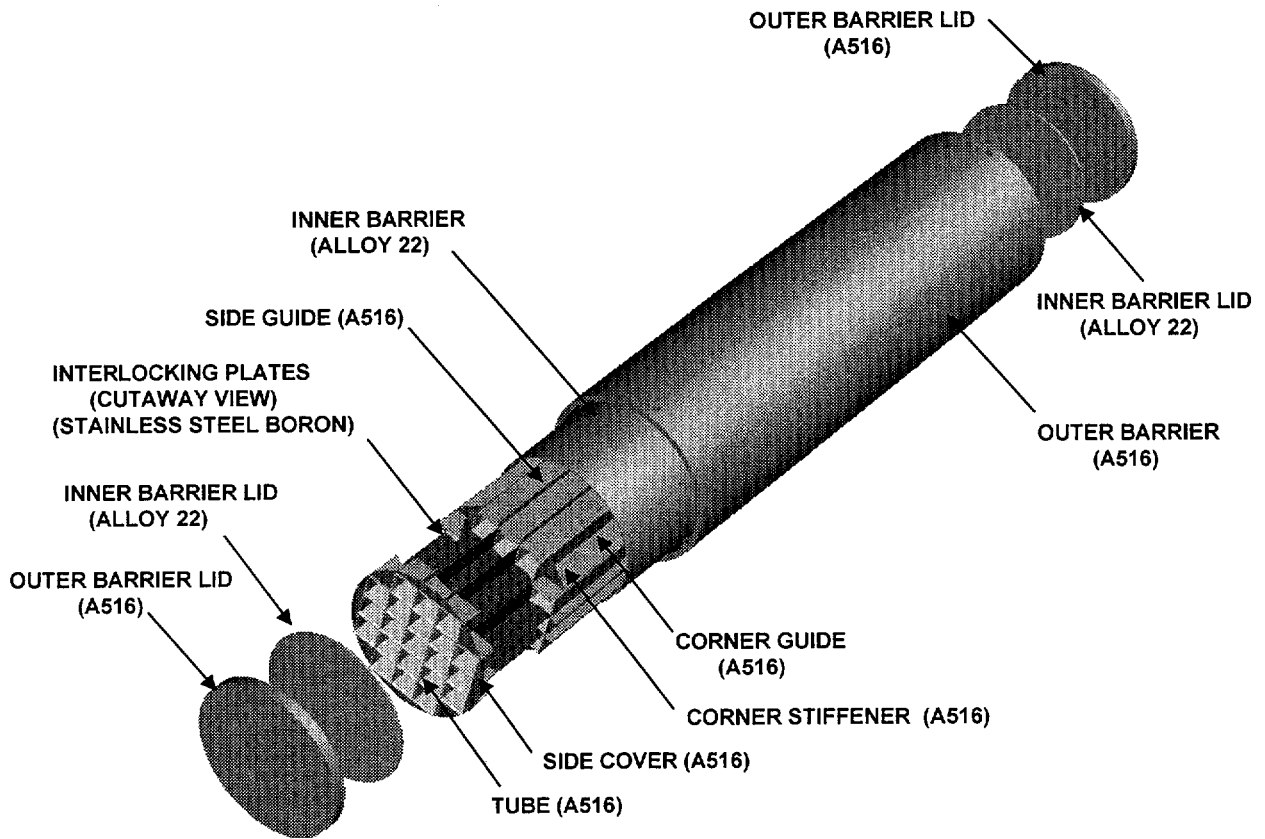


Figure 2-2. 21 PWR UCF Waste Package Assembly

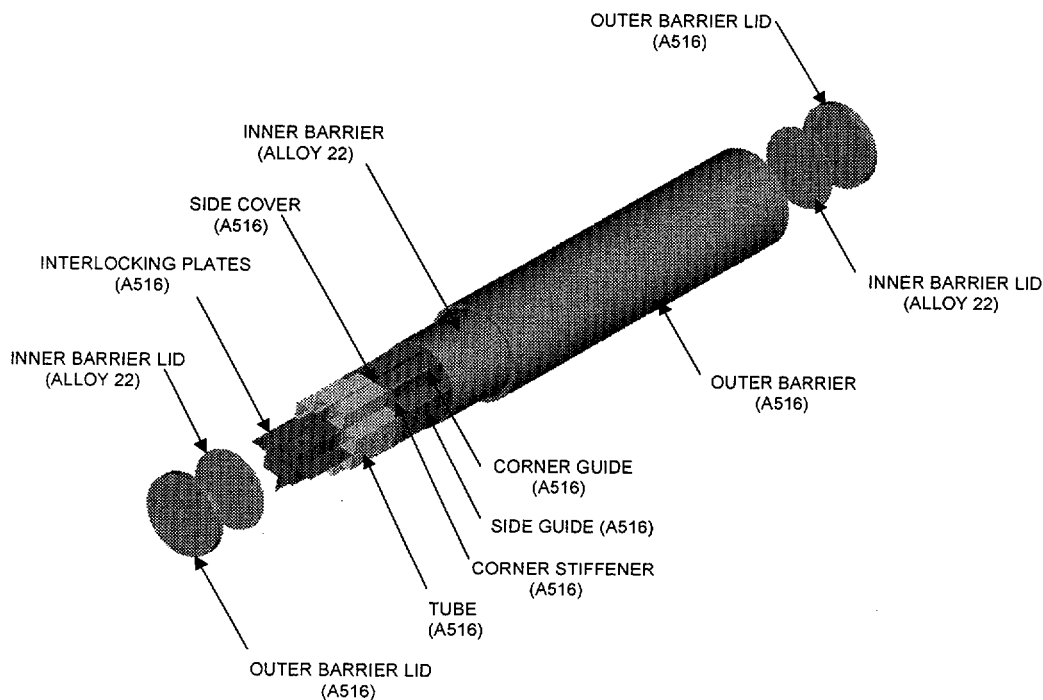


Figure 2-3. 12 PWR UCF Waste Package Assembly

All of the analyses were based on these 21 PWR and 12 PWR WP designs but tailored to the particular analysis as appropriate.

The intact waste package geometry parameters used in this analysis are listed in CRWMS M&O (1998c, Section 5). The general waste package assembly information was obtained from CRWMS M&O (1997f) and CRWMS M&O (1997g). Since the analysis covers both intact and degraded waste forms, representation the chemical behavior of these systems is necessary which requires the chemical compositions of the waste package materials, their masses, surface areas, and corrosion or degradation rates as input. Corrosion product volume information for the 21 PWR WP was calculated for the geochemistry analysis (CRWMS M&O 1998d) and is summarized in Section 2.1.2.1 with the material property data. Corrosion product volumes were calculated for the 12 PWR WP assuming only carbon steel in the basket structure with a mass of 4449.7 kg. Calculating the corrosion product volume for the 12 PWR WP from carbon steel only is conservative since aluminum corrosion products (from thermal shunts) will displace a larger moderator volume than the carbon steel products.

2.1.2.1 Material Properties

Material properties of the 21 PWR MOX SNF WP required for representing the geochemical behavior of the waste package for the criticality analyses include the masses, surface areas, and average corrosion or degradation rates. Only the average values are listed since variation in the corrosion rate had very minimal effect on the amount of iron or aluminum retained in the WP as solids (CRWMS M&O 1998d, p. 32). These properties are listed in Table 2-4 (CRWMS M&O 1998b, Volume I, Table 2.2.1-1). An exception is made, however, for the material of the inner corrosion resistant barrier, which is assumed to react so slowly with the infiltrating water as to have negligible effect on the chemistry (CRWMS M&O 1998d, Section 3).

Table 2-4. Material Properties of 21 PWR WP Components

Component Material	Mass (kg)	Surface Area (m ²)	Corrosion Rate (moles/cm ² /sec)
A 516 Grade 55 Carbon Steel	5443.2	229	1.573e-11
Borated Stainless Steel (SS316B6A)	1882.0	71	1.169e-13
Aluminum (6061 T4)	146.5	43	1.263e-11
SNF	11,054.0	43774	4.419e-14

2.1.3 Waste Stream Quantities

Approximately 200 metric tons (MT) of fissile material (highly enriched uranium (HEU) and Pu) has been declared surplus and withdrawn from the U.S. nuclear stockpile. The disposition of surplus HEU was addressed in a DOE 1996 Record of Decision (DOE 1996). In a 1997 Record of Decision (DOE 1997), the strategy adopted by the DOE for disposition of surplus weapons grade Pu consists partly of direct geologic disposal of Pu immobilized in a ceramic matrix and partly of using the Pu as MOX in one or more commercial reactors with disposal of the SNF according to the Nuclear Waste Policy Act.

There is about 50 MT of Pu in the surplus fissile material. Approximately 17 MT of this material contains significant quantities of impurities and is considered unsuitable for reactor fuel as MOX. This material has been designated for direct disposal by immobilization in a ceramic waste form. The remaining 32 MT of Pu is suitable for incorporation into MOX assemblies for commercial reactors (CRWMS M&O 1998b, Volume I, Section 2.3). The composition of possible MOX SNF assemblies at discharge from a reactor will be substantially different from standard commercial fuel, and, so, must be analyzed to identify potential impacts on the waste package designs and to provide guidance for potential MOX SNF disposal recommendations.

Approximately 1732 MOX assemblies will be required to consume the 32 MT of Pu (CRWMS M&O 1998b, Volume I, Section 2.3). This translates into 19 core reloads of 92 assemblies per reload. The standard LEU 21 PWR and 12 PWR waste package design are proposed for disposal of the MOX SNF. The 21 PWR WP design will be used for assemblies with lower burnup values (and consequently more fissile Pu content) and the 12 PWR WP design will be used for assemblies with high burnup values and corresponding high thermal heating rates. The number of highly burned assemblies can be estimated from the discharge burnup distribution

(Westinghouse Electric Corporation 1998, p. 43). Use of both waste package designs (the 21 PWR and 12 PWR WPs) is necessary to meet the maximum thermal output criteria of 11.8 kW per waste package (CRWMS M&O 1999g, Vol. I, p. 19). This analysis shows that a MOX SNF assembly burnup of approximately 46.5 GWd/MTHM will meet the 18 kW thermal output limit for the 21 PWR WP (850 W per assembly). For the 12 PWR WP, the thermal output criteria limits the maximum output to 1500 W/assembly, well above the highest output value of 1070 W/assembly derived from this analysis. This waste package loading criteria results in 43 of the 21 MOX PWR WPs and 72 of the 12 MOX PWR WPs required for the 1732 MOX assemblies.

2.1.4 Waste Package Criticality Control Measures

The criticality control requirement for emplacement and isolation of radioactive waste is that the system k_{eff} maintains a minimum 5% margin below unity after allowing for biases and uncertainties (YMP 1998, Section 2.1.1). To assure such conditions for long term emplacement of MOX SNF, reactivity control measures are necessarily the same as for LEU SNF. Reactivity control in the waste packages while the system is intact is provided by B-SS absorber plates in the assembly basket structure as shown in Figure 2-2. Insoluble corrosion products from the A 516 carbon steel basket structure (notably hematite [Fe_2O_3]) may provide long term criticality control for breached but structurally intact waste packages because of moderator displacement. This study shows that only the 21 MOX SNF WPs with the larger fissile Pu content will require reactivity control. The 12 MOX PWR WPs remains subcritical under all degradation scenarios because of the smaller initial fissile Pu inventory and subsequent moderator displacement by waste package corrosion products. Thus, no supplemental absorber plates are necessary for reactivity control in this waste package.

2.1.5 Criteria for Evaluating Impacts of MOX Disposal

The WP related impacts of disposition of the MOX waste form have been evaluated against the criteria found in the *Uncanistered Spent Nuclear Fuel Disposal Container System Description Document* (SDD) (CRWMS M&O 1999g, Volume I). The SDD numbers given in brackets are paragraph numbers from the SDD cited. In this section, the key criteria from the SDD are identified for the following areas: structural, thermal, shielding, and intact and degraded criticality.

2.1.5.1 Structural Criteria

- 2.1.5.1.1 “During the preclosure period, the disposal container/waste package, shall be designed to withstand (while in a vertical orientation) a drop from a height of 2 m (6.6 ft) (TBV-245) onto a flat, unyielding surface without breaching. (TBV-245)”
[SDD 1.2.2.1.3]
- 2.1.5.1.2 “During the preclosure period, the disposal container/waste package, shall be designed to withstand (while in a horizontal orientation) a drop from a height of 2.4 m (7.9 ft) (TBV-245) onto a flat, unyielding surface without breaching. (TBV-245)”
[SDD 1.2.2.1.4]

2.1.5.1.3 “During the preclosure period, the waste package shall be designed to withstand (while in a horizontal orientation) the greater stress resulting from a horizontal drop of 1.9 m (6.2 ft) (TBV-245) onto a support in an emplacement drift, or a drop of 2.4 m (7.9 ft) (TBV-245) onto a concrete pier, without breaching by puncture. (TBV-245)”

[SDD 1.2.2.1.5]

2.1.5.1.4 “During the preclosure period, the waste package shall be designed to withstand a tip over from a vertical position with slap down onto a flat, unyielding surface without breaching. (TBV-245)”

[SDD 1.2.2.1.6]

2.1.5.2 Thermal Criteria

2.1.5.2.1 “The waste package shall maintain SNF zircaloy cladding temperature below 350 degrees C (662 degrees F) (TBV-241) under normal conditions, and below 570 degrees C (1,058 degrees F) (TBV-245) for short-term exposure to fire, as specified by Criterion 1.2.2.1.11.”

[SDD 1.2.1.6]

2.1.5.2.2 “The waste package shall be designed to have a maximum thermal output of 11.8 kW.”

[SDD 1.2.4.4]

2.1.5.3 Shielding Criterion

2.1.5.3.1 “Waste Package design shall reduce the dose rate at all external surfaces of a waste package to (TBD-3764) rem/hr or less. This criterion identifies a disposal container interface with the Waste Emplacement/Retrieval System, Disposal Container Handling System, and Performance Confirmation Emplacement Drift Monitoring System.”

[SDD 1.2.4.3]

2.1.5.4 Criteria Related to Postclosure Criticality

None.

2.2 CERAMIC

2.2.1 Waste Stream Quantities

Of the 200 MT of fissile material declared surplus, about 50 MT are Pu. Approximately 17 MT of this material contains impurities considered unsuitable for MOX reactor fuel and have been designated for immobilization in ceramic for disposal. In addition, the DOE has reserved the option of using the immobilization approach for disposal of all the 50 MT of surplus Pu (Shaw 1999, page 4). The proposed immobilization and disposal methods must be analyzed to identify suitable waste package designs and to demonstrate compliance with criticality requirements.

2.2.2 Waste Form Description

The waste form for immobilized Pu will be a ceramic containing approximately 10.5 wt% Pu in the +4 valence state, nominally expressed as PuO_2 . The dominant mineral phase is a titania-based pyrochlore. The basic waste form unit will be a cold-pressed disk. This section provides the current dimensions and composition. The final values will be available as the waste form development project, presently in progress at Lawrence Livermore National Laboratory (LLNL), is completed (Shaw 1999).

A previous study (CRWMS M&O 1996a, Section 8) provided preliminary evaluations of the shielding, thermal, and structural impacts of an immobilized plutonium waste form using the can-in-canister concept. In that study the waste form matrix carrying the plutonium was glass, instead of the current ceramic; other significant differences were:

- Higher Pu loading per canister in the previous study (approximately 51 kg versus 27 kg in the present study).
- 4 Pu-bearing canisters per WP compared with the present baseline of 5.
- 1330 kg of HLW filler glass per Pu-bearing canister compared with the present 1478 kg.

2.2.2.1 Dimensions

Ceramic Disk: 0.94 inch thick and 2.625 inches in diameter, yielding a volume of 5.09 cubic inches, or 88.36 cm^3 . The 20 disks per can will occupy a volume of 101.74 cubic inches, or 1667.28 cm^3 (Shaw 1999, page 4).

Can: Cylindrical shell 20 inches length by 3 inches outside diameter x 0.06 inch thick. The can will displace a volume of 141.4 cubic inches, or 2317 cm^3 (Shaw 1999, page 5).

2.2.2.2 Mass

The WF mass is determined from the above dimensions and an approximate density of the ceramic material, $\rho = 5.5 \text{ g/cm}^3$, resulting in 9.17 kg of ceramic per can (Shaw 1999, page 4).

2.2.2.3 Chemical/Isotopic Composition of the Ceramic Waste Form

The principal chemical components of the waste form are specified in Table 2-5 (Shaw 1999, Table 3.1). The average concentration of impurities in the Pu stream that will be in the final ceramic (i.e., that survive the ceramic formation process) is specified in Table 2-6 (Shaw 1999, Table 3.3). The impurities, plus oxygen, are 27.2 wt% of the total Pu feed, with 72.8 wt% of the feed being Pu. Since the amount of feed is always adjusted so the Pu will be 10.5 wt% of the total ceramic, the impurities in the Pu feed will constitute 3.92 wt% of the total ceramic weight ($= 27.2 \times 10.5/72.8$), for the 17 MT case. Note that the value of the Pu wt% (10.5) is used in this calculation, rather than the value of PuO_2 wt% (11.9) to be consistent with the oxygen of PuO_2 already having been included in the non-Pu component of the feed.

The average initial Pu-related isotopic composition of the feed stream is given in Table 2-7. The data are taken from Tables 4.3 and 4.5 of the LLNL report (Shaw 1999). It should be noted that by the time of any potential criticality, much of the ^{239}Pu would have decayed into ^{235}U . A conservative estimate of this decay at the time of potential criticality is given in with the description of the configurations, which are likely to have criticality potential.

Table 2-5. Input Composition of the Baseline Ceramic Waste Form

Component	wt%
CaO	9.95
HfO ₂	10.65
UO ₂	23.69
PuO ₂	11.89
Gd ₂ O ₃	7.95
TiO ₂	35.86

Table 2-6. Impurities in the Pu Process Input Stream

Element	wt% of Pu Stream
Al	1.856
Am	1.582
B	0.088
Ba	0.208
Ce	0.088
Cr	0.137
Cu	0.094
Fe	0.625
Ga	0.495
K	0.711
La	0.030
Mg	1.141
Mo	0.625
Na	0.357
Ni	0.289
Nd	0.580
Np	0.053
O	15.415
Pb	0.009
Si	1.055
Sn	0.003
Ta	0.964
W	0.019
Zn	0.088
Unknown	0.667
Total	27.18

Table 2-7. Average wt% Isotopic Composition of the Pu and U Feed in 2010

Isotope	17 MT Case	50 MT Case
²³⁵ U	1.91	0.89
²³⁸ U	98.09	99.11
²³⁸ Pu	0.02	0.01
²³⁹ Pu	90.59	92.84
²⁴⁰ Pu	8.41	6.57
²⁴¹ (Pu + Am) ^a	0.89	0.54
²⁴² Pu	0.09	0.04

^a Since ²⁴¹Pu has a half-life of only 14 years, virtually all the ²⁴¹Pu would have decayed into ²⁴¹Am by the time there is any possibility of criticality (upwards of 10,000 years).

The only significant radioactivity in the waste form itself derives from the Pu feed, and will have approximately the distribution indicated in Table 2-8 in the year 2010. This table lists Curies per kg of (Pu + Am) in the feed. This table is taken from Table 4.4 of the LLNL report (Shaw 1999).

Table 2-8. Curies per kg of Total Plutonium plus Americium in 2010

Isotope	Activity (Ci per kg of Pu+Am)	
	50-MT Case	17-MT Case
²³⁸ Pu	2.1	4.2
²³⁹ Pu	57.7	56.3
²⁴⁰ Pu	15.0	19.2
²⁴¹ Pu	99.3	165.
²⁴¹ Am	15.1	25.0
²⁴² Pu	0.00161	0.0034
Total	189.	270.

2.2.2.4 Characteristics of HLW Filler Glass

The baseline mass of the glass per HLW canister is 1680 kg at a density of 2.64 g/cm³ (Shaw 1999, page 3). The chemical composition of the HLW filler glass used for the degradation calculations is given in Table 2-9 (CRWMS M&O 1996b, Attachment I, Table 3.3.8). For the canister containing immobilized Pu, the principal source of radiation during preclosure (up to 300 years) is the HLW glass in which the Pu cans are embedded; there is approximately 1478 kg of HLW per canister. Any shielding requirements will, therefore, be less than, or approximately the same as, what is already required for the HLW glass waste package (as explained further in Section 2.2.6.3).

Table 2-9. HLW Filler Glass Composition

Component	wt%
Ag	0.05
Al ₂ O ₃	3.96
B ₂ O ₃	10.28
BaSO ₄	0.14
Ca ₃ (PO ₄) ₂	0.07
CaO	0.85
CaSO ₄	0.08
Cr ₂ O ₃	0.12
Cs ₂ O	0.08
CuO	0.19
Fe ₂ O ₃	7.04
FeO	3.12
K ₂ O	3.58
Li ₂ O	3.16
MgO	1.36
MnO	2.00
Na ₂ O	11.00
Na ₂ SO ₄	0.36
NaCl	0.19
NaF	0.07
NiO	0.93
PbS	0.07
SiO ₂	45.57
ThO ₂	0.21
TiO ₂	0.99
U ₃ O ₈	2.20
Zeolite	1.67
ZnO	0.08

2.2.2.5 Corrosion Rates

The range of corrosion rates for the waste package solid components used in the EQ6 runs are summarized in Table 2-10. The three ceramic rates were the best available at the time the study began. Very recently, LLNL has provided updated rates that are a factor 3 to 10 times lower for the same conditions. The new LLNL rate data are shown in Figure 5-3 of CRWMS M&O (1999c). While these data offer lower normalized rates, they also suggest the possibility that surface area has been underestimated in EQ6 calculations. Since the total reaction rate for the ceramic is the product of surface area and the fundamental rate constant, the two new observations by LLNL tend to cancel out. Therefore, this study retains the original range of rates, spanning nearly three orders of magnitude.

Table 2-10. Corrosion Rates Used for EQ6 Analyses

Material	Rate
Pu-ceramic^a	
High (pH 2-4, 75°C, metamict)	3×10^{-2} g/m ² /day
Average (pH 2-4, 75°C)	1×10^{-3} g/m ² /day
Low (pH 6, 25°C)	5×10^{-5} g/m ² /day
Stainless Steel (316L, 304L)^b	
High	1 μ m/yr ^c
Average	0.1 μ m/yr
HLW Glass^d	
High	3×10^{-2} g/m ² /day
Low	1×10^{-4} g/m ² /day

^a CRWMS M&O 1999c, Table 5-3

^b CRWMS M&O 1999c, Table 5-1

^c This is the standard unit for corrosion of steel, assuming a flat plate geometry, to convert to g/m²/day, multiply by the density of steel (in kg/m³), by 1000 (to convert kg to g), by 10⁻⁶ (to convert microns to meters), and divide by 365 (to convert years to days).

^d CRWMS M&O 1999c, Table 5-2

It should be noted that the aqueous corrosion (or degradation) of individual solid waste package components does not necessarily lead directly to removal from the waste package of elements or ions from those corroded components. Individual elements may remain in a solid altered state, or precipitate in some insoluble mineral. In particular, the evidence to be discussed in the following sections shows that the primary neutron absorber (Gd) is nearly insoluble over most of the time period and water chemistry of interest, while the secondary neutron absorber (Hf) is completely insoluble over the same range of parameters.

2.2.3 Plutonium Disposition Canister

The waste forms are contained within the waste packages in stainless steel canisters approximately 3 meters overall length, 61 cm outer diameter, and 1 cm wall thickness. The disks are stacked in cans, 20 disks per can. The stainless steel cans are stacked 4 deep in very thin-walled SS 304L tubes. There will also be a mechanism to space and separate the cans within these tubes. The weight, volume, and composition of these tubes and their supports have been neglected. There will be seven of these tubes fastened at the inside wall of a HLW canister. While the final design has not yet been specified, a sketch of a likely arrangement from SRS showing cross section with 4 cans in a tube and 7 tubes in a HLW canister is given in Figure 2-4 (Shaw 1999, page 6). This results in a total of 28 cans, or 560 disks, per HLW canister.

2.2.3.1 Canister Dimensions

- % HLW glass displaced by Pu waste form cans 11%
- % HLW glass displaced by rack for cans 1%
- Mass of HLW canister (empty) 499 kg

With the density of 316 stainless steel = 7.95 g/cm^3 , the following are calculated:

- Ceramic mass per canister 273.15 kg
- Mass of rack 58.5 kg
- Steel can mass per canister 96.7 kg
- HLW glass per canister 1478.4 kg

2.2.3.2 Canister Mass

With these parameters the total loaded canister masses are:

- Ceramic canister 2405 kg
- HLW canister 2179 kg

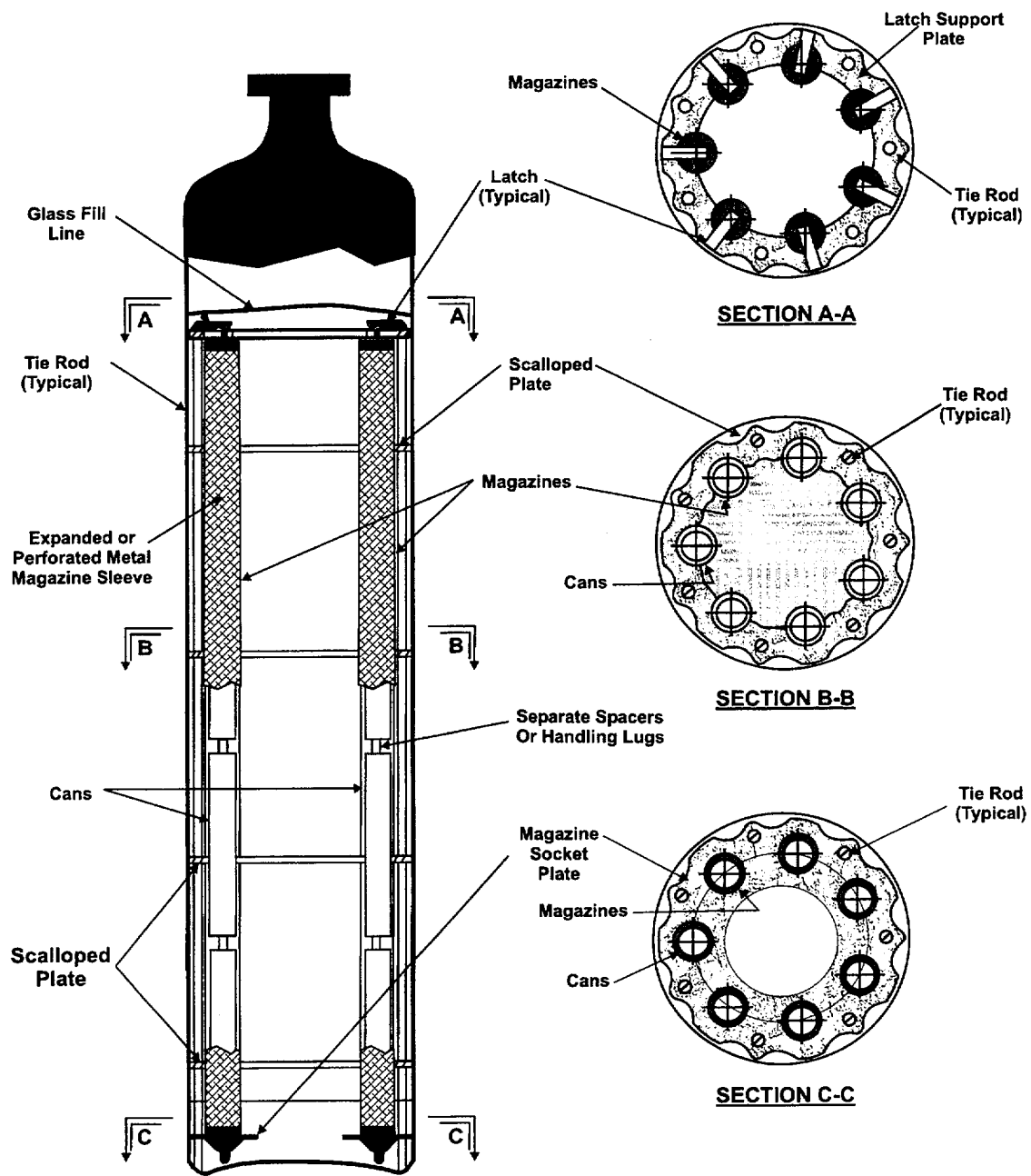


Figure 2-4. Can-in-Canister Sketch

2.2.4 Waste Package Description

The disposal container will be the same 5-DHLW WP (5 Defense High Level Waste Package) design as is planned for the ordinary HLW canisters. An isometric view of the 5-DHLW waste package is given in Figure 2-5, with the lids removed, and showing the inner and outer barriers. The nominal Pu loading per waste package is 5 Pu-loaded canisters per waste package. Previous analyses of ceramic formulations (CRWMS M&O 1997h) have suggested that criticality prevention would be enhanced by limiting the number of Pu-loaded canisters to 1 or 2 per package. However, the results of this study will show that the performance of the current formulation will prevent criticality, even if all 5 canisters are loaded with Pu ceramic.

The disposal container consists primarily of a corrosion allowance outer barrier and a corrosion-resistant inner barrier. The corrosion-allowance outer barrier will be carbon steel 10 cm thick as is used in the Civilian Radioactive Waste Management System (CRWMS) VA design for the commercial spent nuclear fuel waste package. The VA design was chosen because most of the evaluations that support this document were started before the Second Enhanced Design Alternative (EDA-II) was adopted. The inner barrier will be corrosion resistant, high nickel, Alloy 22, 2 cm thick, also corresponding to that planned for the commercial SNF WP. The dimensions and compositions of the intact WP components are provided in Table 2-11 (CRWMS M&O 1998f, p. 10).

Table 2-11. The Main Physical Characteristics of the Five High-Level Waste Canister Waste Package

Component	Number	Material	Inner Diameter (cm)	Outer Diameter (cm)	Thickness (cm)	Inner Length (cm)	Outer Length (cm)
Outer Barrier	1	ASTM A 516 Carbon Steel	177	197	10.0	-----	331
Outer Barrier Lid	2 (top and bottom)	ASTM A 516 Carbon Steel	-----	197	11.0	-----	-----
Inner Barrier	1	ASTM B 575 N06022 (Alloy 22)	173	177	2.0	304	-----
Inner Barrier Lid	2 (top and bottom)	ASTM B 575 N06022 (Alloy 22)	-----	177	2.5	-----	-----
Canister	5	ASTM A 312 Type 304L Stainless Steel	59.055	60.96	0.9525	-----	299.72

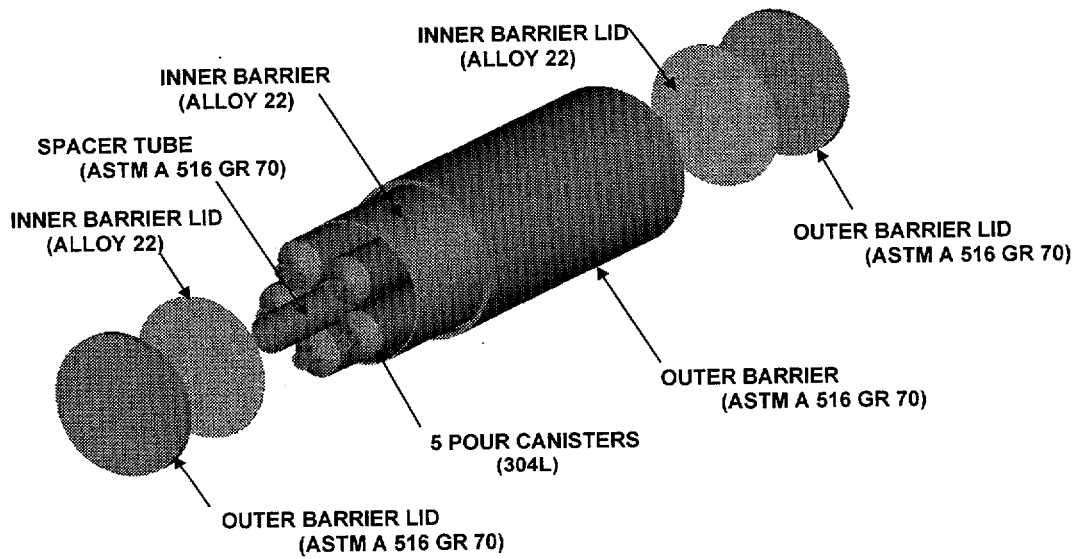


Figure 2-5. 5-DHLW Waste Package to be Used for Plutonium Immobilized in Ceramic

2.2.5 Waste Package and Canister Quantities

For the waste form composition given in Table 2-5 and the loading of 20 disks per can and 28 cans per canister, the total mass of Pu per canister will be 28.68 kg. The total number of canisters required for disposal is summarized in Table 2-12. Also given in the table is the number of waste packages required at 5 canisters per waste package.

Table 2-12. Numbers of Canisters Required for Disposal of Immobilized Pu

	17 MT Case	50 MT Case
Number of Pu containing canisters	635	1744
Net additional canisters to accommodate DHLW filler displaced by the Pu ceramic	77	210
Net additional as a % of total HLW canisters (~12,000)	0.64%	1.75%
Number of waste packages containing Pu	128	348
Net additional waste packages	16	42

It should be noted that since the Pu-bearing canisters contain 88% of their maximum capacity for HLW glass, the impact of immobilized-Pu disposal on the number of waste packages is only the net increase required to make up for the 12% of the HLW displaced by the plutonium bearing cans and their accompanying structure. This net increase is shown for canisters by the second line of Table 2-12, and for waste packages by the fifth line.

2.2.6 Criteria for Evaluating Impacts of Disposal of the Ceramic Waste Form

The WP related impacts of disposition of the ceramic waste form have been evaluated against the criteria found in the *Defense High Level Waste Disposal Container System Description Document* (CRWMS M&O 1999s). The SDD numbers given in brackets are paragraph numbers from the SDD cited. In this section, the key criteria from the SDD are identified for the following areas: structural, thermal, shielding, and intact and degraded criticality.

2.2.6.1 Structural Criteria

- 2.2.6.1.1 “During the preclosure period, the disposal container/waste package, shall be designed to withstand (while in a vertical orientation) a drop from a height of 2 m (6.6 ft) (TBV-245) onto a flat, unyielding surface without breaching. (TBV-245)”
[SDD 1.2.2.1.3]
- 2.2.6.1.2 “During the preclosure period, the disposal container/waste package, shall be designed to withstand (while in a horizontal orientation) a drop from a height of 2.4 m (7.9 ft) (TBV-245) onto a flat, unyielding surface without breaching. (TBV-245)”
[SDD 1.2.2.1.4]
- 2.2.6.1.3 “During the preclosure period, the disposal container/waste package, shall be designed to withstand (while in a horizontal orientation) the greater stress resulting from a drop of 1.9 m (6.2 ft) (TBV-245) onto a support in an emplacement drift, or a

drop of 2.4 m (7.9 ft) (TBV-245) onto a concrete pier, without breaching by puncture. (TBV-245)”

[SDD 1.2.2.1.5]

2.2.6.1.4 “During the preclosure period, the waste package shall be designed to withstand a tip over from a vertical position with slap down onto a flat, unyielding surface without breaching. (TBV-245)”

[SDD 1.2.2.1.6]

2.2.6.2 Thermal Criteria

2.2.6.2.1 “The waste package shall maintain the temperature of HLW glass below 400 degrees C (752 degrees F) (TBV-092) under normal conditions, and below 460 degrees C (860 degrees F) (TBV-245) for short-term exposure to fire, as specified by criterion 1.2.2.1.11”

[SDD 1.2.1.6]

2.2.6.2.2 “The waste package shall be designed to have a maximum thermal output of 11.8 kW.”

[SDD 1.2.4.4]

2.2.6.3 Shielding Criterion

2.2.6.3.1 “Waste package design shall reduce the dose rate at all external surfaces of a waste package to (TBD-3764) rem/hr or less. This criterion identifies a disposal container interface with the Disposal Container Handling System, the Waste Emplacement/Retrieval System, and the Performance Confirmation Emplacement Drift Monitoring System.”

[SDD 1.2.4.3]

2.2.6.4 Criteria Related to Postclosure Criticality

None.

2.3 ENVIRONMENTAL CONDITIONS

2.3.1 Chemical Composition of J-13 Well Water

The water entering the WP has the same composition as J-13 well water contained in Table 2-13. For those elements listed as “trace” constituents in Table 2-13, an arbitrary small molality (10^{-16}) was added to assure numerical stability.

2.3.2 Drip Rate of J-13 Water into a WP

The drip rate onto a WP is the same as the rate at which water flows through the WP. Four drip rates were assumed: 0.0015, 0.015, 0.15, and $0.5 \text{ m}^3/\text{year}$ per package.

Table 2-13. Compositions of J-13 Well Water (from LL980711104242.054)

EQ3NR Input File Constraints for J-13 Water Composition				EQ6 Input File Elemental Molar Composition for J-13 Water	
Component/Species (aq. ^a)	Basis Switch	Concentration	Units	Element	Moles
redox	N/A	-0.7	log fO ₂	N/A	N/A
Na+	N/A	4.580E+01	mg/L	O	5.552E+01
SiO ₂	N/A	6.097E+01	mg/L	Al	2.553E-08
Ca ⁺⁺	N/A	1.300E+01	mg/L	B	1.239E-05
K+	N/A	5.040E+00	mg/L	Ba	1.000E-16
Mg ⁺⁺	N/A	2.010E+00	mg/L	Ca	3.244E-04
Li+	N/A	4.800E-02	mg/L	Cl	2.014E-04
H+	N/A	8.1	pH	Cr	1.000E-16
HCO ₃ ⁻	CO ₂ (g)	-3	log fCO ₂	Cu	1.000E-16
O ₂	N/A	5.600E+00	mg/L	F	1.147E-04
F ⁻	N/A	2.180E+00	mg/L	Fe	3.600E-12
Cl ⁻	N/A	7.140E+00	mg/L	Gd	1.000E-16
NO ₃ ⁻	NH ₃	8.780E+00	mg/L	H	1.110E+02
SO ₄ ⁻⁻	N/A	1.840E+01	mg/L	C	2.094E-03
B(OH) ₃	N/A	7.660E-01	mg/L	P	1.261E-06
Al ⁺⁺⁺	Diaspore	0	Mineral	K	1.289E-04
Mn ⁺⁺	Pyrolusite	0	Mineral	Li	6.915E-06
Fe ⁺⁺	Goethite	0	Mineral	Mg	8.270E-05
HPO ₄ ⁻⁻	N/A	1.210E-01	mg/L	Mn	3.054E-16
Ba ⁺⁺	Trace	1.000E-16	Molality	Mo	1.000E-16
CrO ₄ ⁻⁻	Trace	1.000E-16	Molality	N	1.416E-04
Cu ⁺⁺	Trace	1.000E-16	Molality	Na	1.992E-03
Gd ⁺⁺⁺	Trace	1.000E-16	Molality	Ni	1.000E-16
MoO ₄ ⁻⁻	Trace	1.000E-16	Molality	Np	1.000E-16
Ni ⁺⁺	Trace	1.000E-16	Molality	Pb	1.000E-16
Np ⁺⁺⁺⁺	Trace	1.000E-16	Molality	Pu	1.000E-16
Pb ⁺⁺	Trace	1.000E-16	Molality	S	1.915E-04
Pu ⁺⁺⁺⁺	Trace	1.000E-16	Molality	Si	1.015E-03
TcO ₄ ⁻	Trace	1.000E-16	Molality	Tc	1.000E-16
Ti(OH) ₄	Trace	1.000E-16	Molality	Ti	1.000E-16
UO ₂ ⁺⁺	Trace	1.000E-16	Molality	U	1.000E-16
Zr(OH) ₂ ⁺⁺	Trace	1.000E-16	Molality	Zr	1.000E-16

^a aq. = aqueous

3. STRUCTURAL ANALYSIS

3.1 MOX

The structural design criteria for the 12 and 21 PWR waste packages containing MOX SNF are given in Section 2.1.5.1, with which the results in this section comply. For the criteria evaluated, the tipover accident produces the highest stresses in the waste package since the upper part of the waste package experiences a drop greater than the two-meter criteria. Analyses were performed for the 21 PWR MOX WP (CRWMS M&O 1998h) and 12 PWR MOX WP (CRWMS M&O 1998i) to determine the structural response to a tipover accident design basis event (DBE) dynamic load (CRWMS M&O 1997i, p. 44).

3.1.1 Structural Analysis Method

A three-dimensional finite-element solution was performed by making use of the ANSYS V5.4 finite-element computer code (CSCI: 30040 V5.4) (CRWMS M&O 1998j). ANSYS is qualified as documented in the SQR (CRWMS M&O 1998j). A finite-element representation of the waste package was developed to determine the effects of tipover accident DBE loads on the waste package structural components. The basket structure in the 21 PWR MOX WP was represented with B-SS absorber plates and a combination of A 516 carbon steel and aluminum in the basket structure. The aluminum serves as a heat conduit (thermal shunt) in the waste package and is not a structural material. The basket structure in the 12 PWR MOX WP was represented in a similar manner as the 21 PWR MOX WP except that two calculations were conducted on the waste package, one with and one without B-SS absorber plates. The waste package was represented with an initial orientation of 30° between the symmetry axis and vertical in order to initiate tipping of the waste package, and gravitational acceleration was then applied to the system. Having the waste package represented in this configuration, the simulation was continued throughout the impact until the waste package began to rebound, at which time the peak stresses have been obtained.

The MOX assembly weight is estimated to be 618.8 kg compared to 619.2 kg for the commercial Vantage 5 assembly (CRWMS M&O 1998k, p. 6). Weight changes due to burnup are negligible (less than 25 g at the maximum burnup). The structural analyses show that stresses from the tipover accident for both SNF waste forms are of similar magnitude.

3.1.2 Structural Analysis Results

The structural response of the waste package to tipover accident loads is given as maximum stress values obtained from the finite-element solutions to the problem. These solutions indicate that the maximum stress is located in the region of the inner and outer barrier lids in the vicinity of the impact region between the waste package and the target surface for 12 and 21 PWR waste package designs. The maximum membrane stress plus bending stress of the 21 PWR WP containing MOX SNF due to a tipover accident is 524 MPa in the inner barrier and the inner barrier lid (CRWMS M&O 1998h, p. 8 and Table 6-1) compared to 456 MPa for the 21 PWR WP containing LEU SNF (CRWMS M&O 1998l, p. 11). The maximum membrane stress plus bending stress of the 12 PWR WP containing MOX SNF due to a tipover accident is 404 MPa

(CRWMS M&O 1998i, p. 11 and Table 6-2) in the inner barrier and the inner barrier lid. These maximum stress levels for the 12 PWR (CRWMS M&O 1998i, Table 6-2) and 21 PWR (CRWMS M&O 1998h, Table 6-1) waste package designs are at least 15% below the respective ultimate tensile strength values and thus are within design limits [Section 2.1.5.1, Item 2.1.5.1.4 (SDD 1.2.2.1.6)].

3.2 CERAMIC

The structural analysis for the ceramic waste form is performed in CRWMS M&O (1999d). The structural design criteria for the can-in-canister concept are discussed in Section 2.2.6.1, with which the results in this section comply. A wide range of drop heights, up to 11.58 m, and various orientations are presented in this section to cover those dictated by the handling facility design (Gwyn 1999).

3.2.1 Structural Analysis Method

CRWMS M&O 1999u has concluded that under very conservative assumptions, radionuclide releases from a breach canister could exceed site boundary dose limits without mitigation. As such, the structural integrity of the canister has become important to safety. The evaluation of the structural integrity of the can-in-canister concept is based on computational methods and correlation with previous drop test results performed by Pacific Northwest National Laboratory (PNNL) on the Savannah River Site (SRS) HLW canister (Olson and Alzheimer 1989) (Peterson et al. 1985). Computationally, finite element solution is performed by the use of the commercially available ANSYS V5.4 finite element code. Two-dimensional (2-D) axisymmetric and three-dimensional (3-D) finite element representations for the standard HLW canister and the can-in-canister are developed and analyzed using the dynamic solver. The results of this calculation are provided in terms of strain. Strain is the most meaningful structural parameter to evaluate performance of ductile materials such as SS 304L.

3.2.2 Finite Element Representations and Results

3.2.2.1 Canister Vertical Drop (Standard Glass Canister)

To calculate the structural response of the HLW glass canister to a vertical drop, a 2-D axisymmetric representation is developed to take advantage of the symmetric geometry of the canister. The 2-D representation includes the canister shell containing glass waste form. The canister is assumed to drop onto an unyielding target surface, characterized by a very large modulus of elasticity. Four drop heights were evaluated: 7 m, 8 m, 9 m, and 11.58 m. The total canister mass (approximately 2600 kg) used in the calculation is based on the mass of the can-in-canister heavy configuration indicated in Table 2 of Jones (1998), which bounds all the glass canister masses with or without cans of plutonium ceramic waste form.

The structural response of the canister (standard glass) to vertical drops is reported using strain values at the times when they reach the maximum. For all drop heights analyzed (7 m, 8 m, 9 m and 11.58 m), the maximum strain from the drop impact on the canister shell occurs at the bottom surface portion of the canister, which contacts the target surface first. The tension in the

direction along the target surface is critical for shell material to fail. Figure 3-1 (CRWMS M&O 1999d, p. II-7) is a contour plot representing the strain values along the canister shell for a drop height 11.58 m. For all the drop heights analyzed, the maximum strain values through the shell thickness along the target surface direction do not exceed the ductility limit of SS 304L of 40%.

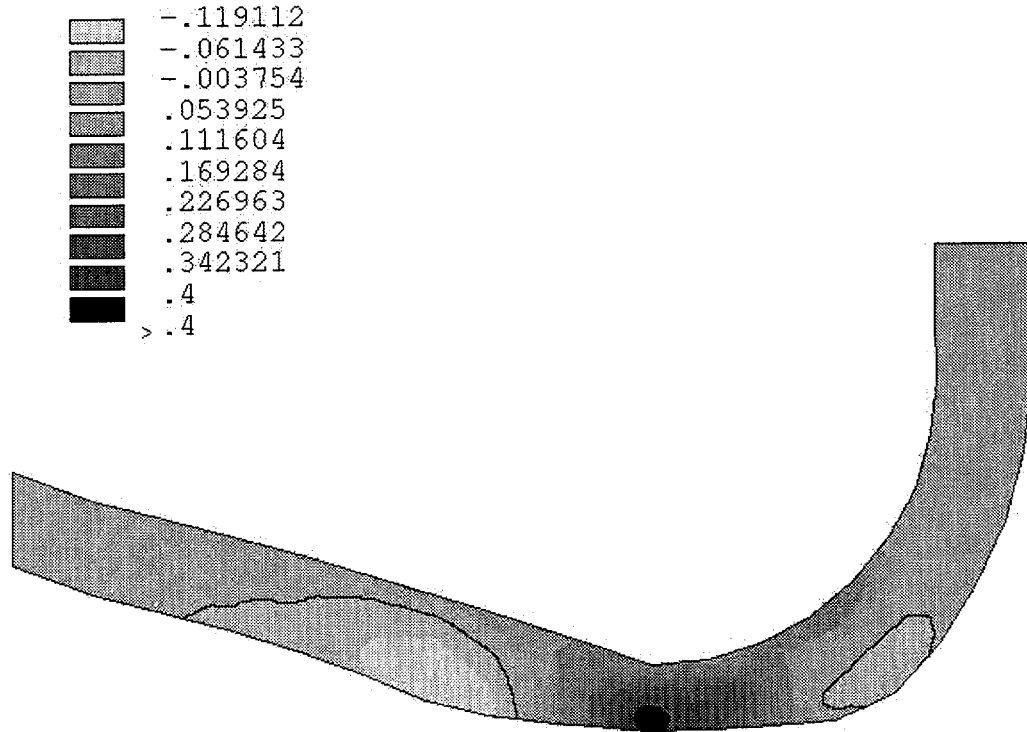


Figure 3-1. Canister Shell Strain Contours Along the Target Surface for 11.58 m Vertical Drop

3.2.2.2 Canister Corner Drop (Standard Glass Canister)

The orientation of the corner drop, which aligns the canister center of gravity with the canister bottom corner along the same vertical line, provides the maximum linear momentum for the canister to convert impact energy to deformation energy. Figure 3-2 shows the initial drop orientation for the canister at vertical and corner drops.

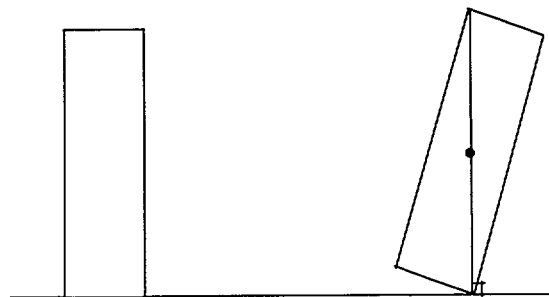


Figure 3-2. Orientation of Vertical and Corner Drops

To calculate the structural response of the HLW glass canister to the corner drop, a half-symmetry 3-D representation of the canister is constructed. The 3-D representation includes the canister shell and the glass waste form. The canister is assumed to drop onto an unyielding target surface with a very large modulus of elasticity specified for the target material. Several drop heights including 2 m, 4 m, 7 m, and 9.14 m are evaluated. The same can-in-canister heavy configuration indicated on Table 2 of Jones (1998) was used, which bounds all the glass canister masses with or without cans of plutonium ceramic waste form.

The structural responses of the canister to standard corner drops are reported using strain values at the times when they reach the maximum. For all drop heights analyzed (2 m, 4 m, 7 m, and 9.14 m), the maximum strain from the drop impact on the canister shell occurs at the localized corner area on the bottom of the canister. The tension in the direction along the target surface is critical for shell material to fail. Figure 3-3 (CRWMS M&O 1999d, p. III-7) is a contour plot representing the strain values along the canister shell for the drop height of 9.14 m. For all the drop heights analyzed, although very high strain is developed on the outer portion of the shell, the maximum strain values along the target surface direction and through the canister shell do not exceed the ductility limit of the SS 304L of 40%.

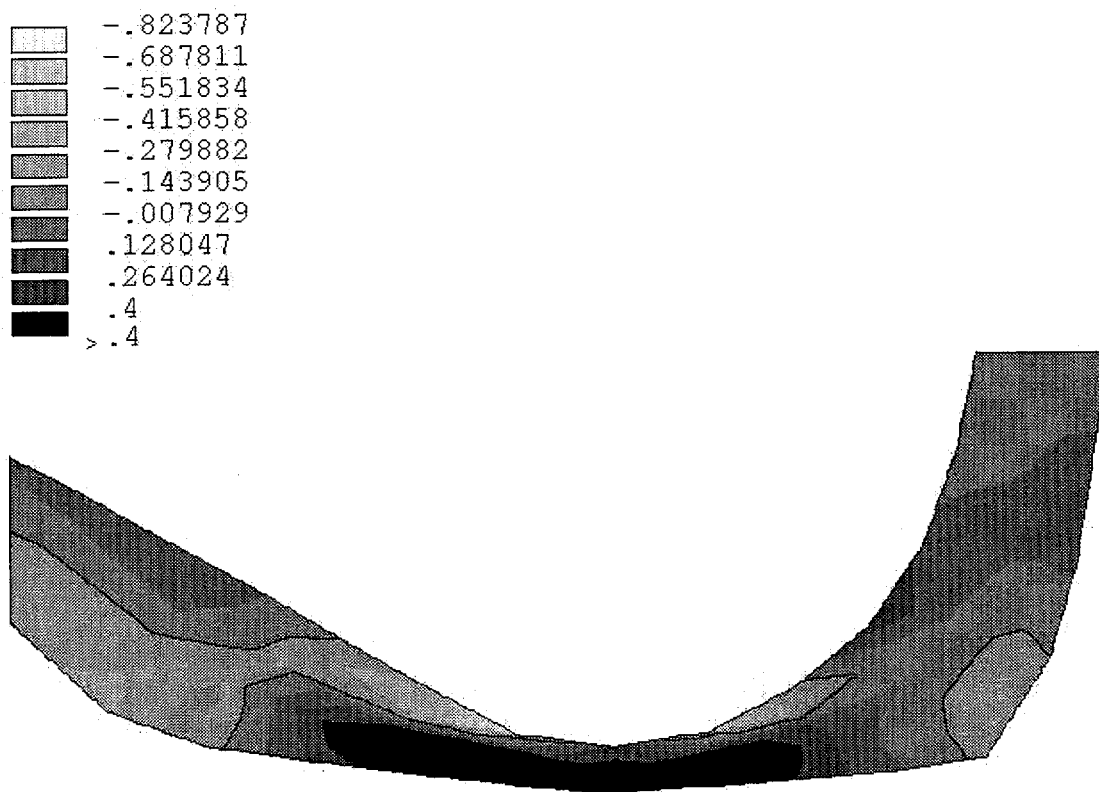


Figure 3-3. Canister Shell Strain Contours Along the Target Surface for 9.14 m Corner Drop

3.2.2.3 Can-in-Canister Vertical Drop (Glass Canister Contains Plutonium Cans)

A 3-D finite element representation of the can-in-canister design is developed in order to determine the effect of the vertical drop on the canister and magazine support. Since there are 7 magazines, evenly spaced about the canister center axis, a 1/14 slice of the canister is used in the calculation. The slice captures almost the whole length of the canister except for the canister neck and head. The representation includes the magazine rack base and glass, however, excludes the portion of the plutonium cans. The rack radial supports, scalloped plates, and tie rods, which provide insignificant structural support, are ignored to simplify the representation.

The computer simulation of the can-in-canister dropping from a certain height takes two steps. First, the canister and the magazines are falling at the same velocity before the canister reaches the target surface. Second, once the canister contacts the target surface, the impact takes place. With the deceleration of the canister, the impact between the canister bottom and target surface, and between the magazine and the magazine support occurs. To evaluate the strain increase from the impact of an additional magazine, a comparison between the canister with and without magazine is performed.

The maximum strain from the drop impact on the canister shell for the case with magazines is 0.12 and 0.23 for the inner surface and outer surface of the canister shell, respectively (CRWMS M&O 1999d, Table 6.3-1). The maximum strain from the drop impact on the canister shell for the case without magazines is 0.11 and 0.23 for the inner surface and outer surface of the canister shell, respectively (CRWMS M&O 1999d, Table 6.3-1). Thus, the maximum strain increase at the contact area due to the additional magazine impact is insignificant.

3.2.3 Effect of Glass Properties on the Calculation

The HLW glass canister contains borosilicate glass, which is considered a brittle material. The stress-strain behavior of brittle material under compression is dependent on the geometry of the material component and loading conditions. Since there is little information available for glass properties, and also the stress on the canister shell rather than the glass is of interest, an elastic-perfectly-brittle representation is generally used in the calculation. In actuality, under the compressive load, the brittle material will experience a non-linear stress-strain curve due to the gradual development of microcracking within the material after the critical stress. Therefore, to evaluate the effect of the glass properties on the calculation, four stress-strain curves are used to evaluate the sensitivity of the results (CRWMS M&O 1999d, Figure 5.3-1).

The results show that for the assumed glass properties, the stresses in the glass are highly dependent on the stress-strain curve that the glass will experience under compressive load. The linear stress-strain curve (elastic) produces the highest stresses in the glass as expected. The stress change in the canister shell due to the change of glass properties is not so pronounced. Assuming glass properties as elastic produces the most conservative results. Since the canister shell is of interest, using elastic glass properties for the calculations reported in Section 3 gives reasonable and slightly conservative results.

4. THERMAL ANALYSIS

4.1 MOX

The thermal design criteria for the 12 and 21 PWR waste packages containing MOX SNF are given in Section 2.1.5.2, with which the results in this section comply. Thermal analyses (CRWMS M&O 1998m) were performed under normal repository disposal conditions on the 21 PWR WP and the 12 PWR WP loaded with MOX to demonstrate that these waste packages can accommodate the entire MOX waste stream. The 46.5 GWd/MTHM heating rates were used in the 21 PWR MOX WP and the 56.5 GWd/MTHM in the 12 PWR MOX WP. In both cases, the SNF assemblies were assumed to have had a 10-year cooling period prior to emplacement in the waste package (CRWMS M&O 1997b, Section 3.2) specifies that the initial SNF for the repository be at least 10 years old).

4.1.1 Thermal Analysis Method

A 2-D, time dependent finite-element calculation was performed by making use of the ANSYS V5.1 finite element computer code (CRWMS M&O 1995), which was the current version of the code at the time the analysis was performed. A 2-D finite-element representation was developed (CRWMS M&O 1998m, Section 5.4) for a midpoint cross section of the waste package. This represents the hottest portion of the waste package because of the non-uniform axial heat source distribution. Aluminum thermal shunts were included in the representation for both the 21 PWR and 12 PWR WP designs to enhance the heat flow rate.

The SNF assembly, which produces a heat load in the waste package, was represented as a lumped parameter solid material placed inside of each tube in the basket assembly. The time-dependent volumetric heat loads were multiplied by an axial peaking factor of 1.25 (CRWMS M&O 1997j, p. 29) to approximate representing the axial center of the waste package with a 2-D representation. The peaking factor conservatively compensates for the lack of a detailed axially non-uniform assembly power shape. The initial heating rates for the MOX SNF were 798 W/assembly for the 21 PWR WP and 1070 W/assembly for the 12 PWR WP. The burnup levels for these assemblies were 46.5 GWd/MTHM and 56.5 GWd/MTHM, which are the hottest assemblies planned for these WPs, respectively. These values compared to 850 W/assembly and 1500 W/assembly for commercial PWR thermal design basis fuel assemblies (CRWMS M&O 1997j, p. 67) in the respective waste packages. The burnup level for the design basis commercial PWR assembly was 60 GWd/MTU. The initial heating rate values for the commercial PWR SNF correspond to different cooling periods prior to inclusion in the repository waste stream.

Temperature boundary conditions at the exterior surfaces of the 21 and 12 PWR MOX WPs for the 2-D thermal calculations were derived from the time-dependent temperature boundary conditions resulting from the 3-D multiple waste package calculation (Wang 1998). The waste package boundary surface temperatures were determined at thermal design basis loading of 85 MTU/acre which gives a constant center-to-center spacing for the 21 PWR WP with absorber plates of 15.4 m and 9.2 m for the 12 PWR WP with no absorber plates (CRWMS M&O 1998n, p. 17). This areal mass loading (AML) is within the AML range (80 to 100 MTU/acre) given on page 3-3 of YMP (1999) as the reference mass loading range. Thus, the MOX SNF will pose no

additional constraints on the repository waste package layout. The source for the thermal calculation was derived from the time-dependent radioactive decay heat sources (CRWMS M&O 1998d). The 2-D thermal analyses of the waste packages were carried out for a time period of 1000 years following a cooling period of 10 years after discharge from the reactor.

4.1.2 Thermal Analysis Results

The temperature history containing the peak fuel (cladding) temperature for 21 PWR MOX SNF WP is shown in Figure 4-1 and for the 12 PWR MOX SNF WP in Figure 4-2. The location of the peak node was at the center of the innermost assembly in both cases (note that the fuel assemblies were represented as a homogenized solid material). The peak values were 336°C for the 21 PWR SNF WP and 302°C for the 12 PWR WP. The WP outer surface boundary condition temperatures for the respective cases are also shown in the figures. The peak values for the surface temperatures were 234°C for the 21 PWR SNF WP and 218°C for the 12 PWR WP. The time of occurrence of the peak WP surface temperature was about 20 years after emplacement for both histories.

The fuel temperature (homogenized assembly material) peaks at approximately 336°C about 7 years after emplacement for the 21 PWR MOX SNF WP and at approximately 302°C about 2 years after emplacement for the 12 PWR MOX WP. Both these peak temperatures are well below the maximum permissible waste package temperature of 350°C given in Section 2.1.5.2.

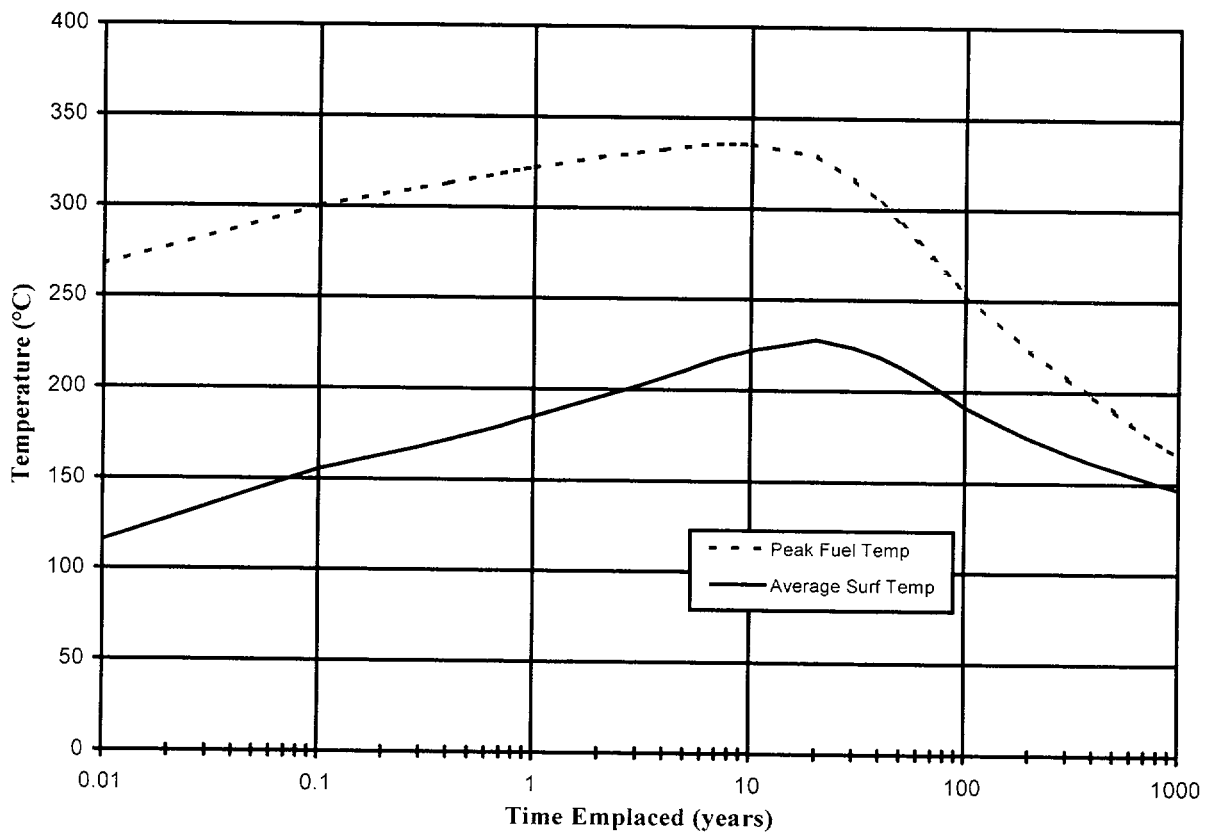


Figure 4-1. Temperature Histories for 21 PWR MOX WP

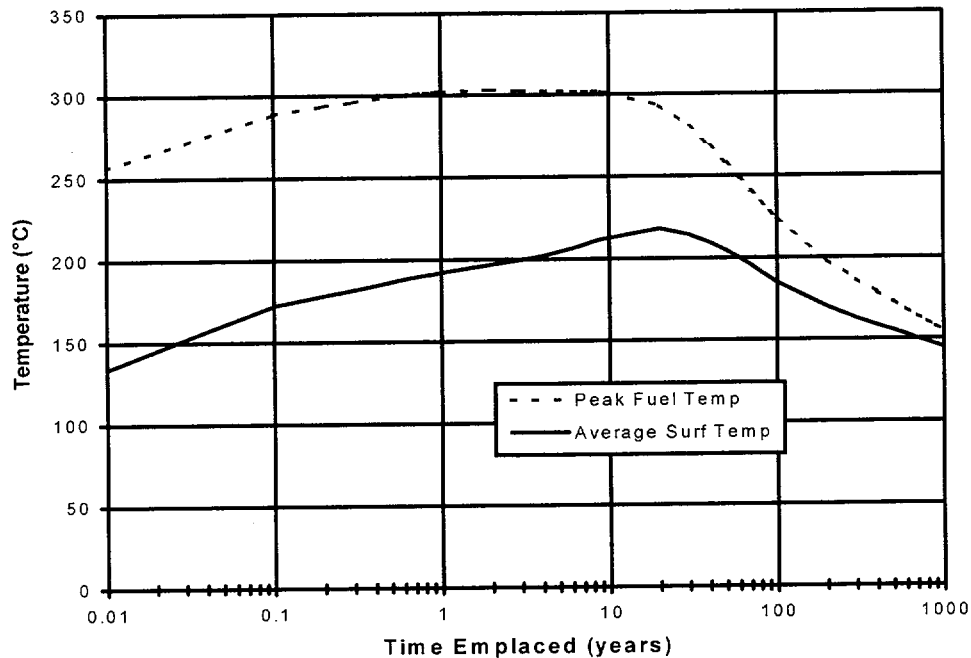


Figure 4-2. Temperature Histories for 12 PWR MOX SNF WP

4.2 CERAMIC

The thermal design criteria for the can-in-canister concept are discussed in Section 2.2.6.2, with which the results in this section comply. The thermal analysis for the ceramic waste form is performed in CRWMS M&O (1999e). By the time the peak temperatures occur (approximately 30 years after emplacement for the peak waste temperature and approximately 60 years after emplacement for the peak WP surface temperature) much of the radioactivity in the HLW has decayed so the principal remaining heat source in the WP is Pu (as is explained in CRWMS M&O 1996a, Section 8.3.3.3). Therefore, the temperature comparison between the immobilized Pu WP and HLW WP should be more favorable to the former in the present case than it was in the previous study, because the present case has a smaller Pu loading per canister and per WP.

4.2.1 Thermal Analysis Method

The solution method to be employed is 2-D ANSYS finite element analysis. The calculation uses multiple WP emplacement thermal evaluation results (CRWMS M&O 1998n, p. 26) for the WP surface temperatures as the boundary condition, and applies the heat loads in the HLW glass and immobilized plutonium to determine the temperatures in the WP. The temperature calculation is performed under transient conditions after emplacement of the waste package in the repository.

4.2.2 Thermal Analysis Results

Figure 4-3 (CRWMS M&O 1999e, Figure 6-2) displays the temperature distribution from the center of the waste package to the surface of the waste package. Temperatures at different times are compared inside the waste package. As expected, the temperature variation inside the waste package becomes less significant as the heat from the glass and ceramic waste decays. The maximum temperature in the waste package, which is 217°C, occurs in the glass matrix towards the center of the waste package basket support tube after 20 years of emplacement. The canister shell reaches its maximum of 212°C after 20 years of emplacement at a point closest to the support tube. The maximum ceramic temperature reaches 215°C at 20 years after emplacement in the location closest to the support tube. The maximum temperature on the outside of the WP shell reaches 194°C at 20 years after emplacement. The maximum temperatures of the ceramic, the canister shell, and the WP outer shell are plotted versus time in Figure 4-4 generated from the tables in Section 6 of CRWMS M&O (1999e). The temperature difference in the canister shell from the coldest point (near WP shell) to the hottest point (near WP support tube) is about 13°C at the time of the peak temperatures.

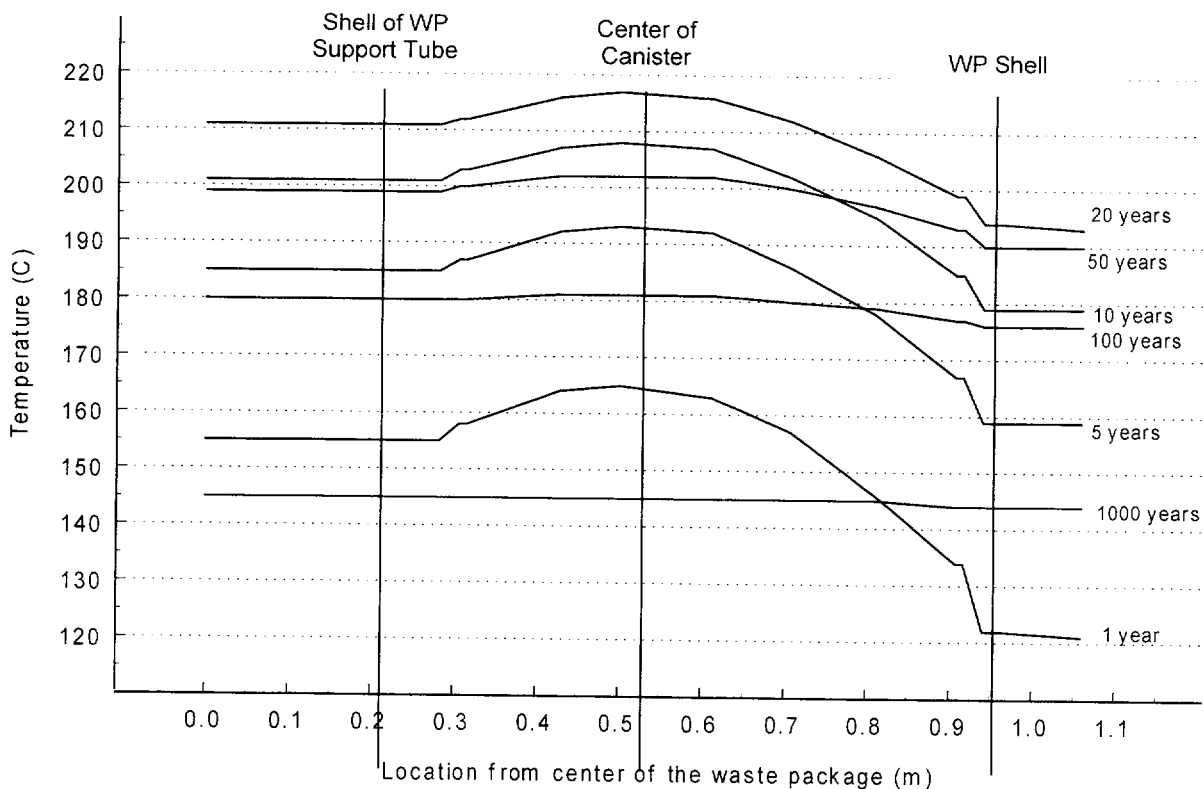


Figure 4-3. Waste Package Temperature Distribution

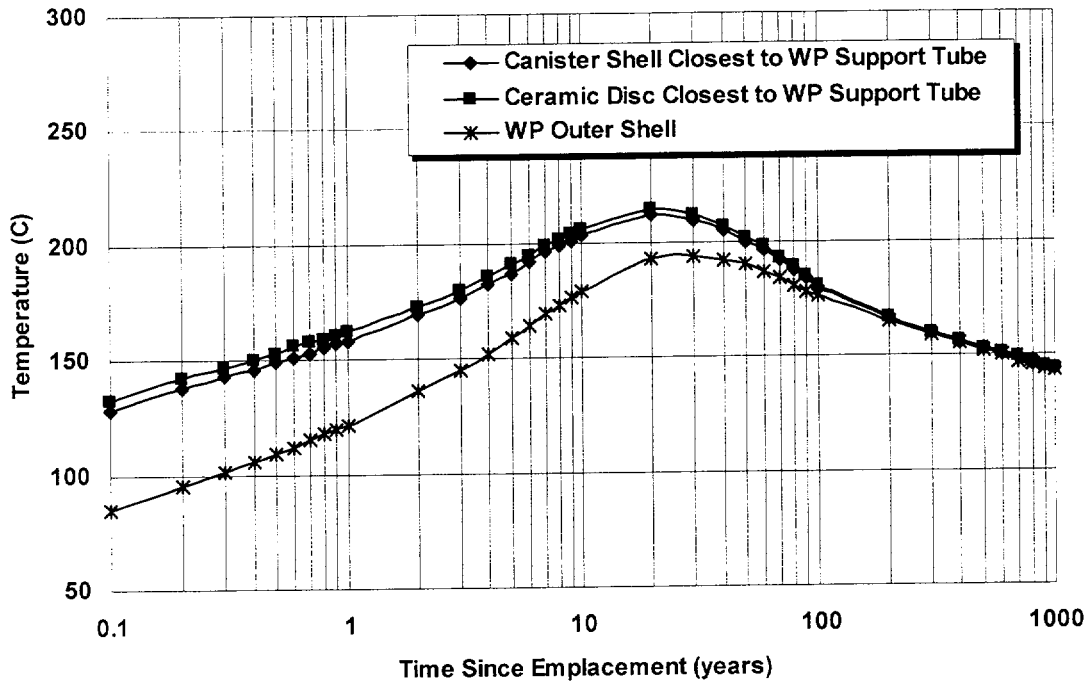


Figure 4-4. Temperature versus Time since Emplacement for Selected Points in the WP

INTENTIONALLY LEFT BLANK

5. SHIELDING ANALYSIS

5.1 MOX

Shielding analyses were performed for the 21 PWR MOX WPs (CRWMS M&O 1998p) using the MOX SNF assembly producing the highest gamma-heating source following discharge from a hypothetical equilibrium PWR MOX reactor (CRWMS M&O 1998a). These analyses required a two step calculation procedure given by:

1. Generation of the appropriate radiation source terms for SNF assemblies (primarily gamma intensity) as a function of time using the SAS2H/ORIGEN-S code sequence from SCALE 4.3, and
2. Use of the calculated source terms as partial input to the MCNP4B2 code (Briesmeister 1997) (CRWMS M&O 1998q) to calculate time-dependent dose rates in rem/hr on various surfaces and external near-field locations around the waste package. MCNP4B2 identified as CSCI 30033 V4B2LV is qualified as documented in the SQR (CRWMS M&O 1998q).

Shielding requirements for UCF waste packages as given in CPA 019 (CRWMS M&O 1999a) states that waste package containment barriers will provide sufficient shielding for protection of waste package materials from radiation enhanced corrosion. Experiments on radiolytic corrosion reported in CRWMS M&O (1996c, Vol. III, p. 8-4) indicate that for iron based materials in an air/steam environment, a 100 rad/hr dose rate at 250°C increased the corrosion rate by a factor of 5 but no change in rates were observed at 150°C. Dose rates from the shielding analysis are given in rem/hr. Dose rates in rad/hr will always be less than or equal to the dose rate in rem/hr.

Methods and results for the shielding calculation are discussed in detail to aid in the interpretation of the time history surface dose rate and to identify the differences between the MOX SNF dose rates and the LEU SNF dose rates.

5.1.1 Shielding Analysis Method

The source terms for the shielding configuration included activation of assembly hardware. The PWR MOX WP source terms are generated from the data files (CRWMS M&O 1998r) developed during the analyses documented in CRWMS M&O (1998a, Section 6). The case chosen for the shielding analysis of the 21 PWR MOX WP from the set of analyses reported in this latter reference was the 56.5 GWd/MTHM burnup case with 4.0 wt% initial fissile Pu in HM. Results of the shielding analysis will be conservative since this case produced the largest gamma-heating source from the MOX analysis.

Shielding calculations have also been carried out for commercial SNF in the 21 PWR WP using a Babcock and Wilcox (B&W) Mark B assembly having an initial enrichment of 5.05 wt% fissile uranium and a burnup of 75 GWd/MTU (CRWMS M&O 1998s, p. 4). This burnup level was used since it is the worst case situation for which shielding must be designed. The commercial SNF calculation provides a frame of reference for the MOX SNF shielding results.

The SAS2H/ORIGEN-S code is used to simulate the irradiation of the fuel and the light elements and to decay the radiation source. Time dependent gamma and neutron sources are generated for each time step requested in ORIGEN-S. To use this information as a source in MCNP4B2, the spectrum and group structure for the sources are entered and normalized by the code. The source strength is then entered in the form of a tally multiplier. This multiplier is calculated by multiplying the total source determined in SAS2H/ORIGEN-S analysis by the number of assemblies in the package and by an axial peaking factor of 1.25. This factor is based on the axial gamma radiation profile from Electric Power Research Institute (EPRI 1989, Fig. 3-19). The peaking factor conservatively compensates for the lack of a detailed axially non-uniform assembly source profile.

The major isotopes contributing to the sources for the shielding calculations are given in Table 5-1 for the MOX PWR SNF and the commercial PWR SNF. The isotopic inventory in both cases was calculated for a 10-year cooling period following discharge from a reactor (CRWMS M&O 1997b, Section 3.2). Contributions from the fuel region included actinides, fission products, and the light elements. Contributions from the lower end fittings, representative of the non-fueled regions, included only the light elements, Table 5-2. The following observations can be made concerning these radiation sources:

1. The MOX SNF actinide curie source was considerably higher than for the commercial SNF but the actinides decay mainly by alpha emission contributing little to the external dose rate.
2. The fission product isotopic distribution from the MOX SNF results in lower relative source contributions from ^{90}Sr and ^{90}Y than from the commercial SNF. This is due partly to the higher burnup in the LEU SNF and due partly to the different fission product inventory (curies) as shown in Table 5-1.
3. The major contributors to the radiation source in the non-fuel regions are ^{60}Co and ^{125}Sb , with the commercial PWR SNF source much larger than the MOX SNF source (Table 5-2).

The variation in radiation sources between the MOX and LEU PWR assemblies results in higher calculated dose rates from the LEU assemblies compared to the MOX assemblies.

Table 5-1. Major Isotopes Contributing to the Fuel Region Radiation Source

Actinides			Fission Products			Light Elements		
Isotope	PWR (curies)	MOX (curies)	Isotope	PWR (curies)	MOX (curies)	Isotope	PWR (curies)	MOX (curies)
²³⁸ Pu	6,080	2,720	⁸⁵ Kr	4,080	1,810	⁵⁵ Fe	56.4	28
²³⁹ Pu	191	267	⁹⁰ Sr	55,800	20,600	⁶⁰ Co	2,670	N/A
²⁴⁰ Pu	400	757	⁹⁰ Y	55,800	20,700	⁶³ Ni	288	N/A
²⁴¹ Pu	63,700	124,000	¹³⁴ Cs	6,930	4,520	^{93m} Nb	28.4	N/A
²⁴¹ Am	1,460	2,950	¹³⁷ Cs	87,900	60,900	¹²⁵ Sb	67.4	146
²⁴⁴ Cm	9,230	8,320	^{137m} Ba	83,000	57,500	^{125m} Te	16.5	36
N/A	N/A	N/A	¹⁴⁷ Pm	6,240	5,700	N/A	N/A	N/A
N/A	N/A	N/A	¹⁵⁴ Eu	3,940	3,800	N/A	N/A	N/A
Total	81,300	140,000	Total	307,000	179,000	Total	3,140	215

Table 5-2. Major Isotopes Contributing to the End Fittings Region Radiation Source

Isotope	PWR (curies)	MOX (curies)
⁵⁵ Fe	88	43
⁶⁰ Co	223	109
⁶³ Ni	56	20
¹²⁵ Sb	179	N/A
^{125m} Te	44	N/A
Total	598	177

Fuel assemblies and their hardware compositions are homogenized over the inside dimension of the waste package in the geometric representation for the MCNP calculation with no shielding credit taken for the waste package basket and basket guide materials. This is a conservative approach for dose rate calculations since: (1) the internal basket structure would attenuate the neutron and gamma ray flux, and (2) homogenizing the assemblies inside the waste package in effect moves the source closer to the outer surface of the waste package, thereby allowing more particles to reach the outer surface. The corrosion allowance barrier in the waste package was assumed to begin degradation when the repository humidity reaches 75% at approximately 700 years after emplacement, thus gradually reducing the original quantity of shielding material.

A different calculation was made for each of four gamma sources representative of four axial regions in the waste package (bottom end, fuel, upper plenum, and top end) and one fuel region neutron source to isolate the contribution from each. These contributions are then summed to yield a total dose.

5.1.2 Shielding Analysis Results

Radiation dose rates were calculated at a number of locations both interior and exterior to the 21 PWR MOX WP. Dose rates were calculated in the radial direction on the inside and outside

surfaces of the corrosion allowance and resistant shells, shown in Figure 5-1 and at the one and two meter distances from the outside surface of the waste package. Axially, the dose rate was determined on the exterior surface and two meters from the waste package. The maximum source strength is in the mid-region of the waste package and maximum dose rates occurred in the radial direction normal to the waste package central axis. The total dose rates, together with the neutron and gamma components, in the radial direction at 10 years following reactor discharge are given in Table 5-3 for the surfaces defined in Figure 5-1. The dose rates at these surfaces are calculated from contributions from all source regions. The dose rate in rem/hr at several radial positions in the waste package mid-region is shown in Figure 5-2 as a function of time. At locations interior to the waste package, the dose rate declines monotonically with time as the source decays. Exterior to the waste package, however, the dose rate rises slightly in the period between approximately 700 and 12,000 years but is always lower than at the initial time. This is primarily due to the loss of shielding material as the corrosion allowance waste package material (A 516 carbon steel) begins to degrade. Axial profiles (vertically along the WP) of the dose rates at the exterior surface of the waste package are shown in Figure 5-3 for various times following emplacement. The gamma dose from the end regions (see Table 5-3) results, in part, from ^{60}Co in the Inconel components as shown in Table 5-2. The spectrum of the gamma radiation from the fuel and end regions differs, resulting in the modest peaks near the assembly ends. These peaks are short-lived as shown in Figure 5-3.

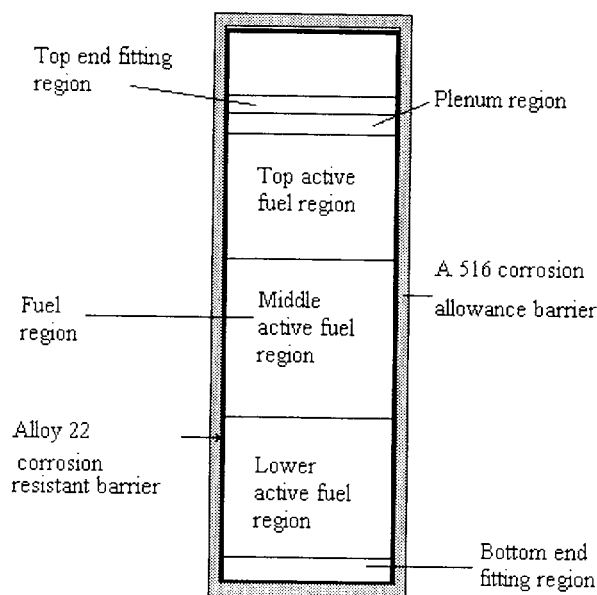


Figure 5-1. Waste Package Surfaces for Radial Dose Rate Calculation.

Dose rates on the surface of the 21 PWR WP for commercial PWR SNF at 10 years following reactor discharge are shown in Table 5-4 (CRWMS M&O 1998s, Table 6.2-3). The commercial SNF used in the shielding calculation was a B&W Mark B assembly having an initial enrichment of 5.05 wt% fissile uranium and a burnup of 75 GWd/MTU. This burnup level was used since it is the worst case situation for which shielding must be designed. As shown, the dose rates at the

waste package surface from Table 5-4 are considerably higher than for the MOX SNF WP consistent with the differences in the source values.

Table 5-3. 10-Year Dose Rates from 21 MOX PWR SNF at External Surface of Waste Package

Region	Total (rem/hr)	Neutron (rem/hr)	Gamma (rem/hr)
Top end fitting region	8.23E+01	3.58E+00	7.87E+01
Plenum region	1.12E+02	5.08E+00	1.07E+02
Top active fuel region	8.92E+01	1.13E+01	7.79E+01
Middle active fuel region	9.01E+01	1.33E+01	7.67E+01
Lower active fuel region	9.05E+01	1.16E+01	7.89E+01
Bottom end fitting region	9.53E+01	5.50E+00	8.98E+01

Table 5-4. 10-Year Dose Rates at the External Surface from Commercial LEU SNF in the 21 PWR Waste Package

Region	Total (rem/hr)	Neutron (rem/hr)	Gamma (rem/hr)
Top end fitting region	1.96E+02	3.40E+00	1.92E+02
Plenum region	2.93E+02	5.31E+00	2.88E+02
Top active fuel region	1.66E+02	1.26E+01	1.53E+02
Middle active fuel region	1.64E+02	1.49E+01	1.50E+02
Lower active fuel region	1.65E+02	1.29E+01	1.52E+02
Bottom end fitting region	1.76E+02	6.06E+00	1.70E+02

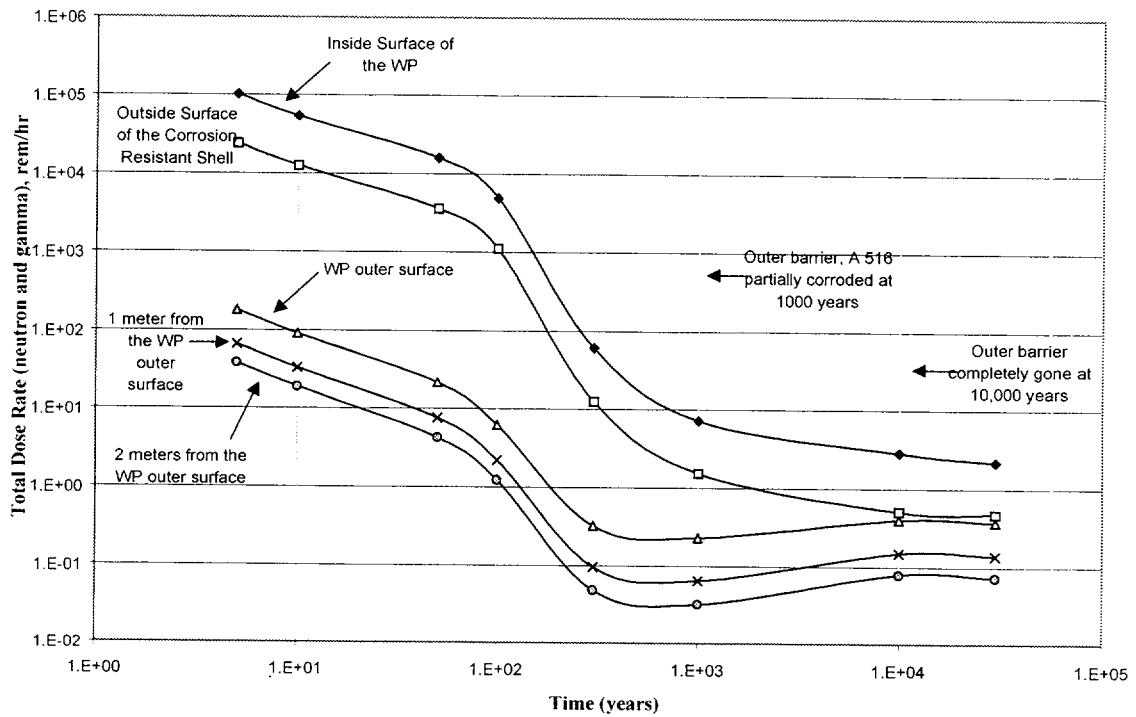


Figure 5-2. Radiation Dose Rate Over Time from the 21 MOX PWR WP Mid-Region

For the 21 MOX SNF WP, the dose rates shown in Figure 5-2 exceeded 10 rem/hr only during the period prior to 100 years when the humidity of the external environment is assumed to be low. High humidity levels were assumed to occur only after approximately 700 years when the waste package surface temperatures are calculated to not exceed approximately 150°C. Thus, it is concluded that there will not be any increase in the waste package barrier corrosion rate due to radiolysis.

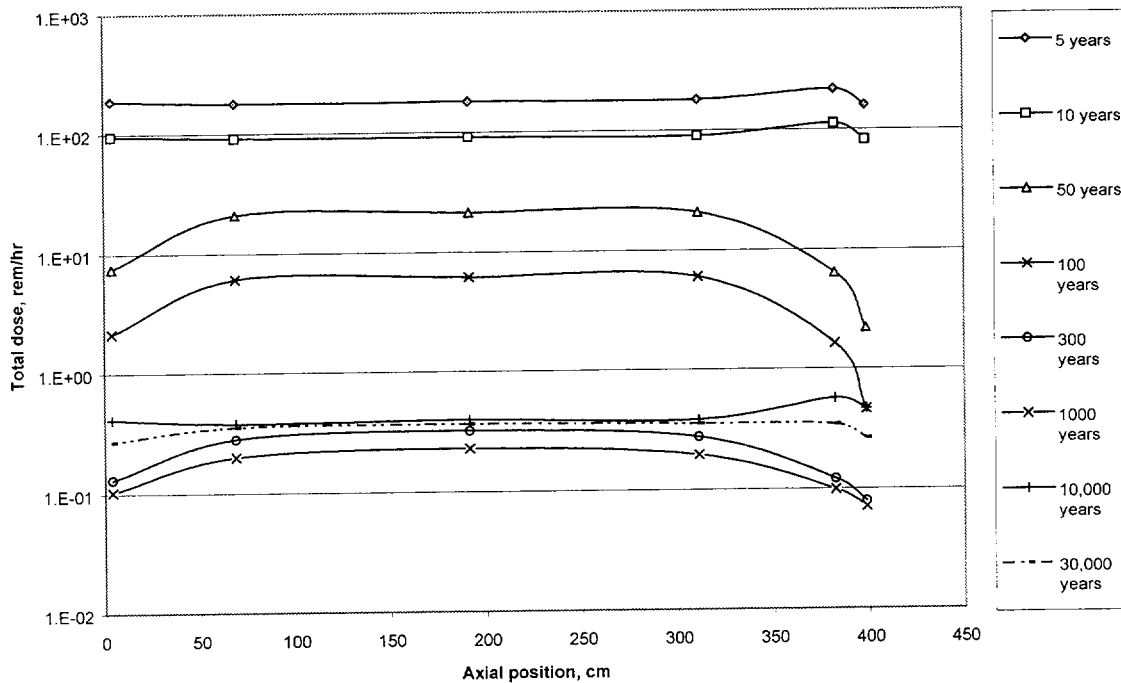


Figure 5-3. Axial Profile of Dose Rates at the Outside Surface of the 21 MOX PWR WP

5.2 CERAMIC

The shielding analysis for the ceramic waste form was performed in CRWMS M&O (1999f). The comparison of the dose rates from the immobilized Pu WP with those for the HLW glass WP given in CRWMS M&O (1996a, Table 8-5), showed the former to have less than half the dose rate of the latter. This ratio between immobilized Pu and HLW glass waste package dose rates (less than 0.5) should remain approximately the same for the present case in which the number of canisters is increased from 4 to 5 per waste package. The fact that the current Pu disposal canister has approximately 10% more filler glass would tend to increase the ratio, since the dominant radiation source at emplacement is the filler glass. However, the magnitude of the increase in the 0.5 dose ratio will be less than this 10% because of the smaller Pu loading per canister in the present case (143 kg Pu compared with 204 kg Pu in the previous study).

5.2.1 Shielding Analysis Method

The method used to perform the shielding calculations documented herein involved the use of the MCNP code system. The MCNP code system uses Monte Carlo techniques to simulate the transport of particles (neutrons/photons) through arbitrary geometries to assess the average behavior of the neutron/photon population in the actual physical system. Figure 5-4 shows the geometry representation. Through use of the MCNP tally option, dose rates are calculated for the configuration of interest. The MCNP calculated parameter of interest in the shielding calculations for the various systems is the dose rate. The dose rate is calculated for various radial and axial positions of the WP.

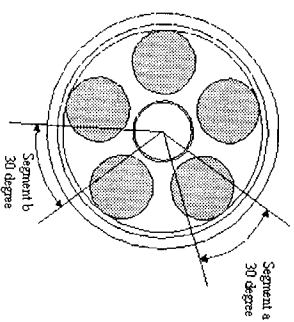
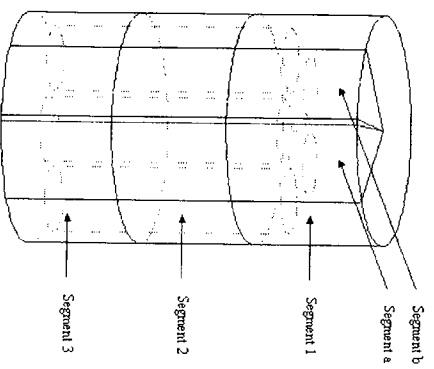
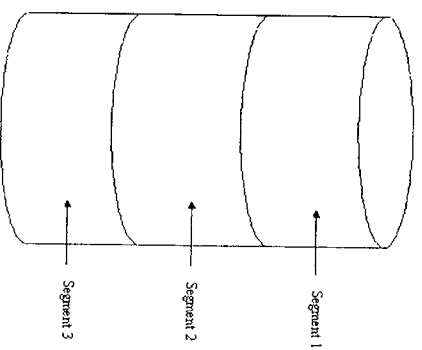
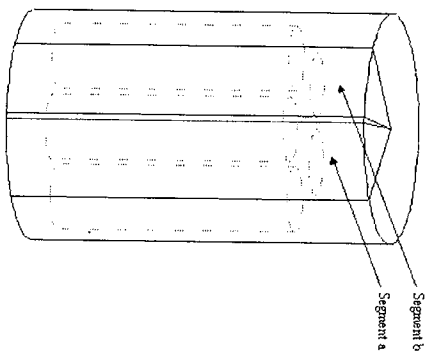


Figure 5-4. MCNP Shielding Representation of 5-DHLW WP Containing Can-in-Canister

5.2.2 Shielding Analysis Results

The results of the can-in-canister shielding calculation are presented in this section. Table 5-5 presents the shielding results for each of the waste package calculations. From Table 5-5, the maximum dose rate at the surface of the WP of 11.8 rem/hr is at the outer surface of the outer barrier in Segment 2.

Table 5-5. Dose Rate Results for the 5-DHLW/DOE Spent Fuel Disposal Container WP Shielding Calculations

Waste Package Location	Neutron Dose Rate (rem/hr / relative error)	Gamma Dose Rate (rem/hr / relative error)	Total Dose Rate (rem/hr / relative error ^a)
Segment 1: inner surface of inner barrier	0.35122 / 0.0059	9099.84 / 0.0019	9100.19 / 0.0062
Segment 1: inner surface of outer barrier	0.25748 / 0.0056	1856.75 / 0.0025	1857.01 / 0.0061
Segment 1: outer surface of outer barrier	0.04819 / 0.0048	9.80420 / 0.0075	9.85239 / 0.0089
Segment 1: 1 m from outer barrier	0.01050 / 0.0035	2.33751 / 0.0065	2.34801 / 0.0074
Segment 1: 2 m from outer barrier	0.00509 / 0.0030	1.12798 / 0.0061	1.13307 / 0.0068
Segment 2: inner surface of inner barrier	0.40251 / 0.0055	10117.7 / 0.0019	10118.1 / 0.0058
Segment 2: inner surface of outer barrier	0.32158 / 0.0052	2248.74 / 0.0024	2249.06 / 0.0057
Segment 2: outer surface of outer barrier	0.06062 / 0.0045	11.7419 / 0.0072	11.8025 / 0.0085
Segment 2: 1 m from outer barrier	0.01887 / 0.0032	4.72061 / 0.0063	4.73948 / 0.0071
Segment 2: 2 m from outer barrier	0.00913 / 0.0032	2.57734 / 0.0065	2.58647 / 0.0072
Segment 3: inner surface of inner barrier	0.35921 / 0.0058	9351.44 / 0.0019	9351.80 / 0.0061
Segment 3: inner surface of outer barrier	0.26515 / 0.0054	1900.63 / 0.0024	1900.90 / 0.0059
Segment 3: outer surface of outer barrier	0.04964 / 0.0048	10.0392 / 0.0074	10.0888 / 0.0088
Segment 3: 1 m from outer barrier	0.01074 / 0.0034	2.39146 / 0.0065	2.40220 / 0.0073
Segment 3: 2 m from outer barrier	0.00519 / 0.0030	1.14956 / 0.00600	1.15475 / 0.0067
Inner barrier top surface	0.32243 / 0.0085	8632.08 / 0.0034	8632.40 / 0.0092
Outer barrier top lid bottom surface	0.22382 / 0.0089	1193.51 / 0.0044	1193.73 / 0.0099
Outer barrier top lid top surface	0.03553 / 0.0083	3.57077 / 0.0174	3.60630 / 0.0193
1 m from outer barrier top lid top surface	0.00706 / 0.0072	0.88284 / 0.0159	0.88991 / 0.0175
2 m from outer barrier top lid top surface	0.00312 / 0.0065	0.40889 / 0.0150	0.41201 / 0.0164
Inner barrier bottom surface	0.33014 / 0.0083	8786.30 / 0.0035	8786.63 / 0.0090
Outer barrier bottom lid top surface	0.24827 / 0.0090	1250.09 / 0.0044	1250.34 / 0.0100
Outer barrier bottom lid bottom surface	0.03813 / 0.0081	3.80757 / 0.0185	3.84570 / 0.0202
1 m from outer barrier bottom lid bottom surface	0.00752 / 0.0070	0.92478 / 0.0162	0.93230 / 0.0177
2 m from outer barrier bottom lid bottom surface	0.00330 / 0.0063	0.42923 / 0.0153	0.43253 / 0.0166

^a The total relative error was calculated by taking the square root of the sum of the squares of the relative errors from the neutron and photon dose rates.

6. DISPOSAL CRITICALITY ANALYSIS

6.1 MOX

The degradation analysis methodology for the MOX SNF and waste package basket structure is discussed in Section 6.1.1. The criticality evaluation of the intact MOX SNF and basket structure is given first in Section 6.1.2. The degraded configurations and results of the criticality analyses of these configurations are discussed in Section 6.1.3. Results of the criticality analyses are summarized in Section 6.1.4.

The criticality control requirement for emplacement and isolation of radioactive waste is that the system k_{eff} maintains a minimum 5% margin below unity after allowing for biases and uncertainties (YMP 1998, Section 2.1.1). Benchmark calculations (CRWMS M&O 1998q, Section 3.1.4) with the MCNP4B2 code showed a maximum difference (or bias) of 3% between the calculated and experimental k_{eff} s for LEU fuel. MOX Commercial Critical benchmark calculations should be performed to show that the same values apply to MOX fuel. The data for these experiments will be supplied by the reactor burning weapons-grade MOX fuel. Statistical uncertainties at the 2σ level in the k_{eff} calculations are normally of the order of 0.2% to 0.3%. Thus the maximum k_{eff} to assure subcriticality is $0.92 = 1.0 - 0.05 - 0.03$. This section describes the MCNP4B2 cases needed to evaluate the k_{eff} of this configuration.

This study is primarily concerned with evaluating the criticality potential of the intact and degraded forms of the MOX SNF. Two variations of the WP VA design have been used: the 21 PWR WP and the 12 PWR WP. The 21 PWR WP holds 21 MOX fuel assemblies and is used for moderately burned MOX SNF. The latter holds only 12 MOX fuel assemblies and is used for the highest burned MOX SNF, in order to satisfy peak temperature limits. This study also includes an evaluation of the structural, thermal, and shielding impacts of the MOX SNF WPs.

6.1.1 Disposal Criticality Analysis Methodology for Intact and Degraded SNF

In this study the methodology for computing k_{eff} values (CRWMS M&O 1998c) for intact and various degraded waste package configurations uses the Monte Carlo N-Particle Code MCNP, Version 4B2 (Briesmeister 1997) (CRWMS M&O 1998q). MCNP4B2 identified as CSCI 30033 V4B2LV is qualified as documented in the SQR (CRWMS M&O 1998q). Fuel region number densities used in this criticality evaluation were calculated simply by homogenizing the isotopic concentrations from CRWMS M&O (1998a) for a particular fuel and decay time throughout the volume of the active fuel region.

The results reported from the MCNP calculations were the combined average values of k_{eff} from the three estimates (collision, absorption, and track length) listed in the final generation summary in the MCNP output.

The following is an evaluation of each of the internal criticality configuration classes of the *Disposal Criticality Analysis Methodology Topical Report* (YMP 1998, Section 3.1.1) applied to the MOX waste package.

1. **Degraded basket with intact waste form**—This class is evaluated in Section 6.1.3, and the results shown in Section 6.1.3. Of the configurations in this class, the only one that can support criticality is IP-3c, which has all the boron flushed from the waste package. IP-3a and IP-3b have some of the borated stainless basket material remaining intact, thereby retaining boron in the waste package. The criticality evaluation results in Section 6.1.2 show that no criticality is possible if there is any boron remaining in the waste package. IP-3d is not applicable because it requires the neutron absorber material to degrade before the structural basket. The material carrying the neutron absorber, stainless steel, corrodes much slower than the structural basket material, carbon steel (YMP 1998, Section 3.1.1). This configuration class is shown in Figure 6-1D. The scenario represented by Figure 6-1 is discussed below.
2. **Degraded basket and degraded waste form**—This class is an evolution (further degradation with time) of Class 1, above, with some degradation of the initial waste form. In fact the only configuration in this class that can become critical is a variant of IP-3c, which has some of the iron oxide and/or fission products removed. Both these processes tend to increase k_{eff} . This class is evaluated in Section 6.1.3. Degradation of the waste form may also include partial collapse of the spacer grids, which will be seen to reduce k_{eff} . In fact, it will be seen (Section 6.1.3.3.3) that for MOX SNF there can be no criticality if there is any significant collapse of the assembly spacer grids. The improbability of any scenario leading to this configuration is discussed with criticality probability in Section 6.3.3.
3. **Fissionable material from the waste form is mobilized and moved away from the neutron absorber**—SNF mobilized (dissolved) and moved away from the absorber material, which, for definition of this configuration class corrodes at a much slower rate. This class does not apply because zircaloy cladding protects the SNF, so that its effective corrosion rate is much slower than the steel basket material (YMP 1998, Section 3.1.1).
4. **Fissionable material accumulates at the bottom of the WP with a moderator**—This class has moderation provided primarily by water trapped in clay. The class does not apply because the MOX waste package has no glass, so the formation of any clay is expected to be extremely slow (YMP 1998, Section 3.1.1).
5. **Fissionable material is distributed throughout a major fraction of the WP with a moderator**—This class has moderation provided primarily by water trapped in clay. The class does not apply because the MOX waste package has no glass, so the formation of any clay is expected to be extremely slow.
6. **Waste form degraded in place with basket intact**—This case does not apply for the same reason as #3.

The scenario sequence leading to configuration Classes 1 and 2 for the MOX waste package, which is the same as the commercial PWR waste package (CRWMS M&O 1998c, Figure 2-1) is shown in Figure 6-1. CRWMS M&O (1998c) Sections 3 and 5 provides a description of the degradation process and corrosion product generation. Since the waste package interior was

inerted with He prior to time of breach, the initial configuration will be the as-built basket (Fig. 6-1A). Within a few hundred years following breach, the carbon steel and aluminum components will degrade to insoluble corrosion products as shown in Figure 6-1B (CRWMS M&O 1998d, Section 5.3). While structural calculations show that the absorber plates can support the load of the assemblies (CRWMS M&O 1997k, p. 27), localized corrosion in the crevice regions at the corners of each cell will likely cause collapse shortly after failure of the structural components. However, the majority of the B-SS absorber plates will be only minimally degraded and remain between the assemblies, with corrosion products from the degraded carbon steel tubes (Fig. 6-1C). Eventually, after thousands of years, general corrosion will also fully degrade the absorber plates, allowing the soluble boron neutron absorber to be flushed out of the package (Fig. 6-1D). As mentioned previously, Figure 6-1D is the representation of configuration class number 1, or configuration IP-3c.

The zircaloy cladding and spacers represent the most corrosion resistant material in the waste package, and thus will be the last to degrade. Collapse of the fuel rods at the bottom of the waste package will likely occur prior to complete cladding degradation (Figure 6-1E), as the spacer grids are typically fabricated from strips of zircaloy that are thinner than the cladding. The final internal configuration (Figure 6-1F) is complete degradation of the entire waste package contents, with only the insoluble materials remaining. Similar configurations would also be expected to form during degradation of the 12 PWR WP, with the exception of configurations B and C, which cannot occur because the 12 PWR WP does not contain B-SS absorber plates.

This study summarizes calculations that considered configurations A, D, E, and F for both the 21 and 12 PWR WP. Configurations B and C have not been specifically evaluated because they are bounded by D. (A is also dominated by D, but it is considered because it is the starting point that can serve as a reference.) Chemical compositions of the remaining basket and fuel corrosion products were obtained from the geochemistry calculations reported in CRWMS M&O (1998d, Section 5.3), both settled and uniform corrosion product distributions will be evaluated for configuration D.

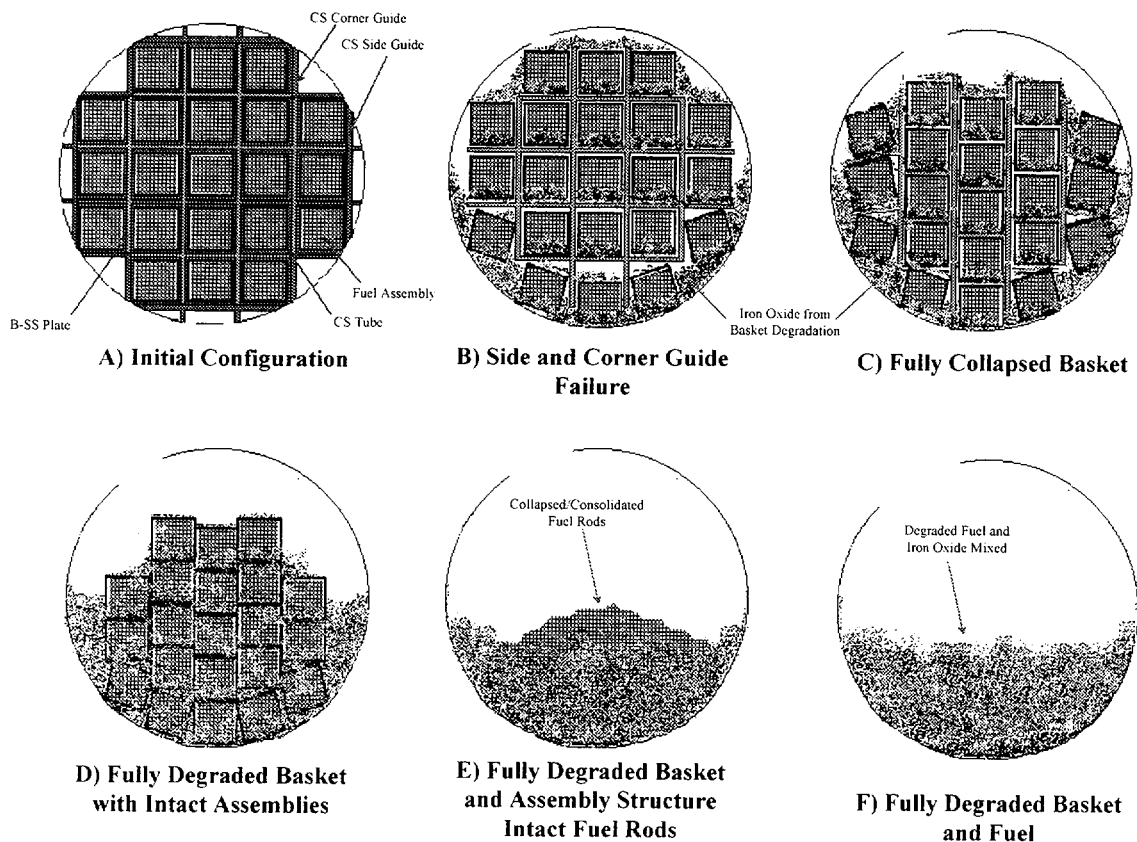


Figure 6-1. Degradation Sequence of the 21 PWR Basket Structure Following WP Breach

6.1.2 Criticality Evaluation of the Intact Configuration

In keeping with the methodology described in Section 6.1, the k_{eff} of the intact MOX SNF WP configuration (Fig. 6-1A) was evaluated for both the 21 and 12 PWR WP designs.

6.1.2.1 Intact Fuel and Intact Basket Criticality Case

The composition and dimensions of the containment barriers and basket components were represented explicitly using the information in Section 2.1.2. Each Westinghouse 17x17 Vantage 5 fuel assembly was treated as a heterogeneous system with the fuel rods and control rod guide tubes represented explicitly using the information contained in Section 2.1.1. The fuel rods are conservatively represented with water in the gap region simulating the effect of penetrated cladding (Zircaloy-4 is highly corrosion resistant but assumed to have sufficient penetration to allow water to fill the gap) (CRWMS M&O 1998c, Section 3). Figure 6-2 shows the details of the MCNP4B2 representation for the 21 PWR WP and Figure 6-3 shows the representation details for the 12 PWR WP. In both representations, the waste package is filled with water and there is a water reflector on the exterior. In addition to the base design discussed in Section 2.1.2, an additional case was evaluated with the central basket plates changed from A 516 carbon steel to aluminum Alloy 6061. This alternative was evaluated because it was being

considered in the thermal analyses of the 12 PWR WP. Each of the intact 21 PWR WP designs was evaluated for the 4.0 wt% fissile Pu in HM, 35.6 GWd/MTHM burnup fuel (fuel #1) and the 4.5 wt% fissile Pu in HM, 39.4 GWd/MTHM burnup fuel (fuel #2), for decay times from 10 years to 250,000 years. In addition, the intact 12 PWR WP designs were evaluated for the 4.0 wt% fissile Pu in HM, 50.1 GWd/MTHM burnup fuel (fuel #3).

In all MCNP cases, even though the environment outside the waste package, whether tuff, water, or a mixture, has no significant impact on the configuration k_{eff} , the waste package is assumed to be water reflected. The amount of outgoing neutrons penetrating the waste package barriers is less than 1% of the total number of neutrons in the system; and typically less than 0.2% based on the evaluation of the neutron activity reported in the outputs. When the factor of four attenuation through the waste package barriers is factored in, even mirror reflection of these neutrons would have no statistically significant effect. Hence, having a different reflector (e.g., tuff, rock, clay, etc.) on the outside of the waste package would have negligible or no effect on the results.

```
02/24/98 22:44:08
UCF 21 PWR WP MODEL V 17x17 MOX
Fuel

probid = 02/24/98 22:25:38
basis:
( 1.000000, .000000, .000000)
( .000000, 1.000000, .000000)
origin:
( .00, .00, 200.00)
extent = ( 100.00, 100.00)
```

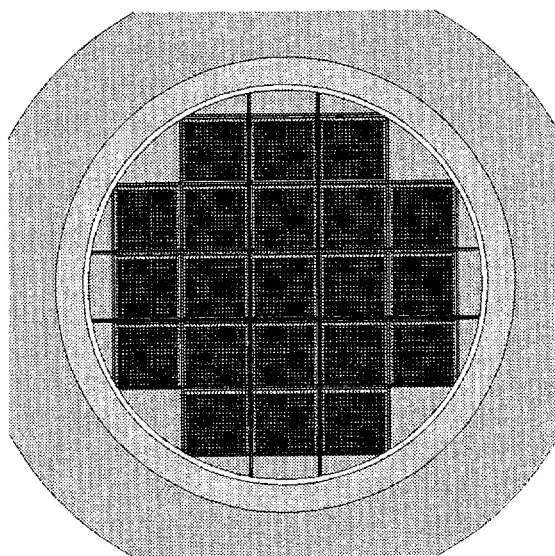


Figure 6-2. Intact 21 PWR MOX Fuel Waste Package

Principal isotopic compositions for the MOX SNF, summarized in Section 2.1.2, as obtained from the SAS2H/ORIGEN-S calculations (CRWMS M&O 1998a) are given in grams per assembly for decay times from a few days out to 1 million years. These were converted to number densities for the criticality calculations with MCNP (CRWMS M&O 1998c, Section 5).

```

02/17/98 10:31:34
L2m1 - UCF 12 MOX PWR WP, V
17A17, Intact, Flooded

probid = 02/17/98 10:16:17
basis:
/ 1.00000, .00000, .00000)
/ .00000, 1.00000, .00000)
origin:
/ .71, -.37, 200.00)
extent = / 69.40, 69.40)

```

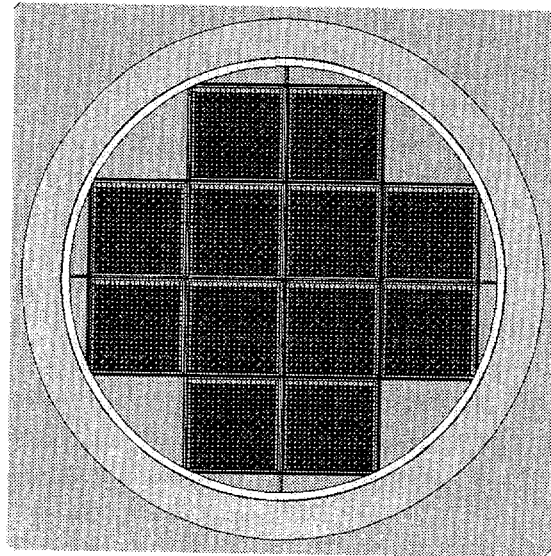


Figure 6-3. Intact 12 PWR MOX Fuel Waste Package

6.1.2.2 Intact Fuel and Intact Basket Criticality Evaluation Results

Results of the criticality analyses of the intact 21 PWR WP and 12 PWR WP and basket are discussed below (CRWMS M&O 1998c, Table 6.1-1 through Table 6.1-3, pp. 26-32). The k_{eff} for all cases was well below the potential critical limit of 0.92. For the first ~ 100 years after being discharged, the k_{eff} of the MOX SNF decreases as the ^{241}Pu (13.2-year half-life) fissile material decays. From ~ 100 years out to ~ 20,000 years the k_{eff} increases as the quantity of ^{240}Pu (6580-year half-life) and other intermediate half-life neutron absorbers are reduced through radioactive decay. After the ~ 20,000 year local peak, the k_{eff} decreases again as the ^{239}Pu (24,400-year half-life) fissile material decays into ^{235}U , which is still highly fissile material but lower fission cross section (Parrington et al. 1996) of ^{239}Pu . These effects on k_{eff} are illustrated in Figures 6-4, 6-5, and 6-6 (CRWMS M&O 1998c, Figures 6.1-1, 6.1-2, and 6.1-3) which show the $k_{eff} \pm 2\sigma$ values as a function of time for the intact 21 PWR WP, 12 PWR WP, and 12 PWR WP with Al thermal shunts, respectively. Assemblies with higher burnup values than shown in the figures will have a lower k_{eff} profile.

The 12 PWR WP designs showed higher k_{eff} values than the 21 PWR WP design for the same fuel type because these waste package designs do not include criticality control plates. The 12 PWR WP with Al thermal shunts showed an $\approx 1\%$ increase in k_{eff} over the 12 PWR WP (CRWMS M&O 1998c, pages 26-32) with the all carbon steel basket primarily because the Al has a much smaller neutron absorption cross section than the Fe that it replaces (Parrington et al. 1996). The 4.0 wt% fissile Pu in HM, 35.6 GWd/MTHM burnup fuel generally showed higher k_{eff} values than the 4.5 wt% fissile Pu in HM, 39.4 GWd/MTHM fuel for all cases evaluated.

No specific comparisons were made of the intact MOX SNF and intact basket criticality results with LEU criticality results since the MOX SNF k_{eff} s were well below critical values. Thus, a criticality event for this configuration is impossible. Probability of criticality for MOX SNF is

discussed in Section 6.3, but since criticality is impossible for this configuration, it is not part of that discussion.

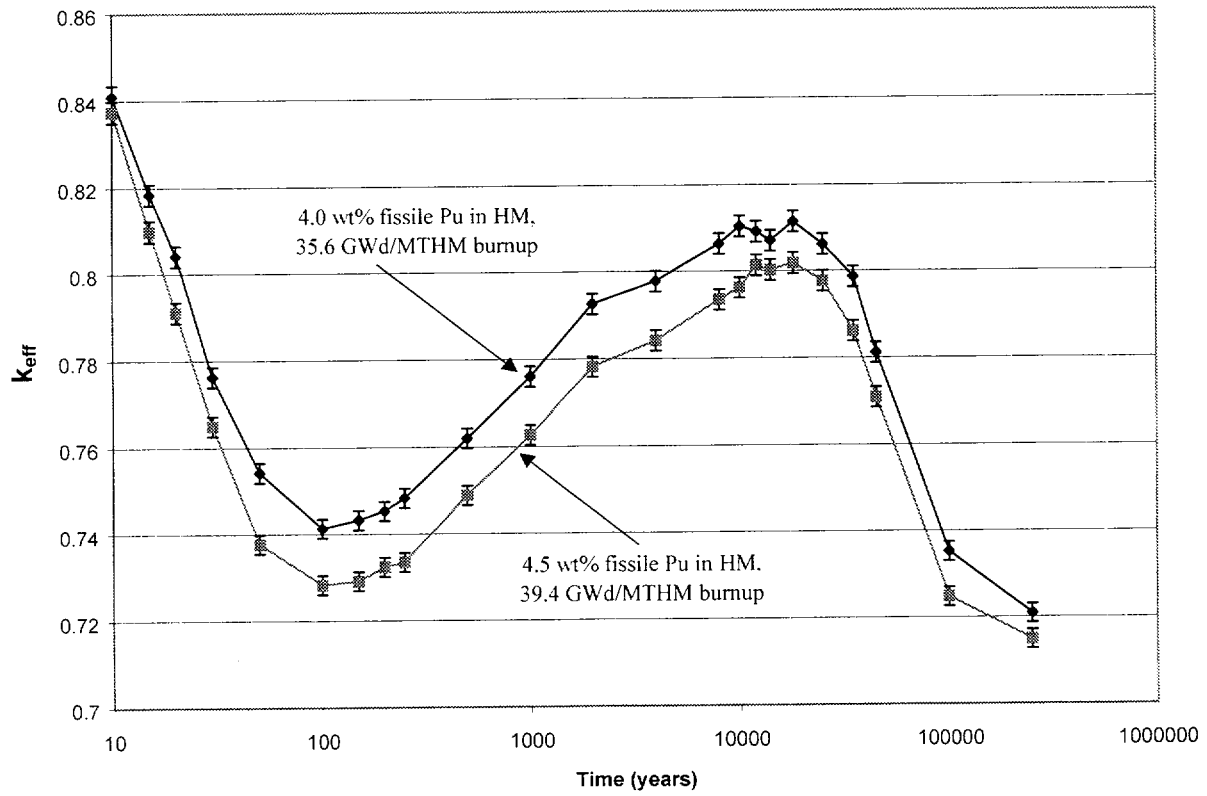


Figure 6-4. Time Effects on k_{eff} for Intact MOX SNF and Intact Baskets in a 21 PWR Absorber Plate WP

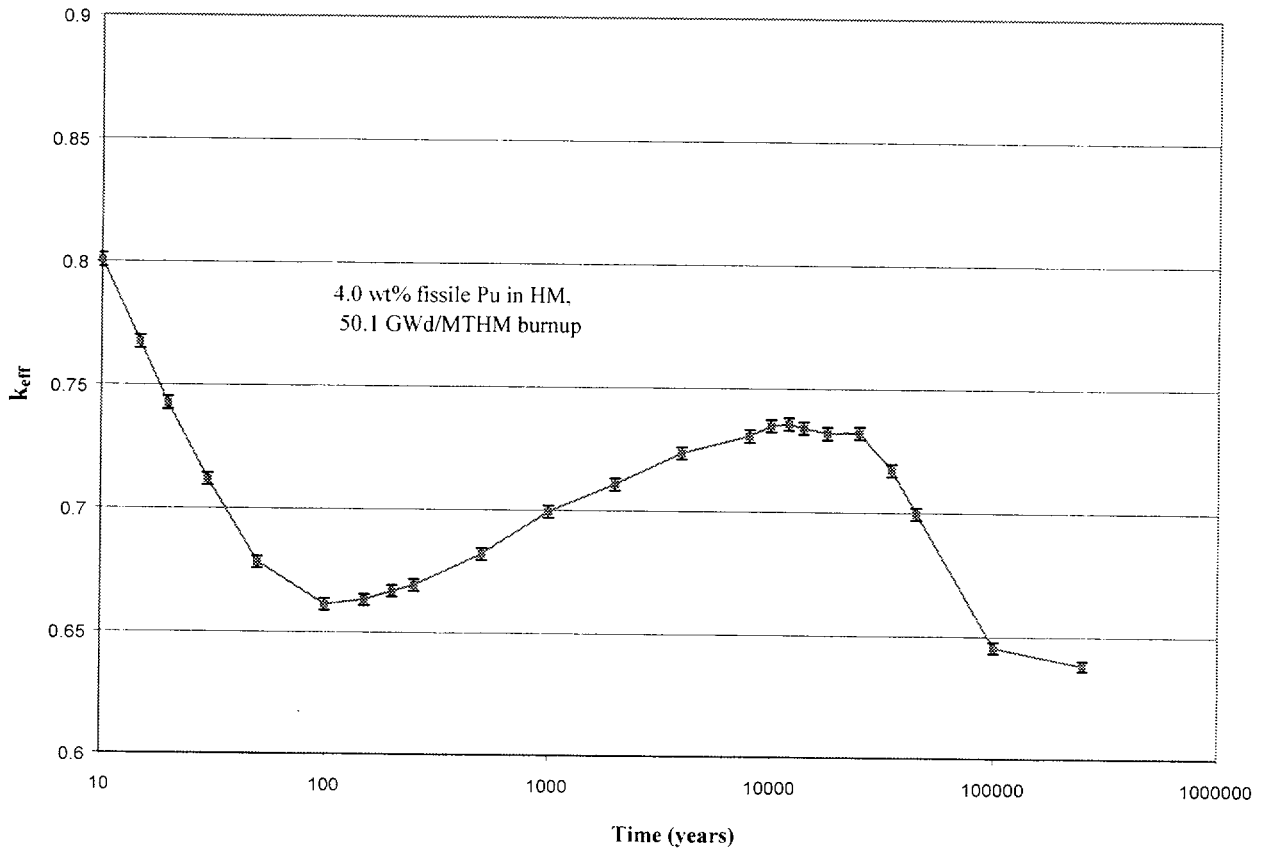


Figure 6-5. Time Effects on k_{eff} for Intact MOX SNF and Intact Baskets in a 12 PWR WP

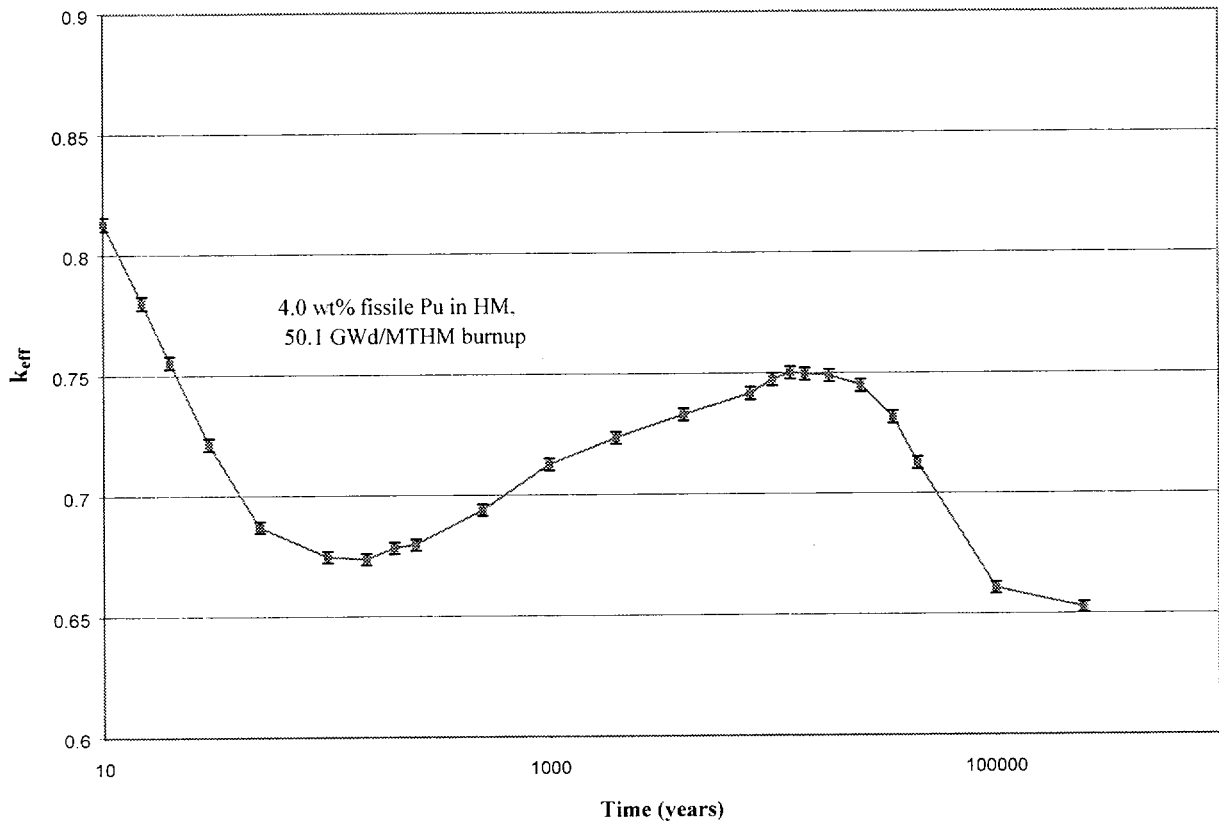


Figure 6-6. Time Effects on k_{eff} for Intact MOX SNF and Intact Baskets in a 12 PWR WP with AI Shunts

6.1.3 Criticality Analysis for Partially Degraded Configurations

Analyses of the intact PWR MOX SNF evaluated the criticality potential of the water-filled waste packages for the fissile and absorber nuclides in the waste package as a function of time. The analysis included radioactive decay of nuclides, geochemical degradation of materials, and removal of soluble compounds. The objectives of the geochemical analyses (CRWMS M&O 1998d, p. 5) were to determine the geochemical conditions under which:

1. Criticality control material suggested for this design will remain in the degraded waste package after the corrosion/dissolution of its initial form (such that it can be effective in preventing criticality), and
2. Fissile plutonium and uranium will be carried out of the degraded waste package by infiltrating water (such that internal criticality is no longer possible, but the possibility of external criticality may be enhanced).

Configurations of the SNF, as derived from the geochemical analyses, having a reasonable chance of occurring in those waste packages, which experience degradation, were discussed generally in Section 6.1.1.

Boron (B) in the form of B-SS was included in the analyses, as were various neutron absorbing fission products, notably Gd and Nd. These elements are important for inclusion in calculations of waste package internal criticality. The results of this analysis were used as input for the criticality evaluations of the degraded waste package configurations to ensure that the type and amount of criticality control material used in the waste package design will prevent criticality. These chemical compositions (and consequent criticality evaluations) were determined for time periods up to 200,000 years.

Geochemistry calculations were not performed for the 12 PWR MOX WP in CRWMS M&O (1998d) since the results can be extrapolated from the 21 PWR WP adjusted for the differences in waste package volumes. The geochemistry results of the 21 MOX PWR WP indicated that all of the Fe from the carbon and stainless steel components was incorporated into Fe_2O_3 , and remained in the package. Since the 12 PWR WP basket is fabricated entirely from carbon steel, the corrosion product resulting from degradation of the basket components will also be Fe_2O_3 . Since the criticality calculation considered only the initial configuration and fully degraded basket configurations (Fig. 6-1), compositions for the 12 PWR WP can be calculated from the initial volumes.

6.1.3.1 Methodology for Determining Degraded Configurations

This section describes the methodology used for the degradation analysis (CRWMS M&O 1998d, pp. 5-6) of both basket materials and the waste form (MOX SNF). Because this analysis was done before the ceramic degradation analysis (Section 6.2.3.1), an earlier version of the geochemistry methodology was used. The methodology used the EQ3/6 V7.2b software package (CRWMS M&O 1998e) and the EQ3/6 7.0b manual (Wolery 1992 and Wolery and Davelier 1992), primarily the EQ6 reaction path code which represents water/rock interaction or fluid mixing in either a pure reaction progress mode or a time mode. EQ3/6 V7.2b is qualified as documented in the SQR (CRWMS M&O 1998e). The overall software package calculates thermodynamic equilibrium, thermodynamic disequilibrium, and reaction kinetics in chemical systems. EQ6 calculates the consequences of irreversibly reacting an aqueous solution with a set of reactants.

The method used for the geochemical analysis of the PWR MOX SNF involves the following steps:

1. Use of basic EQ3/6 program for tracing the progress of reactions with evolution of the chemistry, including the estimation of the concentrations of minerals remaining in solution and the composition of the precipitated solids.
2. Use of the "pseudo flow-through" mode in which:
 - a. Water is added continuously to the waste package and builds up in the waste package over a sequence of time steps. The time period per sequence is constant and is determined from the selected drip rate, e.g., $0.15 \text{ m}^3/\text{year}$ entering the waste package, and the percentage of added water selected.

- b. Flushing action (removal of water added during one EQ6 sequence) is simulated by adjusting the amount of water and solutes for input to the next EQ6 sequence.

For more recent geochemistry calculations the "pseudo flow-through" mode has been replaced by the solid centered flow through (SCFT) code addendum to EQ3/6, which is described in Section 6.2.3.1.

3. Outputs include the following time histories:

- a. Waste package solution composition
- b. Waste package solids composition (precipitates from the products of the degradation of the initial solid components)
- c. Effluent solution composition

Items a and c may differ because conservative assumptions for internal criticality would lead to the maximum retention of fissile material in the waste package, while conservative assumptions for external criticality would lead to the maximum release of fissile material.

6.1.3.2 Degraded Configurations from Geochemistry Analysis

The emphasis in the geochemical analyses was on the composition and composition reactivity, rather than on the physical configurations within different waste packages, although the geometric configurations were used for volume calculations to determine the chemical evolution. As shown in Figure 2-2, a 21 PWR MOX SNF WP consists of SNF assemblies held in a basket and placed inside a corrosion barrier. The design for the corrosion barrier itself specifies an outer corrosion allowance and an inner corrosion resistant metal. A representation of the chemical behavior of this system requires the following characteristics of each material: chemical compositions (CRWMS M&O 1998d, Section 5.1.1.1); masses and surface areas (CRWMS M&O 1998d, Table 5.2.3-3); and corrosion or degradation rates (CRWMS M&O 1998d, Table 5.2.3-2). Elemental compositions for the SNF assemblies were obtained from the output files (CRWMS M&O 1998r) from the SAS2H/ORIGEN-S analysis (CRWMS M&O 1998a) in gram-atoms/assembly. The compositions were decayed, following discharge from the reactor, to 10,000 and 25,000 years after emplacement. The resulting isotopic changes were used to adjust the geochemistry results since the EQ3/6 code package does not account for compositional changes due to radioactive decay.

The geochemistry calculations determined the composition of the corrosion product mixture remaining in the 21 PWR waste package following complete basket degradation. Concentrations of insoluble corrosion products that remain after the basket has completely degraded are given in Table 5.3.2-1 of CRWMS M&O (1998d), which also indicates that this final composition is fairly insensitive to the likely range of possible B-SS degradation rates and drip rates. The elemental composition used for the criticality calculation is determined by the mineral compositions, which are summarized in Table 6-1 (CRWMS M&O 1998c, Table 5.1-6). The

corresponding corrosion product inventory remaining in the 12 PWR WP is derived from the 21 PWR WP values with the appropriate volume ratio.

Table 6-1. Corrosion Products Remaining Following Basket Degradation in the 21 PWR WP

Basket Corrosion Product	Volume per WP (m ³)	Moles/liter H ₂ O	Moles/WP
Diaspore (AlOOH)	1.8392E-01	2.291	10424.05
Hematite (Fe ₂ O ₃)	1.7707E+00	12.77	58103.5
Pyrolusite (MnO ₂)	2.7361E-02	0.35	1592.5
Ni ₂ SiO ₄	3.0867E-02	0.1592	724.36
Nontronite-Ca (Si _{3.7} Ca _{0.33} Al _{0.33} Fe ₂ H ₂ O ₁₂)	1.2874E-02	0.0216	98.28
Nontronite-K (Si _{3.7} K _{0.17} Al _{0.33} Fe ₂ H ₂ O ₁₂)	5.6325E-04	0.0009151	4.163705
Nontronite-Mg (Si _{3.7} Mg _{0.2} Al _{0.33} Fe ₂ H ₂ O ₁₂)	8.9323E-03	0.01513	68.8415
Nontronite-Na (Si _{3.7} Na _{0.33} Al _{0.33} Fe ₂ H ₂ O ₁₂)	9.0407E-04	0.001504	6.8432
TOTAL	2.0362E+00		

An important part of the geochemistry results is the effects that fuel degradation will have on the principal isotope inventory since these isotopes are important for burnup credit. Due to uncertainties in degradation rates as discussed in Section 2.1.2.1, two cases were studied:

1. Fuel degradation concurrent with basket degradation and
2. Fuel degradation beginning after basket degradation is completed.

Figure 6-7 (CRWMS 1998b, Volume I, Figure 6.3.2-1) illustrates graphically the simulated history for these elements for the MOX case in which hematite forms showing the quantity in gram-atoms of selected elements of special interest for criticality computations remaining in the MOX PWR WP for the concurrent degradation case. Times are relative to the initial breach of the corrosion barrier. The assumed inflow rate of water into the waste package was 0.15 m³/year (Section 2.3.2). Mo and Tc are effectively removed as soluble corrosion products from the waste package as the fuel degrades. Consequently, they will be absent from the waste package, except for very minor amounts of adsorbed species or minute traces left in solution, e.g., as a consequence of incomplete mixing of water within the waste package, soon after the SNF is fully degraded. Therefore, Mo and Tc are not shown in the figure at all.

Figure 6-7 also shows the rapid removal of Am, and some early flushing of Sm, and Gd. However, these latter elements stabilize to a (approximately) constant fraction of their original inventory. The solubilities of all the lanthanides (Gd, Nd, Sm, and Eu) are very similar; the different histories reflect differences in their initial inventories in the waste form compositions. Only a small percentage of Nd, Rh, and Ru is removed and nearly all of the Pu and U is retained.

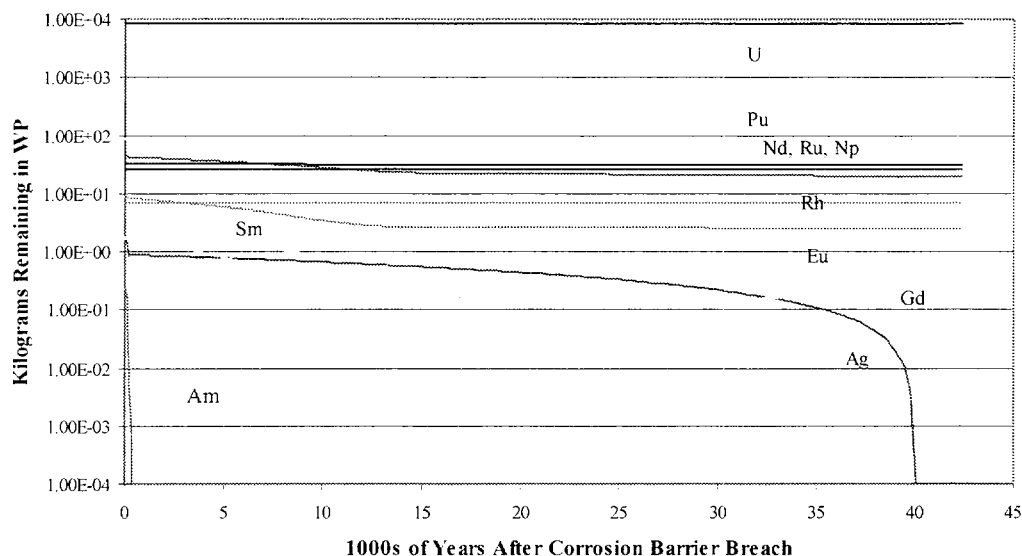


Figure 6-7. Retention History of Elements of Principal Interest for Criticality Remaining in WP

The case in which the fuel degradation was concurrent with the basket degradation resulted in more of the principal isotopes being lost due to lower pH conditions during degradation of the B-SS. It is unlikely that the basket and fuel matrix degradation will significantly overlap, because the zircaloy cladding of the fuel is much more corrosion resistant than the stainless steel of the basket. Nevertheless, this is the more conservative configuration and the results from this case are used in the degraded criticality analyses.

6.1.3.3 Criticality Evaluation of Degraded Waste Package Configurations

As discussed in Section 6.1.3.2, fuel degradation will lead to a reduced inventory of the soluble principal isotopes (summarized in CRWMS M&O 1998c, p. 15). Criticality calculations involving degraded fuel examined cases with the reduced principal isotope inventories, as well as a conservative case including only the U and Pu principal isotopes.

The total volume of corrosion products remaining following full basket degradation is equal to 36.8% of the waste package void space (interior volume minus the volume of the still intact assemblies). If these corrosion products were uniformly distributed throughout the void space, they would participate in 36.8% of the volume density of that void space. If the corrosion products settle to the bottom of the waste package, they will be packed more densely, but will occupy only a fraction of the total void space. The criticality of the package will increase with the packing density of the settled corrosion products. Therefore, it is most conservative to use the highest density found for a common natural particulate material. Packed sand is found to generally occupy 58% of the available volume (CRWMS M&O 1998c, p. 15). At 58% dense packing, if all of the oxides settle to the bottom, they will completely cover the bottom three rows of the Westinghouse 17x17 Vantage 5 MOX SNF assembly stack and cover more than 95%

of the fourth assembly row. Within the assemblies that are covered, this analysis conservatively covers only 94% or 16 of the 17 fuel pin rows (CRWMS M&O 1998c).

If all of the Fe from the 12 PWR WP basket were converted to Fe_2O_3 , as assumed, it would occupy 37.4% of the interior void space of a loaded waste package. If this material were settled to the bottom of the waste package at a 58% dense packing, it would cover all but the top two assemblies in a 12 PWR WP (CRWMS M&O 1998c, p. 15).

6.1.3.3.1 Configurations for Intact Fuel with Fully Degraded Basket

The MCNP cases needed to evaluate the k_{eff} of the 21 PWR MOX SNF and 12 PWR MOX SNF waste package designs with intact fuel and fully degraded basket structures (configuration D from Section 6.1) are described in this section. Both the uniformly distributed corrosion product and the settled corrosion product configurations were evaluated for each waste package. Each Westinghouse 17x17 Vantage 5-fuel assembly was treated as a heterogeneous system with the fuel rods and control rod guide tubes represented explicitly. The fuel rods are conservatively represented with water in the gap region and guide tubes, even when surrounded by water/corrosion product mixtures (CRWMS M&O 1998c, Section 3). The fuel rods are assumed to be breached but otherwise intact while the guide tubes are horizontal. There is no physical mechanism for getting basket corrosion products into these locations while the assembly remains intact. Figure 6-8 shows the geometry details of the MCNP4B2 representation for the 21 PWR WP with a fully degraded basket and uniformly distributed corrosion products. Figure 6-9 shows the geometry details of the MCNP representation for the 21 PWR WP with a fully degraded basket and settled corrosion products. Figure 6-10 shows the geometry details of the MCNP representation for the base 12 PWR WP with a fully degraded basket and uniformly distributed corrosion products. Figure 6-11 shows the geometry details of the MCNP4B2 representation for the base 12 PWR WP with a fully degraded basket and settled corrosion products. Each of the 21 PWR WP configurations was evaluated for the 4.0 wt% fissile Pu in HM, 35.6 GWd/MTHM burnup fuel (fuel #1), and the 4.5 wt% fissile Pu in HM, 39.4 GWd/MTHM burnup fuel (fuel #2), for decay times from 10 years to 250,000 years. In addition, the 12 PWR WP configuration was evaluated for the 4.0 wt% fissile Pu in HM, 50.1 GWd/MTHM burnup fuel (fuel #3).

Similar MCNP calculations were made to evaluate the k_{eff} for commercial LEU SNF in the 21 PWR WP design (CRWMS M&O 1998r, Section 6) with intact fuel and fully degraded basket structures (configuration D from Section 6.1). The commercial PWR assembly design was based on the B&W 15x15 Mark B assembly (B&W Fuel Company 1991, p. II.6-6). Since this assembly type has one of the largest fuel loadings, it is likely to provide a conservative bounding calculation for the degraded mode criticality analysis.

The criticality potential for the LEU SNF waste forms was evaluated over decay times from 10,000 to 45,000 years for a number of enrichment-burnup combinations to identify the time of peak k_{eff} (CRWMS M&O 1998r, Section 6). The MCNP geometry for the LEU SNF calculations was similar to the MOX SNF geometry shown in Figures 6-8 and 6-9. Both the uniformly distributed corrosion product and the settled corrosion product configurations were evaluated for 21 LEU PWR WP. Results from a subset of the LEU enrichment-burnup combinations which are comparable to the MOX SNF wt% fissile Pu in HM-burnup combinations are included with the MOX SNF results in this study to provide a frame of reference for the MOX SNF results. These cases are as follows: 4.0 wt% ^{235}U , 35.0 GWd/MTU and 4.5 wt% ^{235}U , 40.0 GWd/MTU. These results show that, for most configurations, the MOX SNF has a lower criticality potential (k_{eff}) than the B&W LEU SNF waste form.

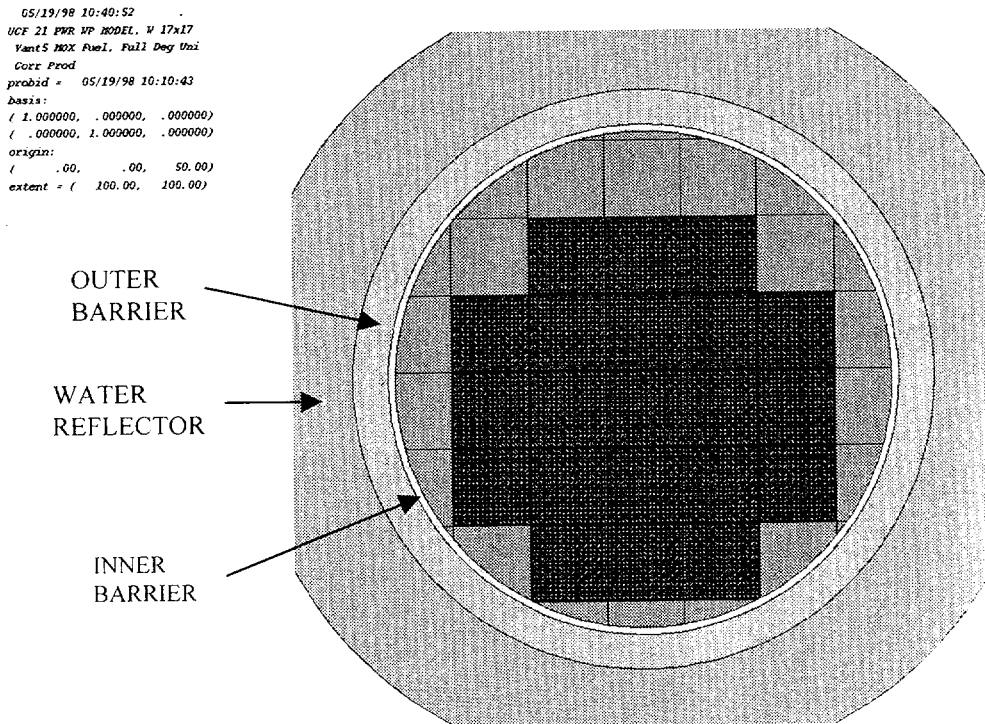


Figure 6-8. Degraded 21 PWR MOX Fuel Waste Package with Uniform Corrosion Product Distribution

```

05/19/98 10:47:04
UCF 21 PWR MP MODEL, V 17x17
YantS MOX Fuel, Full Deg Set
Corr Prod
probid = 05/19/98 10:41:32
basis:
( 1.000000, .000000, .000000)
( .000000, 1.000000, .000000)
origin:
( .00, .00, 50.00)
extent = ( 100.00, 100.00)

```

LEVEL OF
BASKET
DEGRADATION
PRODUCTS

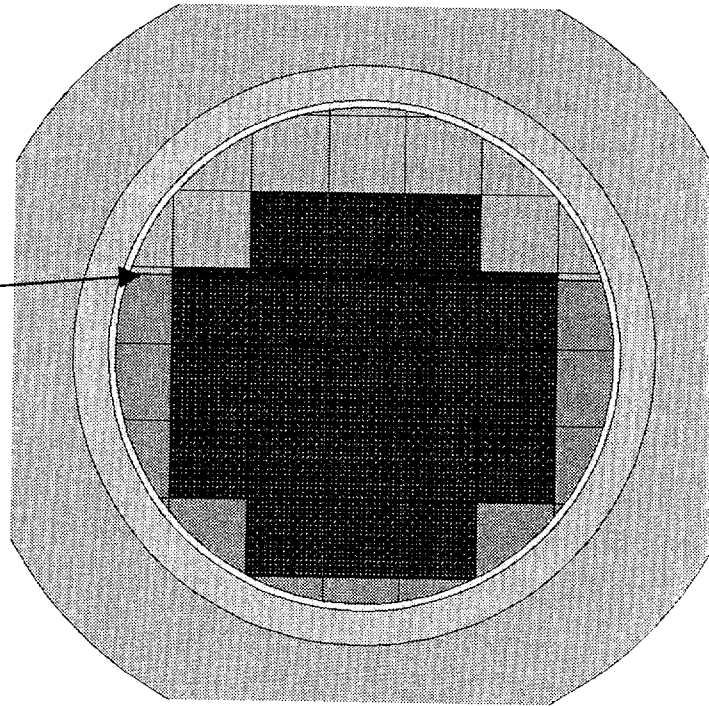


Figure 6-9. Degraded 21 PWR MOX Waste Package With Settled Corrosion Product Distribution (58% solid content)

```

03/17/98 10:49:19
Ibasit - UCF 12 MOX PWR MP, V
17x17, Deg. Basket w/ Uniform
Oxide, Flooded
probid = 03/17/98 10:40:27
basis:
( 1.000000, .000000, .000000)
( .000000, 1.000000, .000000)
origin:
( -.37, -2.55, 206.00)
extent = ( 72.39, 72.39)

```

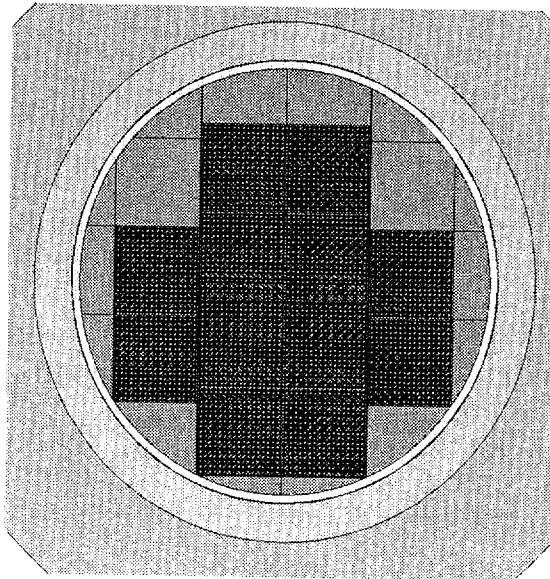


Figure 6-10. Degraded 12 PWR MOX Fuel Waste Package with Uniform Corrosion Product Distribution

```

05/27/98 11:50:04
UCF Base 12 MOX PWR WP, v 17x17
Vant5, Deg. Basket w/ Set
Oxide, Flooded
probid = 05/27/98 11:33:44
basis:
( 1.000000, .000000, .000000)
( .000000, 1.000000, .000000)
origin:
( 1.75, 1.07, 50.00)
extent = ( 70.92, 70.92)

```

LEVEL OF
BASKET
DEGRADATION
PRODUCTS

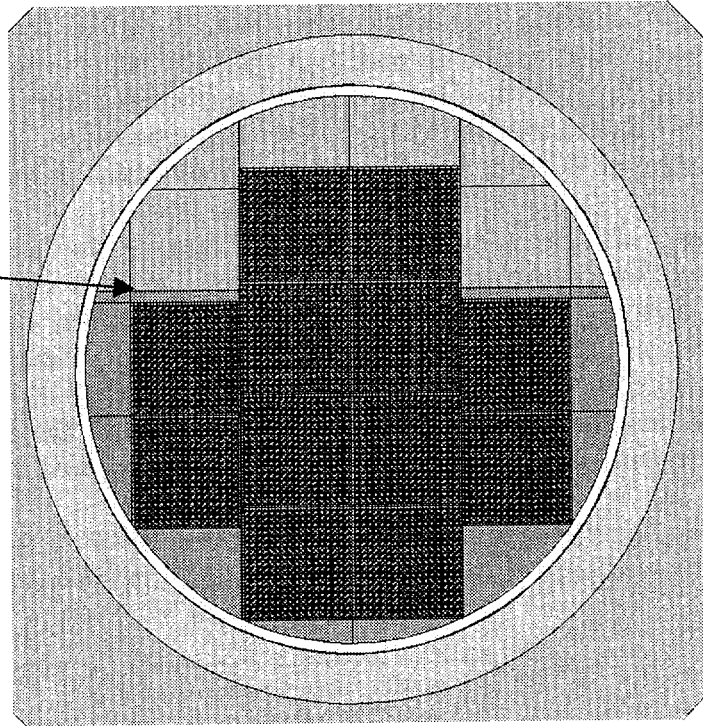


Figure 6-11. Degraded 12 PWR MOX Waste Package With Settled Corrosion Product Distribution (58% solid content)

6.1.3.3.2 Criticality Results for Intact Fuel with Fully Degraded Basket

Results of the criticality analyses of the intact fuel and degraded basket for MOX SNF in the 21 PWR WP and in the 12 PWR WP are shown (CRWMS M&O 1998c, Table 6.2-1 through Table 6.2-4, pp. 35-43) in Figures 6-12, 6-13, 6-14, and 6-15. The figures show the nominal k_{eff} with a 2σ variance shown as error bars. The time effect behavior is essentially the same as for the intact configurations.

As with the intact results presented in Section 6.1.2, all of the degraded cases for the 4.0 wt% fissile Pu in HM, 35.6 GWd/MTHM fuel consistently showed higher k_{eff} values than those for the 4.5 wt% fissile Pu in HM, 39.4 GWd/MTHM fuel. The degraded basket cases for the 21 PWR WP showed increases in k_{eff} over the intact waste package for the same fuel and decay time due to the loss of boron absorber as the B-SS absorber plates degraded. This effect, together with the fissile material inventory, more than compensated for the increased effectiveness (due to volume increase displacing moderator) of the A 516 degradation products in reducing the k_{eff} . The 58 vol% settled corrosion product case showed a 6.8% increase in k_{eff} (measured at the postclosure peak for the 4.0 wt% fissile Pu in HM, 35.6 GWd/MTHM fuel, Fig. 6-13 compared with Fig. 6-4) from the intact configuration, while the uniform corrosion product case showed only a 4.1% increase (Fig. 6-12 compared with Fig. 6-4).

Figures 6-12 and 6-13 also show the k_{eff} results from the LEU SNF calculations of intact fuel and fully degraded baskets. For decay times around 10,000 years the k_{eff} generally reaches a secondary peak. This secondary peak is always lower than the 10-year decay values. The k_{eff} values for the LEU SNF cases are up to 4% higher than for the corresponding MOX SNF cases. Therefore, it is concluded that MOX SNF does not pose any greater, and likely less, criticality concerns in the 21 PWR WP than does LEU SNF of similar burnup and fissile content.

The degraded basket cases for the 12 PWR WP actually showed decreases in k_{eff} over the intact waste package for the same fuel and decay time. This is due solely to the increased volume of the carbon steel degradation products displacing moderator. Unlike the 21 MOX PWR WP, there is no boron to be lost in the basket degradation process and, therefore, no compensating increase in k_{eff} . The 58 vol% settled corrosion product case showed a 4.3% decrease in k_{eff} (measured at the post-closure peak for the 4.0 wt% fissile Pu in HM, 50.1 GWd/MTHM fuel) from the intact configuration, while the uniform corrosion product case showed a 6.8% decrease.

The k_{eff} values were sufficiently far from critical values (0.75 maximum) that a criticality event is virtually impossible and no comparisons with LEU SNF were necessary.

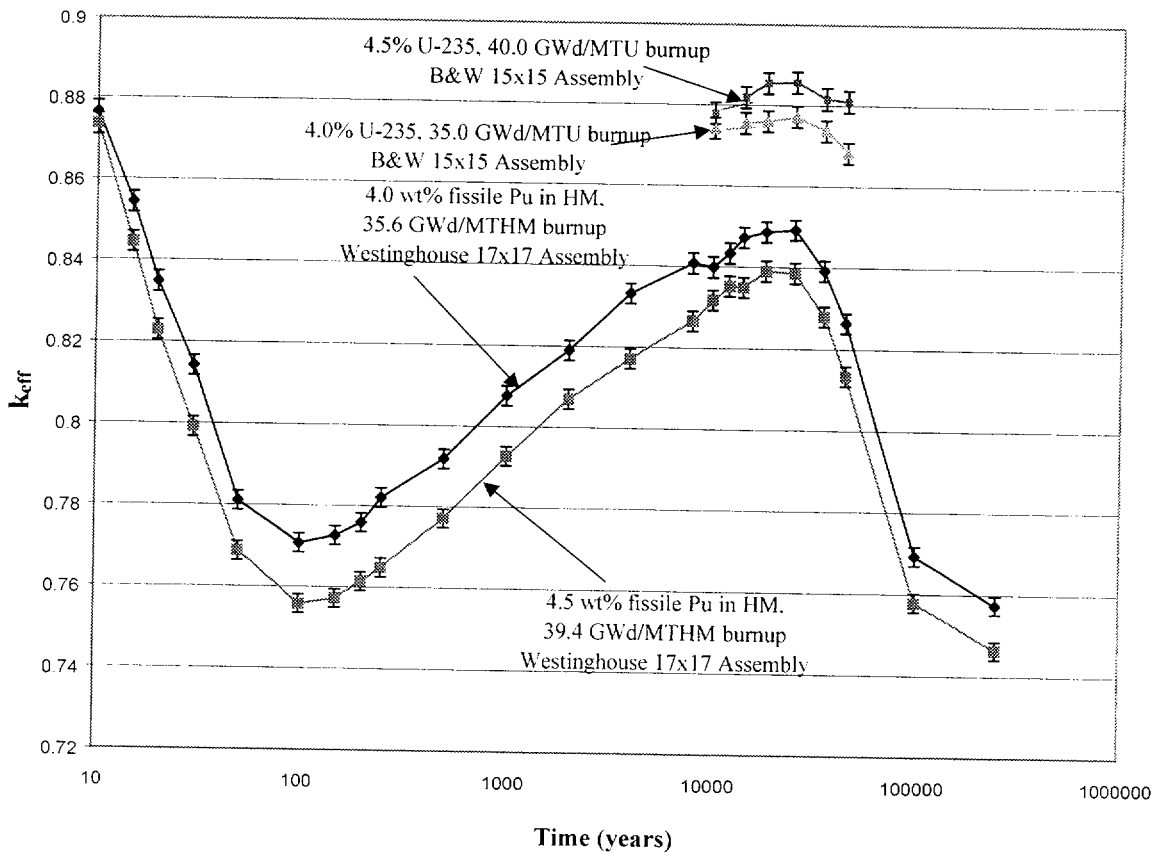


Figure 6-12. Time Effects on k_{eff} for Intact MOX and LEU SNF in a 21 PWR WP with a Fully Degraded Basket (No Boron Remaining) and Uniformly Distributed Corrosion Products

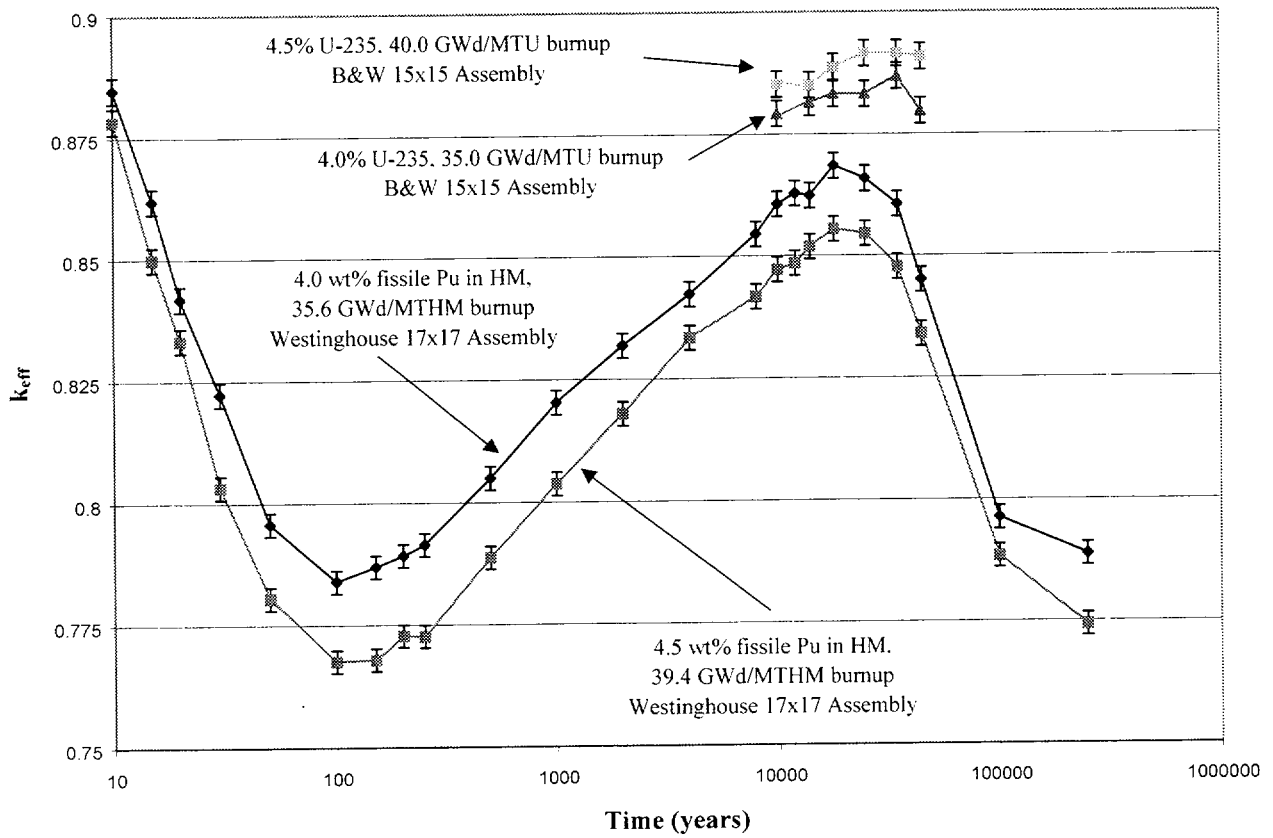


Figure 6-13. Time Effects on k_{eff} for Intact MOX SNF in a 21 PWR WP with a Fully Degraded Basket (No Boron Remaining) and Settled Corrosion Products

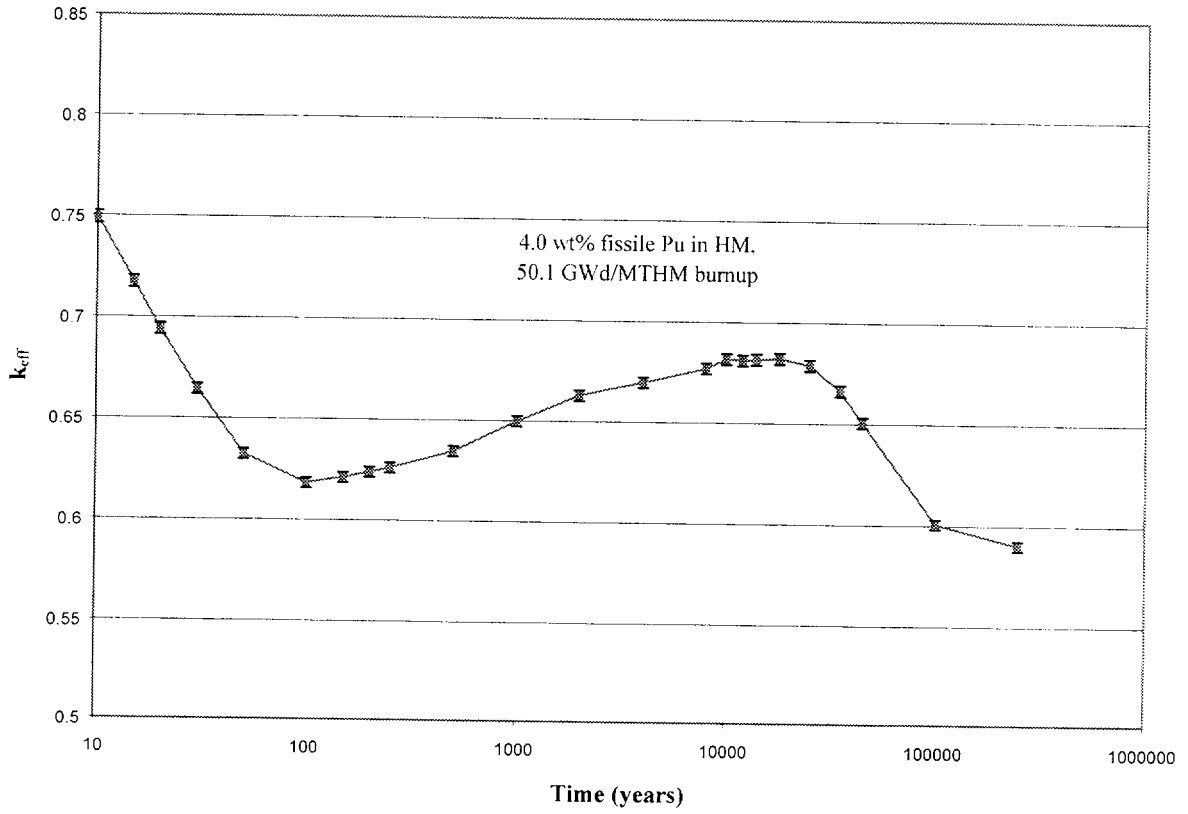


Figure 6-14. Time Effects on k_{eff} for Intact MOX SNF in a 12 PWR WP with a Fully Degraded Basket and Uniformly Distributed Corrosion Products

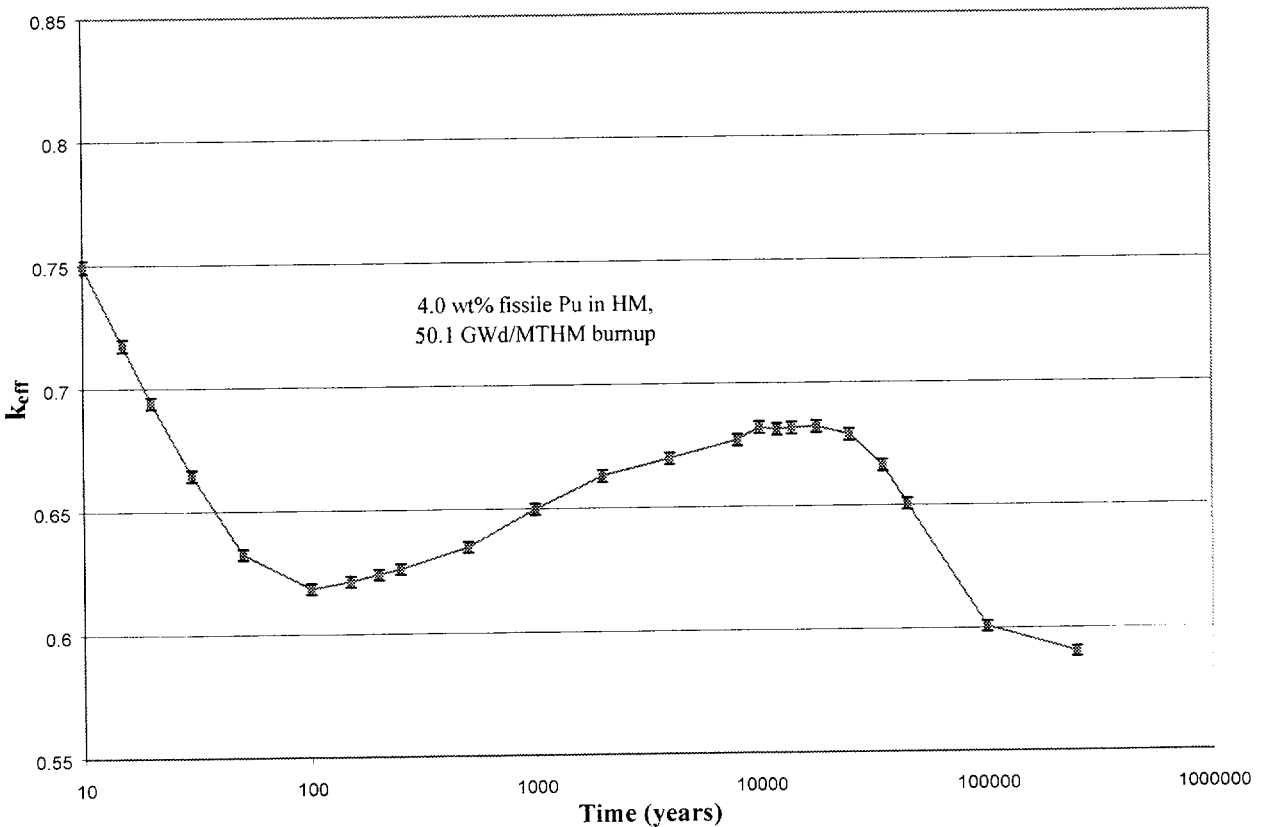


Figure 6-15. Time Effects on k_{eff} for Intact MOX SNF in a 12 PWR WP with a Fully Degraded Basket and Settled Corrosion Products

6.1.3.3.3 Simultaneous Matrix Degradation, Assembly Collapse and Iron Oxide Loss

The purpose of this section is to summarize a recent parametric study (CRWMS M&O 1999h) of effects of various degradation parameters on the reactivity of a WP containing MOX spent fuel. Previous calculations (CRWMS M&O 1998c) have shown that the criticality control features of the waste package are adequate to prevent criticality of a waste package filled with water for all the burnup-enrichment pairs expected for the MOX SNF. In this section, the increase in reactivity resulting from the range of degradation parameters of the waste package criticality control features will be determined. Specifically, this section tests the sensitivity of k_{eff} to loss (from the waste package) of the following: (1) fission product neutron absorbers, or (2) iron oxide that results from the corrosion of steel. The calculations using MCNP4B2 provide the neutron k_{eff} for the spent MOX fuel configurations shown in Figure 6-16 (CRWMS M&O 1999h, Fig. 5-1) for the nominal pitch and fully collapsed cases.

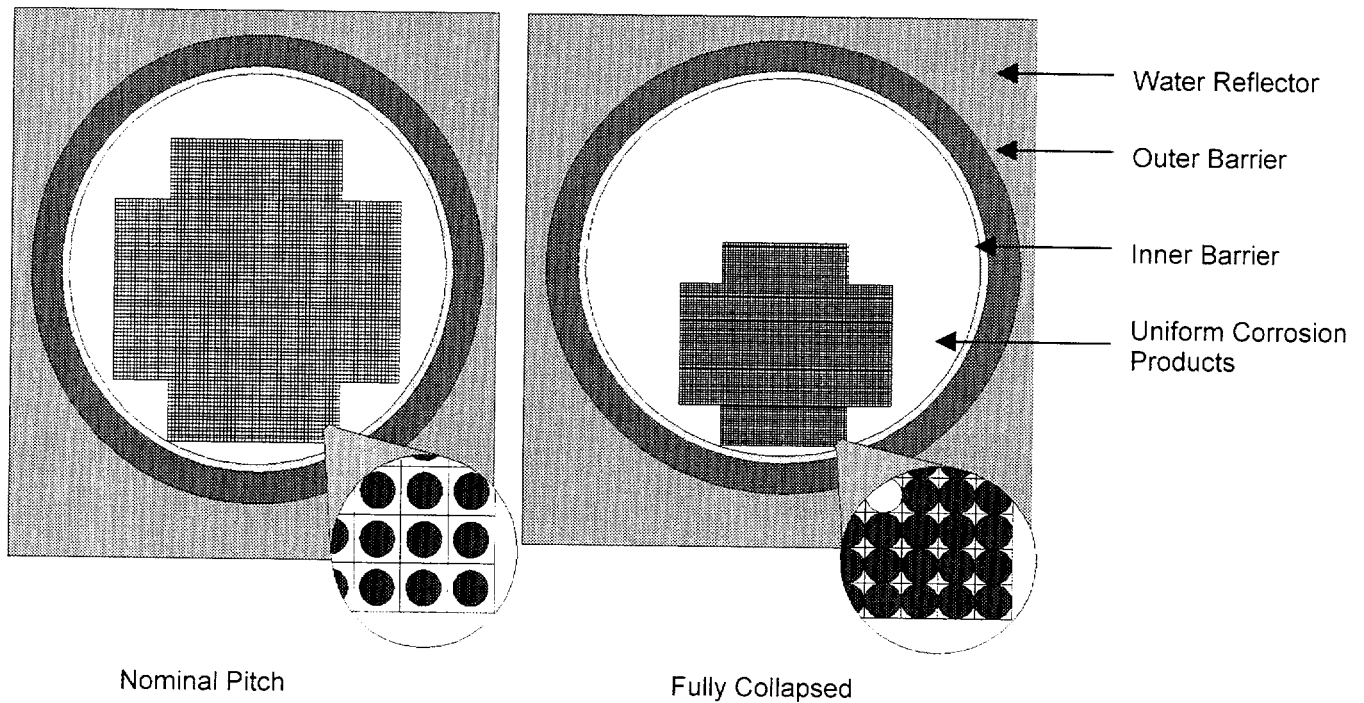


Figure 6-16. Degraded 21 PWR Fuel Waste Package with Uniform Corrosion Product Distribution

This calculation (CRWMS M&O 1999h, Section 5.2) involves varying five parameters: burnup-enrichment, decay time, rod spacing, fission product concentration, and iron oxide concentration. The first two parameters, burnup-enrichment and decay time, affect the atom densities of all of the isotopes in the fuel material.

The third parameter, rod spacing, affects the neutron spectrum of the system, by varying the amount of moderator (water) interspersed through the lattice. The rod spacing is decreased in steps of 25% of the original spacing.

The fourth parameter is fission product concentration. This parameter affects the amount of parasitic absorption (absorption other than fission) occurring in the fuel material. All fission products are conservatively assumed to have the same average solubility while U and Pu isotopes are assumed to be insoluble. The amount (atom density) of fission products in the fuel is decreased in steps of 25% of the original amount, while the atom densities for the actinides and for oxygen remain unchanged. This is intended to represent Fission Product Loss (FPL) over time.

The fifth parameter is iron oxide concentration. This parameter affects the amount of parasitic absorption and the moderator displacement occurring in the moderator material interspersed through the lattice. The amount (moles) of the iron oxide, in the form of hematite (Fe_2O_3), in the water is decreased by up to 75% in four steps (10%, 25%, 50%, and 75% of the original amount). The hematite is replaced with water (H_2O).

The presentation of results is arranged to emphasize the sensitivity of k_{eff} to the most relevant parameters associated with waste package degradation. The cases varying these degradation parameters are divided into two major sets. Tables 6-2 and 6-3 emphasize the variation of k_{eff} with fission product loss for a range of times since discharge and degree of assembly collapse (or interpin pitch) for the 4%, 35.6 GWd/MTHM fuel. In each of these two tables, the individual tables correspond to different degrees of collapse: 0% and 100%. These correspond to a square lattice with the following interpin spacings (center to center, cm): 1.260 and 0.914. Each of these tables is divided into four blocks according to the time since discharge, 10, 25, 45, and 100 thousand years. Within each block the lines cycle through the values of fission product loss: 0%, 25%, 50%, 75%, and 100%.

Table 6-4 emphasizes the variation of k_{eff} with iron oxide loss for a range of times since discharge and degree of assembly collapse (or interpin pitch). Fewer cases were run for this set, corresponding to only two time values (25,000 and 100,000 years) and only two degrees of collapse (0 and 100%), hence the fewer number of tables and the fewer lines per table.

Figure 6-17 is a plot of k_{eff} as a function of fission product loss at the two extreme collapse rates of 0 and 100% and at decay times of 25,000 and 100,000 years for the 4.0 wt%/35.6 GWd/MTHM fuel, which is the fuel with the higher reactivity. Figure 6-18 is a plot of k_{eff} as a function of hematite loss at the two extreme collapse rates of 0 and 100% and at decay times of 25,000 and 100,000 years for the same fuel type. Both figures show an increase in k_{eff} with increase in the independent degradation parameter, fission product loss and iron oxide loss, respectively. There is, however, one significant distinction. All the curves in Figure 6-17 (which are approximately straight lines) are approximately parallel, indicating that the k_{eff} increase with increasing fission product loss is relatively independent of assembly collapse. Figure 6-18 shows that the slope of the lines decreases with increasing collapse. This is because the collapsed configuration has little room for iron oxide between the fuel pins, so the loss of iron oxide does not make much difference.

Table 6-2. Results for the 4.0 wt%/35.6 GWd/MTHM Fuel, 0% Collapse (CRWMS M&O 1999h, Table 6-1)

Decay (yrs.)	Δ_f (%)	k_{eff}	σ
10,000	0	0.83855	0.00125
10,000	25	0.85792	0.00118
10,000	50	0.87967	0.00135
10,000	75	0.90477	0.00125
10,000	100	0.92546	0.00115
25,000	0	0.84689	0.00116
25,000	25	0.86969	0.00116
25,000	50	0.89478	0.00105
25,000	75	0.92102	0.00155
25,000	100	0.94725	0.00114
45,000	0	0.82322	0.00129
45,000	25	0.85307	0.00119
45,000	50	0.87607	0.00116
45,000	75	0.90313	0.00110
45,000	100	0.93413	0.00129
100,000	0	0.77119	0.00099
100,000	25	0.80710	0.00106
100,000	50	0.82493	0.00088
100,000	75	0.85406	0.00122
100,000	100	0.88775	0.00084

Table 6-3. Results for the 4.0 wt%/35.6 GWd/MTHM Fuel, 100% Collapse (CRWMS M&O 1999h, Table 6-5)

Decay (yrs.)	Δ_f (%)	k_{eff}	σ
10,000	0	0.71093	0.00128
10,000	25	0.72484	0.00128
10,000	50	0.74631	0.00115
10,000	75	0.76518	0.00146
10,000	100	0.78893	0.00137
25,000	0	0.72547	0.00123
25,000	25	0.74631	0.00128
25,000	50	0.76777	0.00138
25,000	75	0.79567	0.00136
25,000	100	0.82162	0.00135
45,000	0	0.72511	0.00126
45,000	25	0.74918	0.00139
45,000	50	0.77495	0.00109
45,000	75	0.80146	0.00112
45,000	100	0.83403	0.00149
100,000	0	0.69360	0.00120
100,000	25	0.73466	0.00131
100,000	50	0.74730	0.00118
100,000	75	0.77665	0.00093
100,000	100	0.81507	0.00113

Table 6-4. Results of the Iron Oxide for 4.0 wt%/35.6 GWd/MTHM Fuel (CRWMS M&O 1999h, Table 6-11)

$\Delta_{Fe_2O_3}$ (%)	Δ_s (%)	Decay (yrs.)	k_{eff}	σ
0	0	25,000	0.84689	0.00116
10	0	25,000	0.86085	0.00140
25	0	25,000	0.88371	0.00107
50	0	25,000	0.91950	0.00106
75	0	25,000	0.95234	0.0014
0	100	25,000	0.72547	0.00123
10	100	25,000	0.73440	0.00095
25	100	25,000	0.74537	0.00105
50	100	25,000	0.76436	0.00138
75	100	25,000	0.78441	0.00131
0	0	100,000	0.77119	0.00099
10	0	100,000	0.78719	0.00109
25	0	100,000	0.80619	0.00107
50	0	100,000	0.84332	0.00101
75	0	100,000	0.88409	0.00106
0	100	100,000	0.69360	0.00120
10	100	100,000	0.70139	0.00107
25	100	100,000	0.71517	0.00108
50	100	100,000	0.72881	0.00127
75	100	100,000	0.74765	0.00138

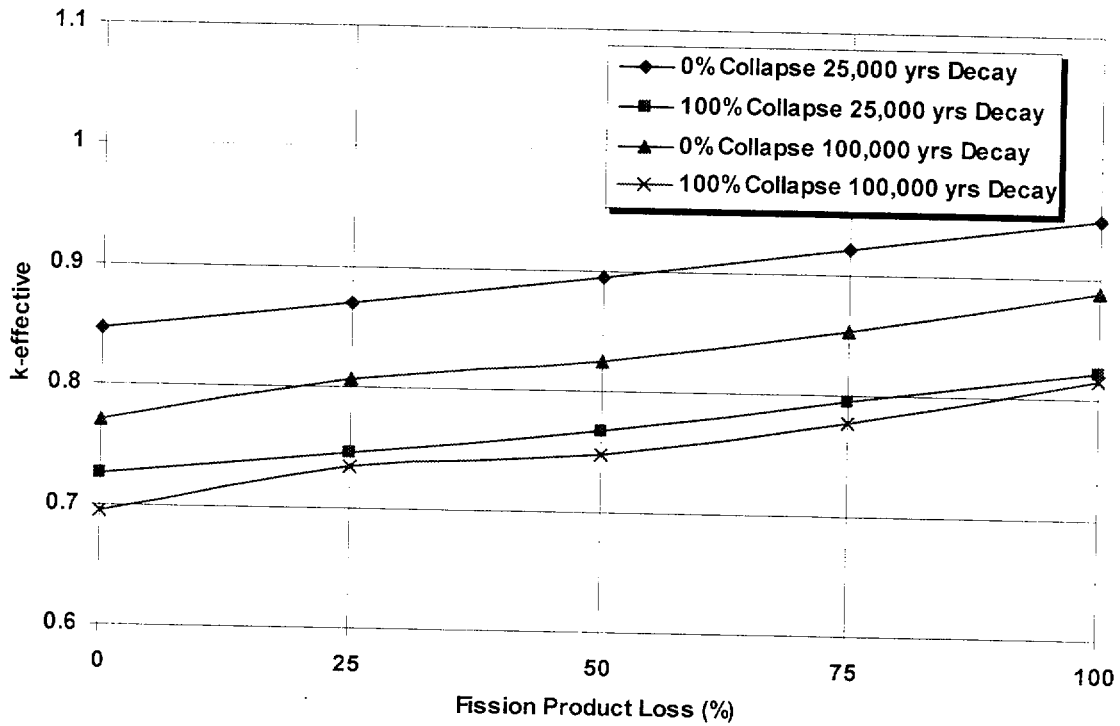


Figure 6-17. k_{eff} as a Function of Fission Product Loss (4.0 wt%, 35.6 GWd/MTHM) (CRWMS M&O 1999h, Fig. 6-1)

These results show that criticality (defined as $k_{eff} > 0.92$) is not possible for the MOX SNF, unless most of the fission products are lost and/or most of the iron oxide is lost while the assembly remains largely uncollapsed. It is possible to construct a curve of constant k_{eff} for fission product loss and for collapse, or for iron oxide loss and collapse. However, such results are most meaningful when used with probability distributions of these parameters to obtain an estimated of expected number of criticalities as a function of time. Such an analysis is given in Section 6.3.

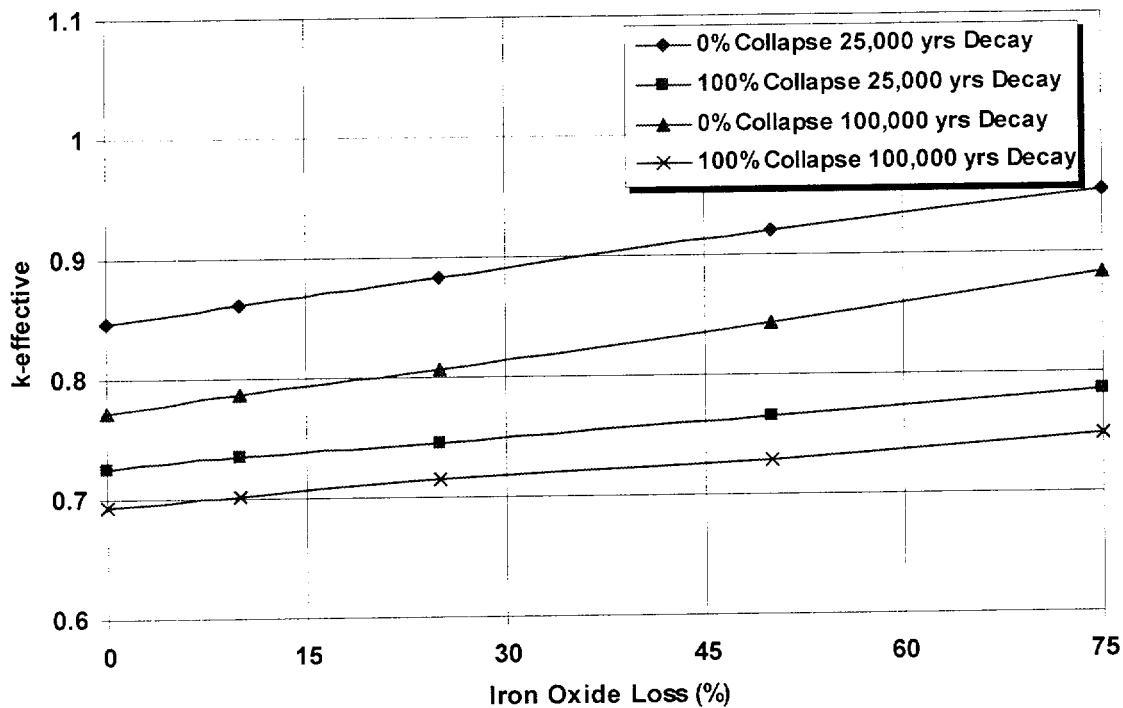


Figure 6-18. k_{eff} as a Function of Iron Oxide Loss (4.0 wt%, 35.6 GWd/MTHM) (CRWMS M&O 1999h, Fig. 6-2)

6.1.3.3.4 Configurations for Degraded Fuel and Fully Degraded Basket

The MCNP4B2 cases needed to evaluate the k_{eff} of the 21 PWR MOX SNF waste package design with fully degraded basket structures and fuel that is partially (structurally intact but allows water to fill the gap region) or fully degraded (configurations E and F from Section 6.1) are described in this section. Configuration E was represented by settling fuel rods into a cylinder segment at the bottom of the waste package in a square lattice arrangement, as is shown in Figure 6-19. The square lattice is the most conservative with respect to criticality since space is available for moderator in the lattice. A more likely arrangement such as a close packed one is less conservative because of greater moderator exclusion evaluated (CRWMS M&O 1998c, Section 6.3). The height of the cylinder segment was calculated to be that which would give a volume equal to 5544 fuel rods (264 rods/assembly x 21 assemblies) in a square lattice at a given pitch. Lattice pitches ranging from 0.9144 cm (rods touching) to 1.2598 cm (as-built fuel rod pitch) were evaluated (CRWMS M&O 1998c, Section 6.3) to represent the range of possible separations between collapsed rods which is expected to be less than the original pitch. The k_{eff} in this sensitivity study decreased as the pin pitch decreased.

The fuel rods were represented explicitly and contained water in the gap region. Only a uniform corrosion product distribution of 36.8 vol% (see Section 6.1.3.3) was evaluated. Cases were run with full isotope burnup credit, as well as for the reduced principal isotope conditions.

The fully degraded fuel and basket configuration (Configuration F) was represented by homogenizing the remaining principal isotopes, zircaloy, and basket corrosion products in the waste package interior volume. The volume of degraded fuel material was assumed to be that which would occur if all of the initial UO₂ degraded to soddyite ([UO₂]₂SiO₄:2H₂O), as is indicated in the geochemistry calculations (CRWMS M&O 1998d). Additional Si, H, and O were also added to the mixture to account for what will be present if the fuel degraded to soddyite. The volume of zircaloy was equivalent to that contained in the cladding and guide tubes of 21 Vantage 5 SNF assemblies. All together, the degraded fuel, zircaloy, and basket corrosion products occupied 62.5% of the waste package interior volume. Water was assumed to fill the remaining void space. Figure 6-20 shows the geometry details of the MCNP4B2 representation for the 21 PWR WP with fully degraded fuel and basket corrosion products uniformly distributed. Cases were run with reduced principal isotopes resulting from 17,500 years of radioactive decay and geochemical degradation. For comparison purposes only, a worst case was run for U and Pu isotopes only with all absorber isotopes removed.

Each of these configurations was evaluated with the most reactive fuel (4.0 wt% fissile Pu in HM, 35.6 GWd/MTHM burnup fuel) for decay times from 1,000 to 250,000 years.

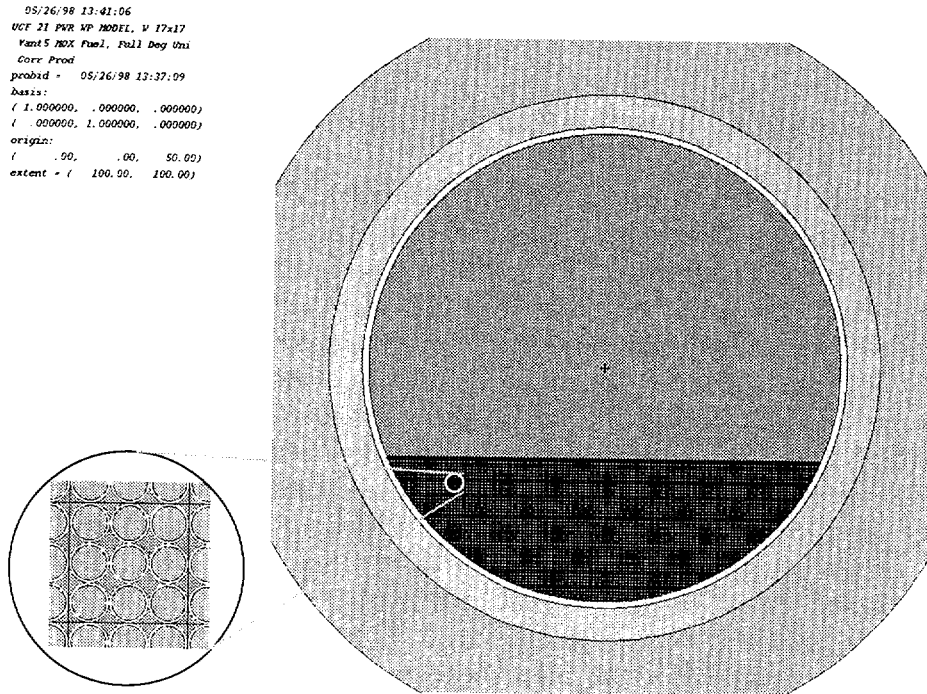


Figure 6-19. Degraded 21 PWR MOX WP with Fuel Rods Collapsed to Bottom of Package Surrounded by Uniformly Distributed Basket Corrosion Products

```

05/26/98 13:19:45
OCT 21 PWR WP MOX Fuel,
Full Deg Basket & Fuel Uni Corr
Prod
period = 05/26/98 13:18:46
basis:
( 1.000000, .000000, .000000)
( .000000, 1.000000, .000000)
origin:
( 00, 00, 00.00)
extent = ( 100.00, 100.00)

```

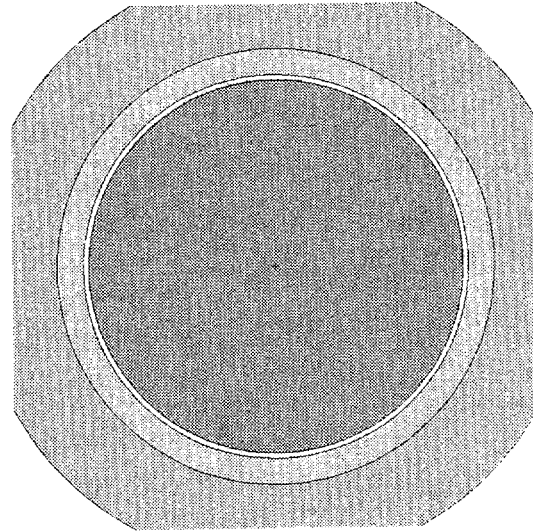


Figure 6-20. Fully Degraded Fuel and Basket Material Uniformly Distributed Throughout Interior Volume of 21 PWR WP

6.1.3.3.5 Criticality Results for Degraded Fuel and Fully Degraded Basket

Results of the criticality analyses of the 21 MOX PWR WP with a fully degraded basket, minimally spaced collapsed fuel rods (0.9144 cm), and a uniform corrosion product distribution are given in Table 6.3-1 of CRWMS M&O (1998c, p. 46). The maximum k_{eff} value was less than 0.675 for these cases, well below the critical limit of 0.92, as shown in Figure 6-21 (MOX labels). All values are for a rod center-to-center spacing of 0.9144 cm (rods touching in square lattice) representative of a nominal configuration. (Note: Nominal configuration; sensitivity to rod spacing is discussed below.) The ultra-conservative assumption (because of the low corrosion rate of zircaloy compared to carbon steel) that SNF degradation begins simultaneously with the baskets (see Section 6.3.2) is made in two of the analyses shown in Figure 6-21 (MOX Curves A and C). A more realistic SNF degradation assumption, where loss of the principal isotopes begins at 10,000 years after the start of basket degradation (MOX Curve B in Fig. 6-21), shows a moderate increase in k_{eff} over time relative to the early loss of the principle isotopes. Also of interest are the reduced peak-and-valley effect with time and the movement of the peak k_{eff} out to ~ 45,000 years. Both effects result from increased resonance absorption due to the harder spectrum of this configuration. The location of the peak shifts outward in time because the increased absorption in ^{240}Pu in a harder spectrum is not matched by an equal increase in ^{239}Pu fission. Thus, longer decay times are required to eliminate the absorption effect from ^{240}Pu .

Results from a similar analysis for the 21 LEU PWR WP (fully degraded baskets, minimally spaced collapsed fuel rods, and uniform corrosion products) (CRWMS M&O 1998p, Section 6) are also shown in Figure 6-21 with the LEU labels. This case utilized the 4.0 wt% ^{235}U , 35.0 GWD/MTU LEU SNF with a 1.0922 cm square pitch (normal pitch is 1.44272 cm). The MOX SNF k_{eff} s were less than those from the similar LEU SNF cases; the maximum LEU SNF k_{eff} was approximately 0.7.

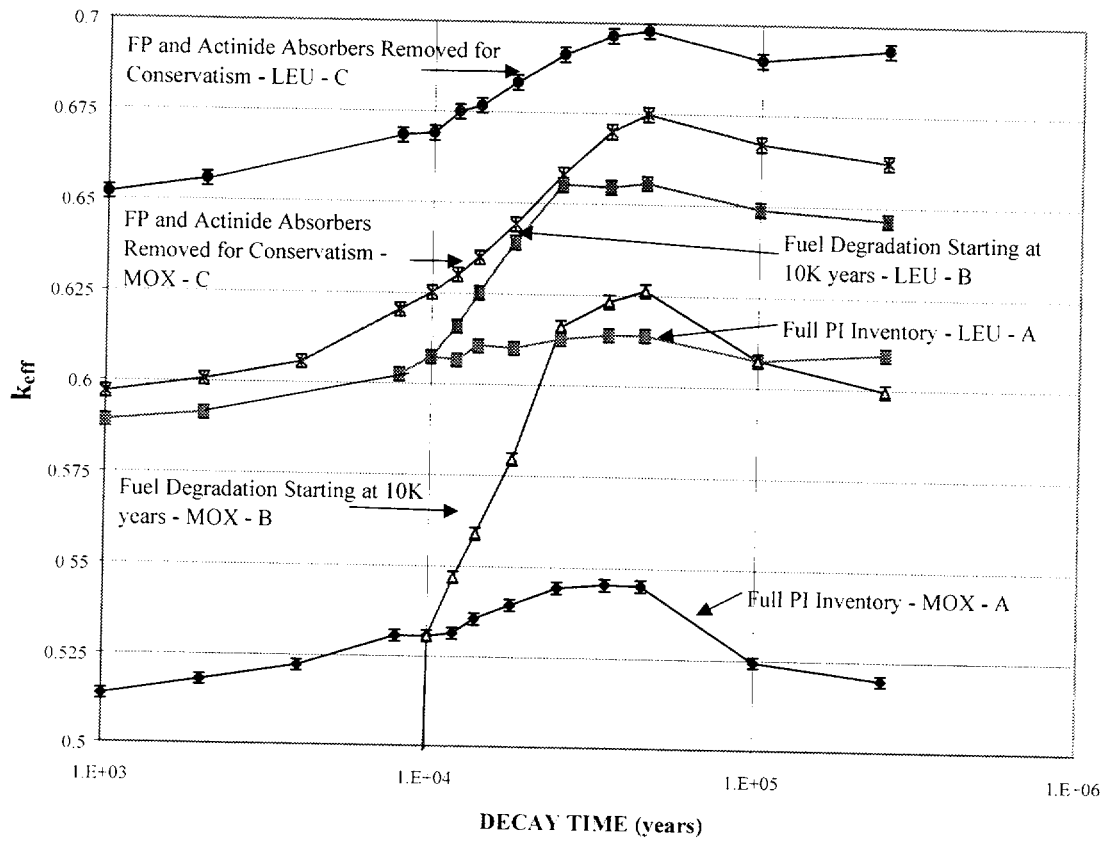


Figure 6-21. Time and Fuel Degradation Effects on k_{eff} for 21 PWR WP with a Fully Degraded Basket, Square Lattice Collapsed Rods (MOX and LEU), and Uniformly Distributed Corrosion Products

Results of the 18,000 and 45,000 year MOX SNF cases run for various fuel rod spacing, up to the original pitch of 1.2598 cm showed that the optimum point of moderation occurs at the original assembly pitch. However, the k_{eff} values only exceeded those of the 21 PWR WP in Configuration D with settled oxide (see Section 6.1) under the combination of extreme fuel degradation (U and Pu principal isotopes only) and rod spacing within ~1 mm of the original pitch. This is not a likely situation, as the original rod geometry (much less the spacing) would not be expected to be retained at such a degree of fuel degradation.

Figure 6-22 shows the k_{eff} results for the fully degraded fuel and basket configuration (Configuration F, Section 6.1 and Fig. 6-20) for both the MOX SNF and the LEU SNF. Note that for this case, the peak k_{eff} for the LEU SNF is approximately 4% less than the MOX SNF value of 0.845. This is well below the critical value of 0.92.

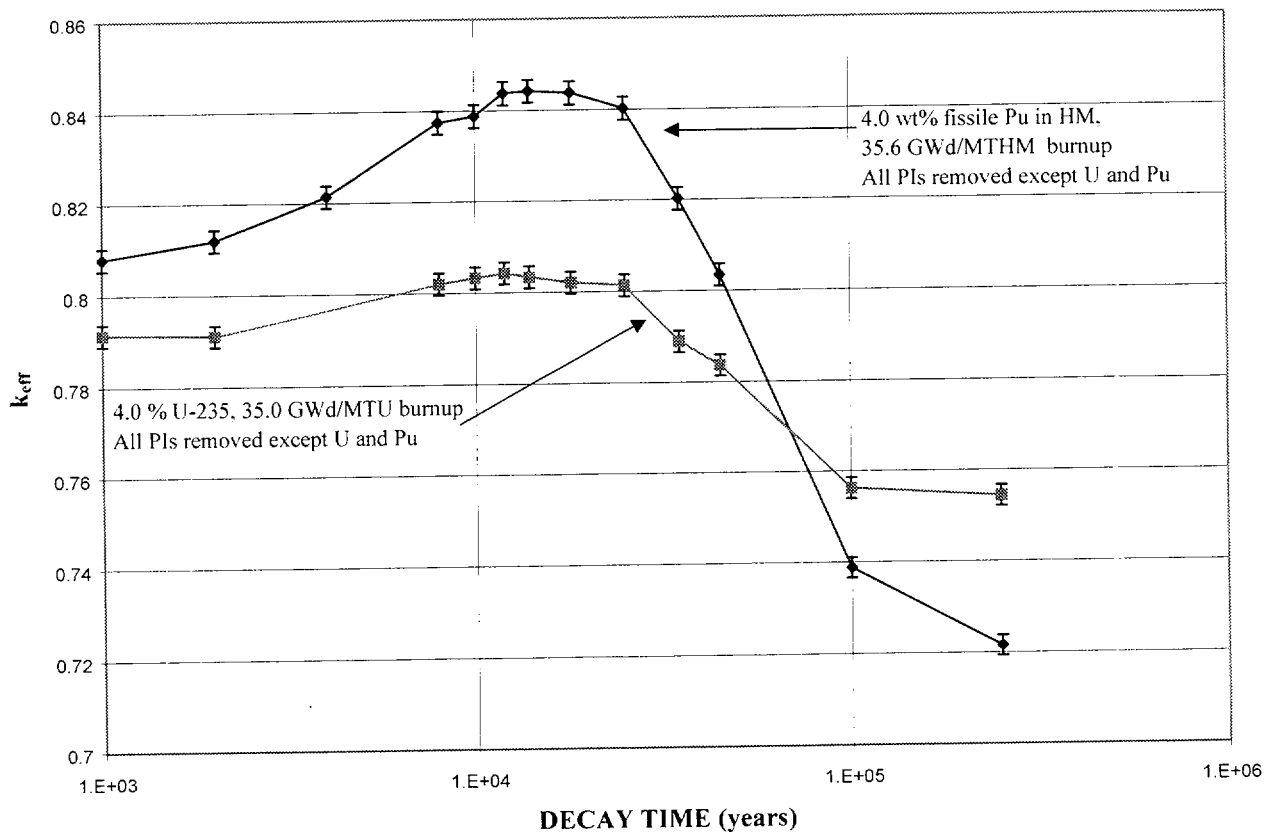


Figure 6-22. Time and Fuel Degradation Effects on k_{eff} for a 21 PWR WP with Fully Degraded Basket and Fuel, and Uniformly Distributed Corrosion Products

6.1.4 Summary of Evaluation of Potential Critical Configurations

Criticality evaluations were performed for the 21 PWR MOX SNF WP and the 12 PWR MOX SNF WP for conditions ranging from intact to fully degraded fuel and baskets. The k_{eff} s peaks are shown in Table 6-5. The following observations on the criticality potential of the PWR MOX SNF can be made:

1. The worst case k_{eff} is below the criticality limit of 0.92 for all waste package designs examined for any credible waste package internal configuration and thus a criticality event is incredible.
2. The 12 PWR WP (last column of Table 6-5) has a higher k_{eff} than the 21 PWR WP for the intact fuel and intact basket because this waste package has no neutron absorber plates (both WP's filled with water).

The 12 PWR WP (last column of Table 6-5) has a lower k_{eff} than the 21 PWR WP for the intact fuel and degraded basket because the iron oxide corrosion products displace more moderator compensating, in part, for the absence of absorber plates (both WP's filled with water).

Table 6-5. Peak k_{eff} for Degraded PWR MOX SNF

SNF Configuration	Burnup (GWd/MTHM)		
	35.6 (4.0 wt% fissile Pu in HM)	39.4 (4.5 wt% fissile Pu in HM)	46.5 (4.5 wt% fissile Pu in HM)
	21 PWR WP	21 PWR WP	12 PWR WP
Intact Fuel, Intact Basket	0.84	0.84	0.86
Intact Fuel, Degraded Basket	0.89	0.88	0.81
Partially Collapsed and Degraded SNF—Full PIs	0.55	N/A ^a	N/A
Partially Collapsed and Degraded SNF – Pu and U PI	0.67	N/A	N/A
Fully Degraded Basket and SNF	0.84	N/A	N/A

^a N/A—Case not run.

6.2 CERAMIC

The degradation analysis methodology for the waste package with plutonium immobilized in ceramic is discussed in Section 6.2.1. The criticality evaluations relating to intact waste forms are given in Section 6.2.2. The chemical and physical descriptions of the degraded configurations, together with the results of the criticality analyses of these configurations are given in Section 6.2.3.

6.2.1 Disposal Criticality Analysis Methodology Applied to Ceramic

In this section the methodology for computing k_{eff} values for intact and various degraded waste package configurations uses the Monte Carlo N-Particle Code MCNP, Version 4B2 (Briesmeister 1997) (CRWMS M&O 1998q). MCNP4B2 identified as CSCI 30033 V4B2LV is qualified as documented in the SQR (CRWMS M&O 1998q).

The following is an evaluation of each of the internal criticality configuration classes of the *Disposal Criticality Analysis Methodology Topical Report* (YMP 1998, Section 3.1.1) applied to the immobilized plutonium (ceramic) waste package:

1. This class does not apply because there is no basket.
2. This class does not apply because there is no basket.
3. Fissionable material mobilized (dissolved) and moved away from the neutron absorber material. This configuration does not apply because the fissionable material is insoluble and cannot be easily mobilized.
4. Fissionable material accumulates at the bottom of the waste package. This configuration class could also apply to the case of fully degraded waste package contents but has been

found, in a previous study (CRWMS M&O 1998t), to be less reactive than the homogeneous distribution of Class 5, below. In that document, Table 6.5.1.1-3 was typical of the completely homogenized distribution; Table 6.5.1.2-1 was typical of fissile material mixed with clay at the top; and Table 6.5.1.3-2 was typical of fissile material mixed with clay at the bottom. A variant of this configuration class is applied to the partly degraded configuration discussed in Section 6.2.3.2.1. In that case the fissile material remains in the ceramic disks, while the Gd neutron absorber is spread uniformly throughout the water filled waste package. This case omits all the other degradation products, in order to focus on the worst case separation of fissile material from neutron absorber.

5. This class is similar to Class 4 above but with the fissionable material distributed throughout a major fraction of the waste package volume. This class is most likely to occur when the waste form degrades faster than the other internal components, so that its degradation products may be released before the intact waste forms can fall to the bottom through the clay from the degraded glass. The immobilized plutonium waste form is generally considered to degrade slower than the other internal components, so this class would not ordinarily occur. However, it is possible for a radiation-damaged ceramic to degrade faster than the glass. The geochemistry analysis in Section 6.2.3.1 shows that the highest loss of the gadolinium neutron absorber occurs if the ceramic and steel components degrade much faster than the glass, which puts the configuration in this class. Therefore, this class is the subject of most of the ceramic geochemistry analysis in this document and most of the ceramic criticality analysis.
6. This class has the waste form degrading while the other components remain completely intact. It is not relevant to the plutonium ceramic waste package that has the other internal components protecting the waste form itself. There is no way that the ceramic waste form can degrade until the other components (can, glass, and canister) have degraded enough to permit the water to reach it. There is no way for the ceramic degradation products to move somewhere until the other components have degraded sufficiently to get out of the way.

The degraded configurations actually evaluated for criticality are described in Section 6.2.3.2.

6.2.2 Criticality Evaluations Relating to Intact Configurations

The intact configuration is described in Sections 2.2.2 and 2.2.3 for the ceramic disk canister containing 28 cans of 20 disks each and the waste package containing 5 canisters.

Criticality Calculations for Intact Configurations—The k_{eff} of the intact configuration has been estimated under two conditions: (1) no water in the waste package, and (2) water in the void spaces within the canister and waste package. The values are $k_{\text{eff}} = 0.12$, and 0.11, respectively (CRWMS M&O 1998u, Table 6-5). Because these k_{eff} values are very small, their time histories are not reproduced here. Such low values of k_{eff} result from the relatively large loading of the ceramic waste form with the neutron absorber materials, gadolinium and hafnium (the former being particularly effective in the thermal region of the neutron spectrum) (Parrington et al. |

1996). While the heavy loading with neutron absorber is unnecessary for intact criticality control, it is important for criticality control in the degraded configurations (Section 6.2.3).

6.2.3 Criticality Evaluations Relating to Degraded Configurations

6.2.3.1 Geochemistry Evaluations of the Degradation Processes and Scenarios

This section provides a summary of the geochemistry evaluations of the ceramic waste package degradation processes and scenarios (CRWMS M&O 1999c). These geochemistry evaluations represent significant refinements from the previous study (CRWMS M&O 1998o, Volume II, Section 3.3.1) and have resolved several issues relating to the impact of parameter uncertainty.

Section 6.2.3.1.1 provides a summary of the improved form of the geochemistry code EQ3/6, called solid centered flow through (SCFT). This more precise representation is necessary for the ceramic degradation products because this waste form makes strong use of criticality control material in the waste form itself. Section 6.2.3.1.2 provides a summary of three geochemistry sensitivity studies that involve the geochemistry parameter sets having the greatest uncertainty. These sensitivity studies are particularly important for the ceramic waste form because there is a need to convincingly demonstrate the very low solubility of the principal neutron absorbers, Gd and Hf. Section 6.2.3.1.3 provides a summary of the actual results of the geochemistry evaluations, showing the worst case Gd loss from the waste package.

6.2.3.1.1 Degradation Methodology and Scenarios

This section describes the solid centered flow through methodology developed for the analysis to meet the comprehensive geochemistry requirements of the ceramic waste form criticality evaluation. Also summarized are the scenarios leading to the largest possible Gd loss (from the waste package). These are found to provide a greater Gd loss than was found in the previous study (CRWMS M&O 1998o, Volume II, Section 3.3.1). However, the scenarios leading to the highest Gd loss are very unlikely (Section 6.2.3.1.4).

Solid Centered Flow through Methodology—This section presents a major improvement in the EQ3/6 methodology over the pseudo flow-through methodology used for the MOX SNF degradation evaluations, Section 6.1.3.1. As with the earlier methodology, the calculations are performed for a unit mass of solution, typically 1 kilogram, within the waste package. Amounts of reactants to be input for this unit mass are determined by scaling the total waste package inventory (and reactant surface areas) according to the amount of water calculated to be in the waste package. Reactants are input in two modes, (1) initial amounts of solute for each dissolved species and (2) reagents which are added continuously (actually in discrete increments at each time step), primarily to simulate the elements that can go into solution or transform into solid corrosion products as the solid materials (waste form (WF) and other internal components (OIC), degrade).

In the pseudo flow-through method, the removal of water was simulated by restarting the program, after the water has built up to 20% above its initial volume, with the total mass of water reduced to the original amount. For this study, the EQ3/6 code was modified with an addendum

to perform the removal of water at each timestep, permitting a more constant volume of solution in the waste package. Details of this SCFT code are given in CRWMS M&O (1999c, Section 4.2). The documentation of this code is given in CRWMS M&O (1999i). As with earlier versions of EQ3/6, all degradation products of the individual waste package components are assumed to be in complete contact with the solution and, via the solution, in contact with each other.

All of the cases are run until the solution and precipitates (minerals deposited in the waste package) have stabilized. In most cases, this is upwards of 500,000 years, although most of these cases show little variation beyond 100,000 years. In most cases the changes in solution concentration of a key element is associated with the complete depletion of a degrading initial solid or the depletion of a mineral that was temporarily holding a relatively insoluble degradation product. The longest runs could be terminated by the complete depletion of all possible reactants and the return to concentration control by the incoming J-13 water.

Scenarios for Previous Studies—This section provides a summary of the prior degradation analysis with the EQ6 flow-through methodology (CRWMS M&O 1998o, Volume II, Section 3.3.1). The principal objective was to determine the amounts of neutronically active materials removed from the waste package. These were the fissile isotopes ^{239}Pu and ^{235}U and the neutron absorbers Gd and Hf. In selecting conditions most likely to lead to removal of these elements, the following guidelines were used. Although uranium and plutonium are generally insoluble, they will be relatively soluble in the alkaline, CO_2 -rich solutions produced when the HLW glass degrades. In contrast, GdOHCO_3 (which is the mineral formed by the Gd released from the degrading ceramic waste form) is soluble in the acid solution that may be produced when stainless steel degrades after the strongly alkaline period of HLW glass degradation.

For the analysis of Section 3.3.1 of CRWMS M&O (1998o, Volume II), two basic types of scenarios were represented. In the first type, all package materials degrade simultaneously, albeit at different rates, and the drip rate of J-13 water into the package is kept constant throughout the run. It was found that this type of scenario maintains a moderate to high pH (minimum value 6.33) and that for only a few thousand years. This is because all the stainless steel is degrading while glass is also degrading so that the steel's pH-lowering effect is overcompensated by the pH-raising effect of the glass degradation. With this relatively high minimum pH (6.33), there was little opportunity for loss of gadolinium. Therefore, only one EQ6 case of this type was reported in CRWMS M&O (1998o, Volume II).

In the second type of scenario considered in CRWMS M&O (1998o, Volume II), the sequence of EQ6 runs was divided into two-stages with different drip rates. This was thought to be the most efficient way to obtain sustained, low pH conditions. The first stage involved an early breach of the 304L stainless steel canisters holding the HLW, followed by fast degradation of the HLW glass and removal of the alkaline components during a period of relatively high drip rate. In the second stage, the SS 304L cans holding the ceramic were allowed to breach, exposing some portion of the Pu-U-Gd-Hf-ceramic to acid conditions. To keep the pH low, the drip rate must be reduced for the second stage.

The sequence of material degradation (glass degrading first) is consistent with the nominal assumption that glass has the highest degradation rate, followed by the stainless steel, while the ceramic has a very low degradation rate and is also somewhat protected from the water by the glass and steel. The first stage lasted as long as the degrading glass or period of high pH; the stage was terminated when the pH dropped to the low pH plateau that signals the onset of the second stage. This plateau occurs after the glass has degraded and solid carbonates, produced by glass degradation, are consumed. During this period of high pH and high drip rate, nearly all the depleted uranium from the HLW filler glass was dissolved and flushed from the waste package. At a lower drip rate, the first stage would last somewhat longer, because some of the glass degradation products would maintain an elevated pH until a major fraction of the silica could be flushed from the waste package by the dripping water.

The second stage chemistry was dominated by the degradation products of the ceramic waste form and possibly the corroding stainless steel (via the formation of chromic acid). During this phase, the pH may then drop to ~5.25, as the stainless steel continues to corrode, and the rate of influx of J-13 (which is mildly alkaline) water is reduced. There follows a period of relatively low pH, which may persist for thousands to tens of thousands of years, in this period of low pH. The solubility of GdOHCO_3 is at its highest, and dissolved Gd concentrations can reach 10^{-3} to 10^{-2} molal. The pH gradually rises, due to several factors: the inherent alkalinity of the J-13 water, the alkalinity built into the ceramic waste form, and the buffering capacity of the clays that were formed in the system. Seven simulations of this second type were run; only four (scenarios 4, 5, 6, and 7) produced a significant loss of Gd (~10 to 15%) from the system.

In summary, the aim of the two-stage runs was to force a "conservative" condition of high acidity by degrading the glass rapidly before all the acid-producing stainless steel is degraded. The early glass degradation and flushing requires very high glass degradation rates: the total effective rate of the glass is further increased by counting cracks as part of the total surface area. An unfortunate side effect of the high glass degradation rates associated with the two-stage calculation was that a slow flush rate could produce unreasonably high ionic strengths (> 1) of glass degradation products. Such high ionic strengths are beyond the applicability of EQ3/6s ionic strength (B-Dot) corrections.

The results of the previous study lead to the following observations (CRWMS M&O 1998o, Volume II, Section 3.3.1, p. 20):

- The amount of Gd lost was not particularly sensitive to the second stage drip rate: the higher drip rate generally means a lower chromic acid concentration (higher minimum pH), which, in turn, means a lower peak Gd concentration in solution. However, this factor is balanced by the fact that the higher drip rate will remove what Gd is in solution at a faster rate.
- A slower corrosion rate for the stainless steel would prolong the acidic period and, hence, will enlarge the width of the aqueous Gd peak.

- A higher ceramic corrosion rate would sharpen the aqueous Gd peak as a function of time (higher peak and narrower width), leading to earlier loss of Gd but would have little effect on the total Gd loss.

While these earlier scenarios covered the entire range of possible ceramic corrosion rates, they did not consider the possibility of glass degradation rate slower than the steel or ceramic. Such conditions are extremely unlikely, but possible. They are considered in the present study, as described below.

Scenarios and Methodology for this Study—In addition to the improved SCFT mode of EQ3/6, the present study also adds a focus on the potential plutonium loss from the waste package in preparation for developing the source term for external criticality (CRWMS M&O 1999c, Section 5.4). However, the principal difference with the previous studies is the focus on a set of conditions that can result in higher loss of Gd from the waste package. These conditions included high glass corrosion rates that would produce high pH and the opposite extreme of very low glass corrosion rates that would produce the lowest possible pH.

In general, low pH conditions will most likely occur if most of the stainless steel degrades while little glass is degrading. As mentioned above in connection with scenarios used in the previous study, it was thought that this would occur most efficiently if the glass degradation proceeded relatively quickly, while most of the steel remained undegraded. However, after careful analysis it was found that the lowest possible pH could be obtained by steel degrading quickly, while the glass degraded so slowly that it did not produce much alkalinity to compensate the acid produced by the corrosion of the steel. This is a single stage process, so there were few two-stage cases in this study (in contrast to CRWMS M&O 1998o, Volume II).

The primary cases for this study included 20 single-stage and 5 two-stage runs, with varied combinations of steel, glass, and ceramic degradation rates and different water fluxes (CRWMS M&O 1999c, Section 5.4). These 25 cases used ambient gas fugacities of 0.2 atm for O₂, and 10⁻³ atm for CO₂. The latter CO₂ pressure is consistent with the long-term ambient assumed for the VA (CRWMS M&O 1998v, Fig. 4-27).

6.2.3.1.2 Input Parameter Sensitivity Studies

Since the issue of the original study of Pu-ceramic degradation geochemistry (CRWMS M&O 1998w), new information became available on the thermochemistry some important mineral phases of the Gd carbonate system. Issues were also raised with the projected long-term composition of the water dripping into the waste package (nominally assumed to be the standard J-13), and with the chemistry of the glass produced by SRS. Therefore, the new, more refined, geochemistry evaluations required some study of sensitivity to uncertainty in important input parameter sets. In general, the waste package degradation calculations predicted that the greatest solubility of U, Pu, and Gd occurs when there is rapid degradation of one or more waste package components. The question is then whether the uncertainty in these parameter sets could dominate the uncertainties in the material and environmental parameters (e.g., corrosion rates and drip rate). It was found that they did not.

Effects of Gd Carbonate Thermochemistry—The previous Pu-ceramic calculations (CRWMS M&O 1998w) used a custom version of the Swedish Nuclear Fuel and Waste Management Co. (SKB) thermodynamic database (Spahiu and Bruno 1995) prepared by LLNL. The Pu-ceramic waste forms contain Gd, but little or no phosphate; the encasing glass contains some phosphate, but not enough to precipitate all the Gd in the ceramic. Thus when these waste forms degrade in J-13 water, Gd phosphate may not be the solubility-limiting phase. When the SKB database was used in the previous study, the calculations indicated that GdOHCO_3 would be the solubility-limiting phase for Gd (CRWMS M&O 1998w, Figs. 5.3.4-2 and 5.3.4-5). However, the thermodynamic data for this phase were originally estimated from the data for NdOHCO_3 , and there was substantial uncertainty in the SKB data for the hydroxyl and carbonate aqueous complexes of Gd.

Recently, Weger et al. (1998) performed experiments to determine the solubility of three solid Gd carbonates and one hydroxide, and estimated the formation constants for several dissolved Gd carbonate and hydroxyl complexes. A version of the SKB database was customized to include the new Weger et al. (1998) data; this new database is hereafter referred to as the Weger database.

To test the consequences of using the Weger database, versus the SKB database, two cases (run numbers 4 and 6 from CRWMS M&O 1998w, Table 5.3-1, p. 23) were repeated with both datasets. To ensure a uniform basis for comparison, both calculations were performed with the SCFT using the new addendum to EQ3/6 (CRWMS M&O 1999c, Section 4.2).

Table 6-6 summarizes the net Gd losses for the two runs, using both databases. Figure 6-23 compares the detailed time behavior for the two datasets for the conditions of run 4; the comparison for run 6 is similar. (The “moles” on the right are for the normalized EQ6 system as discussed in CRWMS M&O 1998w, p. 24.)

Table 6-6. Percent Loss of Gadolinium, for Entire WP, Thermodynamic Data Sensitivity Study (CRWMS M&O 1999c, Table 5-6)

	Run 4	Run 6
SKB database	14.8625%	12.9599%
Weger database	14.4983%	12.9537%

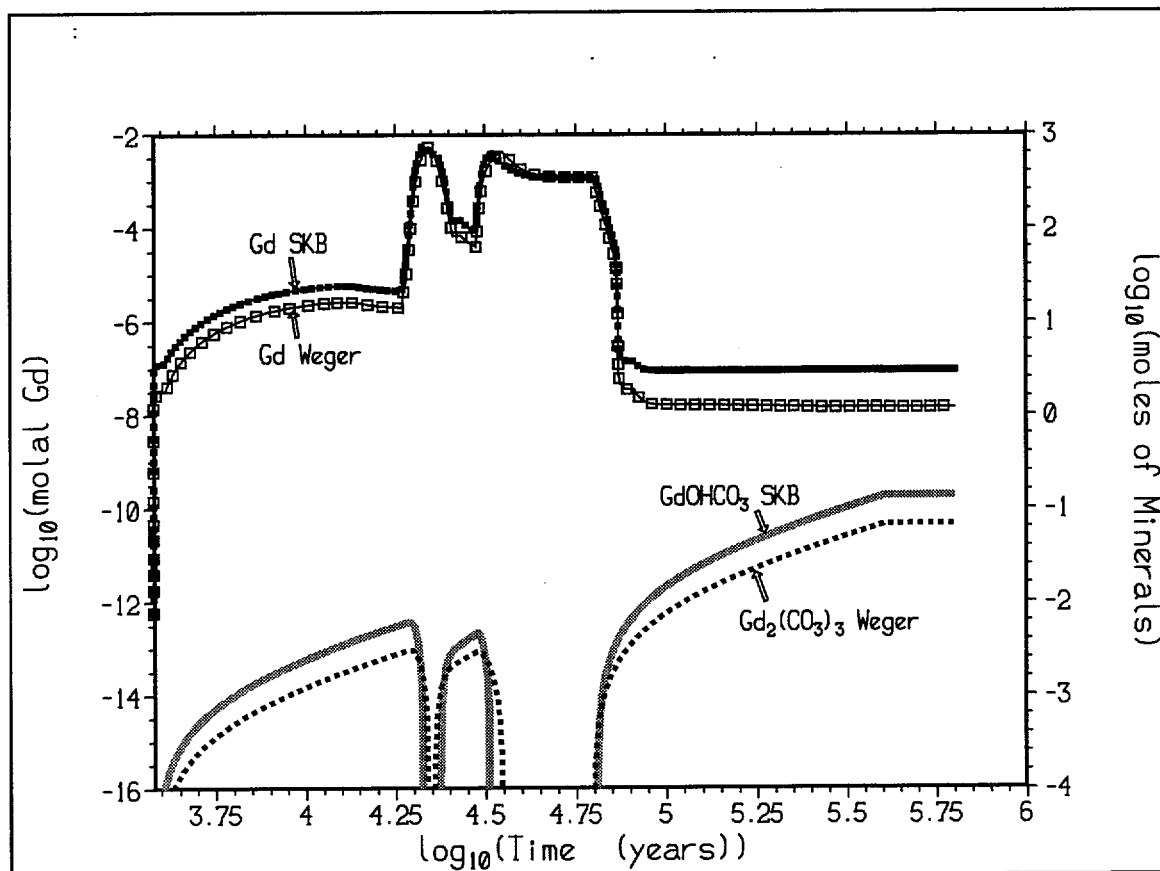


Figure 6-23. Sensitivity of Aqueous Gd Molalities (CRWMS M&O 1999c, Fig. 5-5)

It is apparent from Table 6-6 and Figure 6-23 that the Weger et al. (1998) data do not significantly alter the important aqueous Gd calculation results. Furthermore, the use of the SKB database is slightly conservative for systems where the solid Gd phases are carbonates, because it results in more Gd in solution, and, consequently, more Gd lost from the waste package.

Effects of Possible Compositions of Incoming Water—To reflect the current uncertainty the composition of the *incoming* J-13 water has been varied over a set of likely ranges for its principal parameters.

The parameters most representative of the incoming water uncertainty were Ca concentration and CO₂ fugacity (CRWMS M&O 1999c, Section 5.3.2). Fugacity is defined as an idealized partial pressure; it represents chemical activity, and may not correspond exactly to the actual partial pressure of the gas in solution. Six cases of Ca concentration and CO₂ fugacity were considered, in two sets of three. For one set, the Ca⁺⁺ concentrations were held at saturation with calcite.

For the other set of three, Ca^{++} was fixed at the average value (LL980711104242.054). For each set, the $\log_{10} f\text{CO}_2$ (fugacity of CO_2) values were set at -2.5, -3.0 or -3.5, to encompass the VA mean value, the approximate value suggested in CRWMS M&O (1998d), and the normal ambient value (Weast 1977, p. F-210). For all the cases, the concentrations of Fe^{2+} , Al^{3+} , and Mn^{2+} were set to equilibrium with goethite, diaspore, and pyrolusite, respectively.

Table 6-7 shows the comparison of Gd, Pu, and U losses for the 7 runs. Overall, the differences are small. It is notable that the highest Gd losses occur in the samples with the lowest overall CO_2 fugacity, and that these runs have the highest average pH. However, the runs with $\log_{10} f\text{CO}_2 = -3.5$ have lower dissolved H_2CO_3 and HCO_3^- , and are less able to buffer the system pH during the degradation of metals.

Table 6-7. Gd, Pu, and U% Losses for Indicated Deviations from J-13 Incoming Water Composition (CRWMS M&O 1999c, Table 5-7)

Case	Gd	Pu	U	$\log_{10} f\text{CO}_2$	Calcite Saturation
r4base_ (base case)	13.933	0.000	0.031	-2.539	No
r4cal25	13.192	0.000	0.031	-2.500	Yes
r4cal30	14.147	0.000	0.019	-3.000	Yes
r4cal35	14.712	0.000	0.012	-3.500	Yes
r4noc25	13.663	0.000	0.031	-2.500	No
r4noc30	14.178	0.000	0.019	-3.000	No
r4noc35	14.574	0.000	0.012	-3.500	No

In summary, the Gd loss is relatively insensitive to the uncertainties in the two parameters representative of the uncertainty in incoming water composition. This is not surprising; it only reflects the fact that chemical reactions in the waste package cause much greater changes in solution composition than the uncertainty represented by the range of compositions in Table 6-7. In fact, it will be seen in Section 6.2.3.1.3 that the rapid degradation of waste package components has a larger effect on the waste package aqueous chemistry than does any possible variations from the incoming J-13 water composition. For example, for those waste forms involving codisposal with HLW glass, the rapid glass degradation will often drive the ionic strength to ~1 molal. Steel degradation somewhat faster than normal can drive pH below 5. Under these conditions, the aqueous phase deviates from the nominal J-13 composition by much more than the variety of suggested modifications for the composition of the indripping water.

Effects of Glass Composition Variations—A sensitivity study, investigating effects of glass composition variations, was undertaken for two reasons. First, the previous study of Pu-ceramic degradation used a single composition to represent “typical” HLW glasses produced at the SRS (CRWMS M&O 1998w, Table 5.1.1.1-2, p. 16). A very similar, standardized glass composition was recently developed in CRWMS M&O (1999j, Attachment I, p. I-7). Ultimately, these two compositions trace to a 1987 report, issued before SRS had finalized its glass production process. In addition, other reports suggested large composition ranges for SRS glass (DOE 1992, Table 3.3.8, p. 3.3-15). Second, in the previous calculation, all phosphorus was eliminated from the idealized glass composition. The phosphorus was removed from the previous calculation, to

prevent EQ6 from precipitating low-solubility Gd phosphates; the removal was conservative, since there was uncertainty about the accuracy of glass phosphorus analyses, and elimination of phosphorus would lead to greater Gd losses from the WP.

Six glass compositions were used, a base case used by the previous study (CRWMS M&O 1998w) and five typical glass compositions from the most recent SRS document on glass composition, Fowler et al. (1995). These represent the various types of glass that could be made from the sludge at SRS. They differ primarily in the percentages of Al, Fe, Ca, K, and Mn. The comparison in Table 6-8 shows that the glass compositions from Tables 1 and 2 of Fowler et al. (1995) generate slightly lower Gd losses, than does the base case. The principal reason for the lower loss appears to be the small phosphate content included for these SRS compositions. The phosphate converts some of the Gd into insoluble $GdPO_4 \cdot H_2O$, which lowers overall Gd loss in the system. Overall, the wide variations in the new glass compositions appear to have little effect on the total calculated Gd loss. Other elements (particularly Pb) compete with Gd for the phosphate, so there is no simple correlation between phosphate content and Gd loss.

Table 6-8. Sensitivity of Gd Loss to Glass Composition (CRWMS M&O 1999c, Table 5-9)

Glass	%Gd Loss
Base	13.93
Blend	10.59
Batch1	9.58
Batch3	10.13
HM	9.30
Purex	9.46

6.2.3.1.3 Summary of Results

Table 6-9 summarizes the total percentage Gd, Pu, and U lost at the end of the 36 EQ6 runs covering the range of corrosion rates and drip rates. The values corresponding to the degradation rate indicators for stainless steel (SS), glass (G), and ceramic (C) are given in Table 2-10.

Table 6-9. Gd, Pu, and U Losses for EQ6 Cases
(CRWMS M&O 1999c, Tables 5-10, 5-11, 5-12, and 6-1)

Case	Number of Stages	Degradation Rates ^a	J-13 Drip rates (m ³ /yr)	Years	% Gd Loss	% Pu Loss	% U Loss
1	1	S: avg; G: lo; C: lo	0.0015	633860	0.02	0.17	47.52
2	1	S: avg; G: lo; C: lo	0.15	44871	0.00	0.02	0.01
3	1	S: avg; G: lo; C: hi	0.0015	633860	20.45	0.00	100.00
4	1	S: avg; G: lo; C: hi	0.15	46013	0.69	0.00	0.01
5	1	S: avg; G: lo; C: avg	0.015	416890	8.33	0.41	33.44
6	1	S: avg; G: hi; C: lo	0.0015	634040	0.01	0.91	33.19
7	1	S: avg; G: hi; C: lo	0.15	45672	0.01	0.08	34.48
8	1	S: avg; G: hi; C: hi	0.0015	633860	0.02	29.94	89.16
9	1	S: avg; G: hi; C: hi	0.15	45485	0.36	0.07	59.68
10	1	S: avg; G: hi; C: avg	0.015	442310	17.06	1.80	38.41
11	1	S: hi; G: lo; C: lo	0.0015	633860	0.14	0.62	47.42
12	1	S: hi; G: lo; C: lo	0.15	43280	0.03	0.05	0.07
13	1	S: hi; G: lo; C: hi	0.0015	634200	77.92	0.01	100.00
14	1	S: hi; G: lo; C: hi	0.15	42518	49.01	0.20	0.22
15	1	S: hi; G: lo; C: avg	0.015	415350	0.34	1.42	37.27
16	1	S: hi; G: hi; C: lo	0.0015	634040	0.01	0.59	39.88
17	1	S: hi; G: hi; C: lo	0.15	44467	0.02	0.04	34.55
18	1	S: hi; G: hi; C: hi	0.0015	634200	0.02	13.99	72.95
19	1	S: hi; G: hi; C: hi	0.15	45891	0.09	0.03	56.13
20	1	S: hi; G: hi; C: avg	0.015	401570	0.07	1.62	36.43
21	2	S: hi; G: hi; C: avg	0.5 & 0.015	491560	0.07	0.00	0.33
22 ^b	2	S: hi; G: hi; C: avg	0.5 & 0.015	528010	0.07	0.26	0.49
23 ^b	2	S: hi; G: hi; C: avg	0.15 & 0.0015	634130	0.01	0.00	0.07
24 ^b	2	S: avg; G: hi; C: avg	0.15 & 0.0015	634210	2.28	0.00	0.04
25 ^b	2	S: hi; G: hi; C: hi	0.15 & 0.0015	634130	13.89	0.00	0.04
26 ^c	1	S: avg; G: lo; C: hi	0.0015	634000	1.30	0.00	100.0
27 ^c	1	S: avg; G: lo; C: avg	0.015	424000	10.60	0.00	34.90
28 ^c	1	S: avg; G: hi; C: avg	0.015	447000	15.80	0.00	38.40
29 ^c	1	S: hi; G: lo; C: hi	0.0015	634000	1.40	0.00	100.00
30 ^c	1	S: hi; G: lo; C: hi	0.15	44200	37.50	0.00	0.20
31 ^e	1	S: avg; G: lo; C: hi	0.0015	634070	0.00	0.00	100.00
32 ^e	1	S: avg; G: lo; C: avg	0.015	436000	0.10	0.00	28.20
33 ^e	1	S: avg; G: hi; C: avg	0.015	483000	0.10	0.00	38.40
34 ^e	1	S: hi; G: lo; C: hi	0.0015	634000	0.00	0.00	100.00
35 ^e	1	S: hi; G: lo; C: hi	0.15	43700	0.10	0.00	0.00
36	1	S: hi; G: lo; C: hi ^d	0.0015	634000	32.68	0.07	100.00

^a S = steel, G = glass, C = ceramic; corrosion rates (high [hi], average [avg], low [lo]) are presented in Table 2-10

^b In Cases 22-25, hematite (Fe₂O₃) was suppressed and goethite (FeOOH) was formed.

^c In Cases 26-30, the fugacity of O₂ was lowered from 0.2 to 10⁻¹⁰ bar.

^d In Case 36, the conditions of case 13 are repeated, except the ceramic corrosion rate is reduced by a factor of 3.

^e In Cases 31-35, the fugacity of O₂ was lowered from 0.2 to 10⁻¹⁵ bar.

Eight cases were selected for further detailed examination, and are given in Table 6-10. Cases 3, 13, and 14 were selected because they represent the runs with the highest net Gd loss. Cases 8 and 18 have the highest Pu loss. Case 3 is also compared with Case 26 (its lower *f*O₂ analogue) to illustrate the indirect effect of *f*O₂ on Gd loss. Cases 22 and 25 were selected as representative of the two-stage scenarios; Case 25 is closest to the cases that produced highest Gd loss in the prior study of Pu-ceramic degradation (CRWMS M&O 1998w, Table 5.3-1).

Table 6-10 summarizes several aspects of the selected cases, focussing on conditions tied to Gd loss.

Table 6-10. Gd Loss Characteristics and pH of Selected Cases (CRWMS M&O 1999c, Table 6-2)

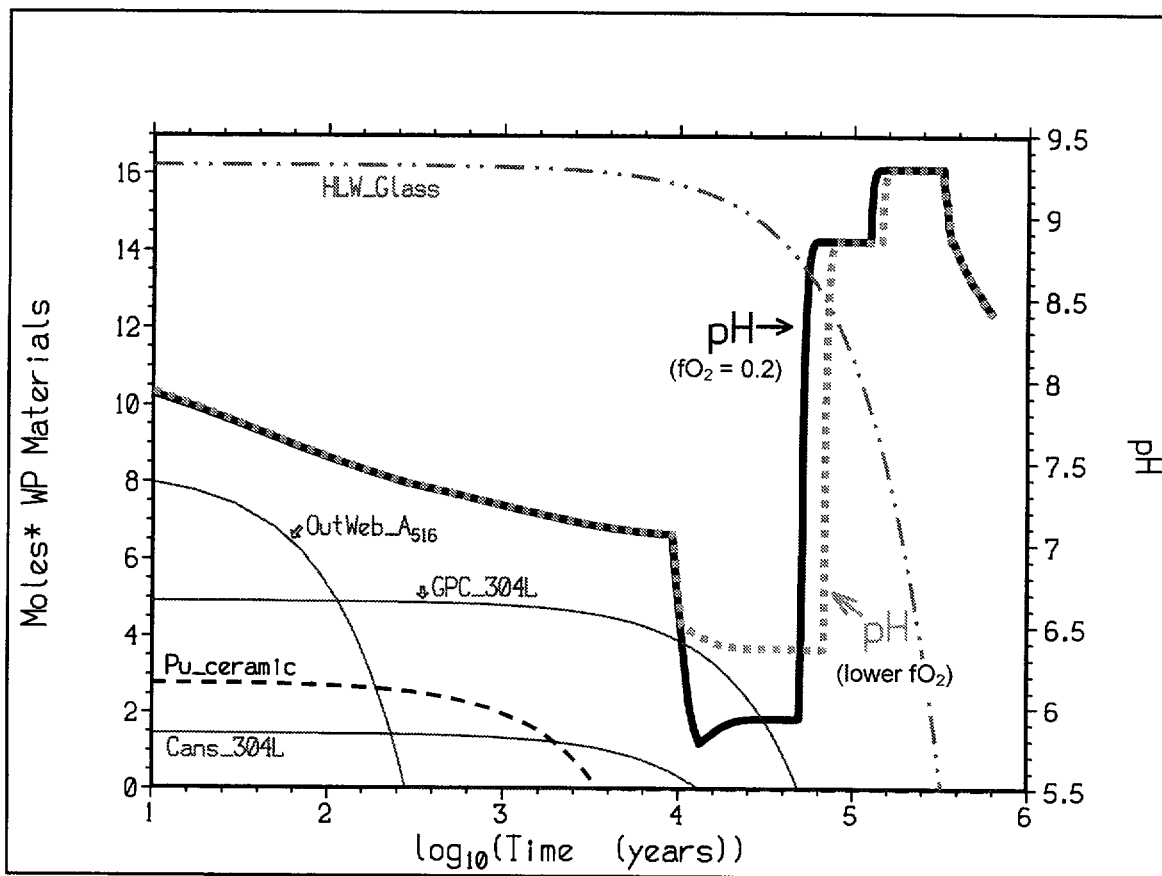
Case	Number of Stages	Corrosion Rates ^a	J-13 Drip Rates (m ³ /yr.)	Simulated Time (yrs.)	pH min/max	Peak ^b Gd Conc. (molal)	Width Gd Peak ^b (yr.)	% Gd Loss
3	1	HLW: low Steel: avg Cer: high	0.0015	6.3e5	5.8 / 9.4	7.2e-3; 1.4e-3	3.6e3; 3.3e4	20.45
8	1	HLW: high Steel: avg Cer: high	0.0015	6.3e5	7.3 / 10.1	4.9e-6; 5e-7	4.6e3; 1e4	0.02
13	1	HLW: low Steel: high Cer: high	0.0015	6.3e5	5.3 / 9.3	5e-2	5.4e3	77.92
14	1	HLW: low Steel: high Cer: high	0.15	4.3e4	5.8 / 8.2	9.7e-4; 3.9e-4	1.1e3; 1.4e3	49.01
18	1	HLW: high Steel: high Cer: high	0.0015	6.3e5	7.9 / 10.0	3.9e-6; 2.6e-7; 7.3e-8	2.2e3; 1.6e5; 3.3e5	0.02
22	2	HLW: high Steel: high Cer: medium	0.5 / 0.015	3.1e3 / 5.3e5	5.2 / 8.6	6e-8	4.7e5	0.07
25	2	HLW: high Steel: high Cer: high	0.15 / 0.0015	3.5e3 / 6.3e5	5.0 / 8.1	4.4e-2	1.2e3	13.89
26 ^c	1	HLW: low Steel: avg Cer: high	0.0015	6.3e5	6.3 / 9.3	8.3e-5	5.7e4	1.30

^a See Table 2-10 for rates.

^b Most cases have multiple "peaks".

^c Analogous to Case 3, except $\log_{10}(fO_2) = -10$ (vs. -0.7).

The results of Case 3 and its corresponding sensitivity test, Case 26, are plotted in Figures 6-24 through 6-26 to demonstrate the general consequences of WP component degradation. The consequences include changes in pH, variations in the dissolved Gd, Pu, and U content of the water flushed from the WP, and the formation of solubility-controlling and space-filling minerals and solid solutions. Comparison of Figures 6-25 and 6-26 also demonstrates the indirect effects of oxygen fugacity on pH and Gd loss. The following paragraphs explain this behavior.



NOTE: Cases 3 [$fO_2 = 0.2$ atm, Solid pH Line] and 26 [$fO_2 = 10^{-10}$ atm, Dashed pH Line]
Moles in the EQ6 Normalized [1 Liter Fluid] System

Figure 6-24. Effect of fO_2 on pH (CRWMS M&O 1999c, Fig. 6-1)

Figure 6-24 illustrates the dependence of pH on degradation of the initial solids. Under the hypothesis that the chromium from the stainless steel components is mostly oxidized to chromate, forming chromic acid, the pH in the WP decreases with stainless steel degradation, until the steels are exhausted. The decrease in pH is gradual for the first 10,000 years, at which time there is a sharp drop in pH from just above 7 to well below 6. This sharp drop is produced by the exhaustion of precipitated calcium carbonate. The amount of this mineral is not given in Figure 6-24, but it is given in CRWMS M&O (1999c, Figs. 6-6 and 6-7), for Cases 3 and 26, respectively. The exhaustion of the 304L stainless steel of the cans, shortly after 10,000 years, produces a small upswing in the pH. However, the pH does not have a major rise until all the steel is degraded at approximately 56,000 years, which corresponds to the exhaustion of the canister steel, GPC_304L. Since this example assumes a low glass degradation rate, the alkalinity from glass is insufficient to neutralize the pH until all the steel is consumed. The Mg and Ca carbonate minerals formed from glass dissolution do not fully neutralize the acid produced from steel degradation. It should be noted that during the time between the complete degradation of the ceramic at approximately 3200 years and the sharp decrease in pH at just over 10,000 years, nearly all the Gd in the waste package will be in a carbonate mineral.

It should be noted that the quantities and rates of change depicted in Figure 6-24 are the same for both Cases 3 and 26, which differ only in the assumed fO_2 , except for the pH. The lower fO_2 means that a considerable fraction of the Cr released by stainless steel is only oxidized to the +4 valence state and precipitates as CrO_2 , instead of being fully oxidized to chromate and chromic acid, which is immediately flushed from the waste package, because it is soluble. After all the steel is corroded, Case 26 still has a Cr reservoir in the CrO_2 , which can serve as a source of Cr for chromic acid for nearly 1000 years after the exhaustion of the stainless steel. The CrO_2 is not shown in Figure 6-24, but can be seen in CRWMS M&O (1999c, Fig. 6-5).

After the steel is completely corroded and its associated acidity is flushed from the system, the pH climbs well above 7 (at ~50,000 years) due to glass dissolution. Once the glass is consumed, the pH gradually drops to the ambient for J-13 water at $fCO_2 = 10^{-3}$ atm. However, in the sensitivity test (Case 26), the lower oxygen fugacity ($fO_2 = 10^{-10}$) in the WP restricts complete oxidation of the Cr, thereby preventing the pH from decreasing until $\sim 10^{4.81}$ years, which is $\sim 10^4$ years later than in the case with 0.2 atm fO_2 . The rapid pH increase occurs when the Pu-ceramic and "Out Web_A516" (the carbon steel support structure) have been exhausted, and while the GPC_304L and Cans_304L continue to degrade as show in Figure 6-24.

The concentrations of aqueous Gd, U, and Pu as functions of time are shown in Figures 6-25 and 6-26 for Cases 3 and 26, respectively. The solubility-limiting phase for Gd is $GdOHCO_3$; like most carbonates, this phase is more soluble under acid conditions, thus the times of highest aqueous Gd correspond to times of low pH. Therefore, the case with lower fO_2 (Case 26) also yields lower Gd loss (1.5%, versus 20.45% for Case 3; Table 6-9).

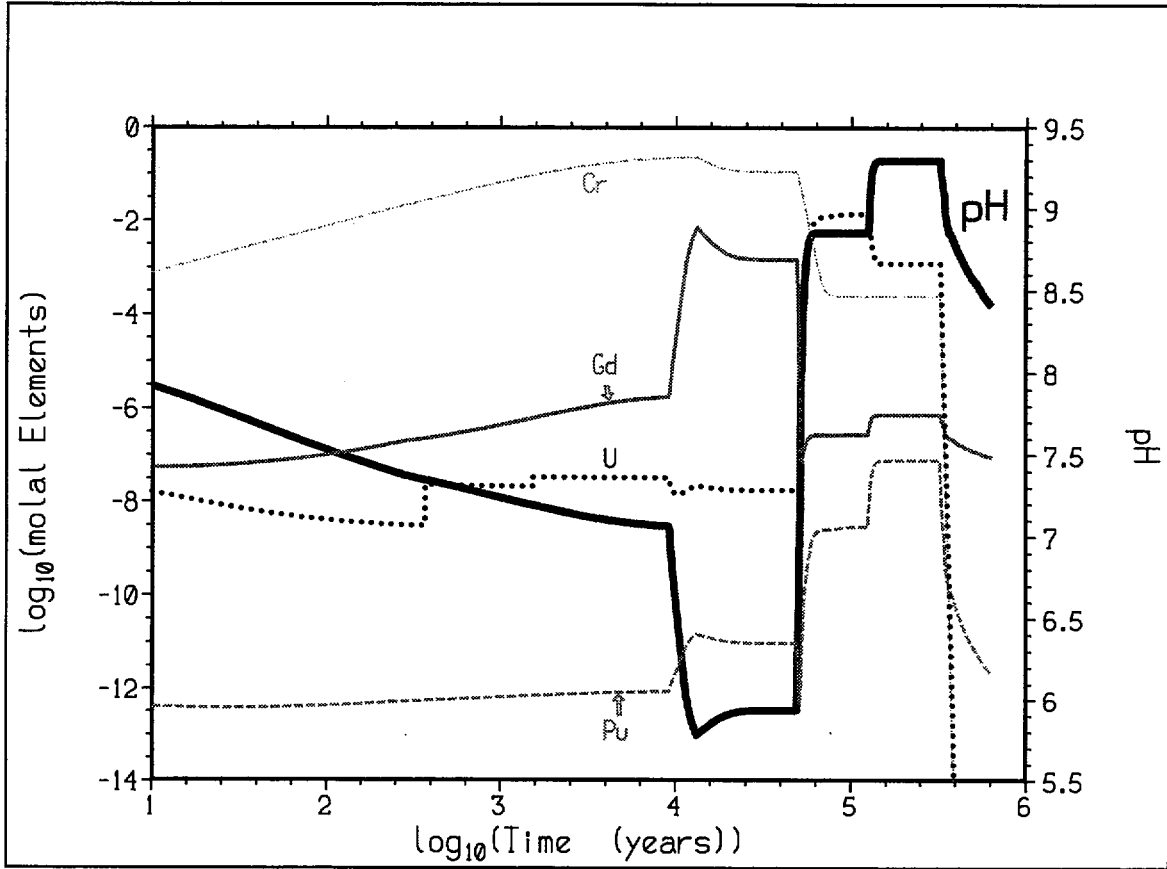


Figure 6-25. Aqueous Concentrations of Important Elements and pH for Case 3 (CRWMS M&O 1999c, Fig. 6-2)

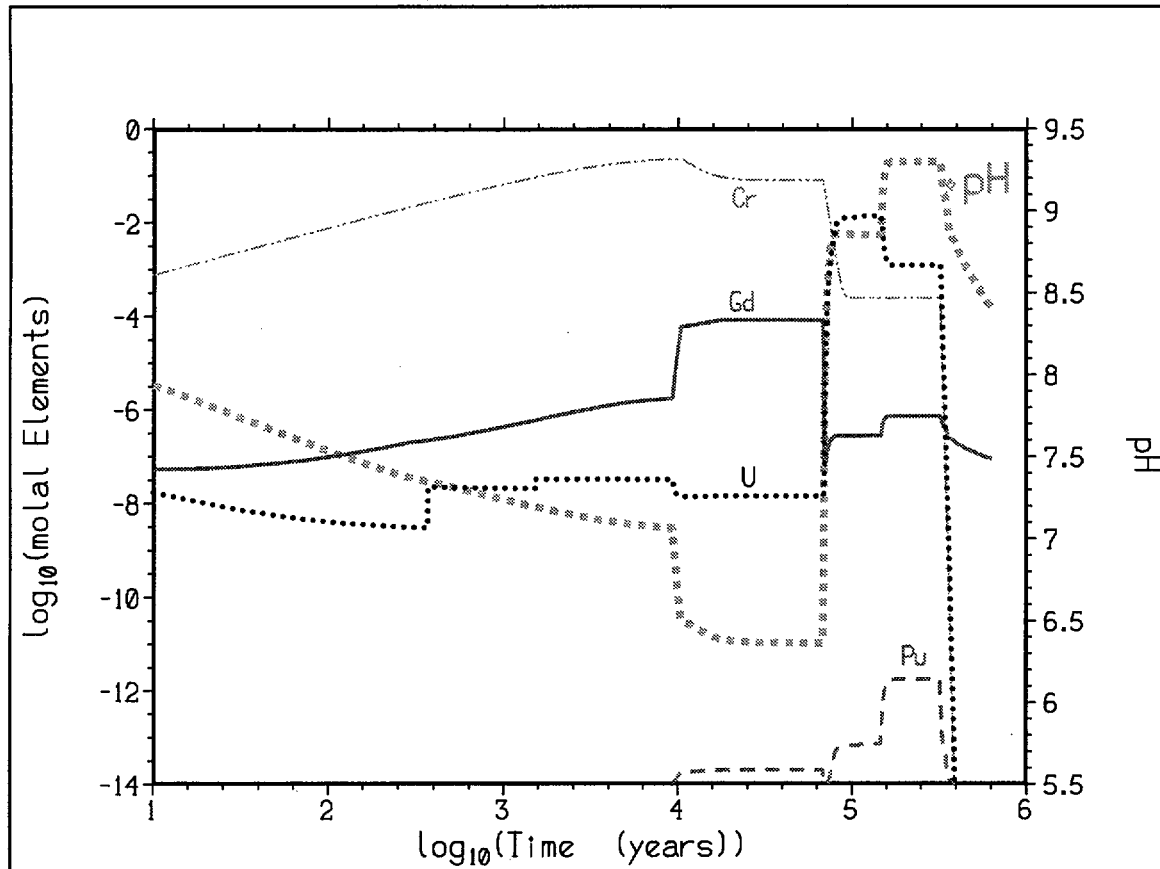


Figure 6-26. Aqueous Concentrations of Important Elements and pH for Case 26 (CRWMS M&O 1999c, Fig. 6-3)

It should be noted that both Figures 6-25 and 6-26 show two relatively high plateau steps for U in solution 56,000 years and 316,000 years. This is due to the very slow glass dissolution rate, which maintains a relatively high pH condition for this period of time. Although these are not the highest examples of U concentration in solution, they last for such a long time that all the U is ultimately lost from the waste package.

The Gd loss is inferred from the amount of Gd remaining, as calculated by EQ6. It can also be computed by numerically integrating the product of the Gd concentration in solution, multiplied by the outflow from the waste package (approximated by the drip rate into the waste package). It will be noted that the Gd concentration in Figures 6-25 and 6-26 have relatively well defined peaks, or plateaus over a limited range of time, and are much smaller elsewhere. This suggests that the major portion of the Gd loss occurs over the relatively brief period of time when the aqueous Gd peaks.

A simple calculation can be used to illustrate this fact that most of the Gd is lost while its aqueous concentration is at a peak value. The numerical integral mentioned in the previous paragraph can be approximated by multiplying the drip rate by the peak Gd concentration in solution multiplied by the width of the peak. For Case 3 there are two peaks, one triangular perched on top of a broader plateau. The corresponding calculation is

$0.0015*157*(0.0072*3600+0.0014*33000) = 17$ kg; dividing by the initial 94 kg Gd gives a percent loss of 18%, which is close to the 20% from the EQ6 calculation, as given in Table 6-9. For those scenarios that do not lead to a significant peak, there will be no significant Gd loss at all. It should be noted that this discussion is for illustration only, the precise calculation of Gd loss is determined from the EQ6 output, and given in the last column of Table 6-9.

6.2.3.1.4 Observations

The following observations can be made from the geochemistry calculation results given in Tables 6-9 and 6-10:

- The highest Gd losses occur for those cases in which the glass degrades slowly, but the ceramic and stainless steel degrade quickly. Under these circumstances a low pH situation is set up relatively early, before much of the slowly degrading glass is able to contribute much alkalinity to raise the pH. The case with the highest Gd loss, Case 13 with 78% loss, has the most rapid degradation of the stainless steel and ceramic, so that the period of low pH (and high Gd solubility) lasts for the shortest time (only 5400 years, from Table 6-10). In this case, however, the pH has such a low value (approximately 5.5, from CRWMS M&O 1999c, Fig. 6-11) that it creates a very high Gd solubility that results in the highest Gd loss. Some of the two-stage cases of CRWMS M&O (1998o, Volume II), which have the opposite condition (glass completely degrading before any of the other components) produce significant Gd loss also, but not as high as the conditions identified here (e.g., Cases 3, 13, 14, and 30 of Table 6-9).
- Even if the glass degrades much more slowly than the other components, a large Gd loss will not occur unless there is a high enough oxygen fugacity. Otherwise there will not be sufficient support for the oxidation of chromium to chromate (e.g., contrast Cases 3 and 26 of Table 6-9)
- In those cases with the glass degrading last, there will be a long period of relatively high pH (approximately 9 in Figs. 6-24, 6-25, and 6-26) after all the pH-lowering potential of the corroding stainless steel has been removed. This long period of high pH (Table 6-10) can result in loss of most, or all, of the uranium (Cases 3, 13, 18, 19, 26, 29, 31, 34, 36 of Table 6-9). This loss of uranium occurs too late to completely prevent internal criticality, but it will increase the risk of external criticality, to be discussed in REV 01 of this document.

6.2.3.2 Degraded Configurations

6.2.3.2.1 Partially Degraded Configuration

This section summarizes the criticality evaluation of an extreme case of relative displacement between the fissile material and the neutron absorber (CRWMS M&O 1999k, p. 9). The absorbers (Gd and Hf) were assumed to become soluble and uniformly distributed throughout the water in the WP filled with water as shown in Figure 6-27. This configuration can be considered as a variant of class 4 of Section 6.2.1. The composition of the discs is conservatively

represented with initial weight fraction of Pu listed in Table 2-5. Five cases were represented. The first case used the initial compositions of the disks. The other cases had the Gd and Hf spread uniformly throughout the waste package volume, in both the water and the remainder of the ceramic disks. In the first of these cases all the Gd and Hf remained in the waste package. In the three other cases the percentages of initial Gd and Hf retained were 50, 25, and 0%.

Neither the glass nor the steel was included. This is conservative because the water is a more efficient moderator than the silica in the glass, and the steel contains neutron absorbers and displaces water.

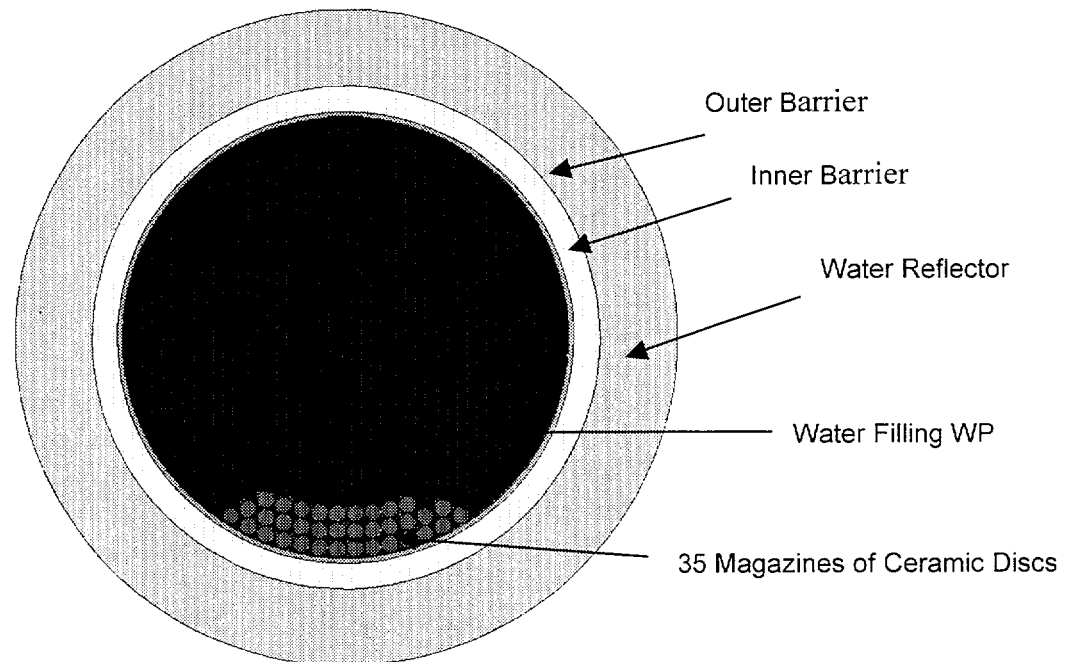


Figure 6-27. A Cross-sectional View of a Horizontally Emplaced Waste Package for the Partial Degradation Configuration (CRWMS M&O 1999k, Fig. 5-1)

The k_{eff} values and their standard deviations are listed in Table 6-11 for the partially degraded cases described in Section 6.2.3.2.1.

Table 6-11. MCNP Calculated k_{eff} for Partially Degraded Cases (CRWMS M&O 1999k, Table 6-1)

Gd and Hf Remaining in WP (%)	Gd and Hf Presence	k_{eff}	Standard Deviation
100	Ceramic Discs	0.38801	0.00072
100	Throughout WP	0.53098	0.00124

The explanation of this behavior is as follows:

- Spreading the neutron absorbers throughout the waste package volume increases the k_{eff} , but not anywhere near enough to reach criticality.
- Removing neutron absorber from the waste package, while continuing to have the same relative geometry between the fissile material (in the disks) and the neutron absorber (spread uniformly throughout the waste package), increases k_{eff} but still does not reach criticality, because the geometry of the disks at the bottom of the waste package is so unfavorable.

6.2.3.2.2 Fully Degraded Configuration

The fully degraded mode criticality configurations of the WP are evaluated in CRWMS M&O (1999k) where the WP internals have lost their original intact configurations and compositions and settled (depicted in Figure 6-28). Note that the bottom of the WP contains a settled mixture of degradation products and non-degraded WP internals. Water fills the remaining volume above the sludge. The most abundant elements in the homogenized mixture of the fully degraded sludge at various times in life after WP breach are taken from the geochemistry degradation analysis for Case 14 and Case 13 as discussed in Section 6.2.3.1.2. The compositions at the different times in life are given in moles per liter of waste package void volume (4593.965 total liters) to preserve consistency with the geochemistry calculations and mole fraction percent normalized to 100%. The quantities of uranium and plutonium are reported by EQ6 at the elemental level. The isotope breakdown of U and Pu, at the approximate time of WP emplacement, is given in Table 2-7.

The criticality analysis is performed at times of approximately 10,000; 30,000; and 43,000 years after the initial breach of the WP (10,000 years) for Case 14 (CRWMS M&O 1999k, Section 6.2.1). Based upon the results obtained for Case 14, the only time calculated for Case 13 (CRWMS M&O 1999k, Section 6.2.2) is the 13,000-year time step since it results in the highest reactivity. To search for the optimum sludge dilution, the criticality evaluations were performed for cases where the homogenized mixture of the degradation products and non-degraded WP internals contained added percentages of water by volume. Cases were also run for comparison with total removal of the principal neutron absorbers Gd and Hf, which is unrealistic. Additional cases were run with partial replacement of the two neutron absorbers with water for Case 14 in order to find the minimum amount of absorbers needed to maintain subcriticality. The partial replacement cases demonstrated that only small amounts of either absorber are needed to maintain subcriticality.

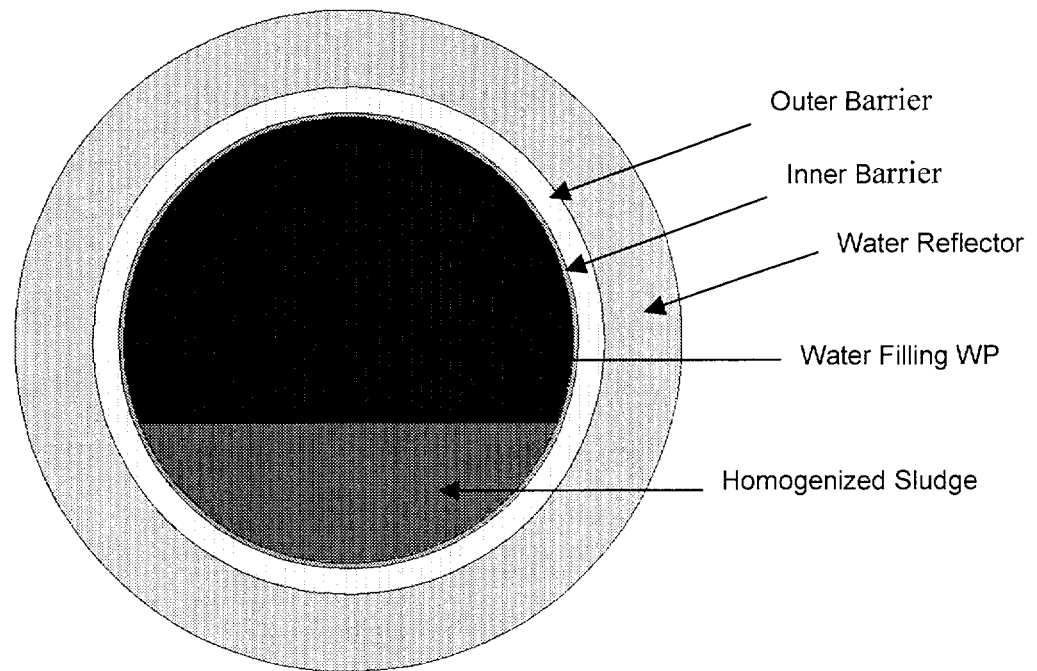


Figure 6-28. A Cross-sectional Front View of a Horizontally Emplaced Waste Package for the Full Degradation Configuration (CRWMS M&O 1999k, Fig. 5-2)

The k_{eff} values for the fully degraded configuration with various amounts of water added are shown in Figure 6-29 for Case 14 (CRWMS M&O 1999k, Section 6.2.1). Note that the amount of water added to the sludge and homogenized varies from no water added to the addition of water equal to 50% of the final volume. That is, the initial volume of sludge was doubled with the 100% water addition. Three times after the breach of the WP were evaluated. These times were approximately 10,000; 30,000; and 43,000 years after WP breach. For the decay of plutonium isotopes, 10,000 years have to be added to the above times to account for the assumed emplacement time before WP breach.

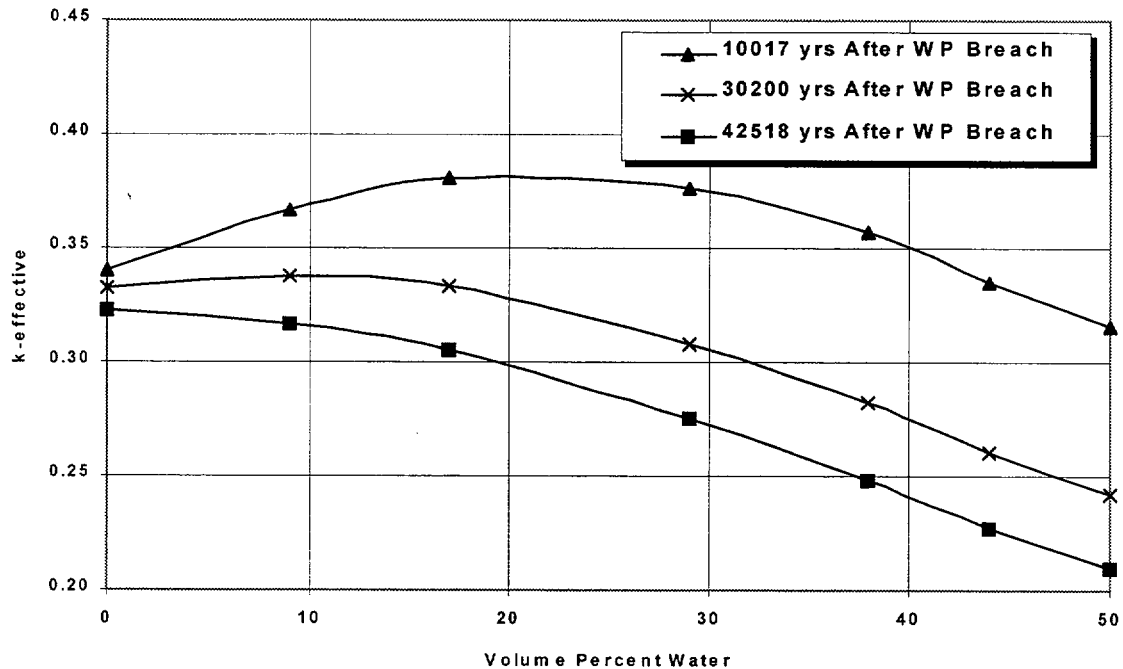


Figure 6-29. MCNP k_{eff} for Case 14 (49% Gd lost, CRWMS M&O 1999k, Fig. 6-1)

From Figure 6-29, the k_{eff} is shown to be low for any amount of water added to the sludge. To see if the degraded material could stay subcritical with a total loss of both of the primary neutron poisons, cases were run with all the Gd and Hf material removed (Fig. 6-30) (CRWMS M&O 1999k, Section 6.2.1). From the results it can be seen that the system cannot have all of both the primary poison materials removed and stay subcritical. Additional cases were run with small quantities of the poison material retained. For the 10,017-year time step, which gave the highest k_{eff} , (a) only 1% of the original Gd and 50% of Hf were retained, (b) next only 1% of the original Gd was retained, and (c) only 50% of Hf was retained. Figure 6-31 (CRWMS M&O 1999k, Section 6.2.1) presents the results of these partial-poison-retention cases. Note that about 50% of the Hf or only about 1% of the initial Gd is needed to maintain subcriticality under all dilution situations. k_{eff} for the 0% Gd, 50% Hf case keeps increasing with additional water, which indicates that Hf is a less effective absorber in the thermal region since the resonance integral is much larger for Hf than its thermal absorption cross section (Parrington et al. 1996).

Table 6-12 (CRWMS M&O 1999k, Table 6-5) and Figure 6-32 (CRWMS M&O 1999k, Fig. 6-4) show the minimum required Hf to maintain subcriticality as a function of time after WP breach. Figure 6-32 was generated by linearly interpolating and extrapolating from the data in Table 6-12. The following is an explanation of this behavior:

- The reactivity in the waste package decreases as the ^{239}Pu decays into the less reactive ^{235}U (Parrington et al. 1996).
- There is no peak in reactivity as a function of time because the waste form contains very little ^{240}Pu . This isotope is a strong neutron absorber and, if there is enough of it, its

relatively rapid decay (6560-year half-life) (Parrington et al. 1996) causes a temporary increase in reactivity, which is ultimately reduced by the slower decay of ^{239}Pu .

- Beyond 42,000 years so much Pu has decayed to U that the configuration can no longer go critical.

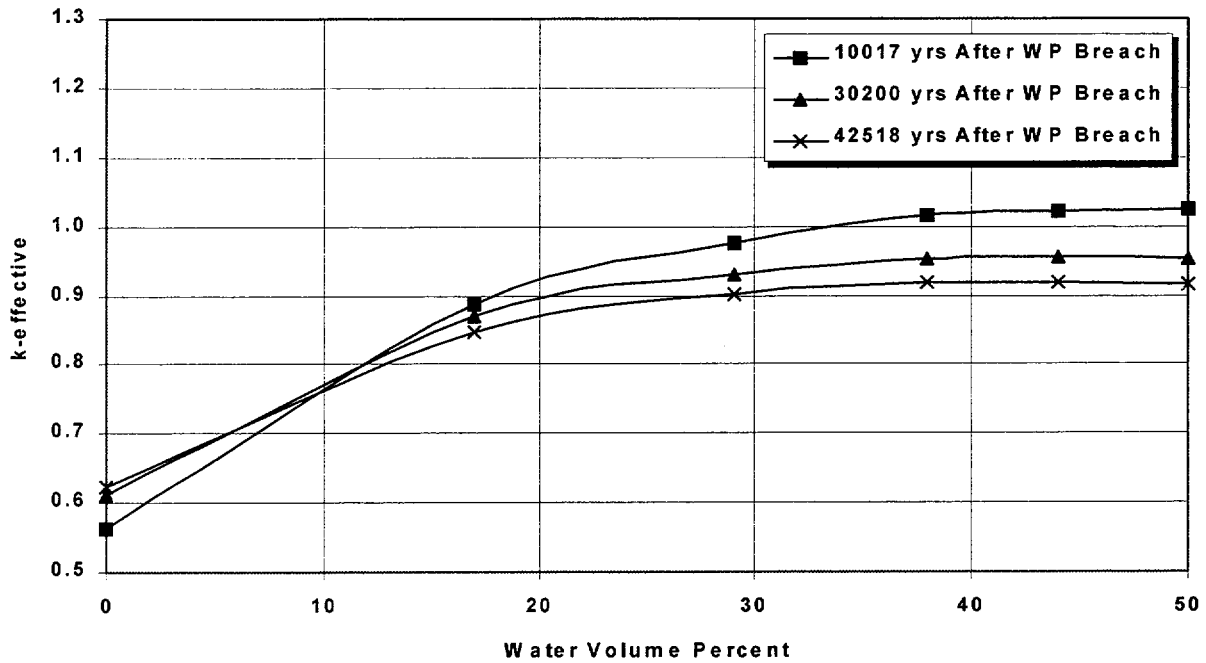


Figure 6-30. MCNP k_{eff} for Case 14 with All Gd and Hf Removed (CRWMS M&O 1999k, Fig. 6-2)

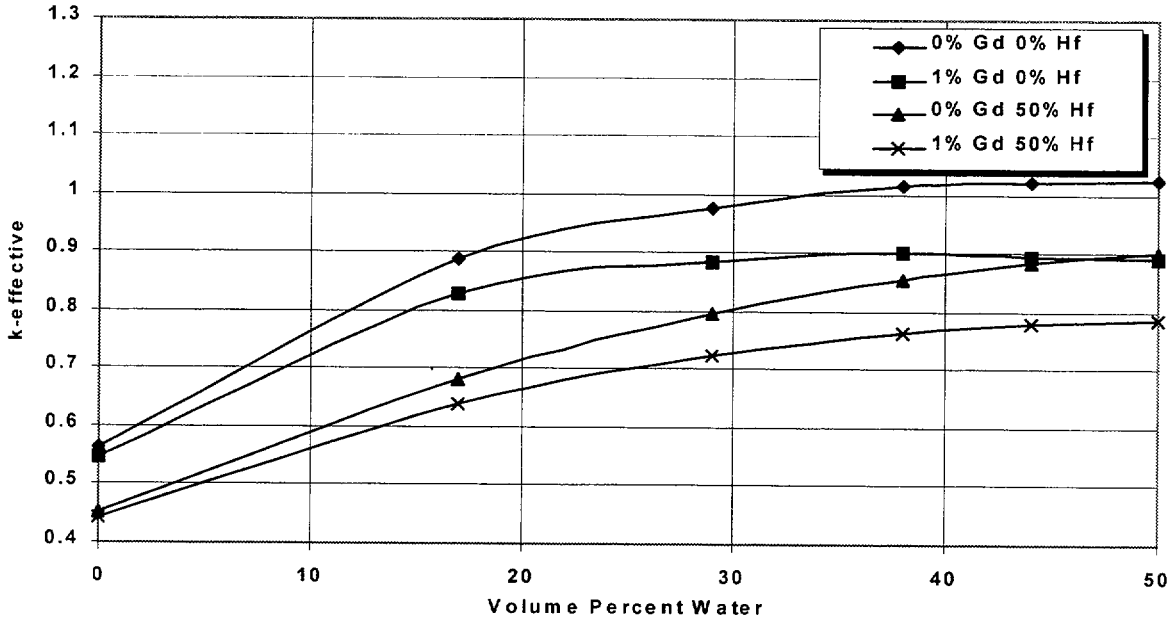


Figure 6-31. MCNP k_{eff} for Case 14 with Partial Gd and Hf Removed (CRWMS M&O 1999k, Fig. 6-3)

Table 6-12. Minimum Hf Required to Maintain Subcriticality

Time Since WP Breach ¹ (yr.)	Volume % Water	Percent Initial Gd Present	Percent Initial Hf Present	k_{eff}	Standard Deviation
10,017	50	0	50	0.90218	0.00114
10,017	50	0	40	0.92370	0.00098
10,017	50	0	30	0.94466	0.00103
20,000	50	0	25	0.92727	0.00068
20,000	50	0	20	0.93963	0.00062
20,000	50	0	15	0.95226	0.00062
30,200	50	0	5	0.94017	0.00098
30,200	50	0	0	0.95391	0.00077
42,518	50	0	0	0.91494	0.00093

¹ Assumed 10,000 years after discharge from reactor

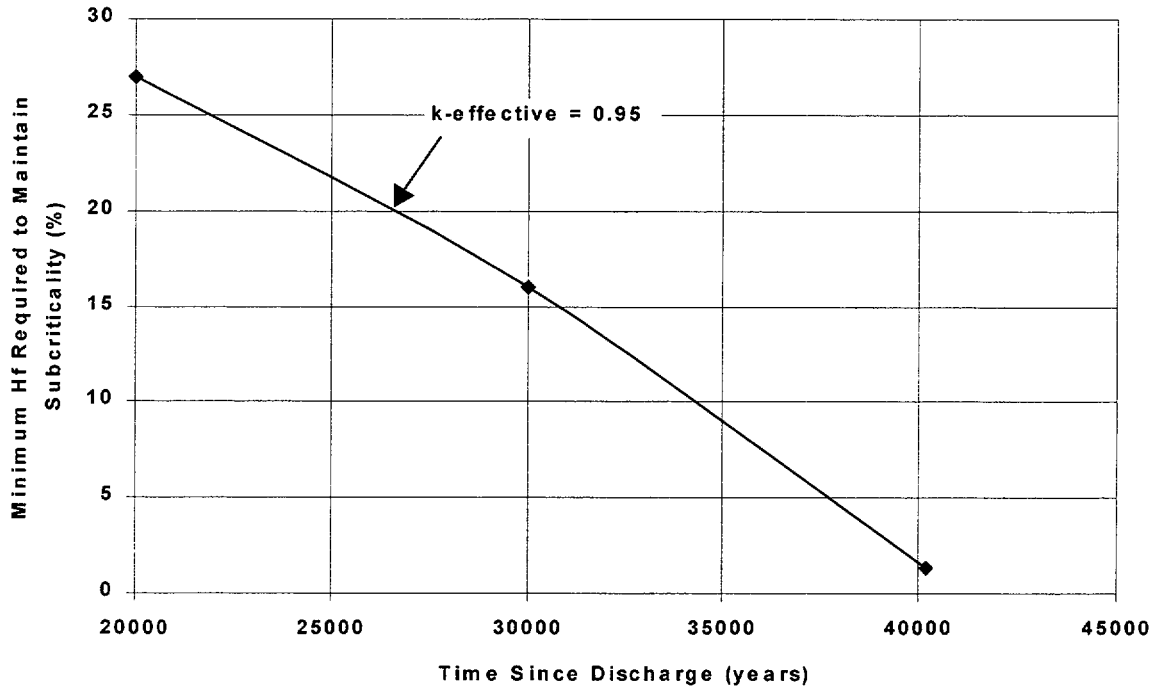


Figure 6-32. Minimum Hf Required to Maintain Subcriticality versus Time since Discharge

A second degradation scenario was evaluated that had approximately 78% of the Gadolinium removed from the sludge 13,175 years after breach of the WP. This was Case 13 discussed in Section 6.2.3.1.3. Case 14 evaluated earlier only had about 49% of the Gd removed 42,518 years after WP breach. Figure 6-33 (CRWMS M&O 1999k, Fig. 6-5) shows a plot of the Case 13 results along with the 10,017 years results from Case 14. A comparison of the functions plotted in Figure 6-33 shows the effects of the higher Gd loss in Case 13 compared with Case 14.

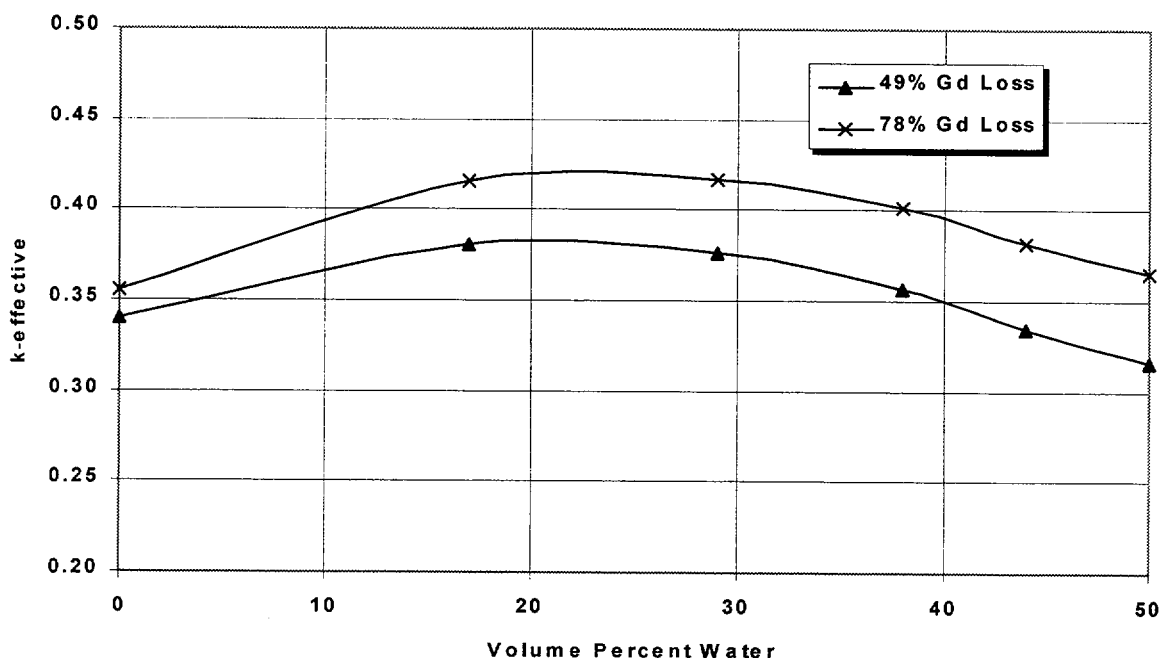


Figure 6-33. Calculated k_{eff} for Maximum Gd Loss Cases

The criticality evaluations presented in this section show two types of results:

- The maximum Gd removal from the waste package computed by the geochemistry code, EQ3/6 still leaves enough Gd in the waste package to be safely sub-critical.
- Complete removal of the Gd (leaving only Hf as a neutron absorber) may produce criticality, but only if enough Hf is removed and only before 40,000 years after creation of the waste form. This result is presented only as a point of reference. There is no physical mechanism for producing such large removal of the Gd without also removing most of the other waste package contents, including the fissile material.

6.3 PROBABILITY OF INTERNAL CRITICALITY

The purpose of these probability calculations is to provide a conservative estimate (upper bound) of the probability of criticality for MOX PWR SNF. There is no probability calculation for the ceramic waste form because there were no credible configurations that had a k_{eff} greater than 0.54, and even those were very unlikely (Section 6.2.3.2).

6.3.1 Method

The details of this method are provided in CRWMS M&O (1999), Sections 2, 5, and 6). This calculation uses a Monte Carlo methodology to generate k_{eff} statistics for the 21 PWR waste package. Probability distributions are developed from these statistics. The Monte Carlo

methodology generates values for key parameters using random sampling from recognized probability distributions for those parameters. Each set of parameters that completely determines a value of k_{eff} is called a Monte Carlo realization. For each realization it would be possible to calculate k_{eff} using MCNP. However, reasonable statistics over the range of parameters of interest requires tens of thousands of realizations, and it would be impractical to do so many MCNP calculations.

The Monte Carlo methodology is efficiently implemented by setting up two tables from the MCNP cases discussed in Section 6.1.3.3. One table is for the 200 cases with fission product loss, and the other is for the 40 cases with iron oxide loss. Each of these tables contains equal numbers of cases for the two batches of MOX fuel that have significant criticality potential, (1) 304 assemblies with initial 4% ^{239}Pu loading and 35.6 GWd/MTHM burnup and (2) 76 assemblies with initial 4.5% ^{239}Pu loading and 39.3 GWd/MTHM burnup. The methodology implicitly assumes that the waste package is homogeneously loaded with assemblies having the same burnup and initial Pu, so these numbers imply approximately 15 and 4 waste packages, respectively. The remaining assemblies out of the total of 1732 can be seen to be non-critical in the analysis of Section 6.1.3.3.

Each batch (or burnup-Pu loading pair) is subjected to 30,000 Monte Carlo realizations. Each Monte Carlo realization begins with a random selection of whether the package is dripped on and whether the package is breached on the top before it is breached on the bottom. For realizations that satisfy both conditions, the time before breach and the time between first top breach and first bottom breach (duration of waste package "bathtub" configuration) are randomly generated.

Also generated at this time are start and finish times for the assembly collapse process, the fission product loss process, and the iron oxide loss process. Then the data for each successive time step are generated. These are primarily the secondary degradation parameters: fission product loss, pitch between fuel pins, and loss of iron oxide. Each of these is generated in a two-step process. First, a nominal value is computed by taking the parameter to be fractionally degraded in proportion to the time from the start of the degradation process. Next a fluctuation is added, which is normally distributed with zero mean. The standard deviation, or amplitude, of this fluctuation is an input parameter. After these parameters are generated, the k_{eff} is calculated by table lookup and interpolation. As mentioned in the previous paragraph, for the fission product loss cases, the lookup table consists of 200 lines (k_{eff} values). For the iron oxide loss case, the lookup table consists of 40 lines. The lines of the k_{eff} tables must be arranged so that the sequence of parameters listed corresponds to the frequency of cycling, with a latter listed parameter cycling faster than the earlier listed parameter. In addition, the cycles must go from low value to high. The order for the parameters in the 200-value table is enrichment, pitch, time, and fission product loss. The order for the parameters in the 40 oxide loss cases is enrichment, pitch, time, and iron oxide loss. Both these table files are given in Attachment V of CRWMS M&O (1999).

If k_{eff} exceeds the potential critical limit (CL), then a criticality will be recorded. For this purpose, the total number of criticalities is incremented by the number of assemblies in the batch (304 or 76). It should be noted that the criticality is for a waste package, but the bookkeeping is on a per assembly basis for convenience, since neither batch leads to an integral number of waste

packages. The expected number of waste package criticalities will be computed by dividing the number of artificial *assembly criticalities* by the number of assemblies per waste package, 21. The occurrence of a criticality is also logged according to the time of occurrence of the criticality using an array of bins, with one bin for each time step. For this purpose, the bin corresponding to this time step is also incremented by the number of assemblies in the batch. The simulation then moves to the next realization. If, on the other hand, the $k_{\text{eff}} < \text{CL}$, then the simulation moves to the next time step. If the time steps reach to the duration of the bathtub, the realization is considered to have had no criticality, and the next realization will begin.

After all the realizations have been processed for the two batches, the summary statistics are generated over the time period covered, 100,000 years. The fraction of assemblies participating in a criticality is determined by dividing the total number of criticalities by the number of chances for criticality. This number of chances is the product of two factors: the total number of assemblies, and the number of Monte Carlo realizations. The probability density function (pdf, more properly called a frequency function, ff, since a distribution characterized by discrete time steps is considered) is similarly computed by dividing the number of criticalities in each bin by the same number of chances for criticality. The cumulative distribution function (CDF) as a function of time is then calculated by summing the pdfs (or ffs) to that point in time. Although this fraction has been calculated as a fraction of assemblies that could be critical, it is equally valid as a fraction of waste packages since x% of assemblies would also be x% of waste packages. The expected number of packages that will experience criticality is then the fraction of packages that become critical (which is the probability of criticality) multiplied by the total number of packages (which is the total number of assemblies divided by the number of assemblies per package, 21).

6.3.2 Probability Distributions of Secondary Degradation Processes

As mentioned previously, the primary degradation process, corrosion of the basket materials (carbon steel, borated stainless steel, and aluminum) is assumed to take place initially (Figure 6-1A through D). Since this results in no criticality (Section 6.1.3.3) the calculation begins with the assumption that all these processes have taken place completely and that all the boron has been removed from the waste package. The three principal degradation processes considered in this calculation are the ones that follow this initial set. These are assembly collapse, FPL, and iron oxide loss; they may be referred to as secondary degradation processes. These processes take the configuration from D through E and F of Figure 6-1. Each of these processes is assumed to proceed at a constant rate between a specified start and finish time, as described in Section 6.3.1.

Although none of these processes is likely to take place in the first 100,000 years following emplacement, the purpose of this calculation is to test the sensitivity to assumptions of when they could occur. Since the zircaloy spacer grids (Toledo Edison 1998, Table 4.2-1) are two thirds the thickness of the zircaloy fuel pin cladding (CRWMS M&O 1998x, p. 26), and since the spacer grids are exposed to corrosion from both sides while the cladding is only exposed to corrosion from one side, the assemblies are more likely to collapse before significant degradation of the fuel matrix itself. However, the Monte Carlo simulation does consider the possibility of

these processes occurring simultaneously, with appropriate probability weighting, to ensure that the final result represents a conservative estimate.

For the nominal cases the start times for all three processes are generated randomly according to a uniform distribution between 10,000 and 20,000 years. The finish times are generated randomly according to a uniform distribution between 80,000 and 90,000 years. These cases are called nominal for reference purposes only. They represent scenarios that are very unlikely. For the nominal fission product loss scenarios, the corrosion of the basket and the fuel matrix must overlap in time, or there will be very little fission product loss, as explained in Section 6.1.3.2. The iron oxide loss scenarios are so unlikely as to be incredible, since iron oxide is very insoluble. The iron oxide loss scenarios are included only because there has been some conceptualization of mechanical disturbances that might produce such an effect.

It will be seen in Section 6.3.3, below, that the nominal scenarios do not lead to any criticality for the MOX SNF.

6.3.3 Criticality Probability

The results of the probability calculations can be summarized in terms of expected number of criticalities in 100,000 years. These are given in Table 6-13 together with a brief characterization of the key parameters for 12 scenarios. An analysis of the results for each scenario follows the table. It should be re-emphasized that these are all very conservative scenarios for reasons given in Section 6.3.1; the scenario with the highest number for expected criticalities, Scenario 8, is characterized by two very unlikely conditions favorable to criticality: iron oxide loss before 35,000 years, and assembly collapse after 100,000 years.

Table 6-13. Expected Number of Criticalities for 83 MOX Waste Packages (CRWMS M&O 1999, Table 6-1)

Scenario	Number at 100,000 yr.
1. Nominal FPL ^a and collapse, no oxide loss	0
2. Nominal FPL, no collapse, no oxide loss	0.0157
3. Early FPL, nominal collapse, no oxide loss	0.0066
4. Early FPL, no collapse, no oxide loss	0.0804
5. Nominal oxide loss, nominal collapse, no FPL ^c	0
6. Nominal oxide loss, no collapse, no FPL	0.0019
7. Early oxide loss, nominal collapse, no FPL	0.0078
8. Early oxide loss, no collapse, no FPL	0.0653
9. Nominal FPL, collapse, high fplcv ^a	0
10. Nominal FPL, no collapse, high fplcv	0.0432
11. Nominal oxide loss, collapse, high oxlosscv ^b	0
12. Nominal oxide loss, no collapse, high oxlosscv	0.0134

^a Coefficient of variance (cv) of the fission product loss parameter = 0.7, as compared with the nominal 0.3.

^b Coefficient of variance of the iron oxide loss parameter = 0.7, as compared with the nominal 0.3.

^c No fission product loss.

^d FPL: fission product loss.

Scenarios 1 and 5 are the least conservative. They have been identified as nominal in Section 6.3.2. Since neither of these scenarios shows any criticality in 100,000 years in any of the

60,000 Monte Carlo realizations, scenarios that are even more conservative are examined. Scenarios 2 through 4 represent more conservative variations on Scenario 1. In these cases early fission product loss means all the fission product neutron absorbers are lost from the waste package by 50,000 years. No collapse means that the start of any reduction in assembly pitch is delayed beyond 100,000 years. This requires two very unlikely conditions. In the first place, the corrosion of the spacer grids must be delayed beyond the time of the corrosion of the cladding, which is extremely unlikely because of the relative thicknesses and exposure to water, as explained in Section 6.3.2. Equally important, the cladding must retain structural integrity while having enough holes to permit major fission product loss. Although it is possible to imagine a fuel pin cladding with half the surface area covered with regularly spaced holes, in such a manner that the structural rigidity was not compromised, any randomness in the location of these holes would certainly lead to a number of overlapping holes and a complete breaking of the fuel pin.

The increase in expected number of criticalities with time for these three alternative scenarios is shown in Figure 6-34. This figure shows that the expected number of criticalities remains constant after approximately 60,000 years for all three scenarios. This is because the k_{eff} decreases with time beyond 25,000 years due to the decay of the more reactive fissile isotope, ^{239}Pu , to the less reactive isotope, ^{235}U . Therefore, there are no new criticalities possible ($k_{eff} > \text{CL}$) beyond 60,000 years for these scenarios.

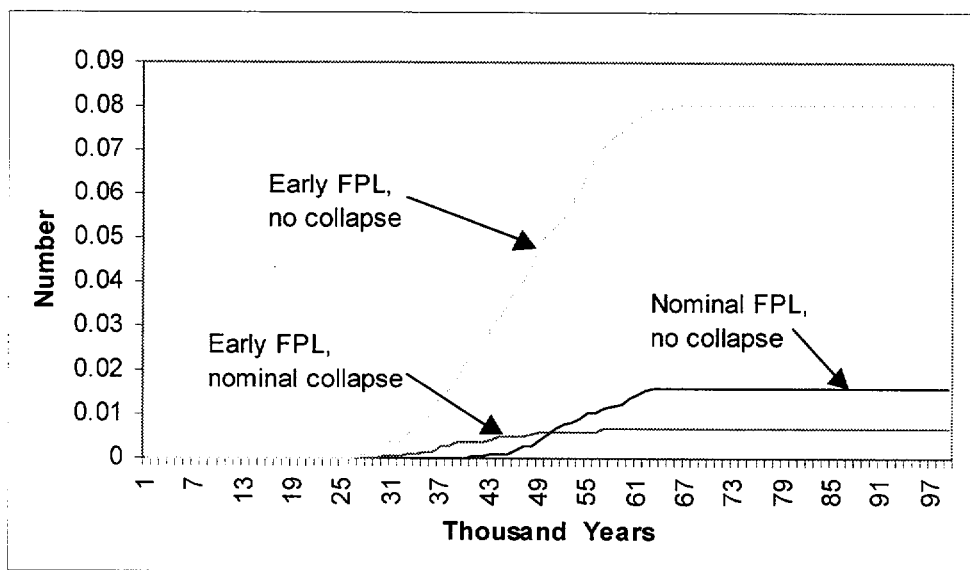


Figure 6-34. Expected Criticalities for Alternative Fission Product Loss Scenarios (CRWMS M&O 1999I, Fig. 6-1)

Scenarios 5 through 8 examine the effects of iron oxide loss. Since the nominal iron oxide loss scenario (Scenario 5) shows no criticality, Scenarios 6 through 8 are examined as alternatives that are more conservative. These scenarios add the following unlikely conditions, either individually (Scenarios 6 and 7) or jointly (Scenario 8): early oxide loss (in less than 50,000 years) and no (or delayed) assembly collapse. These are seen to have approximately the same order of magnitude expected number of criticalities at 100,000 years as the corresponding

Scenarios 2 through 4. The cumulative expected number of criticalities as a function of time, under these extremely conservative scenarios, are shown in Figure 6-35. This group also shows no increase in the number of criticalities beyond 60,000 years.

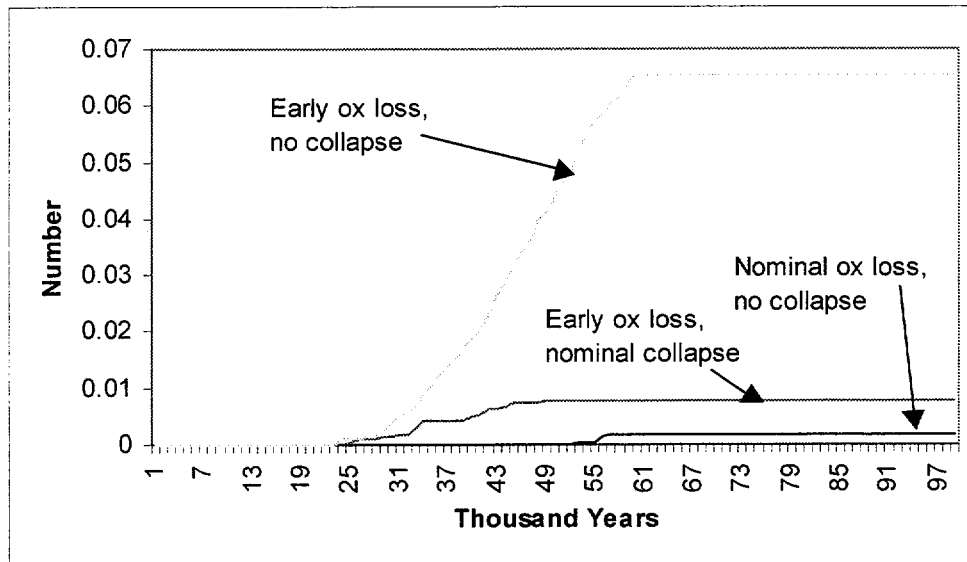


Figure 6-35. Expected Criticalities for Alternative Iron Oxide Loss Scenarios (CRWMS M&O 1999l, Fig. 6-2)

Sensitivity analysis for this calculation is performed with respect to the spread in the distribution of random uncertainty that is added to the linear interpolation for the two degradation parameters, fission product loss and iron oxide loss. The amount of this spread is determined by the coefficient of variation, which is the ratio between the standard deviation and the mean of the normal distribution generating the values of the parameter in question. The coefficient of variation is indicated by the suffix “cv” in Table 6-13. The nominal value for the coefficient of variation is 0.3 for all three of the secondary degradation parameters. The sensitivity to the coefficient of variation is tested by increasing this value to 0.7 for fission product loss in Scenarios 9 and 10 and for iron oxide loss in Scenarios 11 and 12. Scenarios 9 and 11 show no criticalities, indicating that increasing the coefficient of variation does not significantly increase the probability of criticality if the corresponding scenarios for the lower coefficient of variation (Scenarios 1 and 5, respectively) show no criticality to begin with. However, Scenarios 10 and 12 do show significant increase in expectation of criticality over the corresponding scenarios with lower coefficient of variation, Scenarios 2 and 6, respectively. The cumulative expected number of criticalities as a function of time, under these extremely conservative scenarios, are shown in Figure 6-36.

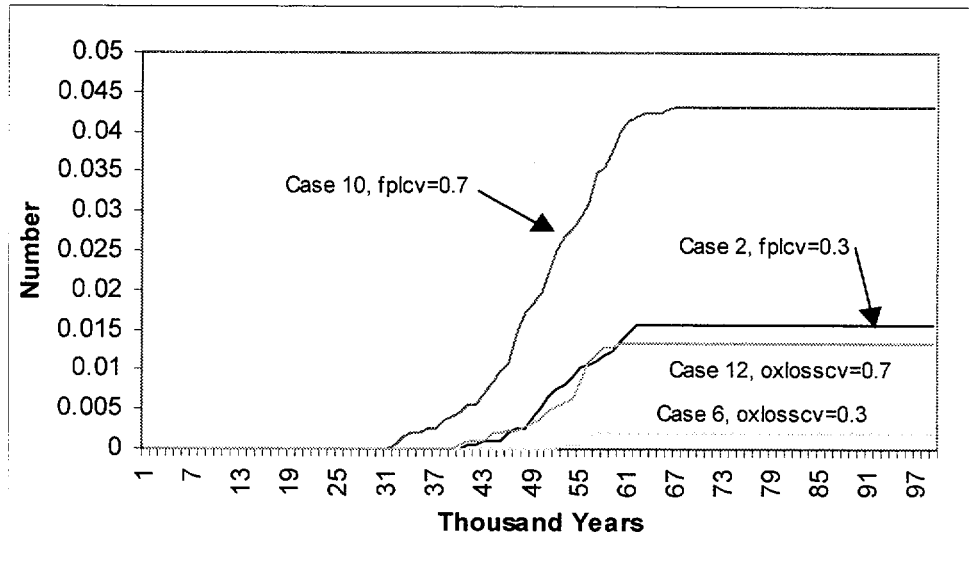


Figure 6-36. Expected Criticalities with Alternative Coefficients of Variance for Oxide Loss and Fission Product Loss (CRWMS M&O 1999I, Fig. 6-3)

The probability evaluations of this section can be summarized as follows:

- Only those scenarios with at least two unlikely conditions more conservative than the nominal lead to criticality.
- Of the scenarios leading to criticality, those requiring the largest number of unlikely conditions lead to the highest number of expected criticalities.
- Because of the decay of Pu to U, there can be no criticalities beyond 60,000 years.

6.4 INTERNAL CRITICALITY CONSEQUENCES

This section presents a summary of the criticality consequence evaluation for the MOX SNF, which is described in detail in CRWMS M&O (1999m). The most conservative configuration to start a criticality has the waste package basket completely corroded (with loss of all the boron from the borated stainless steel), but with the assembly completely intact. Any collapse of the assemblies would reduce the reactivity, as was shown by the partly collapsed cases in Section 6.1.3.3. In this configuration the iron oxide remaining from the corrosion of the basket components plays a major role in preventing criticality.

The potential criticalities can be divided into two categories: transient and steady state. The transient criticality arises when an event results in an increase in reactivity that takes the k_{eff} from just below 1 to just above 1. An example of such an event is a re-arrangement of the iron oxide due to a seismic disturbance. The principal consequences of the transient criticality are an increase in pressure and temperature within the waste package. These increases are associated with steam production and removal from the waste package. Removal of water from the waste package reduces k_{eff} and shuts down the criticality before there can be significant increase in

radionuclide inventory. If the reactivity increase is very slow, or just enough to take the configuration to $k_{\text{eff}} = 1$ and no higher, the amount of water lost by steam blowoff may be so small that the criticality stabilizes, instead of being shut down. This leads to a steady state criticality, which can lead to an increase in radionuclide inventory, if the duration is long enough (upwards of 10,000 years). The consequences of both types of criticality are evaluated in the remainder of this section.

If the penetration area through the WP is sufficiently small, inflow will be smaller and less likely. This will lengthen the time required for flooding the WP. This, in turn, will delay, or prevent the occurrence of any criticality events. If a criticality event does occur, the penetration area becomes the exit area through which steam must flow out of the waste package to provide the negative feedback that will ultimately limit the criticality. A smaller penetration area will limit the exit area available for the required outflow, thereby reducing the negative reactivity effect of voiding the WP because the water/vapor escape rate will be lowered. This, in turn, leads to higher heat output, higher internal pressure, and higher temperatures. The higher pressure and density of the water vapor will increase the mass flow out of the waste package, so that eventually the negative reactivity from voiding the system becomes dominant, and the criticality event shuts down.

Consequences must assume a start with $k_{\text{eff}} = 1$, but critical configurations are nominally identified at lower values of k_{eff} to account for bias and uncertainty. In fact the worst case values of k_{eff} given in the figures of Section 6.1.3.3.2 and the tables of Section 6.1.3.3.3 are all less than 1, but greater than conservative thresholds that have been considered in the past for regulatory purposes (e.g., 0.95 or even 0.92). The criticality consequence calculations can bypass this issue. For the transient criticality, increases in pressure and temperature are calculated (as described in Section 6.4.1.1). These increases are ultimately controlled by the total feedback, which, in turn, is computed from the calculated values of the derivatives of k_{eff} with respect to the various parameters effecting reactivity control. If the actual values of k_{eff} are close to 1, the derivatives should be close to the values they would have if k_{eff} were actually equal to 1. The methodology for steady state criticality control calculates the radionuclide inventory increment, based on the power level, which determines the number of fissions per unit time, as described in Section 6.4.2, below.

6.4.1 Transient Criticality

Since the primary control measure for a transient criticality is steam blowoff, reducing the total cross section area of waste package penetrations (exit area for steam) will allow a greater increase in pressure before the criticality shuts itself down. Therefore, the transient criticality consequence analyses calculate peak overpressure for a range of exit areas.

The light water reactor transient analysis code, RELAP5/MOD3.2 (INEEL 1995a) was used to calculate the time evolution of the power level and other characteristics of a criticality event involving PWR MOX SNF. RELAP5/MOD3.2 was previously obtained from SCM in accordance with appropriate procedures. RELAP5/MOD3.2 is qualified and used only within the range of validation as documented in the SQR (CRWMS M&O 1999n)

6.4.1.1 Transient Criticality Methodology

The methodology for evaluating transient criticality consequences involving intact PWR SNF in a degraded WP has been documented previously (CRWMS M&O 1997l). The methodology places primary reliance on RELAP5 code that is used for calculating the consequences of a transient criticality. This code is used extensively to represent nuclear reactor transients. It is designed for use with fundamentally one-dimensional hydraulic systems but does include multi-directional flow representation under restricted conditions (INEEL 1995b, pp. 2-14 through 2-16). The RELAP5 representation for the degraded WP contains flow connections in the two directions normal to the WP cylinder axis but not parallel to the axis. For the quasi-two dimensional representation used here, the fuel bundles were represented at one-fifth their actual length with appropriate adjustments to the representation parameters. The principal elements of the representation description include the geometric representation, flow connections, friction factors, and heat conductors. These elements are described in the following sections. Note that RELAP5 input quantities are specified in English units.

The simulated criticality event is driven by a linear rate of reactivity insertion up to a maximum of 14.18 \$ (CRWMS M&O 1997l, Section 7) and held constant thereafter. The 14.18 \$ reactivity value was derived from the LEU WP reactivity change between a homogeneous and settled distribution of Fe_2O_3 (CRWMS M&O 1997l, Section 7, and CRWMS M&O 1999m, Section 2.1) and used in this calculation to maintain a consistent basis for purposes of comparison. The principal condition required for this reactivity insertion is that the iron oxide be in a maximally controlling geometry (uniform throughout the waste package) and then be shaken in such a way that it settles into a minimally controlling geometry (settled to the bottom of the waste package). Since these are the extremes of the possible geometries, the condition for the high reactivity insertion must be regarded as extremely unlikely. The calculation was performed for time scales corresponding to a rapid reactivity insertion rate of 0.158 \$/s and a much slower rate of 0.0004 \$/s. The rapid reactivity insertion rate was derived from the time required (\cong 90 seconds) for a spherical particle of Fe_2O_3 to fall one meter in water at a Reynolds number of \sim 1.0 (CRWMS M&O 1997l, Attachment III), hence the value $0.158 \text{ \$/s} = 14.18 \text{ \$/90 sec}$. This time provides an upper bound on the rate that reactivity in the WP can be increased through absorber redistribution.

The low reactivity insertion rate approximates a more likely gradual shift in conditions conducive to criticality. One possible mechanism is a sudden increase in the flow rate into the waste package which could cover all the assemblies in approximately 10 hours, starting from a partially covered (30 - 35%) condition for the top fuel assemblies, corresponding to the 14.18 \$ total reactivity addition.

6.4.1.2 Transient Criticality Results

The transient criticality results are presented separately for the two types of reactivity insertion rate: rapid and slow, where the former is has a timescale of seconds, and the latter has a timescale of hours. This classification will be seen to be justified by the behavior of peak overpressure as a function of exit area. The peak overpressure for the fast reactivity insertion

rate cases increases strongly with decreasing exit area, but not for the slow reactivity insertion rate.

The increase in radionuclide inventory for transient criticality is negligible, as can be seen from the relatively small increment in burnup for transient criticality. For the rapid insertion rate, the total burnup over one event is approximately 4.2×10^{-6} GWd/MTHM (CRWMS M&O 1999m, Section 6.1). For the slow insertion rate, the total burnup is 5×10^{-7} GWd/MTHM (CRWMS M&O 1999m, Section 6.2). This is certainly negligible by comparison with the upwards of 35 GWd/MTHM burnup received over the lifetime in the reactor. It is also negligible by comparison with the 2.7 GWd/MTHM received in a 10,000 year steady state criticality, Section 6.4.2.2, below.

6.4.1.2.1 Rapid Reactivity Insertion Rate Results

A series of cases having a rapid reactivity insertion rate were run with decreasing exit junction area as a variable parameter (CRWMS M&O 1999m, Section 6.1). The reactivity insertion rate for these cases was 0.158 \$/s corresponding to the maximum reactivity of 14.18 \$ added in 90 seconds (Section 6.4.1.1). As expected, peak values of the system pressure and fuel temperature were insensitive to the exit area until the area was decreased to extremely small values. The results for these variables are summarized in Table 6-14.

Table 6-14. Maximum Temperature and Pressure Values for PWR MOX SNF for a Reactivity Insertion Rate of 0.158 \$/s (CRWMS M&O 1999m, Table 6.1-1)

Exit Area (cm ²)	Temperature		Pressure	
	(K)	(°F)	(Pa)	(psi)
10.0	413.91	285.37	1.15E+05	1.67E+01
5.0	413.91	285.37	1.15E+05	1.67E+01
0.5	413.92	285.39	1.43E+05	2.08E+01
0.375	413.92	285.38	1.63E+05	2.37E+01
0.25	453.23	356.15	9.17E+05	1.33E+02
0.10	493.70	428.99	5.89E+06	8.55E+02

Figure 6-37 shows the pressure histories (as a function of time) for a representative interior location in the WP and Figure 6-38 shows the temperature histories for a representative SNF assembly. Figure 6-39 shows the exit junction mass flow rates. It should be noted that the smallest exit area, case F, shows a secondary peak in flow rate at approximately 65 seconds, corresponding to a secondary pressure peak at approximately the same time, as can be seen from Figure 6-37.

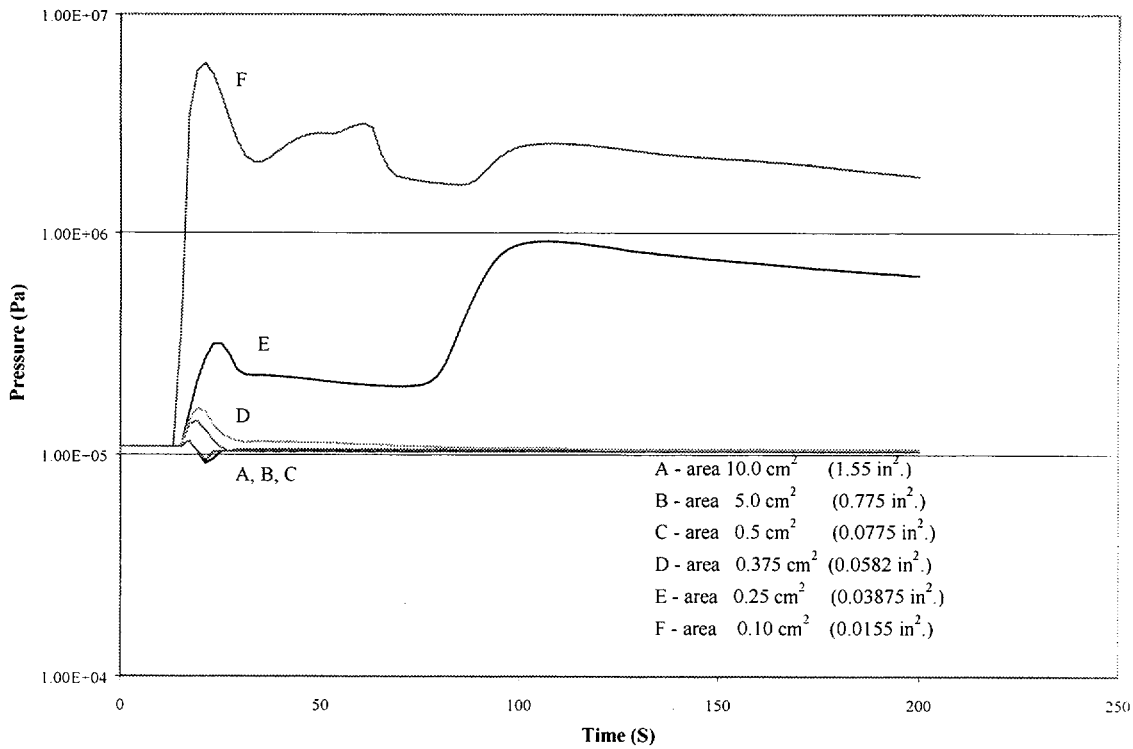


Figure 6-37. Pressure for 0.158 \$/s Insertion Rate (CRWMS M&O 1999m, Fig. 6.1-3)

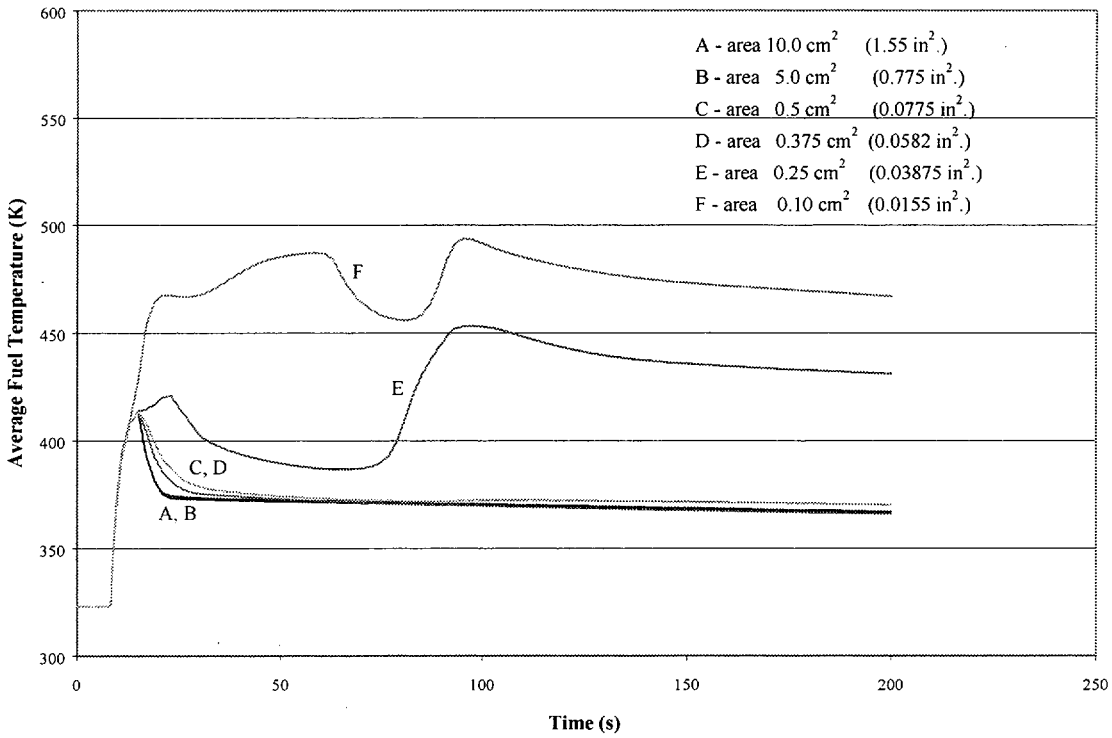


Figure 6-38. Fuel Temperature for 0.158 \$/s Insertion Rate (CRWMS M&O 1999m, Fig. 6.1-4)

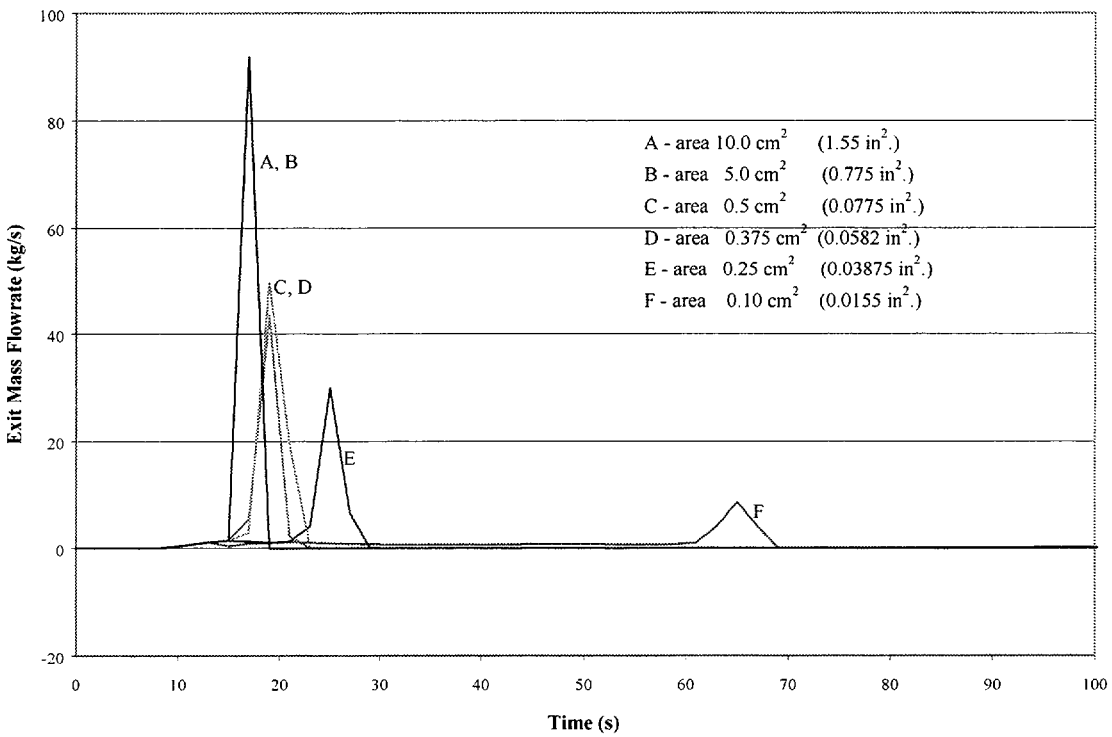


Figure 6-39. Exit Flow 0.158 \$/s Insertion Rate (CRWMS M&O 1999m, Fig. 6.1-9)

6.4.1.2.2 Slow Reactivity Insertion Rate

The consequences to a WP containing MOX PWR SNF of a criticality event with a low reactivity insertion were calculated for events having a reactivity addition rate of 0.0004 $\$/s$ and for quasi-static events (CRWMS M&O 1999m, Section 6.2). The 0.0004 $\$/s$ rate is the same as used for the commercial PWR SNF reactivity consequence sensitivity calculation (CRWMS M&O 1999o, Section 2). This latter calculation showed that results had little sensitivity to the exit area. Consequently, only two exit areas were used for this calculation; a 10.0-cm² and 0.1-cm² area. These results are shown in Figure 6-40.

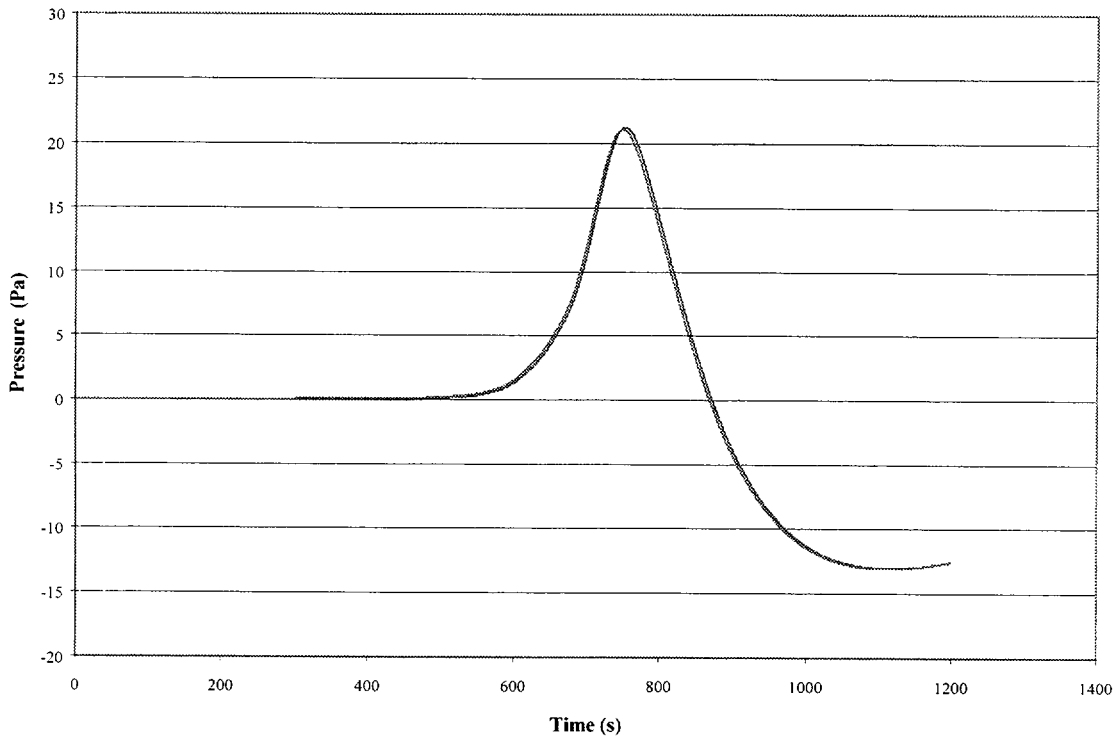


Figure 6-40. Pressure for 0.0004 $\$/s$ Insertion Rate (for both 10.0 cm² and 0.1 cm² exit areas) (CRWMS M&O 1999m, Fig. 6.2-1)

6.4.2 Steady State Criticality

6.4.2.1 Steady State Criticality Methodology

In a steady state criticality the radionuclide inventory increment is determined by the power level and the duration. The physical factors that control the power level, and their interactions, are described as follows. Consider a configuration that has the assemblies nearly covered with water, so that criticality is reached as water is added slowly. As the criticality is reached the increased heat will raise the temperature so that the water evaporates faster. At some temperature the rate of water loss by evaporation will just equal the rate of water addition by dripping into the waste package. The steady state power level will provide just enough power to supply the heat loss by conduction (through the rock beneath and beside the waste package) by radiation (to the drift wall or intermediate surface such as drip shield), and by heating and

evaporating the incoming water. For calculating evaporation rate it is conservatively assumed that airflow is stagnant in a drift during postclosure, and evaporation can be represented as diffusion of water vapor into air. The basis for this assumption and the details of the heat transfer calculations summarized in the following paragraphs are given in Section 5.3 of CRWMS M&O (1999m).

The approximate mean rate of water dripping on a waste package during a long-term super-pluvial climate in Total System Performance Assessment (TSPA)-VA was approximately 0.5 m³/yr. (DOE 1998b, pp. 3-15 and 3-23). The waste package would produce sufficient power to maintain the water in the waste package at a temperature of 73°C, as well as compensate for other mechanisms of heat loss, to match this drip rate. The surface area of the water just above the upper row of assemblies (~8 cm from inner barrier inner surface) is taken to be 3 m² (CRWMS M&O 1996d, p. VII-4).

As stated above, additional heat losses will also occur due to radiation and/or conduction heat transfer to the local environment. The actual configuration of the drift thousands of years after emplacement cannot be defined sufficiently to allow a detailed heat transfer estimate. It is highly likely that a portion of the waste package may be covered with rubble, possibly as a result of the gradual collapse of the drift, and both radiation and conduction mechanisms will be active. However, examination of ideal radiation-only and conduction-only systems should respectively provide an upper and lower bound on the heat loss from a waste package with a bulk water temperature of 73°C. Heat losses due to radiation alone can be estimated by treating the WP and drift as a system of concentric cylinders, with the waste package surface at 73°C, and the drift wall assumed to maintain a constant 30°C.

The radiation heat loss from a 73°C WP is estimated to be 6558 W. The surface temperature of 73°C indicates that 728 W will be lost if all heat transfer occurs by conduction through crushed tuff. Assuming the more likely configuration of a waste package covered halfway with rubble, the heat loss may be approximated (i.e., not specifically accounting for the radiation heat transfer between the rubble and the drift wall) by taking the mean of the above two extremes plus 37 W. The fact that the power can be completely dissipated by these mechanisms indicates that evaporation alone will be sufficient to remove the incoming water, and bulk boiling will not occur.

Once the bounding power level is determined, the calculation of the number of fissions and the amounts of fission products and actinides was performed with the SAS2H-ORIGEN-S modules from the SCALE4.3 code system (CRWMS M&O 1997a) for the PWR MOX assembly with a fissile Pu content of 4.0 wt% HM and burnup of 35.6 GWd/MTHM. A baseline case was run with only the decay option and a criticality case run with a burn subcase included in the ORIGEN-S data at 25,000 years through 35,000 years followed by decay to one million years. For a conservative calculation, the larger power source $((6558 + 37)/21 = 314 \text{ W/assembly})$ was used for the ORIGEN-S burn subcase.

6.4.2.2 Steady State Criticality Results

Results from the steady state criticality calculation are given in terms of the excess radionuclide inventory in curies produced during the postulated criticality event. The excess inventory is referenced to the baseline levels from the MOX SNF in a decay only mode. Table 6-15 lists the total radionuclide inventory levels for the 21 PWR MOX WP for the time period from 1000 years after the criticality event and extending to 20,000 years past the end of the criticality. The radionuclide inventory level was approximately 18% over the baseline level at 1000 years following the criticality event but fell to less than 3% over the baseline level by 20,000 years after termination of the criticality event. The baseline activity level in this time period is primarily due to the Pu isotopes (> 90%) and these are the principal activity contributors for the criticality case also (> 70%) (CRWMS M&O 1999m). The individual isotopic activity levels for the same time period are given in CRWMS M&O (1999m, Table 6.3-2).

Table 6-15. Total Activity for 21 PWR MOX SNF Waste Package for Steady State Criticality Event (CRWMS M&O 1999m, Table 6.3-1)

Time following Emplacement (yr.)	Time Following Criticality Termination (yr.)	Total Activity No-Criticality (Ci)	Total Activity 10K yr. Criticality (Ci)	Percent Increase over Baseline Case
36000	1000	3.98004E+03	4.70748E+03	18.3
45000	10000	2.96840E+03	3.19413E+03	7.6
55000	20000	2.23317E+03	2.28937E+03	2.5

The steady state power of 314 W/assembly (Section 6.4.2.1), maintained for 10,000 years, yields a total of 2.7 GWd/MTHM. This is approximately a factor of 12 smaller than the 35 GWd/MTHM received in the reactor to begin with, and six orders of magnitude greater than the burnup experienced in the transient criticality, Section 6.4.1.2.

7. EXTERNAL CRITICALITY

7.1 SOURCE TERMS

Continued dripping of water into a breached WP may ultimately lead to transport, out of the WP, of degradation products including dissolved fissile elements from the waste form. The potential concentrations of fissile material in this effluent solution constitute the source terms for analyses of the transport and deposition of fissile material external to the WP for the purpose of assessing possible external criticality events.

Source term calculations using the EQ3/6 V7.2b software (CRWMS M&O 2000e) were used to provide descriptions of the predicted effluent solution chemistry. In particular, the Pu and U content where the latter includes the U-235 that results from the decay of Pu-239. The source term calculations with EQ3/6 used the SCFT methodology (described in detail in Section 6.2.3.1.1) for solutions in the WP which are also the concentration in the effluent. This methodology represents a "bathtub" situation where water constantly drips into the package, mixes thoroughly with the water already resident in the package, then exits the package at a rate equal to the drip rate. The "bathtub" representation is used for all the SCFT runs referenced in this document. This is consistent with the approach taken in Sections 6.1.1 and 6.2.1 of this document. Furthermore, the bathtub representation generally maximizes the loss of fissile materials, because the constant dilution lowers the chance that the aqueous solution will reach the solubility limits for the U and Pu solids.

The source terms from the MOX waste form are summarized in Section 7.1.1 and from the Pu-ceramic waste form in Section 7.1.2.

7.1.1 Source Term from the MOX Waste Package

Since the Pu solubility has not been precisely characterized, source terms from the MOX WP were calculated for two Pu solubility ranges (CRWMS M&O 2000a, Section 6): 1) a nominal one allowing formation of PuO₂ solid and using normal data base solubility product values; and 2) an increased Pu solubility for conservatism generated by suppressing PuO₂ formation and decreasing the equilibrium constant for solid Pu(OH)₄ by four orders of magnitude. For each Pu solubility range, calculations were carried out for a representative low and high drip rate (0.015 m³/y and 0.15 m³/y, respectively, from Section 2.3.2) using a two-stage process in which fissile material was not reacted until most of the metals had dissolved. In this manner the spent fuel is not exposed to the low pH conditions that might arise from corroding steel. In all cases, there is an early peak in Pu concentration (while there is still undissolved fuel to serve as source) followed by a long period of constant (steady-state) concentration. This steady state lasts until the Pu in the WP is exhausted. Sensitivity studies using a single stage process where the fissile material begins dissolving immediately showed similar steady-state Pu concentration but with the initial peak occurring earlier in the process (CRWMS M&O 2000a, Section 6, page 20).

The highest concentration of fissile material in the effluent resulted from low drip rates into the WP and high Pu solubility (CRWMS M&O 2000a, Section 6.2, second paragraph). The Pu concentration was about 4 orders of magnitude higher for this case compared to a nominal Pu

solubility case (CRWMS M&O 2000a, Figure 6.7) compared with Figure 6.2 of CRWMS M&O 2000a. The resulting Pu concentration of about 5×10^{-9} molality is more in line with concentrations found experimentally (Wilson and Bruton 1989, Table 3), and is about three orders of magnitude less than U concentrations found experimentally (Wilson and Bruton 1989, Table 3). Pu and U concentrations in water exiting the WP for high Pu solubility rates are shown in Table 7-1 (CRWMS M&O 2000a, Table III-1) and low drip rates and in Table 7-2 (CRWMS M&O 2000a, Table III-2) for high drip rates. Concentrations of both Pu and U approach a constant value as shown in Table 7-1 (Isotopic decay not modeled in the calculations).

Table 7-1. Aqueous Concentration for Low Drip Rate and High Pu Solubility

Element	Aqueous Concentration (mole/L) at Indicated Years					
	10,534 y	16,511 y	23,624 y	41,818 y	64,560y	91,851 y
Pu	1.23E-07	6.79E-09	6.51E-09	5.07E-09	5.07E-09	5.07E-09
U	6.09E-06	2.14E-05	2.24E-05	1.15E-04	1.15E-04	1.15E-04

Table 7-2. Aqueous Concentration for High Drip Rate and High Pu Solubility

Element	Aqueous Concentration (mole/L) at Indicated Years			
	10,223 y	12,010 y	14,253 y	15,850 y
Pu	3.64E-08	3.70E-08	6.58E-09	4.75E-09
U	6.10E-06	6.07E-06	2.25E-05	7.93E-05

7.1.2 Source Term from the Ceramic Waste Package

Through most of the time of this study the (activities activities leading to Rev 00 of this document) the degradation rates were taken from a study prepared at the Lawrence Livermore National Laboratory for the DOE (LLNL 1998). At that time, the ceramic dissolution experiments, run by LLNL, were incomplete, and temperature and pH effects were estimated with extreme conservatism. Because of this uncertainty, a set of "low," "average," and "high" Pu-ceramic rates were chosen for Pu degradation (Rev 00 of this document, CRWMS M&O 1999c, Table 5-3) designated as the "older" rates. The "newer" rates (Shaw 1999, Section 6) reflect much more experimental work (Shaw, 1999, Figure 6-1) and pH-dependent rates for Pu-ceramic. In particular, the newer rates show less temperature- and pH-dependence than was previously estimated (LLNL 1998). It will be seen in the analyses of external accumulation (Sections 7.2.2.1 and 7.2.2.2, for near-field and far-field, respectively) that the newer, lower, rates lead to lower waste stream fissile concentration, and, hence, lower accumulations. As explained below, in connection with Table 7-3, the "older" rates were used for worst case comparison for the far-field accumulation.

Most of the runs reported in this calculation are based on the newer LLNL data using the 50 °C rates for radiation-damaged ceramic (Shaw, 1999, Section 6) as the baseline "high" degradation rate, since temperatures over 50 °C are not expected after the WPs breach. The pH dependence, however, was abandoned in favor of a simpler, constant rate. There are several motivations behind this simplification. First, EQ3/6 7.2bLV (CRWMS 1998e, Wolery 1992, and Wolery and Daveler, 1992) can model radioactive decay in reactants, but only if the reactants are not defined

as minerals since stoichiometry is strictly preserved. Radioactive decay transmutes one element to another, thereby violating stoichiometry, thus radioactive decay in reactants, and pH-dependent degradation rates cannot be handled in the same code simultaneously. In addition, it was determined that a constant rate of $8 \cdot 10^{-15}$ moles/(cm²·s) and the pH-dependent rate produced extremely similar results (CRWMS M&O 2000b, Figure 5-9). For Pu-ceramic calculations, a "mole" is defined as 100g.

In addition to the change in Pu-ceramic degradation rate, the baseline solubility-controlling solid in this calculation was taken as Pu(OH)₄ (with the stability constant lowered by 4 orders of magnitude), instead of PuO₂. The change in Pu-controlling phases was made because experiments typically show the Pu solubility much higher than that of PuO₂ (Rai and Ryan 1982). While the choice of PuO₂ as the controlling solid is conservative for internal criticality studies (as it lessens the likelihood of Pu leaving the package), this choice is not conservative for external criticality studies.

The choice of WP source term scenarios was based on Table 6-1 in Reference CRWMS M&O (1999c). The highest Pu losses were found for conditions that involved slow water influx (0.0015 m³/y) and very fast Pu-ceramic degradation rates. Case 8 of that study produced the highest Pu loss, ~29.94%. For conditions with more moderate influx (0.015 m³/y), Case 10 of that study produced the highest Pu loss (1.8%). These two scenarios were selected as potential source terms.

Source terms for the Pu-ceramic were calculated for the "older" and "newer" Pu-ceramic degradation rates (CRWMS M&O 2000b, Section 5) as given in Table 7-3. The "older" Pu-ceramic degradation rate was used for the source term referred to as pe0a1231 and the "newer" rate for pw2a1231. Sensitivity source terms (pw7a1231 and pw8a1231 were developed by varying the Pu-ceramic degradation rate by factors of 10 and 100 above the baseline value, thus bracketing the "older" degradation rate (pe0a1231), resulted in similar maximum Pu concentrations as calculated for case pe0a1231. Except where otherwise indicated, pw2a1231 is the nominal source term for the cases in Table 7-4 (which is the same as Table 6-1 of CRWMS M&O 2000b). The exceptions are those cases in the 9xx group of Table 7-4 that identify the use of pw7a1231 and pw8a1231. The pe0a1231 source term is used extensively in CRWMS M&O 2000c, and is identified as such.

Table 7-3. Pu-ceramic Degradation Rates for Source Term Calculations

Case ID	Degradation Rate (moles/cm ² ·s)	Decay of Pu-239 To U-235
pe0a1231	3.472e-13 ^a	No
pw2a1231	8.0e-15 ^b	Yes
pw7a1231	8.0e-14 ^c	Yes
pw8a1231	8.0e-13 ^c	Yes

^a CRWMS M&O 1999c, Table 5-3.

^b CRWMS M&O 2000b, Section 5.3.1.2

^c CRWMS M&O 2000b, Section 5.3.1.2, identified as 10 times and 100 times in the last sentence of the section.

The Pu source terms in moles per liter of WP effluent solution for the two Pu-ceramic degradation rates (pe0a1231 and pw2a1231) are given in Figure 7-1 (CRWMS M&O 2000b, Figure 5-6, Pu_e0 and Pu_w2 data). The corresponding U source terms are shown in Figure 7-2. These curves are from CRWMS M&O 2000b. The curve labeled pi0a1231 is from Figure 5-7 labeled U_VA. The other curve is from Figure 5-9 labeled U_con. It should be noted that Figure 5-9 of CRWMS M&O 2000b also shows the insensitivity of fissile concentrations to whether the degradation rate was pH dependent (curves labeled with the suffix _TST) or constant (curves labeled with the suffix _con).

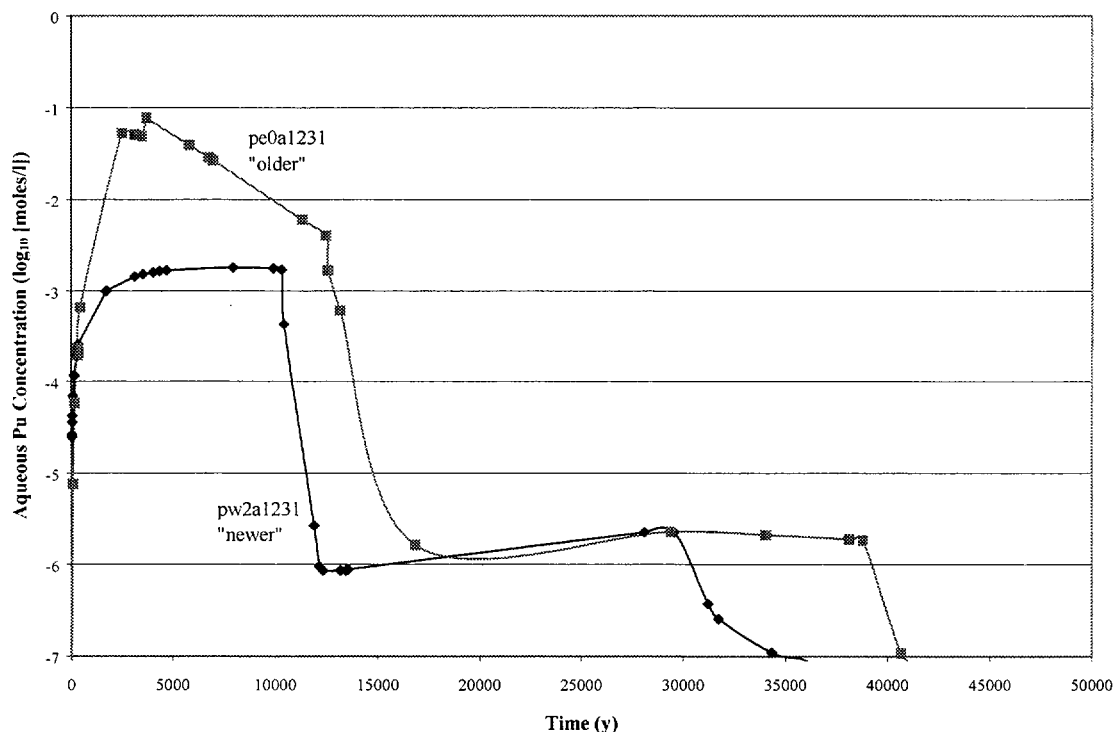


Figure 7-1. EQ3/6 Pu Source Terms

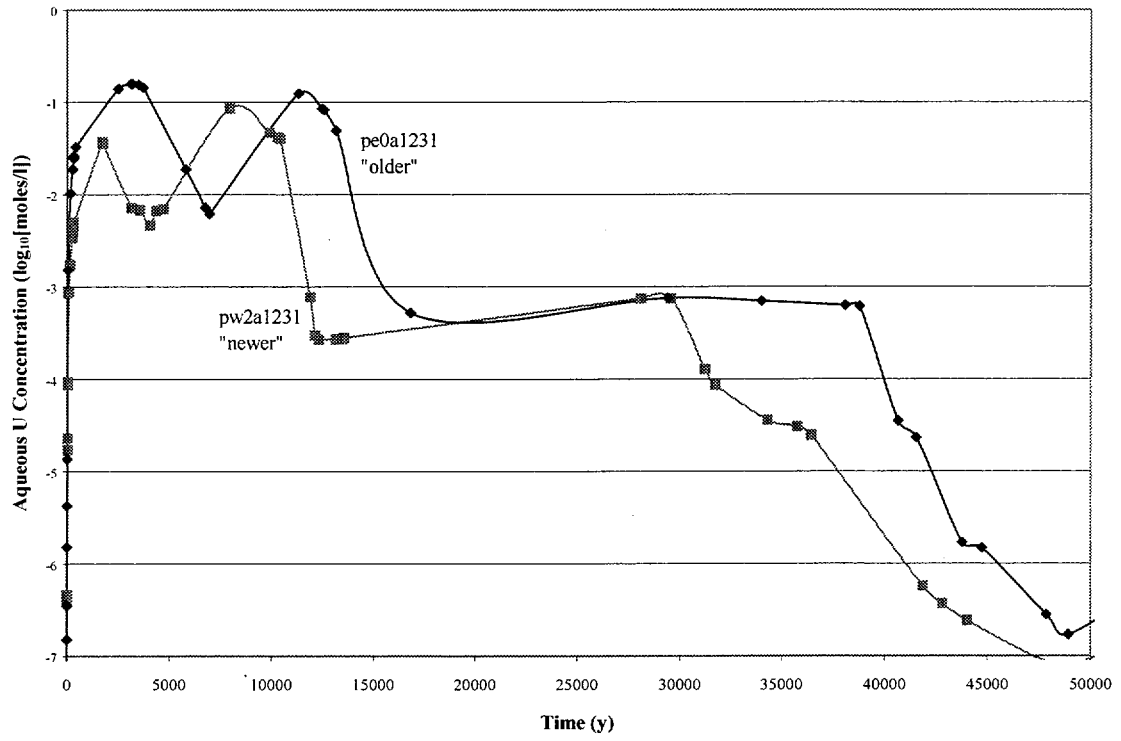


Figure 7-2. EQ3/6 U Source Terms

7.2 ACCUMULATION OF FISSILE MATERIAL

7.2.1 Accumulation from the MOX Source Term

Comparison of the highest fissile concentrations of the MOX source term (Table 7-1) with the peak concentrations for the ceramic source term (Figure 7-1 and 7-2 for Pu and U, respectively), shows that the fissile concentrations in the MOX source term are at least 5 orders of magnitude smaller. This is primarily because the ceramic waste package can have a high pH due to rapid glass degradation, while no comparable mechanism for increasing pH occurs in the MOX SNF waste package. Without the high pH, the solubility of the fissile material, from the MOX SNF is too low to present a significant source term. Consequently, the few accumulation calculations showed no significant concentrations (CRWMS M&O 2000c, Section 6.1).

7.2.2 Accumulation from the Ceramic Source Term

7.2.2.1 Accumulation in the Invert

7.2.2.1.1 Accumulation in the Invert: Mechanisms

Of the suggested geologic invert materials, crushed tuff has the highest potential for chemically reacting with actinide-laden solutions. This is because of its high specific surface area, high Ca-silicate content, high Fe(II) content, and the presence of phases (cristobalite and clinoptilolite) that buffer silica activity well above the solubility of quartz. The invert design is still not finalized, but crushed tuff with particle size between 2 and 4.75 mm has been assumed (GS980808312242.015). However, it is probable that only the very small fines (~200 mesh, approximately 0.1 mm) will be sifted out in the size selection process. Such incomplete sifting will result in a larger mixture of particle sizes, so the effective surface area may be much larger than the geometric surface area calculated for a uniform, cm-sized aggregate. In addition, the tuff probably has micro pores. It is conservative to overestimate the specific surface area, since contact between actinide-bearing solutions and tuff can induce precipitation by the mechanisms discussed below. Hence for all the calculations reported here, the surface area was taken as corresponding to mm-sized cubes. The other major component of the invert is expected to be magnetite from partially oxidized steel that will be used in the invert for structural support of the waste package (CRWMS M&O 1999q, Figure 5). It is possible that the iron in the steel will completely oxidize to hematite (or goethite) within a few thousand years, in which case it would no longer have the capability to reduce, and thereby precipitate, the dissolved fissile material. It is, therefore conservative to assume the presence of magnetite, which is not fully oxidized.

The EQ3/6 calculations included consideration of three possible mechanisms for precipitation of actinides in the invert:

- Loss of dissolved carbonate, by conversion of calcium silicates to calcite (CaCO_3), and the accompanying destabilization of aqueous Pu and U carbonate complexes
- Reduction of Pu and U via oxidation of Fe(II) to Fe(III), which are available in magnetite
- Precipitation of uranium silicates.

7.2.2.1.2 Accumulation in the Invert: Results

Table 7-4 summarizes results of the primary accumulation calculations. These cases are discussed in greater detail in Section 6.1 of CRWMS M&O 2000b. The cases listed in Table 7-4 test the sensitivity of accumulation calculations to several primary factors. With the exception of the case codes beginning with the number 3, all cases included decay of Pu-239 to U-235, according to a half-life of $2.41 \cdot 10^4$ years. Most of the case groups used the source term developed from the nominal ceramic degradation rate, as described in Section 7.1.2. The exceptions were Group 3, which used a source term developed from 1.4 times the nominal ceramic aqueous degradation rate, and Group 9, which used source terms developed from 5x, 10x, and 100x the degradation rate.

The first three case groups, and groups 8 and 10, considered the waste package effluent spread in the invert over the footprint of the entire waste package. The remaining groups considered the effluent focused into a cross sectional area 1/10 the waste package footprint. This would result from the release of the effluent through one hole in the bottom of the waste package, rather than through many holes distributed along the entire length of the waste package. The comparison of the focused versus non-focused cases provided in Group 4 showed that the principal effect of the focusing was to increase the density of accumulation, but the total accumulation was found to be approximately the same. Since the reduced cross-section of the focused flow brings the volume into a more nearly spherical shape, the neutron leakage is greatly reduced, making the focused flow cases more conservative, with respect to criticality, than the non-focused. Therefore, only criticality evaluations for the focused flow cases are reported in Section 7.3, below.

Group 1: This group (1a, 1c, 1s, and 1u) tests the effects of database choice for scenarios with oxidizing conditions in the WP and in the invert. The flow out of the WP is not focused; that is, it is spread evenly over the footprint of the WP. All cases yield very low Pu accumulation, and cases 1a, 1c, and 1s yield approximately the same U accumulation, despite the precipitation of different solubility-controlling phases (haiweeite and soddyite for 1a and 1c, and Na boltwoodite for 1s) and significant differences in the U silicate thermodynamic data. Case 1u produces not only the highest Pu accumulation, but more than twice the U accumulation of the other members of this group (CRWMS M&O 2000b, Section 6.1).

Group 2: This group (2a, 2s, and 2u, with the alphabetic characters having the same meaning as the Group 1 cases) tests the effects of thermodynamic database choice for scenarios with oxidizing conditions in the WP, and reducing conditions in the invert. The flow out of the WP is not focussed; that is, it is spread evenly over the footprint of the WP. To maintain reducing conditions in the invert, the pore spaces must stay saturated with water, and the water must be anoxic, for most of the time before release of fissile material from the WP. Otherwise, the remnants of the carbon steel invert support structure would oxidize and become inert, before the fissile material could reach them. Although Pu and U accumulations are much greater than for Group 1 (oxidizing conditions in invert), there is little difference among the cases in this group, so it may be concluded that the represented thermodynamic database differences are relatively unimportant (CRWMS M&O 2000b, Section 6.1).

Group 3: This is the only group in the table (3aa, 3sa, 3ua, and 3na) to use a source term with higher influx of dripping water (0.015 m^3 , versus 0.0015 m^3 for the rest of the groups.). The flow out of the WP is not focussed; that is, it is spread evenly over the footprint of the WP. This is also the only group without decay of Pu to U. Yet deposition is much lower in group 3, essentially because the higher influx of dripping water flushes out dissolved HLW components, which lowers pH and dissolved carbonate, thus greatly reducing the solubility of the actinides (CRWMS M&O 2000b, Section 6.1).

Group 4: This group (4aa, 4ao, and 4uo) tests the effects of focussing the flow through $1/10^{\text{th}}$ the footprint under the WP. The comparable non-focussed cases are 1a, 2a, and 2u. Comparison of the first cases shows an increase in density of accumulation by a factor of less than 3, but comparison for the other two cases shows an increase in density of by a factor of 10. It is therefore concluded that the principal effect of the focusing is to increase the density but keep the total accumulated mass approximately the same (CRWMS M&O 2000b, Section 6).

Group 5: This single case (5) is used to estimate the fraction of U that originates from HLW, versus the Pu-ceramic. The estimate is made by replacing all the UO_2 in the HLW with chemically similar NpO_2 (since both are actinides). Any accumulation of U is then known to come from the ceramic waste form. The difference between the original U accumulation and that remaining after replacement of the glass U by Np will then be the accumulation of U from the glass. By comparison of case (5) with case 4ao, it is estimated that approximately 50% of the U originates from the HLW. In this case the principal accumulation mechanism is the reduction by iron; the baseline Pu-ceramic degradation rate is used; and the flow out of the waste package is focused into $1/10^{\text{th}}$ the waste package footprint. (CRWMS M&O 2000b, Section 6.1).

Group 6: This single case (6) tests the effects of pre-decaying the Pu in the ceramic by one half-life of ^{239}Pu (2.41×10^4 years). The Pu deposition is reduced by $\sim 1/2$. This result is not surprising, since no stable Pu solid forms in the WP during the time of Pu deposition in the invert. Thus, the Pu concentration in the WP is determined almost entirely by the competition between the ceramic degradation rate and the influx of water (CRWMS M&O 2000b, Section 6.1).

Group 7: This group (7ho, 7lo, 7ha, 7la) tests the effects of varying the stability constants of the Pu solubility-controlling phases (either $\text{Pu}(\text{OH})_4$ or PuO_2). Case 7sa tests sensitivity to the dominant silica polymorph. For the reduced cases (7ho and 7lo), the effect is small; this is expected for two reasons. First, there is no stable Pu solid in the WP at the time of highest aqueous Pu, so the Pu concentration entering the invert is independent of the stability constants. Second, the reduced invert is so far from equilibrium with the oxidized WP solutions, that even soluble Pu solids are adequate to cause precipitation. Although the maintenance of oxidizing conditions in the WP and reducing conditions in the invert is unlikely, as is explained further in Section 7.4.1, these cases are considered for conservatism. For the oxidized cases (7ha and 7la), the low-solubility PuO_2 (7la) produces ~ 238 as much deposition; however, the amount of deposited Pu is still quite small. Case 7sa shows that the effects of assuming cristobalite saturation, instead of chalcedony saturation are quite small. This result may seem remarkable, given that the precipitation of U-silicates depends heavily on the dissolved silica concentration, and cristobalite engenders a much higher dissolved silica; however, the silica concentration in

these runs is actually controlled by other silicates (clays, zeolites or Ni_2SiO_4) during the times of greatest U-silicate deposition (CRWMS M&O 2000b, Section 6.1).

Group 8: This single case (8) tests the effect of changing the saturation to only 10% of the void space of the porous invert (all other cases assume 100% saturation). The flow out of the WP is spread evenly over the footprint of the WP, since the spreading of flow out of the waste package is consistent with the lower saturation. Effectively, this case increases the mass and surface area of invert minerals seen by the fluid that passes through the invert. However, it also decreases the residence time of the fluid in the invert. Compared to 1a, Pu deposition is reduced by a factor ~ 8 , but U deposition in the invert is approximately the same (CRWMS M&O 2000b, Section 6.1).

Group 9: This group (9o6[^], 9o6, 9o7, and 9o8) provides a sensitivity study on the importance of the Pu-ceramic corrosion rate. The first of these cases (9o6[^]) can be compared with case 6 (pre-decay the ^{239}Pu to ^{240}U over one half-life of ^{239}Pu , 24,100 years). The other three cases can be compared with 4ao. It is seen that the increase in Pu deposition varies almost linearly with the increase in ceramic corrosion rate, up to a factor 10 increase in the corrosion rate. At corrosion rates higher than 10x, the aqueous Pu concentration in the WP source term becomes mass-limited. These results are expected. As outlined above, the Pu concentration in the WP source term is expected to vary almost linearly with ceramic corrosion rate (since no Pu solid precipitates in the WP during the time of peak Pu loss). In addition, the invert conditions are so out of equilibrium with the source term, that almost every bit of Pu that enters the invert precipitates (CRWMS M&O 2000b, Section 6.1). The cases with pre-decay of Pu are useful for simulating the effect of the delay of waste package breach. As explained in Section 7.4, the decay of Pu-239 to U-235 reduces the criticality of the waste package because the latter is less efficient than the former at neutron fission.

Group 10: This group tests the effects of increasing the amount of diluting J-13-like water added to the invert (by diversion around the WP, as discussed in Section 5.4 of Ref 3); the cases may be compared with 2u. The flow out of the WP is not focussed; that is, it is spread evenly over the footprint of the WP. The effect of increasing the dilution by a factor of 100 is remarkably small (CRWMS M&O 2000b, Section 6.1).

Table 7-4. Summary of Invert U and Pu Accumulations (CRWMS M&O 2000b, Table 6-1)

Case	Max Pu mols / liter Void ^a	Max U mols / liter Void ^a	Comments
1a	5e-5	0.0174	This group tests the effects of different thermodynamic data files (p0a, p0c, p0s, p0u). Oxidizing conditions in WP and invert, outlet fluence spread over entire shadow of WP. 1a and 1c both produce haiweeite and soddyite as principal U solids. 1s and 1u produce Na boltwoodite (reported U adjusted for formula unit).
1c	4e-5	0.0140	
1s	3.9e-4	0.0152	
1u	4.9e-4	0.0356	
2a	0.0104	0.264	Baseline "reducing" cases. All have Fe ₃ O ₄ that degrades over 10 ³ years. O ₂ diffuses in from drift. Requires constant saturation (all pore space filled with water), which is improbable.
2s	0.0109	0.298	
2u	0.0112	0.223	
3aa	4e-5	1.7e-4	Group 3 is the only group in table to use a WP source term with higher water fluence (0.015 m ³ /y, as opposed to 0.0015 m ³ /y in remainder of table). One reduced case. Shows dramatic effect of lowering pH and ionic strength of WP solutions, by flushing system more rapidly.
3sa	4e-5	3e-5	
3ua	6.6e-5	4e-5	
3an	0.0016	0.034	
4aa	1.3e-4	0.231	Test effects of focussing flow through 1/10 th of the WP footprint. Two reduced cases (o in sixth character place), one to test database effects. Compare to 1a, 2a, and 2u.
4ao	0.104	0.370	
4uo	0.112	0.564	
5	0.105	0.186	Estimate fraction of U deposited is from HLW (~50%), by using HLW with all U replaced by Np. Compare with 4ao.
6	0.053	0.329	Test effect of pre-decaying system by one ²³⁹ Pu half-life. Compare with 4ao.
7ho	0.123	ND ^c	Effects of varying solubility from base case. H and L in fifth character are for high (default EQ6 "Lemire" Pu(OH) ₄) and low (PuO ₂) solubility controls, respectively. S in the fifth place means SiO _{2(aq)} controlled by cristobalite (not chalcedony). Compare with 4ao and 4aa.
7lo	0.0902	ND	
7ha	0 ^d	ND	
7la	0.031	ND	
7sa	1.2e-4	~0.2 ^e	
8	4e-6	0.0192	Effects of varying saturation to 10% of pore space. Compare with 1a.
9o6^	0.246	≥ 0.59	Pu-ceramic corrosion rate sensitivity. "6" in fifth character is for source term with 5 times base case rate; "7" has 10 times base case rate, "8" has 100 times base case rate. 9o6^ pre-decays ²³⁹ Pu one half-life.
9o6	0.488	≥ 0.67	
9o7	0.941	ND	
9o8	2.02	ND	
10a!	3.5e-5	0.0223	Test effects of increasing J-13-like side-fluence from default of 1x WP fluence (j or k ending) to 10x (! Ending) and 100x (@ ending). Compare with 1u (for 10a!) and 2u (for 10o! and 10o@). Effect is insignificant.
10o!	0.0112	0.236	
10o@	0.0112	0.228 ^f	

7.2.2.2 Accumulation in the Far-Field

7.2.2.2.1 Accumulation in the Far-Field: Mechanisms

In addition to accumulation mechanisms present in the invert, far-field accumulations also offer the likely addition of dilution of the WP egress water. Dilution leads to a shift in equilibrium

leading itself to possible precipitation of actinides. Dilution of the effluent from the waste package occurs through two mechanisms: (a) local dilution due to water flowing around the drift applicable to unsaturated cases and (b) classical dispersion resulting from the dispersion of effluent over a complex network of fractures below the drift applicable to both unsaturated and saturated cases.

Local Dilution-When the successive engineered barriers divert the percolation flux, a "dry shadow" builds up underneath the drift (Philip et al., 1989). As little as 1% of the total seepage flow actually flows through the WP, and that only after failure/breach of the drip shield. As the flow proceeds downwards, water progressively invades this volume. Local dilution is a plausible dilution mechanism within a limited distance below the drift. With local dilution alone, the area where precipitation occurs is limited to the vertical "shadow" of the drift and the envelope of Pu-U mineralization is box-like.

Classical Dispersion-With classical dispersion, the mineralization region is more spread out than it is with local dilution. The shape of the Pu-U mineralization envelope resembles a more or less hollow cone with diameter increasing with depth. Because the solution near the source and toward the center of the envelope may be too concentrated to allow precipitation of Pu-U, a region free of mineralization may remain in the center of the envelope at some distance from the source. However, far from the source, the solution toward the center of the envelope becomes dilute enough to allow precipitation, so that a horizontal bridge of mineralization fills in the mineralization envelope, leaving a region free of mineralization near the source and in the center of the envelope.

Examples-The qualified geochemical software PHREEQC (CRWMS M&O 1999r) calculates the dilution through the keyword MIX that mixes the content of a cell with a water of known composition (J-13 water most of the time) in given proportions. Figure 7-3a displays a case of local dispersion and assumes that the 1% seepage fraction is progressively diluted in 100 cells to reach 100% of the seepage existing in the undisturbed conditions above the drift. Fig. 7-3b shows classical transverse dilution.

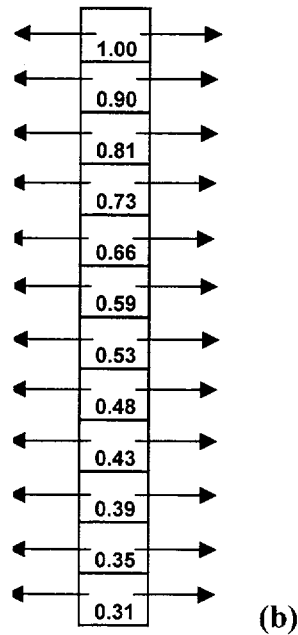
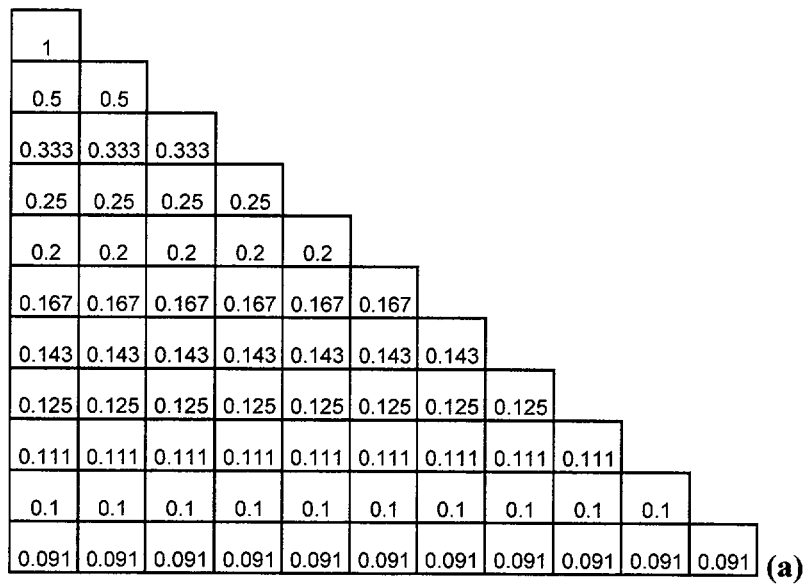


Figure 7-3. Schematics of Handling of Dilution: a) Local Dilution; b) Classical Dispersion (CRWMS M&O 2000c, Figure 2-1)

Two ideal systems, bounding cases of the general system, are considered. In one system, Case A, the fracture system underneath the repository is unsaturated. Local dilution is the main mechanism and the vertical column where minerals can precipitate is the region directly below the footprint of the WP. A realistic surface area is 1,000,000 cm²/liter of water (CRWMS M&O 2000c, page 27). The other system, Case B, results from assuming saturated flow along the active fractures. In Case B, dilution can happen only by transverse dispersion laterally and longitudinal dispersion at the front. The cross section of the cone-like region affected by the mineral deposition can be much larger than the footprint of the WP. It is nevertheless

conservatively assumed that the mineralization is contiguous and convex. In this case, a realistic surface area is 20,000 cm²/liter of water (CRWMS M&O 2000c, page 27).

7.2.2.2.2 Accumulation in the Far-Field: Results

Case A (EQ6 run pe0a1231 source term) (CRWMS M&O 2000c, Section 6.1.1.1)

The total number of moles precipitated in 2,500 years is extrapolated from the incremental precipitation in 50 years because the precipitation rates are fairly constant through time and thus can be scaled to any duration. In fact this constancy only applies after the thermal pulse. This fact is recognized in the selection of times for use in Table 7-5, below (greater than 2500 years). The spatial distribution of the mineralization is plotted on Figure 7-4.

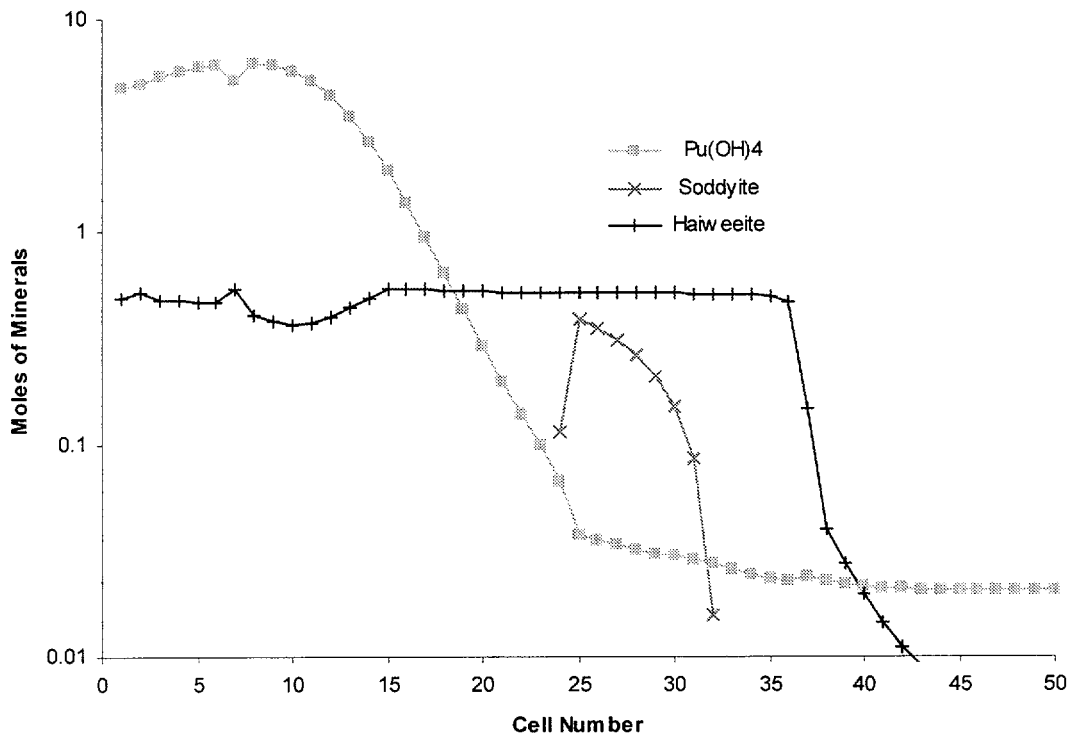


Figure 7-4. Spatial Distribution of Actinide Minerals after 2,500 Years of Precipitation (SA=1,000,000 cm²) (CRWMS M&O 2000c, Figure 6-4)

If a water velocity of 0.03 m/year is assumed, the surface area over which infiltration takes place is fairly large (150 m²). On the other hand, if a reasonable volume is used (cross-section comparable to the waste package footprint), the mineralization is elongated in the vertical direction. Because the worst case geometry for criticality corresponds to a sphere, which can be approximated by a cube, initial mineralization dimensions can be made more conservative and can integrate at the same time uncertainties about the water velocity by recalculating their dimensions to obtain a cube (Table 7-5).

Case B (EQ6 run pe0a1231 source term) (CRWMS M&O 2000c, Section 6.1.1.2)

Case B assumes classical dispersion. In this case, the treatment can only be qualitative; however, it is conservative because PHREEQC is fundamentally a one-dimensional code. The actinide accumulation can be bounded by collapsing it close to the central axis of the plume. The collapsed configuration will generally be more reactive, as can be seen by comparing the large and small volume cases in Table 7-12. Figure 7-5 displays the amounts of uranium minerals present in a cell at a given time step. It can be seen that Haiweeite precipitates initially in cells 60 and beyond but then very slowly dissolves away. Haiweeite mass is smaller than that of soddyite in Case B because the surface area available to dissolution is much less, thereby reducing the availability of Ca from anorthite dissolution.

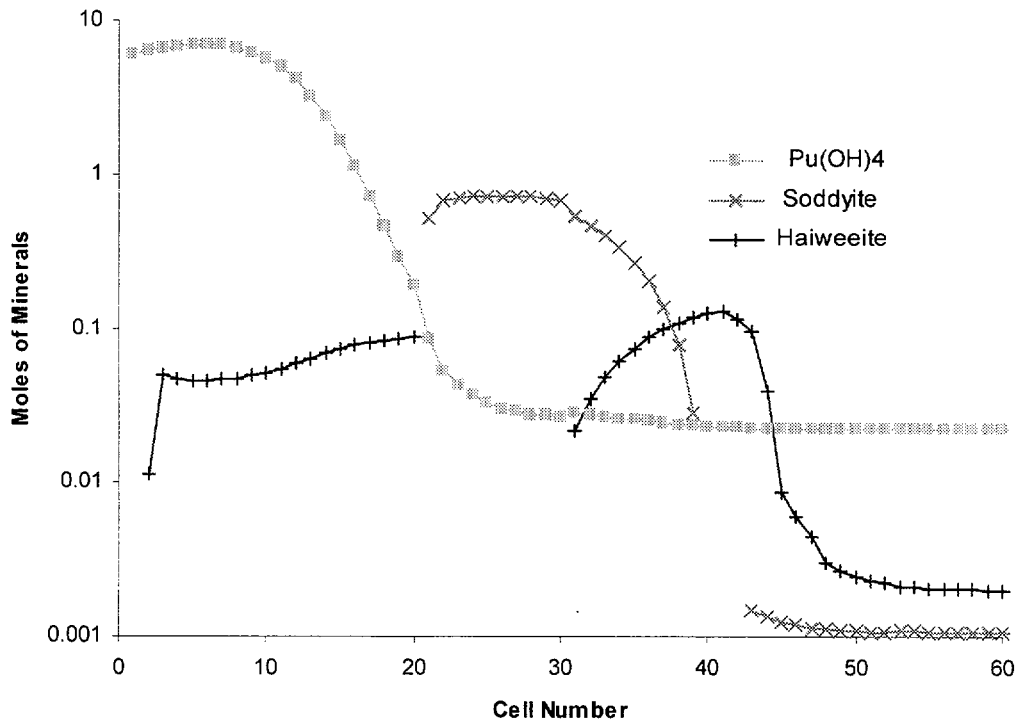


Figure 7-5. Moles of Pu and U Minerals Precipitated as a Function of Cell Number (SA=20,000 cm² for 2,500 years) (CRWMS M&O 2000c, Figure 6-6)

Table 7-5. Summary of Results (pe0a1231): Accumulation Starts 2,500 Years After Breach Time for 2,500 Years(CRWMS M&O 2000c, Table 6-1)

Case A (Unsaturated) SA=1,000,000 cm²/liter	Case B (Saturated) SA=20,000 cm²/liter
78.5 moles Pu 39.7 moles U # of cells = 40	85.3 moles Pu 23.2 moles U # of cells = 40
$A = 5.85 \times 5.85 \text{ m}^2$ $l_c = 0.146 \text{ m}$	$A = 1.6 \times 1.6 \text{ m}^2$ $l_c = 0.04 \text{ m}$
Average Density: 0.4 moles/m ³ Pu 0.2 moles/m ³ U	Average Density: 21.3 moles/m ³ Pu 5.8 moles/m ³ U

Results for different Pu decay values and surface areas are presented in Tables 7-6 and 7-7 (EQ6 run pe0a1231 source term) and 7-8 and 7-9 (EQ6 run pw2a1231 source term).

Table 7-6. Summary of Results for Case pe0a1231 for Different Pu Decay (SA=20,000 cm²) (CRWMS M&O 2000c, Table 6-3)

	Pu all Pu	U all Pu	Pu half Pu	U half Pu	U No Pu
Total Accumulation in the first 50 cells	85.4 moles	23.3 moles	30.2 moles	36.4 moles	57.4 moles
% of Total Actinide mass going through the system	42.8 %	4.5 %	30.3 %	5.9 %	8.0 %
Total Actinide in the first 50 cells	108.6 moles		66.6 moles		57.4 moles

Table 7-7. Summary of Results for Case pe0a1231 for Different Pu Decay (SA=1,000,000 cm²) (CRWMS M&O 2000c, Table 6-4)

	Pu all Pu	U all Pu	Pu half Pu	U half Pu	U no Pu
Total Accumulation in the first 50 cells	77.0 moles	39.0 moles	26.8 moles	51.2 moles	124.5 moles
% of Total Actinide mass going through the system	38.6 %	7.5 %	26.9 %	8.4 %	17.3 %
Total Actinide in the first 50 cells	116.1 moles		79.0 moles		124.5 moles

Table 7-8. Summary of Results for Case pw2a1231 for Different Pu Decay (SA=20,000 cm²) (CRWMS M&O 2000c, Table 6-5)

	Pu all Pu	U all Pu	Pu half Pu	U half Pu	U No Pu
Total Accumulation in the first 50 cells	0.32 moles	8.07 moles	6.12 moles	8.20 moles	8.32 moles
% of Total Actinide mass going through the system	1.8 %	1.6 %	1.3 %	1.6 %	1.6 %
Total Actinide in the first 50 cells	8.39 moles		8.32 moles		8.32 moles

Table 7-9. Summary of Results for Case pw2a1231 for Different Pu Decay (SA=1,000,000 cm²) (CRWMS M&O 2000c, Table 6-6)

	Pu all Pu	U all Pu	Pu half Pu	U half Pu	U No Pu
Total Accumulation in the first 50 cells	0.3 moles	15.0 moles	0.1 moles	15.2 moles	0 moles
% of Total Actinide mass going through the system	0.2 %	2.9 %	0.1 %	2.5 %	0 %
Total Actinide in the first 50 cells	15.3 moles		15.3 moles		Moles

7.2.2.2.3 Sensitivity Studies

Dilution Factor-The dilution factor is a proxy for the importance of dispersion. Both U and Pu have a fairly constant total accumulation (Figure 7-6) and show little dependence on dispersion except if no dilution is assumed (dilution=0%).

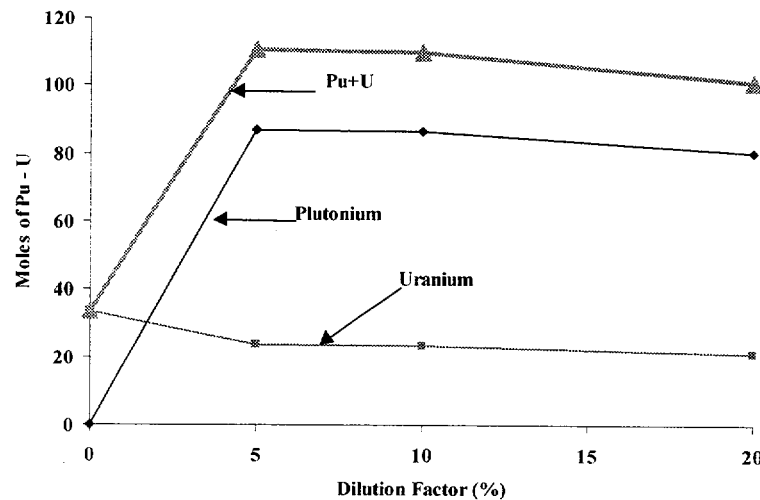


Figure 7-6. Total Number of Moles of Actinide Precipitated as a Function of Dilution (SA=20,000 cm²) (CRWMS M&O 2000c, Figure 6-11)

Surface Areas-Surface areas have little influence on the total amount deposited except for high values where the U accumulation increases (Figures 7-7 and 7-8).

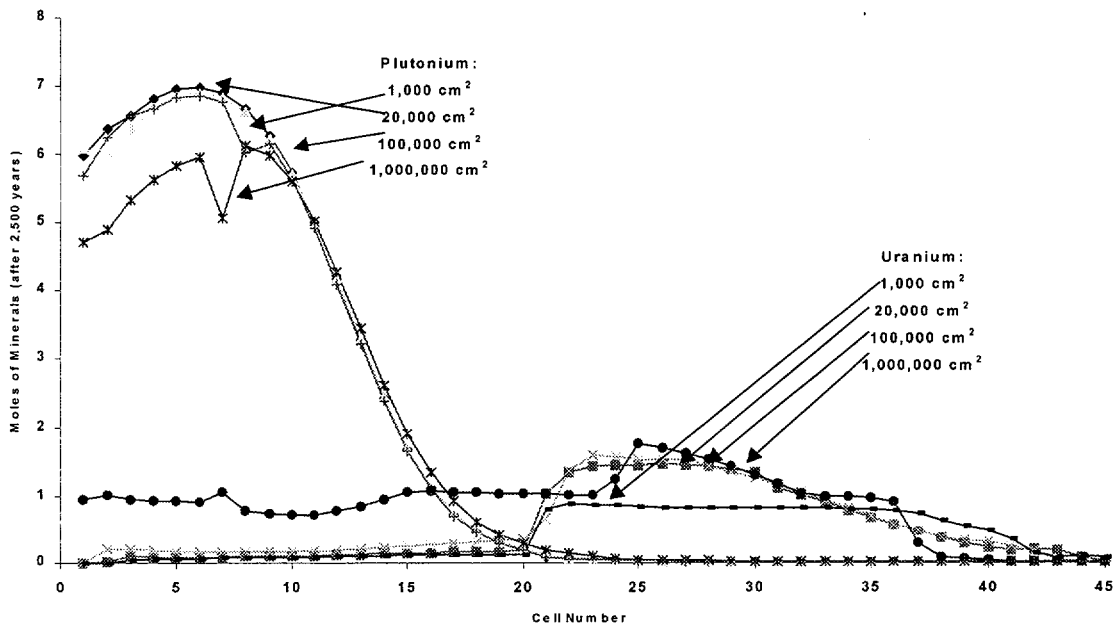


Figure 7-7. Sensitivity Analysis for Surface Areas (dilution factor of 10%) (CRWMS M&O 2000c, Figure 6-12)

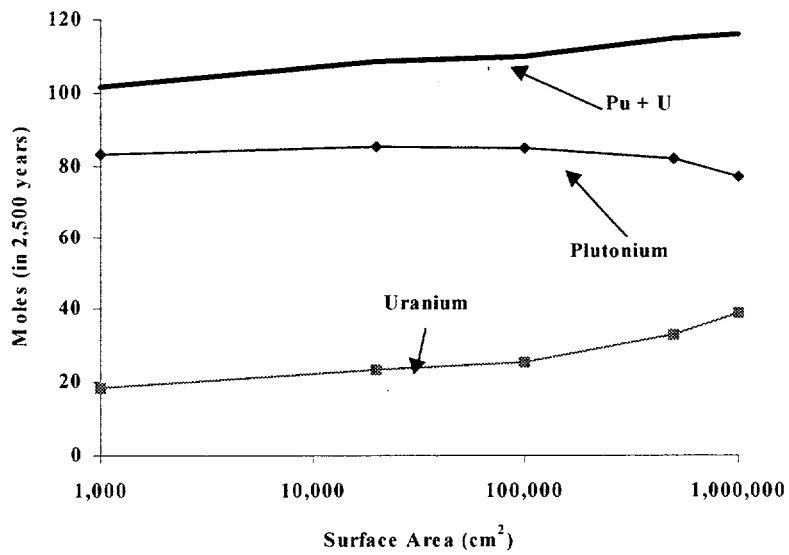


Figure 7-8. Total Number of Moles of Actinide Precipitated as a Function of Surface Area (dilution factor of 10%) (CRWMS M&O 2000c, Figure 6-13)

7.3 CRITICALITY EVALUATIONS OF EXTERNAL ACCUMULATIONS

The objective of this section is to present the criticality evaluations of those significant accumulations of fissile material external to the WP containing the plutonium disposition waste forms, where such accumulations have been defined by the calculations using the geochemistry-transport codes.

Two separate zones for fissile material accumulation were considered: near-field and far-field. The near-field criticality is presented in Section 7.3.1. Section 7.3.2 presents the far-field criticality. Fissile material potentially accumulates in the near-field in large interstices between small rock fragments in the invert, while it potentially accumulates on fracture walls in the far-field (CRWMS M&O 2000d, Page 8). Table 7-10 lists tuff composition and density.

Table 7-10. Tuff Composition (CRWMS 1997m, Table 4.1.3-1)

Element	Weight Percent (wt.%)	Element	wt.%
SiO ₂	76.83	Na ₂ O	3.59
Al ₂ O ₃	12.74	K ₂ O	4.93
FeO	0.84	TiO ₂	0.1
MgO	0.25	P ₂ O ₅	0.02
CaO	0.56	MnO	0.07
Particle Density = 2.54 g/cm ³ (Flint 1998, Extracted from Table 7)			

7.3.1 Criticality Evaluations for Accumulations in the Near-Field

The near-field is defined as the drift outside the waste package. The only location in the drift where there can be a significant accumulation of fissile material is beneath the waste package in the invert. Figure 7-9 gives a representation of the near-field (CRWMS M&O 1999q, Figure 5). The invert is made up of crushed tuff (CRWMS M&O 1999a, Page 54a).

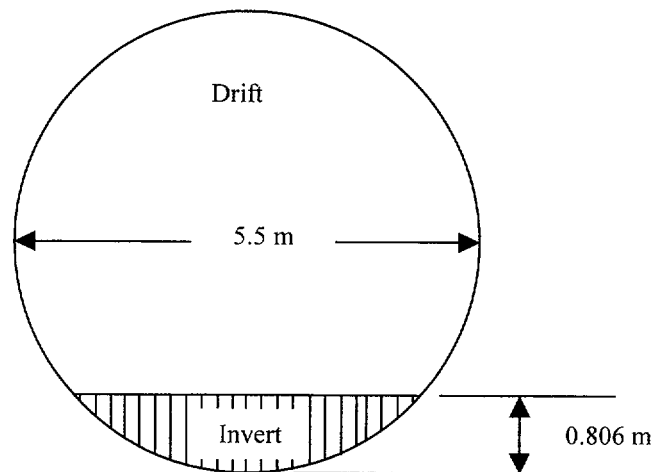


Figure 7-9. Invert Dimension (not to scale) (CRWMS M&O 1999q, Figure 5)

Significant accumulation in the invert only occurs under waste packages containing the plutonium disposition ceramic waste form (CRWMS M&O 2000b, Section 6.1). The source term of fissile material from waste packages containing plutonium disposition MOX waste form is very small (CRWMS M&O 2000b, Section 6.1) which results in insignificant accumulations of fissile material that have no criticality consequence. Table 7-11 is a listing of the cases with significant fissile material accumulations (CRWMS M&O 2000b, Table 6-1). The k_{eff} values are also listed in Table 7-11 (CRWMS M&O 2000d, Section 6.1). The only scenario in Table 7-11 that results in sufficient accumulation of fissile material to pose a criticality concern is Case 011. The reason for the high accumulation of fissile material is the use of a ceramic aqueous degradation (corrosion) rate an order of magnitude higher than nominal.

Table 7-11. Near-Field Criticality Evaluation of Plutonium Disposition Ceramic Waste Form (CRWMS M&O 2000d, Table 5-2 and Table 6-1)

Case	Max Pu moles/liter Void	Max U moles/liter Void	Decay (years)	Corrosion Rate	Flow Volume	Density (g/cm ³)			$k_{eff} + 2\sigma$
						Total accumulation (kg)			
						Pu-239	U-235	U-238)	
011	0.941	Not Determined	No Decay	10x	1/10 th WP Footprint	0.0787 51.66	N/A	N/A	1.30923
012	0.0104	0.264	No Decay	1x	WP Footprint	0.0008 7 5.709	N/A	N/A	0.28144
013	0.104	0.370	No Decay	1x	1/10 th WP Footprint	0.0087 5.709	N/A	N/A	0.89132
014	0.053	0.329	24,100	1x	1/10 th WP Footprint	0.0044 2.91	0.0054 3.55	0.0219 14.39	0.82168
N/A – Not determined or conservatively not represented.									

7.3.2 Criticality Evaluations for Accumulations in the Far-Field

The far-field is defined as the rock beyond the drift. The fracture matrix matrix and aperture detail is modeled as shown in Figure 7-10. The dimensions given in this figure are consistent with the discussion of the fracture network given in CRWMS M&O 2000c, Section 2.2. The accumulation cases were run with models of the matrix (W) varying between 1.6 m and 5.58 m. The appropriate volume is determined by the accumulation calculations (CRWMS M&O 2000c, Section 6.1.1.3). The fracture aperture and spacing are shown in Figure 7-10. Significant accumulation in the far-field only occurs under waste packages containing the plutonium disposition ceramic waste form (CRWMS M&O 2000c, Section 6.1). The source term of fissile material from waste packages containing plutonium disposition MOX waste form is very small (CRWMS M&O 2000c, Section 6.4, Figure 6-20) which results in insignificant accumulations of fissile material that has no criticality consequence. Table 7-12 is a listing of the cases with significant fissile material accumulation (CRWMS M&O 2000c, Section 6). The k_{eff} values are also listed in Table 7-12 (CRWMS M&O 2000d, extracted from Sections 6.1, 6.2 and 6.3). The only scenario in Table 7-12 that results in sufficient accumulation of fissile material to pose a criticality concern is Case 204. The reason for the high accumulation of fissile material is the use of a ceramic aqueous degradation rate an order of magnitude higher than nominal along with a very small accumulation surface area.

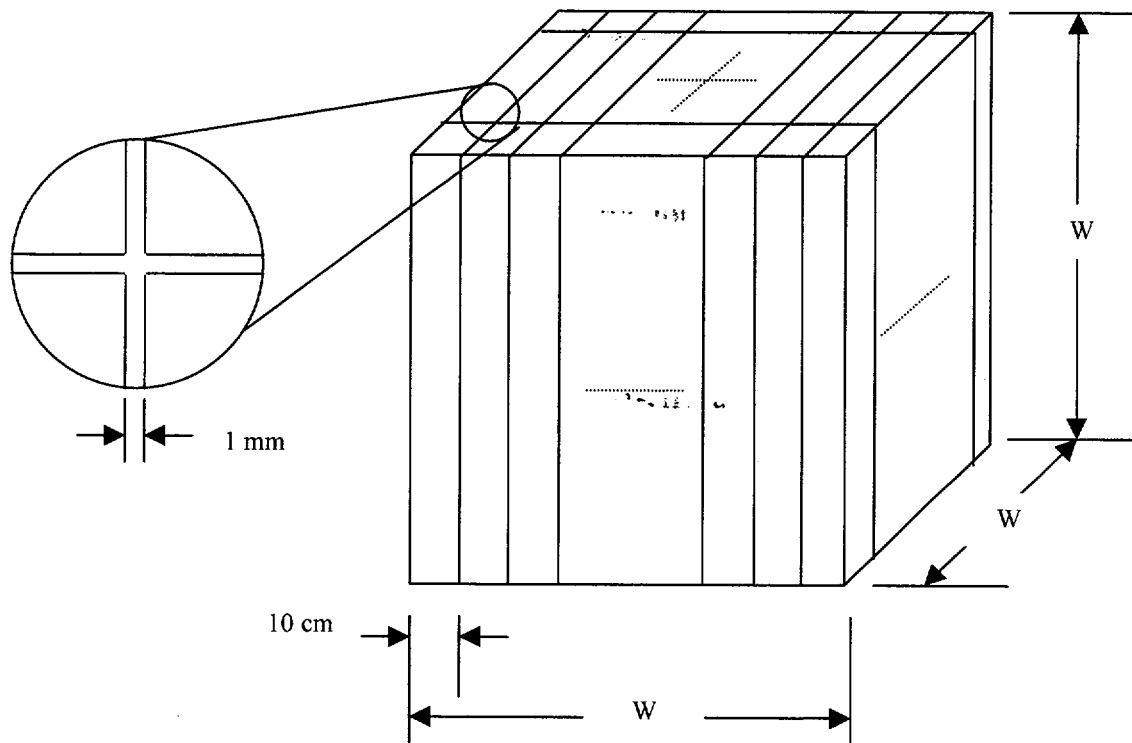


Figure 7-10. Fracture Matrix with Aperture Detail (not to scale) (CRWMS M&O 2000d, Figure 5-2)

Table 7-12. Far-Field Criticality Evaluation of Plutonium Disposition Ceramic Waste Form (CRWMS M&O 2000d, Table 5-3 and Table 6-2)

Case	Cube Volume (m ³)	Degradation Rate	Decay	Total Accumulation (Moles)		Density in apertures (g/cm ³) Total accumulation (kg)			k _{eff} + 2σ
				Pu	U	Pu-239	U-235	U-238)	
201	195.1	10x	No Decay	78.6	39.8	0.0048 18.79	N/A	N/A	0.05307
202	195.1	10x	24,100 years	29.3	52.2	0.0018 7.00	0.0006 2.45	0.0026 9.94	N/A
203	195.1	10x	Complete Decay of Pu-239	N/A	124.5	N/A	0.0026 9.95	0.0050 19.56	0.01586
204	4.1	10x	No Decay	85.4	23.2	0.2505 20.42	N/A	N/A	0.97088
205	4.1	10x	24,100 years	30.2	36.4	0.0886 7.22	0.0210 1.71	0.0850 6.93	0.60072
206	4.1	10x	Complete Decay of Pu-239	N/A	57.4	N/A	0.0563 4.59	0.1106 9.02	0.24582
207	4.1	1x	No Decay	0.32	8.07	0.0009 0.08	N/A	N/A	N/A
208	19.7	10x	No Decay	84.6	25.3	0.0516 20.22	N/A	N/A	0.42159

N/A – Not determined or conservatively not represented.

7.4 PROBABILITY OF EXTERNAL CRITICALITY

7.4.1 Occurrence of Criticality

Table 7-4 shows that the accumulations required for external criticality from the immobilized ceramic waste form could only occur for the highest degradation rates of this waste form. The only critical case for the invert accumulation is seen to be the ones from the 10x ceramic aqueous degradation rate and having accumulation by the reducing mechanism (cases 9o7 from Table 7-4). This case was considered in the accumulation calculations and in the resulting criticality calculations to demonstrate the range of possible geochemistry considerations. In addition to the fact that the large corrosion rate is extremely unlikely, the following are reasons why the reducing accumulation in the invert is virtually impossible:

1. It would require oxidizing conditions in the waste package (to make Pu soluble) and reducing conditions in the invert pond. This is unlikely because the water that drips from the waste package into the invert, carrying the dissolved fissile material, will also carry the dissolved oxygen from the oxidizing environment of the waste package.
2. Even if the differing environments could be maintained (by some mechanism that could remove the oxygen from the water dripping into the invert), the magnetite must reduce all

the Pu in a time less than 1000 years or oxygen diffusing from the surface of a stagnant pond will completely oxidize the iron and prevent further reduction of fissile material.

3. Water saturation in the invert will likely be prevented by the design requirement that the system shall allow free-liquid-phase water to drain out of emplacement drifts, via the emplacement drift floor [through a mechanism such as sand drains] (CRWMS M&O 1999t, Section 1.2.1.8). Therefore, the system will certainly not allow the *anoxic* saturation required to prevent complete oxidation of the iron before the complete reduction (precipitation) of the fissile material.

For these reasons, the results for the reducing accumulation in the invert should not reflect adversely on the acceptability of this waste form for repository disposal, and will not be considered in the calculation of the upper bound to the probability of criticality.

7.4.2 Upper Bound to the Probability of Criticality

For those accumulations found to be critical (or near-critical), an upper bound to the probability of criticality is estimated. CRWMS M&O 2000b and CRWMS M&O 2000c have provided estimates of the fissile accumulations in the invert and the far-field, respectively under various assumptions of determining parameters (e.g., waste form degradation rates, environmental parameters, both inside and outside the waste package). A comprehensive estimate of probability of criticality would require probability distributions for all such parameters. Unfortunately, the only probability distributions presently available are for degradation rates of the waste package materials, and for the environmental parameters relating to water dripping into the waste package. These distributions have been used to develop a model of waste package degradation, which provides a distribution of waste package breach times, which is explained in CRWMS M&O 2000d, Section 5.3.

For plutonium-bearing waste forms, the time of breach is an important determinant of criticality. With increasing time of breach increasing amounts of Pu-239 are decayed into U-235. Since the latter is less reactive with respect to criticality, and since the latter is accompanied by neutron absorbing U-238, a delay of waste package breach will also decrease the probability of criticality because more of the plutonium-239 will have decayed to the less reactive U-235. This can be seen by comparing case 013 with 017 in Table 7-11, and comparing case 201 with 202 and 204 with 205 in Table 7-12. To produce a significant decrease in the amount of accumulated Pu-239, the delay of breach would generally need to be on the order of the Pu half-life, but the example below shows how a shorter delay can be crucial for conditions that are only slightly above critical with the full Pu accumulation.

The methodology for calculation of the upper bound of criticality probability starts with the recognition of the fact that the amount of Pu accumulated is approximately linearly proportional to the amount of Pu present in the waste package at the time of breach. This fact is demonstrated for the invert accumulations in Table 7-4, by comparing the cases 4a0 and 9o6 with the cases in which the waste package does not breach until one half-life of Pu-239, cases 6 and 9o6[^], respectively. The members of the latter pair are seen to have approximately half the Pu accumulation of the corresponding member of the former pair, which is consistent with their

having half the amount of undecayed Pu-239 at the time of breach. This is also seen to be approximately true for the far-field accumulations summarized in Table 7-12. Case 204 corresponds to breach at time zero, and case 205 corresponds to breach at 24,100 years.

The next step in the methodology is the identification of the minimum amount of fissile accumulation (primarily Pu-239) required for criticality. The minimum far-field accumulation is identified from the data in Table 7-12 (illustrated in the following paragraph). For a given initial amount of Pu-239, there is a maximum Pu-239 time that can be tolerated without leaving an amount of Pu-239 that will be too small to lead to a critical mass accumulation. This maximum decay time will simply be the decay time that reduces the initial Pu inventory by the same ratio as the minimum accumulation needed for criticality divided by the maximum possible accumulation (which is only achieved if waste package breach occurs at time zero). Finally, the probability upper bound is estimated as the probability that the waste package breach time is less than this maximum decay time.

Details of the calculation are given in Section 6.3 of CRWMS M&O 2000d, using the breach time distribution parameters discussed in the last paragraph of Section 5.3 of that document. The Pu far-field accumulation required for criticality is determined by interpolating between two cases bracketing $k_{\text{eff}} = 0.95$ in the worst case volume, 4.1 m^3 , 204 and 205 of Table 7-12. This interpolation gives the minimum accumulation of 19.7 kg. The maximum permitted decay time before basket degradation is 1100 years. The upper bound for the probability of criticality is calculated from the distribution as 1.3×10^{-4} per waste package. The upper bound to the expected number of criticalities is computed by multiplying the upper bound for the probability by the number of waste packages with the ceramic waste form, 128 (Table 2-12), to give an upper bound for the expected number of criticalities = 0.017 for all the ceramic waste packages for all time.

The following observations should be made concerning the relatively short criticality preventing decay time (1100 years) for the example of the previous paragraph. First, the low time is a result of the fact that the k_{eff} of case 204 in Table 7-12 is only slightly above critical. Second, this short a time is within the time of the high temperature thermal pulse, when there can be no liquid water in the waste package.

INTENTIONALLY LEFT BLANK

8. FINDINGS AND CONCLUSIONS

This document and its conclusions may be affected by technical product input information that requires confirmation. Any changes to the document or its conclusions that may occur as a result of completing the confirmation activities will be reflected in subsequent revisions. The status of the input information quality may be confirmed by review of the Document Input Reference System database.

8.1 MOX

The following findings are based on the currently available data on the hypothetical Westinghouse MOX design and fuel cycle.

8.1.1 Structural

The most severe structural design basis event that was postulated for the waste package is the tipover accident, considering that any events beyond SDD criteria are beyond-design-basis events. The finite element analyses of both the 21 PWR and the 12 PWR WPs for this postulated event show that the peak stress at any location in either of the waste packages will be at least 15% less than the ultimate material tensile strength and thus are within design limits. Calculated stresses in the MOX PWR WPs were of similar magnitude to stresses calculated for a tipover accident in similar waste packages containing commercial PWR SNF (Section 3.1.2).

8.1.2 Thermal

The initial heating rates for MOX SNF were 798 W/assembly for the 21 PWR WP loaded with the highest heat source MOX SNF to be placed in that package, i.e., assemblies having no greater burnup than 46.5 GWd/MTHM. The initial heating rates were 1070 W/assembly for the 12 PWR WP loaded with the MOX SNF generating the highest heat source, i.e., assemblies with 56.5 GWd/MTHM burnup. This loading strategy for the MOX SNF meets the maximum thermal output design criteria of 11.8 kW per waste package. For the 21 PWR waste package, the peak cladding temperature was approximately 234°C. The peak cladding temperature for the 12 PWR waste was approximately 218°C. The fuel temperature (homogenized assemblies) peaks at approximately 336°C for the 21 PWR MOX SNF and at approximately 302°C for the 12 PWR MOX WP. Both of these peak temperatures are well below the maximum permissible waste package fuel temperature of 350°C given in Section 2.1.5.2.

The waste package surface temperatures were determined at the thermal design basis loading of 85 MTU/acre, which is within the AML range (80 to 100 MTU/acre) given on page 3-3 of YMP (1999) for the repository.

In summary, analysis of the effects of placing MOX SNF in the 21 and 12 PWR waste packages will not result in the thermal design criteria for the waste packages being exceeded, provided that burnup levels for assemblies placed in the 21 PWR WP are restricted to less than 46.5 GWd/MTHM (Section 4.1.2).

8.1.3 Shielding

Maximum dose rates at the waste package exterior surfaces were less than 110 rad/hr for the 21 MOX PWR WP loaded with the highest burnup MOX SNF at 56.5 GWd/MTHM 10 years after reactor discharge. This is conservative since this configuration produces the largest radiation source, thus maximizing the surface dose rate. The 12 MOX PWR WP design has an equivalent amount of shielding with a smaller source, which will result in smaller surface dose rates.

No significant increase in the waste package barrier corrosion rate from the radiolytic effects of high surface dose rates is likely since this requires a steam-air environment combined with a greater than 100 rad/hr dose rate which is a very unlikely repository condition.

The radiation levels were shown to be much less than the values from commercial LEU PWR SNF of similar burnup which were calculated to be greater than 150 rem/hr. This is due primarily to the differences in the isotopic inventory in the two waste forms contributing to the radiation source (Section 5.1.2).

8.1.4 Criticality

Most of the criticality conclusions are with respect to the conservative threshold of $k_{\text{eff}} = 0.92$. Only very unlikely configurations would cause the MOX SNF waste package k_{eff} to exceed this value. Therefore, it is expected that the MOX SNF will satisfy the anticipated risk-based regulatory requirements. Furthermore, the MOX SNF is more robust with respect to criticality than a significant fraction of the commercial LEU SNF.

Configurations that could lead to $k_{\text{eff}} > 0.92$ were found to be extremely unlikely. Specifically, it was found that:

- The loss of all fission products from the SNF matrix while the fuel pins are still uncollapsed produced k_{eff} greater than 0.92, but less than 0.95 (Section 6.1.3.3.3). Such an event should be considered extremely unlikely because it would require the spacer grids to remain uncollapsed while the cladding becomes sufficiently degraded to permit most of the fuel matrix to be leached. Further unlikely required conditions are that the cladding would have to retain its structural integrity while having enough holes to leach most of the fuel matrix (Section 6.3), and that the stainless steel basket and fuel matrix degrade simultaneously (Section 6.1.3).
- The loss of 75% of the iron oxide (which came from the corrosion of the basket steel) can produce a k_{eff} just above 0.95, but, again, only if the assembly remains uncollapsed (Section 6.1.3.3.3). Furthermore, the low solubility of iron oxide makes it incredible that any significant amount would get lost at all (Section 6.3).

With respect to the probability of criticality, it is found that for the worst case fission product loss scenario, the expected number of criticalities in 100,000 years is approximately 0.08. However, as mentioned above, this worst case fission product loss scenario can occur only if three unlikely processes occur over the same time period: (1) spacer grids remain uncollapsed,

(2) cladding retains structural integrity while having enough holes to permit major fission product loss, and (3) basket and fuel matrix degrade simultaneously. If a comprehensive evaluation of the probability of these processes could be developed, each should reduce the probability of criticality by a factor of 100. As a result, a more realistic estimate of the expected number of criticalities due to fission product loss could be six orders of magnitude less than the 0.08 value (Section 6.3.3). For the worst case iron oxide loss scenario, the expected number of criticalities is 0.07 in 100,000 years. The conditions required for this scenario (75% iron oxide loss and no spacer grid collapse) are even less likely than for the fission product loss scenario because there is no known mechanism for a significant amount of iron oxide loss.

With respect to the consequences of a steady state criticality, it was found that, for a criticality lasting 10,000 years, the maximum radionuclide inventory increment at 1000 years following the criticality shutdown is 18% (in Curies) of the radionuclide that would be present without the criticality. At 20,000 years following the criticality shutdown, the increment has decayed to only 2.5% (in Curies) more than would be present without the criticality (Section 6.4.2.2).

With respect to the consequences of a transient criticality with a fairly rapid insertion rate, the peak overpressure and temperature are inversely correlated with the available exit area (holes in the waste package surface). For a total opening area of 0.1 cm² (which is extremely unlikely to permit enough water to enter and exit the waste package) the peak overpressure is less than 60 atmospheres and the peak temperature is only 220°C. These results are not significantly different from those found for a waste package containing LEU PWR SNF (Section 6.4.1.2).

The concentration of fissile material in the MOX source term for external criticality is at least 5 orders of magnitude smaller than the corresponding concentration in the source term for the ceramic waste form. (Section 7.1.1 compared to Section 7.1.2). Therefore, the accumulation is correspondingly smaller, as is shown for far-field accumulation (Section 7.3.2).

8.2 CERAMIC

8.2.1 Structural

The canister containing the Pu-bearing ceramic disks and the HLW glass has been shown analytically to withstand a corner drop from a height of 9.14 meters without being breached (Section 3.2.2.2).

8.2.2 Thermal

Thermal impacts are comparable to, or less than, those of the corresponding HLW waste package (Section 4.2.2).

8.2.3 Shielding

Shielding impacts are comparable to, or less than, those of the corresponding HLW waste package (Section 5.2.2).

8.2.4 Criticality

The following are the primary criticality findings:

- Criticality for the intact configuration is not possible, since the maximum calculated $k_{\text{eff}} = 0.11$ when all of the void space in the waste package is filled with water (Section 6.2.2).
- Criticality is not possible for the partly degraded configuration (maximum credible separation between fissile and neutron absorber), since the maximum calculated $k_{\text{eff}} = 0.54$ (Section 6.2.3.2.1).
- Criticality is not credible for the fully degraded configuration. If both fissile and absorber are uniformly distributed throughout the waste package, and 78% of the Gd is lost from the waste package (worst case calculated by EQ3/6) the k_{eff} is still less than 0.45 (Section 6.2.3.2.2).
- Beyond 40,000 years following discharge from the reactor, sufficient Pu has decayed to U that no configuration can go critical (Section 6.2.3.2.1).
- Accumulations sufficient for external criticality only occur, in the invert or far-field, for the rapid ceramic degradation rate, which is at least 10 times the nominal value provided by LLNL report (Shaw, H., ed. 1999). This is because only the high degradation rate will release significant quantities of fissile material while the pH is high (from the rapid degradation of the filler glass). (Section 7.4.1)
- Criticality in the invert requires the additional accumulation mechanism of reduction on partially oxidized iron (from the partial degradation of drift structural steel). This mechanism is very unlikely for a number of reasons, most of which are expected to be evaluated prior to licensing, to demonstrate a probability below the screening threshold. (Sections 7.4.1 and 7.2.2).

The following are secondary findings that provide insight into the effects of the various degradation scenarios:

- The EQ3/6 degradation calculations are relatively insensitive to the most likely alternative inputs for thermodynamic data (geochemistry calculation constants), deviation of the incoming water composition from the nominal J-13, and HLW glass composition (Section 6.2.3.1.2).
- The highest Gd losses occur for those cases in which the glass degrades slowly, but the ceramic and stainless steel degrade quickly. Under these circumstances a low pH situation is set up relatively early, before much of the slowly degrading glass is able to contribute much alkalinity to raise the pH. The case with the highest Gd loss, Case 13 with 78% loss, has the most rapid degradation of the stainless steel and ceramic. These conditions are extremely unlikely (Section 6.2.3.1.4).

- Even if the glass degrades much more slowly than the other components, a large Gd loss will not occur unless there is a high enough oxygen fugacity. Otherwise there will not be sufficient support for the oxidation of chromium to chromate (e.g., contrast Cases 3 and 26 of Table 6-9) (Section 6.2.3.1.4).
- In those cases with the glass degrading last, there will be a long period of relatively high pH after all the pH-lowering potential of the corroding stainless steel has been removed. This long period of high pH (Table 6-10) can result in loss of most, or all, of the uranium (Cases 3, 13, 18, 19, 26, 29, 31, 34, 36 of Table 6-10). This loss of uranium occurs too late to completely prevent internal criticality, but it will increase the risk of external criticality (to be discussed in the next revision of this document) (Section 6.2.3.1.4).
- Near-field (in the invert) total accumulation of fissile material is relatively insensitive to: (1) alternative thermodynamic data file and (2) volume over which the accumulation takes place. Accumulation increases significantly (greater than 30%) with: (1) decreasing flow rate and (2) increasing ceramic degradation rate. (Section 7.2.2.1.2).
- Far-field accumulations of fissile material from the waste package are relatively insensitive to (1) the degree of water saturation, (2) the amount of surface area in the fracture network and (3) the total amount of dilution of the source term (for dilution factor greater than 5%). Accumulation increases significantly (greater than 30%) with increasing ceramic degradation rate. (Section 7.2.2.2.3).

INTENTIONALLY LEFT BLANK

9. REFERENCES

9.1 DOCUMENTS CITED

B&W Fuel Company 1991. *Final Design Package Babcock & Wilcox BR-100 100 Ton Rail/Barge Spent Fuel Shipping Cask*. Volume 2 of 2. 51-1203400-01. DBABE0000-00272-1000-00014. Lynchburg, Virginia: B&W Fuel Company. ACC: MOV.19960802.0083.

Briesmeister, J.F., ed. 1997. *MCNP- A General Monte Carlo N-Particle Transport Code*. LA-12625M Version 4B. Los Alamos, New Mexico: Los Alamos National Laboratory. ACC: MOL.19980624.0328.

CRWMS M&O 1995. *Software Qualification Report for ANSYS Version 5.1HP*. CSCI: 30003 V5.1HP. DI: 30003-2006 Rev. 01. Las Vegas, Nevada: CRWMS M&O. ACC: MOL.19980908.0167.

CRWMS M&O 1996a. *Report on Evaluation of Plutonium Waste Forms for Repository Disposal, Revision 1*. A00000000-01717-5705-00009 REV 01. Vienna, Virginia: CRWMS M&O. ACC: MOL.19961210.0066.

CRWMS M&O 1996b. *DHLW Glass Waste Package Criticality Analysis*. BBAC00000-01717-0200-00001 REV 00. Las Vegas, Nevada: CRWMS M&O. ACC: MOL.19960919.0237.

CRWMS M&O 1996c. *Engineered Barrier Segment/Waste Package*. Volume III of . *Mined Geologic Disposal System Advanced Conceptual Design Report*. B00000000-01717-5705-00027 REV 00. Las Vegas, Nevada: CRWMS M&O. ACC: MOL.19960826.0096.

CRWMS M&O 1996d. *Second Waste Package Probabilistic Criticality Analysis: Generation and Evaluation of Internal Criticality Configurations*. BBA00000-01717-0200-00005 REV 00. Las Vegas, Nevada: CRWMS M&O. ACC: MOL.19960924.0193.

CRWMS M&O 1997a. *Software Qualification Report for The SCALE Modular Code System Version 4.3*. CSCI: 30011 V4.3. DI: 30011-2002 Rev. 01. Las Vegas, Nevada: CRWMS M&O. ACC: MOL.19970731.0884.

CRWMS M&O 1997b. *Waste Quantity, Mix and Throughput Study Report*. B00000000-01717-5705-00059 REV. 01. Las Vegas, Nevada: CRWMS M&O. ACC: MOL.19971210.0628.

CRWMS M&O 1997c. *Disposal Criticality Analysis Methodology Technical Report*. B00000000-01717-5705-00020 REV 01. Las Vegas, Nevada: CRWMS M&O. ACC: MOL.19980108.0700.

CRWMS M&O 1997d. *Waste Package Materials Selection Analysis*. BBA000000-01717-0200-00020 REV 01. Las Vegas, Nevada: CRWMS M&O. ACC: MOL.19980324.0242.

CRWMS M&O 1997e. *Determination of Waste Package Design Configurations*. BBAA00000-

01717-0200-00017 REV 00. Las Vegas, Nevada: CRWMS M&O. ACC: MOL.19970805.0310.

CRWMS M&O 1997f. *21-PWR Waste Package Disposal Container Assembly*. BBAA00000-01717-2700-15998 REV 00. Las Vegas, Nevada: CRWMS M&O. ACC: MOL.19971222.0299.

CRWMS M&O 1997g. *12-PWR Waste Package Disposal Container Assembly*. BBAA00000-01717-2700-16086 REV 00. Las Vegas, Nevada: CRWMS M&O. ACC: MOL.19980119.0362.

CRWMS M&O 1997h. *Degraded Mode Criticality Analysis of Immobilized Plutonium Waste Forms in a Geologic Repository*. Predecisional Document. A00000000-01717-5705-00014 REV 01. Las Vegas, Nevada: CRWMS M&O. ACC: MOL.19980422.0911.

CRWMS M&O 1997i. *Waste Package Design Basis Events*. BBA000000-01717-0200-00037 REV 00. Las Vegas, Nevada: CRWMS M&O. ACC: MOL.19971006.0075.

CRWMS M&O 1997j. *Preliminary Design Basis for WP Thermal Analysis*. BBAA00000-01717-0200-00019 REV 00. Las Vegas, Nevada: CRWMS M&O. ACC: MOL.19980203.0529.

CRWMS M&O 1997k. *Criticality Evaluation of Degraded Internal Configurations for the PWR AUCF WP Designs*. BBA000000-01717-0210-00056 REV 00. Las Vegas, Nevada: CRWMS M&O. ACC: MOL.19971231.0251.

CRWMS M&O 1997l. *Criticality Consequence Analysis Involving Intact PWR SNF in a Degraded 21 PWR Assembly Waste Package*. BBA000000-01717-0200-00057 REV 00. Las Vegas, Nevada: CRWMS M&O. ACC: MOL.19980106.0331.

CRWMS M&O 1997m. *Evaluation of the Potential for Deposition of Uranium/Plutonium from Repository Waste Packages*. BBA000000-01717-0200-00050 REV 00. Las Vegas, Nevada: CRWMS M&O. ACC: MOL.19980216.0001.

CRWMS M&O 1998a. *Westinghouse MOX SNF Isotopic Source*. BBA000000-01717-0210-00007 REV 00. Las Vegas, Nevada: CRWMS M&O. ACC: MOL.19980818.0131.

CRWMS M&O 1998b. *MOX SNF. Volume I of Report of Intact and Degraded Criticality for Selected Plutonium Waste Forms in a Geologic Repository*. BBA000000-01717-5705-00020 REV 01. Las Vegas, Nevada: CRWMS M&O. ACC: MOL.19981217.0113.

CRWMS M&O 1998c. *Criticality Evaluation of Intact and Degraded PWR WPs Containing MOX SNF*. A00000000-01717-0210-00002 REV 00. Las Vegas, Nevada: CRWMS M&O. ACC: MOL.19980701.0482.

CRWMS M&O 1998d. *EQ6 Calculations for Chemical Degradation of PWR LEU and PWR MOX Spent Fuel Waste Packages*. BBA000000-01717-0210-00009 REV 00. Las Vegas, Nevada: CRWMS M&O. ACC: MOL.19980701.0483.

CRWMS M&O 1998e. *EQ3/6 Software Installation and Testing Report for Pentium Based*

Personal Computers (PCs). CSCI: LLYMP9602100. Las Vegas, Nevada: CRWMS M&O. ACC: MOL.19980813.0191.

CRWMS M&O 1998f. *Criticality Evaluation of Plutonium Disposition Ceramic Waste Form: Degraded Mode*. BBA000000-01717-0210-00014 REV 01. Las Vegas, Nevada: CRWMS M&O. ACC: MOL.19980918.0003.

CRWMS M&O 1998g. Not Used.

CRWMS M&O 1998h. *21 MOX PWR WP Tipover Calculations*. BBAA00000-01717-0210-00003 REV 00. Las Vegas, Nevada: CRWMS M&O. ACC: MOL.19980716.0045.

CRWMS M&O 1998i. *12 PWR MOX Waste Package Tipover Calculations*. BBAA00000-01717-0210-00006 REV 00. Las Vegas, Nevada: CRWMS M&O. ACC: MOL.19980918.0085.

CRWMS M&O 1998j. *Software Qualification Report for ANSYS V5.4, A Finite Element Code*. CSCI: 30040 V5.4. DI: 30040-2003, REV 00. Las Vegas, Nevada: CRWMS M&O. ACC: MOL.19980609.0847.

CRWMS M&O 1998k. *Estimation of the Westinghouse 17 x 17 MOX SNF Assembly Weight*. A00000000-01717-0210-00001 REV 00. Las Vegas, Nevada: CRWMS M&O. ACC: MOL.19980716.0557.

CRWMS M&O 1998l. *UCF WP Tipover Analysis*. BBAAA0000-01717-0210-000001 REV 00. Las Vegas, Nevada: CRWMS M&O. ACC: MOL.19980625.0326.

CRWMS M&O 1998m. *Thermal Evaluation of the PWR UCF Waste Package Loaded with MOX SNF*. BBAA00000-01717-0210-00008 REV 00. Las Vegas, Nevada: CRWMS M&O. ACC: MOL.19980909.0155.

CRWMS M&O 1998n. *Multiple WP Emplacement Thermal Response – Suite 1*. BBA000000-01717-0210-00001 REV 00. Las Vegas, Nevada: CRWMS M&O. ACC: MOL.19980807.0311.

CRWMS M&O 1998o. *Immobilized in Ceramic*. Volume II in *Report of Intact and Degraded Criticality for Selected Plutonium Waste Forms in a Geologic Repository*. BBA000000-01717-5705-00020 REV 01. Las Vegas, Nevada: CRWMS M&O. ACC: MOL.19981217.0112.

CRWMS M&O 1998p. *Time Dependent Source Term Generation and Shielding Analysis for MOX Fuel in the 21 PWR Waste Package*. BBAC00000-01717-0210-00002 REV 00. Las Vegas, Nevada: CRWMS M&O. ACC: MOL.19980811.0596.

CRWMS M&O 1998q. *Software Qualification Report for MCNP Version 4B2 A General Monte Carlo N-Particle Transport Code*. CSCI: 30033 V4B2LV. DI: 30033-2003 Rev. 01. Las Vegas, Nevada: CRWMS M&O. ACC: MOL.19980622.0637.

CRWMS M&O 1998r. *Supplemental Criticality Evaluation for Degraded Internal*

Configurations of a 21 PWR Waste Package. BBA000000-01717-0210-00022 REV 00. Las Vegas, Nevada: CRWMS M&O. ACC: MOL.19980918.0086.

CRWMS M&O 1998s. *Time Dependent Shielding Analysis for Commercial SNF in the 21 PWR Waste Package.* BBAC00000-01717-0210-00003. Las Vegas, Nevada: CRWMS M&O. ACC: MOL.19981109.0382.

CRWMS M&O 1998t. *Evaluation of Codisposal Viability for Aluminum-Clad DOE-Owned Spent Fuel: Phase II Degraded Codisposal Waste Package Internal Criticality.* BBA000000-01717-5705-00017 REV 01. Las Vegas, Nevada: CRWMS M&O. ACC: MOL.19981014.0038.

CRWMS M&O 1998u. *Criticality Evaluation of Plutonium Disposition Ceramic Waste Form: Intact Mode.* BBA000000-01717-0210-00012 REV 00. Las Vegas, Nevada: CRWMS M&O. ACC: MOL.19980811.0635.

CRWMS M&O 1998v. "Waste Form Degradation, Radionuclide Mobilization, and Transport Through the Engineered Barrier System." Chapter 6 of *Total System Performance Assessment-Viability Assessment (TSPA-VA) Analyses Technical Basis Document.* B00000000-01717-4301-00006 REV 01. Las Vegas, Nevada: CRWMS M&O. ACC: MOL.19981008.0006.

CRWMS M&O 1998w. *EQ6 Calculations for Chemical Degradation of Pu-Ceramic Waste Packages.* BBA000000-01717-0210-00018 REV 00. Las Vegas, Nevada: CRWMS M&O. ACC: MOL.19980918.0004.

CRWMS M&O 1998x. *Summary Report of Commercial Reactor Criticality Data for Crystal River Unit 3.* B00000000-01717-5705-00060 REV 01. Las Vegas, Nevada: CRWMS M&O. ACC: MOL.19980728.0189.

CRWMS M&O 1999a. *Monitored Geologic Repository Project Description Document.* B00000000-01717-1705-00003 REV 00 DCN 01. Las Vegas, Nevada: CRWMS M&O. ACC: MOL.19991117.0160.

CRWMS M&O 1999b. *FY1999 Plutonium Disposition Waste Package Critically Tasks.* TDP-DDC-MD-000001 REV 00. Las Vegas, Nevada: CRWMS M&O. ACC: MOL.19990729.0059.

CRWMS M&O 1999c. *EQ6 Calculation for Chemical Degradation of Pu-Ceramic Waste Packages: Effects of Updated Materials Composition and Rates.* CAL-EDC-MD-000003 REV 00. Las Vegas, Nevada: CRWMS M&O. ACC: MOL.19990928.0235.

CRWMS M&O 1999d. *HLW Canister and Can-in-Canister Drop Calculation.* BBAA00000-01717-0210-00023 REV 00. Las Vegas, Nevada. CRWMS M&O. ACC: MOL.19990922.0321

CRWMS M&O 1999e. *Thermal Calculation of the Can-in-Canister 5-DHLW Waste Package.* BBAA00000-01717-0210-00021 REV 00. Las Vegas, Nevada: CRWMS M&O. ACC: MOL.19990831.0075.

CRWMS M&O 1999f. *Shielding Calculations for the 5-DHLW/DOE Can-in-Canister Waste Package*. B00000000-01717-0210-00075 REV 00. Las Vegas, Nevada. CRWMS M&O. ACC: MOL.19990319.0306.

CRWMS M&O 1999g. *Uncanistered Spent Nuclear Fuel Disposal Container System Description Document*. DI: SDD-UDC-SE-000001 Rev. 00. Las Vegas, Nevada: CRWMS M&O. ACC: MOL.19991217.0512.

CRWMS M&O 1999h. *Evaluation of Internal Criticality of the Plutonium Disposition MOX SNF Waste Form*. CAL-EBS-NU-000005 REV 00. Las Vegas, Nevada: CRWMS M&O. ACC: MOL.19990928.0238.

CRWMS M&O 1999i. *Addendum to: EQ6 Computer Program for Theoretical Manual, Users Guide, & Related Documentation*. Software Change Request (SCR) LSCR198. UCRL-MA-110662 PT IV. Las Vegas, Nevada: CRWMS M&O. ACC: MOL.19990305.0112.

CRWMS M&O 1999j. *DOE SRS HLW Glass Chemical Composition*. BBA000000-01717- 0210-00038 REV 00. Las Vegas, Nevada: CRWMS M&O. ACC: MOL.19990215.0397.

CRWMS M&O 1999k. *Evaluation of Internal Criticality of the Plutonium Disposition Ceramic Waste Form*. CAL-EBS-NU-000006 REV 00. Las Vegas, Nevada. CRWMS M&O. ACC: MOL.19990929.0046.

CRWMS M&O 1999l. *Probability of Criticality for MOX SNF*. CAL-EBS-NU-000007 REV 00. Las Vegas, Nevada: CRWMS M&O. ACC: MOL.19990929.0047.

CRWMS M&O 1999m. *Criticality Consequence Calculation Involving Intact PWR MOX SNF in a Degraded 21 PWR Assembly Waste Package*. CAL-EBS-NU-000008 REV 00. Las Vegas, Nevada: CRWMS M&O. ACC: MOL.19990929.0048.

CRWMS M&O 1999n. *Validation Test Report (VTR) for RELAP5/MOD3.2 V1.0*. SDN: 10091-VTR-1.0-00. Las Vegas, Nevada: CRWMS M&O. ACC: MOL.19990929.0036.

CRWMS M&O 1999o. *Sensitivity Study of Reactivity Consequences to Waste Package Egress Area*. CAL-EBS-NU-000001 REV 00. Las Vegas, Nevada: CRWMS M&O. ACC: MOL.19990928.0239.

CRWMS M&O 1999p. *FY99 Pu Criticality, 2101 9074 M1*. Activity Evaluation, March 5, 1999. Las Vegas, Nevada: CRWMS M&O. ACC: MOL.19990330.0479.

CRWMS M&O 1999q. *Geometrical and Material Properties of the Steel Invert Structure*. Input Transmittal WP-SSR-99398.T. Las Vegas, Nevada: CRWMS M&O. ACC: MOL.19991209.0055.

CRWMS M&O 1999r. *Software Validation Test Plan (VTP) for PHREEQC Version 2.0 (beta)*. SDN: 10068-VTP-2.0-00. Las Vegas, Nevada: CRWMS M&O. ACC: MOL.19990716.0156.

CRWMS M&O 1999s. *Defense High Level Waste Disposal Container System Description Document*. SDD-DDC-SE-000001. Las Vegas, Nevada: CRWMS M&O. ACC: MOL.19991217.0510.

CRWMS M&O 1999t. *Emplacement Drift System Description Document*. SDD-EDS-SE-000001 REV 00. Las Vegas, Nevada: CRWMS M&O. ACC: MOL.20000121.0119.

CRWMS M&O 1999u. *Plutonium Can-in-Canister - Design Basis Event Analysis*. ANL-WPS-SE-000002 REV 0. Las Vegas, Nevada: CRWMS M&O. ACC: MOL.19990720.0407.

CRWMS M&O 2000a. *Calculation of External Criticality Source Terms for the Waste Package Containing Pu Disposition MOX*. CAL-EBS-GS-000001 REV 00. Las Vegas, Nevada: CRWMS M&O. ACC: MOL.20000127.0095.

CRWMS M&O 2000b. *Near-Field Accumulation of Fissile Material from Waste Packages Containing Plutonium Disposition Waste Forms*. Input Transmittal WP-WP-00025.T. Las Vegas, Nevada: CRWMS M&O. ACC: MOL.20000125.0608.

CRWMS M&O 2000c. *Far-Field Accumulation of Fissile Material from Waste Packages Containing Plutonium Disposition Waste Forms*. Input Transmittal WP-WP-00024.T. Las Vegas, Nevada: CRWMS M&O. ACC: MOL.20000125.0610.

CRWMS M&O 2000d. *Probability of External Criticality of Plutonium Disposition Waste Forms*. Input Transmittal WP-WP-00026.T. Las Vegas, Nevada: CRWMS M&O. ACC: MOL.20000125.0609.

CRWMS M&O 2000e. *Validation Test Report for EQ6 V7.2bLV*. SDN: 10075-VTR-7.2bLV-00. Las Vegas, Nevada: CRWMS M&O. ACC: MOL.20000124.0135.

DOE (U.S. Department of Energy) 1992. *Characteristics of Potential Repository Wastes*. DOE/RW-0184-R1, Volume 1. Washington, D.C.: U.S. Department of Energy, Office of Civilian Radioactive Waste Management. ACC: HQO.19920827.0001.

DOE (U.S. Department of Energy) 1996. *Disposition of Surplus Highly Enriched Uranium Final Environmental Impact Statement*. DOE/EIS-0240. Two Volumes and Summary. Washington, D.C.: U.S. Department of Energy, Office of Fissile Materials Disposition. TIC: 231278.

DOE (U.S. Department of Energy) 1997. *Record of Decision for the Storage and Disposition of Weapons-Usable Fissile Materials, Final Programmatic Environmental Impact Statement*. Washington, D.C.: U.S. Department of Energy. TIC: 239425.

DOE (U.S. Department of Energy) 1998a. *Quality Assurance Requirements and Description*. DOE/RW-0333P, Rev. 8. Washington, D.C.: U. S. Department of Energy, Office of Civilian Radioactive Waste Management. ACC: MOL.19980601.0022.

DOE (U.S. Department of Energy) 1998b. *Total System Performance Assessment*. Volume 3 of *Viability Assessment of a Repository at Yucca Mountain*. DOE/RW-0508. Washington, D.C.: U.S. Department of Energy, Office of Civilian Radioactive Waste Management . ACC: MOL.19981007.0030.

EPRI (Electric Power Research Institute) 1989. *Testing and Analyses of the TN-24P PWR Spent-Fuel Dry Storage Cask Loaded with Consolidated Fuel*. EPRI NP-6191. Palo Alto, California: Electric Power Research Institute. TIC: 207047.

Flint, L.E. 1998. *Characterization of Hydrogeologic Units Using Matrix Properties, Yucca Mountain, Nevada*. Water-Resources Investigations Report 97-4243. Denver, Colorado: U.S. Geological Survey. ACC: MOL.19980429.0512.

Fowler, J.R.; Edwards, R.E.; Marra, S.L.; and Plodinec, M.J. 1995. *Chemical Composition Projections for the DWPF Product (U)*. WSRC-IM-91-116-1, Rev. 1. Aiken, South Carolina: Westinghouse Savannah River Company. TIC: 232731.

Gwyn, D.W. 1999. "Drop Heights – DHLW Canister." Interoffice correspondence from D.W. Gwyn (CRWMS M&O) to T.W. Doering, March 30, 1999, LV.SA.RPM.03/99-036. ACC: MOL.19990402.0100.

INEEL (Idaho National Engineering and Environmental Laboratory) 1995a. *Code Structure, System Models, and Solution Methods*. Volume 1 *RELAP5/MOD3 Code Manual*. NUREG/CR-5535. Washington, D.C.: U.S. Nuclear Regulatory Commission. TIC: 238741.

INEEL (Idaho National Engineering and Environmental Laboratory) 1995b. *User's Guide and Input Requirements*. Volume 2 of *RELAP5/MOD3 Code Manual*. NUREG/CR-5535. Washington, D.C.: U.S. Nuclear Regulatory Commission. TIC: 243017.

Jones, R.H. 1998. "Weight of Can-in-Canister Assembly." Interoffice Memorandum from R.H. Jones (WSRC) to E.P. Maddux (WSRC), December 3, 1998, NMP-PLS-980153. TIC: 243808.

LLNL (Lawrence Livermore National Laboratory) 1998. *Plutonium Immobilization Project Data for Yucca Mountain Total Systems Performance Assessment, Rev. 1*. PIP 98-012. Livermore, California: Lawrence Livermore National Laboratory. ACC: MOL.19980818.0349.

Olson, K.M. and Alzheimer, J.M. 1989. *Defense Waste Processing Facility Canister Impact Testing*. PNL-6812. Richland, Washington: Pacific Northwest Laboratory. ACC: NNA.19891127.0312.

Parrington, J.R.; Knox, H.D.; Breneman, S.L.; Baum, E.M.; and Feiner, F. 1996. *Nuclides and Isotopes, Chart of the Nuclides*. 15th Edition. San Jose, California: General Electric Company and KAPL, Inc. TIC: 233705.

Peterson, M.E.; Alzheimer, J.M.; and Slate, S.C. 1985. *Impact Testing of Simulated High-Level Waste Glass Canisters*. PNL-5251. Richland, Washington: Pacific Northwest Laboratory. ACC:

NNA.19890713.0219.

Philip, J.R., Knight, J.H., and Waechter, R.T. 1989. "Unsaturated Seepage and Subterranean Holes: Conspectus, and Exclusion Problem for Circular Cylindrical Cavities." *Water Resources Research*, 25,(1), 16-28. Washington, D.C.: American Geophysical Union. TIC: 239117.

Rai, D. and Ryan, J. L. 1982. "Crystallinity and Solubility of Pu(IV) Oxide and Hydrated Oxide in Aged Aqueous Suspensions." *Radiochimica Acta*, 30, 213-216. Munchen, Germany: R. Oldenbourg Verlag. TIC: 219107.

Shaw, H., ed. 1999. *Plutonium Immobilization Project Input for Yucca Mountain Total Systems Performance Assessment*. PIP 99-107. Livermore, California: Lawrence Livermore National Laboratory. TIC: 245437.

Spahiu, K. and Bruno, J. 1995. *A Selected Thermodynamic Database for REE to be Used in HLNW Performance Assessment Exercises*. SKB Technical Report 95-35. Stockholm, Sweden: Swedish Nuclear Fuel and Waste Management Company. TIC: 225493.

Toledo Edison 1998. "Table 4.2-1 Fuel Assembly Dimensions and Materials," "Table 4-1. Fuel Design Parameters," and Addendum 1, "Davis-Besse Nuclear Power Station Unit 1, Cycle 12 - Reload Report." Volume 6 of *Davis-Besse Nuclear Power Station No. 1, Updated Safety Analysis Report*. Rev. 21. Toledo, Ohio: Toledo Edison. TIC: 245410.

Wang, H. 1998. "Temperature Results of the Emplacement Multiple Waste Packages Thermal Calculation." Interoffice Correspondence from H. Wang (CRWMS M&O) to J.H. Jones and D.C. Copenhaver, May 27, 1998, LV.WP.HW.5/98-109 with Attachments. ACC: MOL.19980730.0161.

Weast, R.C. 1977. *CRC Handbook of Chemistry and Physics*. 58th Edition. Pages B-121 and F-210. Cleveland, Ohio: CRC Press. TIC: 242376.

Weger, H.T.; Rai, D.; Hess, N.J.; and McGrail, B.P. 1998. *Solubility and Aqueous-Phase Reactions of Gadolinium in the K-Na-CO₃-OH-H₂O System*. PNNL-11864. Richland, Washington: Pacific Northwest Laboratory. TIC: 242377.

Westinghouse Electric Corporation 1994. *Plutonium Disposition in Existing Pressurized Water Reactors*. DOE/SF/19683-6. Pittsburgh, Pennsylvania: Westinghouse Electric Corporation. TIC: 237140.

Westinghouse Electric Corporation 1998. *Plutonium Disposition Study, Implementation of Weapons Grade MOX Fuel in Existing Pressurized Water Reactors*. DOE/SF/19683-7, Rev. 1. Pittsburgh, Pennsylvania: Westinghouse Electric Corporation. TIC: 245436.

Wilson, C.N. and Burton, C.J. 1989. *Studies on Spent Fuel Dissolution Behavior Under Yucca Mountain Repository Conditions*. PNL-SA-16832. Richland, Washington: Pacific Northwest Laboratory. ACC: HQX.19890918.0047.

Wolery, T.J. 1992. *EQ3/6, A Software Package for Geochemical Modeling of Aqueous Systems. Package Overview and Installation Guide (Version 7.0)*. UCRL-MA-110662 PT I. Livermore, California: Lawrence Livermore National Laboratory. TIC: 205087.

Wolery, T.J. and Daveler, S.A. 1992. *EQ6, A Computer Program for Reaction Path Modeling of Aqueous Geochemical Systems: Theoretical Manual, User's Guide, and Related Documentation (Version 7.0)*. UCRL-MA-110662 PT IV. Livermore, California: Lawrence Livermore National Laboratory. TIC: 205002.

YMP (Yucca Mountain Project) 1998. *Disposal Criticality Analysis Methodology Topical Report*. YMP/TR-004Q, Rev. 0. Las Vegas, Nevada: Yucca Mountain Site Characterization Office. ACC: MOL.19990210.0236.

YMP 1999. *Monitored Geologic Repository Requirements Document*. YMP/CM-0025, Rev. 3, DCN 01. Las Vegas, Nevada: Yucca Mountain Site Characterization Office. ACC: MOL.19990429.0228.

9.2 SOURCE DATA

GS980808312242.015. Water Retention and Unsaturated Hydraulic Conductivity Measurements for Various Size Fractions of Crushed, Sieved, Welded Tuff Samples Measured Using a Centrifuge. Submittal date: 08/21/1998.

LL980711104242.054. Report of the Committee to Review the Use of J-13 Well Water in Nevada Nuclear Waste Storage Investigations. Submittal date: 08/05/1998.